

ANALYTICA CHIMICA ACTA

An international journal devoted to all branches of analytical chemistry

EDITORS

HARRY L. PARDUE (West Lafayette, IN, U.S.A.)

ALAN TOWNSHEND (Hull, Great Britain)

J.T. CLERC (Berne, Switzerland)

WILLEM E. VAN DER LINDEN (Enschede, The Netherlands)

PAUL J. WORSFOLD (Plymouth, Great Britain)

Editorial Advisers

F.C. Adams, Antwerp
M. Aizawa, Yokohama
J.F. Alder, Manchester
C.M.G. van den Berg, Liverpool
A.M. Bond, Bundoora, Vic.
S.D. Brown, Newark, DE
J. Buffle, Geneva
P.R. Coulet, Lyon
S.R. Crouch, East Lansing, MI
R. Dams, Ghent
L. de Galan, Vlaardingen
M.L. Gross, Lincoln, NE
W. Heineman, Cincinnati, OH
G.M. Hieftje, Bloomington, IN
G. Horvai, Budapest
T. Imasaka, Fukuoka
D. Jagner, Gothenburg
G. Johansson, Lund
D.C. Johnson, Ames, IA
A.M.G. Macdonald, Birmingham
D.L. Massart, Brussels
P.C. Meier, Schaffhausen
M.E. Meyerhoff, Ann Arbor, MI

J.N. Miller, Loughborough
H.A. Mottola, Stillwater, OK
M.E. Munk, Tempe, AZ
M. Otto, Freiberg
D. Pérez-Bendito, Córdoba
C.F. Poole, Detroit, MI
S.C. Rutan, Richmond, VA
J. Ruzicka, Seattle, WA
A. Sanz-Medel, Oviedo
S. Sasaki, Toyohashi
T. Sawada, Tokyo
K. Schügerl, Hannover
M.R. Smyth, Dublin
M. Thompson, Toronto
G. Tóig, Dortmund
Y. Umezawa, Tokyo
E. Wang, Changchun
J. Wang, Las Cruces, NM
H.W. Werner, Eindhoven
C.S. Wolfbeis, Graz
Yu.A. Zolotov, Moscow
J. Zupan, Ljubljana

ANALYTICA CHIMICA ACTA

Scope. *Analytica Chimica Acta* publishes original papers, preliminary communications and reviews dealing with every aspect of modern analytical chemistry. Reviews are normally written by invitation of the editors, who welcome suggestions for subjects. Preliminary communications of important urgent work can be printed within four months of submission, if the authors are prepared to forego proofs.

Submission of Papers

Americas

Prof. Harry L. Pardue
Department of Chemistry
1393 BRWN Bldg, Purdue University
West Lafayette, IN 47907-1393
USA
Tel: (+1-317) 494 5320
Fax: (+1-317) 496 1200

Computer Techniques

Prof. J.T. Clerc
Universität Bern
Pharmazeutisches Institut
Baltzerstrasse 5, CH-3012 Bern
Switzerland
Tel: (+41-31) 654171
Fax: (+41-31) 654198

Other Papers

Prof. Alan Townshend
Department of Chemistry
The University
Hull HU6 7RX
Great Britain

Tel: (+44-482) 465027
Fax: (+44-482) 466410

Prof. Willem E. van der Linden
Laboratory for Chemical Analysis
Department of Chemical Technology
Twente University of Technology
P.O. Box 217, 7500 AE Enschede
The Netherlands

Tel: (+31-53) 892629
Fax: (+31-53) 356024

Prof. Paul Worsfold
Dept. of Environmental Sciences
University of Plymouth
Plymouth PL4 8AA
Great Britain

Tel: (+44-752) 233006
Fax: (+44-752) 233009

Submission of an article is understood to imply that the article is original and unpublished and is not being considered for publication elsewhere. *Anal. Chim. Acta* accepts papers in English only. There are no page charges. Manuscripts should conform in layout and style to the papers published in this issue. See inside back cover for "Information for Authors".

Publication. *Analytica Chimica Acta* appears in 14 volumes in 1993. The subscription price for 1993 (Vols. 267-280) is Dfl. 4214.00 plus Dfl. 462.00 (p.p.h.) (total approx. US\$ 2816.75). *Vibrational Spectroscopy* appears in 2 volumes in 1993. The subscription price for *Vibrational Spectroscopy* (Vols. 4 and 5) is Dfl. 700.00 plus Dfl. 66.00 (p.p.h.) (total approx. US\$ 461.50). The price of a combined subscription (*Anal. Chim. Acta* and *Vib. Spectrosc.*) is Dfl. 4592.00 plus Dfl. 528.00 (p.p.h.) (total approx. US\$ 3084.25). All earlier volumes (Vols. 1-266) except Vols. 23 and 28 are available at Dfl. 259.50 (US\$ 156.25), plus Dfl. 18.00 (US\$ 10.75) p.p.h., per volume. The Dutch guilder price is definitive. The U.S. dollar price is subject to exchange-rate fluctuations and is given only as a guide. Subscriptions are accepted on a prepaid basis only, unless different terms have been previously agreed upon.

Our p.p.h. (postage, packing and handling) charge includes surface delivery of all issues, except to subscribers in the U.S.A., Canada, Australia, New Zealand, China, India, Israel, South Africa, Malaysia, Thailand, Singapore, South Korea, Taiwan, Pakistan, Hong Kong, Brazil, Argentina and Mexico, who receive all issues by air delivery (S.A.L.-Surface Air Lifted) at no extra cost. For Japan, air delivery requires 25% additional charge of the normal postage and handling charge; for all other countries airmail and S.A.L. charges are available upon request.

Subscription orders. Subscription orders can be entered only by calendar year and should be sent to: Elsevier Science Publishers B.V., Journals Department, P.O. Box 211, 1000 AE Amsterdam, The Netherlands. Tel: (+31-20) 5803 642, Telex: 18582, Telefax: (+31-20) 5803598, to which requests for sample copies can also be sent. Claims for issues not received should be made within six months of publication of the issues. If not they cannot be honoured free of charge. Readers in the U.S.A. and Canada can contact the following address: Elsevier Science Publishing Co. Inc., Journal Information Center, 655 Avenue of the Americas, New York, NY 10010, U.S.A. Tel: (+1-212) 6333750, Telefax: (+1-212) 6333990, for further information, or a free sample copy of this or any other Elsevier Science Publishers journal.

Advertisements. Advertisement rates are available from the publisher on request.

Detailed "Instructions to Authors" for *Analytica Chimica Acta* was published in Volume 256, No. 2, pp. 373-376. Free reprints of the "Instructions to Authors" of *Analytica Chimica Acta* and *Vibrational Spectroscopy* are available from the Editors or from: Elsevier Science Publishers B.V., P.O. Box 330, 1000 AH Amsterdam, The Netherlands. Telefax: (+31-20) 5862845.

US mailing notice - *Analytica Chimica Acta* (ISSN 0003-2670) is published biweekly by Elsevier Science Publishers (Molenwerf 1, Postbus 211, 1000 AE Amsterdam). Annual subscription price in the USA US\$ 2816.75 (subject to change), including air speed delivery. Second class postage paid at Jamaica, NY 11431. *USA Postmasters:* Send address changes to *Anal. Chim. Acta*, Publications Expediting, Inc., 200 Meacham Av., Elmont, NY 11003. Airfreight and mailing in the USA by Publication Expediting.

**FOR ADVERTISING
INFORMATION
PLEASE CONTACT OUR
ADVERTISING
REPRESENTATIVES**

USA/CANADA

Weston Media Associates

Mr. Daniel S. Lipner

P.O. Box 1110, GREENS FARMS, CT 06436-1110
Tel: (203) 261-2500, Fax: (203) 261-0101

GREAT BRITAIN

T.G. Scott & Son Ltd.

Tim Blake/Vanessa Bird

Portland House, 21 Narborough Road
COSBY, Leicestershire LE9 5TA
Tel: (0533) 753-333, Fax: (0533) 750-522

JAPAN

ESP - Tokyo Branch

Mr. S. Onoda

20-12 Yushima, 3 chome, Bunkyo-Ku
TOKYO 113
Tel: (03) 3836 0810, Fax: (03) 3839-4344
Telex: 02657617



REST OF WORLD
**ELSEVIER
SCIENCE
PUBLISHERS**

Ms. W. van Cattenburch
Advertising Department

P.O. Box 211, 1000 AE AMSTERDAM,
The Netherlands

Tel: (20) 515.3220/21/22, Telex: 16479 els vi nl
Fax: (20) 683.3041

*The first place to look for the data you need
on all common analytical reagents*



**Dictionary of
Analytical Reagents**

FREE 32 PAGE SAMPLE AVAILABLE

- only compilation to include all commonly used analytical reagents in a single volume
- chemical, structural and bibliographic data on over 5,000 analytical reagents
- a wealth of information designed specifically for the analytical chemist, such as pKa, solubilities and uv data
- principal analytical applications given for each reagent
- labelled references allow direct access to the primary literature, saving time and money
- unique Type of Compound Index allows you to locate the information you require by use, by analyte or by compound group

June 1993: Hardback: 0-412-35150-1: 280x210mm: c.1184 pp: £595

**Save £100 by ordering today - special offer price of
£495 until June 1993**



Send your orders/enquiries to:
Steve Hawe, Dept ACA, Chapman & Hall, 2-6
Boundary Row, London SE1 8HN, UK
Tel: +44 71 865 0066 Fax: +44 71 522 9621

003

**PLEASE
MENTION
THIS
JOURNAL
WHEN
ANSWERING
ADVER-
TISEMENTS**

CATALOGUE 1993 ON CD-ROM

Elsevier Science Publishers - the world's largest scientific publisher - presents for the first time details of all its publications on CD-ROM

ADVANTAGES

- Easy to use.
- Get more comprehensive information than ever before.
- Make fast and effective searches.
- Find what you want even with incomplete information.
- Compile special lists of products without typing.
- Improve your control of scientific product information.
- Enhance service to clients.

PRODUCT DESCRIPTION

The CD-ROM contains descriptions of all Elsevier products.

- All the journals, with complete information about journal editors and editorial boards
- Listings of recently published papers for many journals
- Complete descriptions and contents lists of book titles
- Independent reviews of published books
- Forthcoming title information
- Book series
- All other products, e.g. software, CDs, dictionaries, wallcharts.

In addition, the CD-ROM features easy-to-use search tools, making the information

accessible and useful. For example, searches can be made by subject area, by year of publication, by author/editor or title and by "free text" search.

Full book and journal information can be printed to initiate your order.

If you do not find what you need, or wish to know more about Elsevier's publishing programme, the CD-ROM can supply you with the name, address and fax number of the correct person to contact.

AUDIENCE

Librarians, booksellers, researchers, agents and information specialists.

SYSTEM REQUIREMENTS

The CD-ROM has been designed to run under Microsoft® Windows™ 3.0, on IBM PC-ATs and compatibles. The CD-ROM is Microsoft® Windows™ 3.1 compatible.

The minimum requirements are:

- IBM or IBM-compatible PC with a 80286 or higher processor
- 2 MB or more RAM
- MS-DOS® 3.3 or higher installed
- Microsoft® Windows™ 3.0 (or 3.1) installed
- Microsoft® Windows™ compatible mouse or other pointing device
- VGA graphics adapter (colour or monochrome)
- Hard disk with at least 2 MB free disk space
- CD-ROM drive which is accessible from Microsoft® Windows™
- For faster operation a 80386SX or higher processor is recommended, as well as a fast CD-ROM drive (access time less than 0.4 seconds).

The CD-ROM can be installed in a local area network.

For further information please contact

ELSEVIER SCIENCE PUBLISHERS
Attn. Vivian Wong Swie San
Marketing Services Department
P.O. Box 211
1000 AE Amsterdam
The Netherlands
FAX: (020) 5862 425
In the USA & Canada
Journal Information Center
P.O. Box 882
Madison Square Station
New York, NY 10159, USA
FAX: (212) 633 3764



ELSEVIER
SCIENCE PUBLISHERS

ANALYTICA CHIMICA ACTA

An international journal devoted to all branches of analytical chemistry

(Full texts are incorporated in CJELSEVIER, a file in the Chemical Journals Online database available on STN International; Abstracted, indexed in: Aluminum Abstracts; Anal. Abstr.; Biol. Abstr.; BIOSIS; Chem. Abstr.; Curr. Contents Phys. Chem. Earth Sci.; Engineered Materials Abstracts; Excerpta Medica; Index Med.; Life Sci.; Mass Spectrom. Bull.; Material Business Alerts; Metals Abstracts; Sci. Citation Index)

VOL. 272 NO. 2

CONTENTS

FEBRUARY 12, 1993

<i>Sensors</i>	
Optical sensing of pH and pCO ₂ using phase-modulation fluorimetry and resonance energy transfer J.R. Lakowicz, H. Szmazinski and M. Karakelle (Baltimore, MD, USA)	179
Single drop method for determination of ions using an electrodeless piezoelectric quartz crystal T. Nomura, Y. Ohno and Y. Takaji (Matsumoto, Japan)	187
<i>Atomic Spectrometry</i>	
Preconcentration of palladium, platinum and rhodium by on-line sorbent extraction for graphite furnace atomic absorption spectrometry and inductively coupled plasma atomic emission spectrometry M.L. Lee, G. Tölg, E. Beinrohr and P. Tschöpel (Dortmund, Germany)	193
<i>Enzyme Immunoassay</i>	
Automatic apparatus for heterogeneous enzyme immunoassays based on electrocatalytic detection of the enzyme and electrochemical regeneration of the solid phase D. Huet and C. Bourdillon (Compiègne, France)	205
Amperometric enzyme immunoassay for urinary human serum albumin using plasma-treated membrane S. Kaku, S. Nakanishi, K. Horiguchi and M. Sato (Kyoto, Japan)	213
<i>Electroanalytical Chemistry</i>	
Polarographic study of the Eu(III)-triethylenetetraaminehexaacetic acid complex and determination of europium by oscillopolarography X.-T. Fu (Anda City, China), C.-M. Wang and Y.-X. Zhang (Lanzhou, China)	221
Simultaneous determination of copper, nickel, lead, cobalt and cadmium by adsorptive voltammetry Z.-Q. Zhang, S.-Z. Chen, H.-M. Lin and H. Zhang (Changsha, China)	227
Determination of colloidal electrolytes: conductimetric titration of hydroxyzine hydrochloride with ammonium molybdate R. Mikulski and B. Dembiński (Toruń, Poland)	233
<i>Flow-Injection Analysis</i>	
Determination of chemical oxygen demand by a flow-injection method using cerium(IV) sulphate as oxidizing agent T. Korenaga, X. Zhou, K. Okada, T. Moriwake and S. Shinoda (Okayama, Japan)	237
Determination of bromide in sodium chloride matrices by flow-injection analysis using blank peak elimination and kinetic discrimination W.J.M. Emaus and H.J. Henning (Hengelo, Netherlands)	245
<i>Chemiluminescence</i>	
Continuous-flow chemiluminometric determination of dihydralazine, rifampicin and rifamycin SV by oxidation with N-bromosuccinimide S.A. Halvatzis, M.M. Timotheou-Potamia and T.P. Hadjiioannou (Athens, Greece)	251

(Continued overleaf)

ห้องสมุดกรมวิทยาศาสตร์บริการ

- 2 มี.ค. 2536

Contents (continued)

Flow-injection chemiluminometric determination of sodium cyclamate I.M. Psarellis, E.G. Sarantonis and A.C. Calokerinos (Athens, Greece)	265
<i>Chromatography and other Separation Methods</i>	
Liquid chromatographic assay of microbially derived phloroglucinol antibiotics for establishing the biosynthetic route to production, and the factors affecting their regulation P. Shanahan, J.D. Glennon, J.J. Crowley, D.F. Donnelly and F. O'Gara (Cork, Ireland)	271
Substoichiometric ion-pair extraction and determination of barium(II) with macrocyclic crown ether and cryptand T. Fukaya, H. Imura and N. Suzuki (Sendai, Japan)	279
Influence of ring substituents and matrix on lithium / sodium selectivity of 14-crown-4 and benzo-13-crown-4 compounds R.A. Bartsch, M.-J. Goo (Lubbock, TX, USA), G.D. Christian, X. Wen (Seattle, WA, USA), B.P. Czech, E. Chapoteau and A. Kumar (Tarrytown, NY, USA)	285
Liquid-liquid extraction of lanthanides with a highly acidic extractant, 3-phenyl-4-benzoyl-5-isoxazolone, in the presence and absence of tri- <i>n</i> -octylphosphine oxide Q.T.H. Le, S. Umetani, H. Takahara and M. Matsui (Kyoto, Japan)	293
<i>Chemometrics</i>	
Optimized prediction of ¹³ C NMR spectra using increments L. Chen and W. Robien (Vienna, Austria)	301
Characteristics and application of an electrochemical concentration modulator in correlation chromatography. Part 2. Computational aspects, modelling and application M. Engelsma, H.F.M. Boelens, D.J. Louwerse, W.Th. Kok and H.C. Smit (Amsterdam, Netherlands)	309
Ambient error weighted partial least-squares regression: a new receptor model S. Wang (Taichung, Taiwan) and T. Larson (Seattle, WA, USA)	333
Computer method for the simultaneous kinetic determination of compounds in mixtures based on the use of diode-array spectrophotometry A. Cladera, E. Gómez, J.M. Estela, V. Cerdà (Palma de Mallorca, Spain) and J.L. Cerdà (Barcelona, Spain)	339
<i>Book Reviews</i>	345
<i>Author Index</i>	351
<i>News Brief</i>	355

Optical sensing of pH and pCO₂ using phase-modulation fluorimetry and resonance energy transfer

Joseph R. Lakowicz, Henryk Szmazinski and Mutlu Karakelle

*Center for Fluorescence Spectroscopy, Department of Biological Chemistry, University of Maryland, School of Medicine,
108 North Greene Street, Baltimore, MD 21201 (USA)*

(Received 7th May 1992; revised manuscript received 2nd October 1992)

Abstract

We have developed optical sensors for pH and/or pCO₂ based on phase shift and modulation measurements of time-resolved fluorescence energy transfer. pH-insensitive donors and pH-sensitive acceptors were encased in CO₂-permeable silicon membranes. The extent of energy transfer depends on the pH-dependent absorption spectra of the acceptor. The measurements were made insensitive to inner-filter effects of the total intensity by using the phase-modulation method to determine the donor decay times. The general applicability of this method was demonstrated using three donor-acceptor pairs, all of which can be excited with an inexpensive green 543-nm He-Ne laser.

Keywords: Fluorimetry; Donor-acceptor complexes; Energy transfer; pCO₂; pH

Optical measurements of pH and/or pCO₂ are of wide interest in analytical and clinical chemistry [1–3]. At present, most optical sensing of pH/pCO₂ is based on measurements of the steady-state fluorescence intensity, as determined by the absorptive and emissive properties of the sample [4–7]. Steady-state intensity measurements are sensitive to light losses, lamp drift, probe bleaching, and the optical properties of tissues, and such measurements require frequent recalibration. To compensate for these difficulties, wavelength-ratiometric methods have been proposed, particularly using the pH-sensitive fluorophore pyranine [8,9]. However, the use of wavelength-ratiometric compensation requires that the optical artifacts affect both wavelengths

in a similar manner. Furthermore, there are relatively few wavelength-ratiometric probes available, particularly with long-wavelength absorption and emission maxima. Pyranine cannot be excited with inexpensive laser sources, and its use requires two excitation wavelengths which are not conveniently available using laser sources.

The difficulties described above can be circumvented using time-resolved fluorescence and sensors containing a fluorescence donor and a pH-sensitive acceptor (Scheme 1). pH sensors based on intensity-based measurements and energy transfer have been described previously by Walt and coworkers [10–13]. The use of lifetime or decay time measurements offers many advantages for sensing applications [14] because decay times are generally not dependent on the macroscopic optical properties of the sample, and are not sensitive to the total intensity. Fluorescence lifetime measurements are generally thought to require sophisticated instrumentation. Advances

Correspondence to: J.R. Lakowicz, Center for Fluorescence Spectroscopy, Department of Biological Chemistry, University of Maryland, School of Medicine, 108 North Greene Street, Baltimore, MD 21201 (USA).

in lasers, optics and electronics make it easily conceivable to develop inexpensive and robust instruments based on the phase shift and/or demodulation methods [15]. However, construction of practical instrumentation requires the use of simple and inexpensive laser sources [15–17].

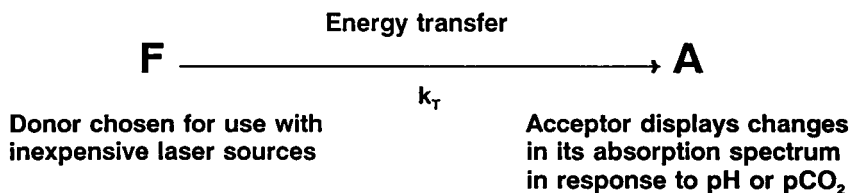
Decay time sensing of pH(pCO₂) is limited by the lack of pH probes which can be excited with simple laser sources such as He–Ne or diode laser. The fluorescence pH(pCO₂) sensor must display good absorption of the laser light, a high quantum yield, and sensitivity in the desired pH range. It is difficult to obtain all these requirements in a single chromophore. However, these characteristics are more easily obtained by using a two-part sensor (Scheme 1). In this case the fluorescent donor can be selected for its absorption, emission and decay time characteristics, without concern for its sensitivity to pH(pCO₂). The acceptor need not be fluorescent, and need only display a change in absorption in response to pH(pCO₂) in the wavelength range of the donor emission. The donor and acceptor can be covalently linked (see Discussion) or simply mixed together as described in this report.

The mechanism of inducing a pH(pCO₂)-dependent change in the donor decay time is fluorescence resonance energy transfer (FRET). The phenomenon of FRET is non-radiative energy transfer from the fluorescent donor to the acceptor, without emission and reabsorption of a photon. This latter process of emission and reabsorption is an inner-filter effect which depends on the size and macroscopic optical properties of the sample. In contrast, FRET is a through-space interaction which can be reliably predicted based on the spectral properties of the donor and acceptor. Importantly, FRET decreases the mean decay time of the donor, whereas radiative energy

transfer (i.e., reabsorption and emission) does not yield easily predictable changes in the donor decay time.

For unlinked donor–acceptor pairs the phenomenon of FRET requires an acceptor concentration in the range of 1–10 mM [18]. Such acceptor concentrations result in high optical densities at the excitation and emission wavelengths, making intensity measurement difficult to use in a quantitative manner [12]. At these high acceptor concentrations there are, in addition to FRET, inner-filter effects which depend on the excitation and observation wavelength and on the detailed macroscopic properties of the sample and detection optics. For instance, an increase in absorption can decrease the observed intensity of the donor due to preferential absorption of the incident light by the acceptor. However, the increased absorption will also change the penetration depth of the incident light into the sample, which also alters the observed intensity.

The non-ideal optical properties of real-world samples result in additional difficulties. High absorbance or turbidity results in low signal levels and difficulties in measuring small changes in the signal intensity. These difficulties can be avoided by measurement of fluorescence decay times, which are independent of the total intensity so long as the donor emission is detectable. The lifetime can be determined by the rate of change following pulsed excitation. However, these nanosecond timescale processes can be more easily measured by the phase-modulation method [19–22]. The decay time information is contained in the phase shift (θ) and modulation (m) of the emission relative to the incident light. In the present report we describe pH(pCO₂) sensing based on three different donors and two acceptors. The donors were selected to be excitable



Scheme 1. Schematic of pH/pCO₂ sensors based on energy transfer.

with a 543-nm He–Ne laser. Since the phenomenon of FRET is predictable, this method can be extended to use with modulated laser diode sources by the selection of alternative donor–acceptor pairs.

MATERIALS AND METHODS

Fabrication of the pH(pCO₂) sensors

Poly(2-hydroxyethyl methacrylate) (polyHEMA) was synthesized as follows: 2-hydroxyethyl methacrylate (Aldrich) monomer was mixed with 1% (w/w) 2,2'-azobisisobutyronitrile (Polysciences) initiator and degassed. The monomer–initiator mixture was placed in a template well between two glass plates and cured at 75°C for 60 min. The polyHEMA film was subjected to repeated water extractions for removing unreacted monomer and catalyst residues.

Silicone rubber membrane was prepared using a two-part platinum catalyst curing formulation (FGB 001, Admiral). Parts A and B were mixed according to the supplier directions and degassed. The mixture was cast on a PTFE-coated glass plate using Doctor's knife and cured at 150°C for 30 min.

The donors and acceptors were dissolved at concentrations listed in Table 1 in a 40 mM NaHCO₃ (Aldrich) solution. PolyHEMA hydrogel disks were soaked in the donor–acceptor–bicarbonate solution for 48 h for reaching an equilibrium intake. The equilibrated hydrogel disks were blot-dried and sandwiched between two circular silicone rubber membranes. The circular silicone membranes were glued together using a moisture cure silicone adhesive (DC 3145, Dow

Corning). The resultant sensors were completely sealed and retained their indicator solutions. The sensors were stored at 100% relative humidity conditions for retaining their equilibrium water uptake. The acceptor concentrations are those expected for significant energy transfer using these donor–acceptor pairs. Acceptor concentrations in this range result in a significant fraction of the donor population being within the characteristic Förster distances for energy transfer, which is near 50 Å.

The donor concentrations were chosen to be as low as possible consistent with an ability to easily observe the emission. Low donor concentrations were also used to avoid FRET between the donors. While such transfer could result in increased transfer to the acceptor [23,24], we wished to avoid donor-to-donor transfer so that the experiments revealed the usefulness of donor-to-acceptor transfer for pH(pCO₂) sensing.

Frequency-domain measurements

Multi-frequency phase and modulation data were collected on the frequency-domain instruments described previously [21,22]. For the multi-frequency measurements, we used 568-nm excitation from a cavity-dumped dye laser [22]. For testing the pH(pCO₂) response of the sensors we used a 543-nm He–Ne laser, which was intensity modulated with an acousto-optic modulator. This light source was chosen because it is practical for analytical or clinical sensing applications.

In phase-modulation fluorimetry, the sample is excited with an intensity-modulated light source. The experimental observables are the phase shift of the emission (θ) and its modulation (m), both relative to the phase and modulation of the source

TABLE 1

Concentrations and wavelengths used in the pH(pCO₂) sensors

Donor ^a		Acceptor		Excitation (nm)	Emission filter (nm)
Identity	Concentration (M)	Identity	Concentration (M)		
Eosin	5 × 10 ⁻⁴	PR	4 × 10 ⁻³	543/563	580
R6G	1 × 10 ⁻⁴	PR	4 × 10 ⁻³	543/568	600
TRH	3 × 10 ⁻⁵	BTB	2 × 10 ⁻³	543/568	600

^a Control (donor-alone) sensors were identical but did not contain acceptor.

[19]. These quantities are related to apparent phase (τ_p) and modulation (τ_m) lifetimes by

$$\tan \theta = \omega \tau_p \quad (1)$$

$$m = (1 + \omega^2 \tau_m^2)^{-1/2} \quad (2)$$

where ω is the modulation frequency in rad s^{-1} . The qualifier “apparent” is used because the lifetimes (τ_p and τ_m) are true decay times only for single-exponential intensity decays. It is known that energy transfer between randomly distributed donors and acceptors results in more complex (multi-exponential) intensity decays [25,26].

RESULTS

Absorption and emission spectra of the three donors [Eosin, Rhodamine 6G (R6G) and Texas Red Hydrazide (TRH)], are shown in Fig. 1. The donors each show significant absorption at 543 nm. The absorption and emission spectra of the donors are not significantly sensitive to the pH from 6.5 to 9.2.

Absorption spectra of the acceptors are shown in Fig. 2. The absorption of both Phenol Red (PR) and Bromothymol Blue (BTB) increases for decreasing partial pressures of CO_2 . The increased absorption is the result of the increase in pH which occurs upon removal of CO_2 (Fig. 2, inset). Importantly, these acceptors display sensitivity to pH in the physiologically relevant range of 6–8, and to pCO_2 in the physiologically relevant range of 0–40 Torr. The sensitive range can be optimized as needed by adjusting the bicarbonate and/or acceptor concentration. The sensors could be made sensitive to pH rather than pCO_2 by using water-permeable membranes. If needed, the donor and acceptors could be covalently linked to a polymeric matrix to prevent dilution of the chromophores. At high pH the absorbance increases in the region of the donor emission, so that increased energy transfer is expected at high pH. It is also possible to identify donor–acceptor pairs in which the extent of energy transfer and/or spectral overlap decreases at high pH.

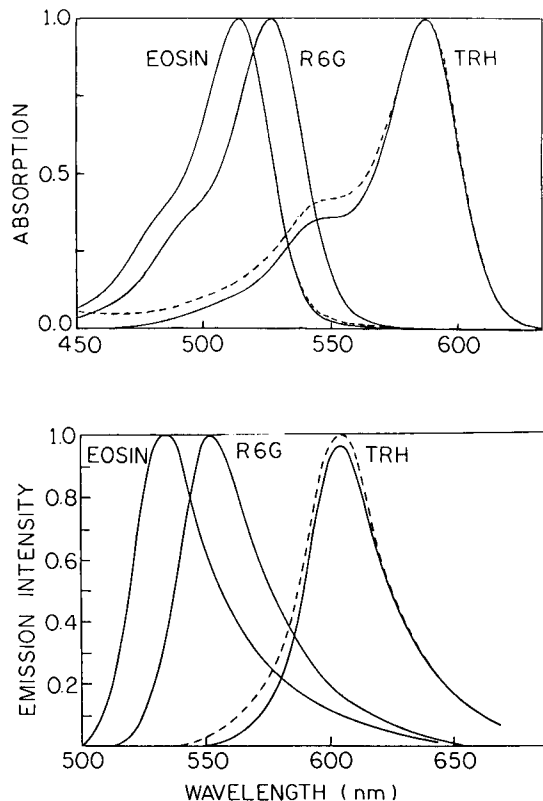


Fig. 1. Absorption and emission spectra of the donors Eosin, Rhodamine 6G and Texas Red Hydrazide; (—) pH 9.2; (---) pH 6.5.

Frequency response curves of the donor alone controls and the donor plus acceptor-containing sensors are shown in Fig. 3. The frequency responses shift to higher frequencies in the presence of acceptor, as seen for R6G–PR (top) and TRH–BTB (bottom). A less dramatic acceptor-dependent shift was seen for Eosin–PR (not shown). The short lifetime of Eosin prevented us from observing its entire frequency response using an upper frequency limit of 200 MHz. While we are capable of measuring at higher frequencies [22,27], we did not do so because we felt 200 MHz was a reasonable upper limit for lifetime-sensing instrumentation, which is not likely to use the higher-speed microchannel plate photomultiplier tubes.

A functional sensor for pH or pCO_2 does not require measurement of a complete frequency response. Measurement at a single light-modula-

tion frequency is adequate. Such measurements are shown in Figs. 4 and 5 for phase and modulation, respectively. In these measurements we used the 543-nm He–Ne laser with an acousto-optic modulator. The phase angles increased monotonically with increased partial pressures of CO₂ (Fig. 4), and the modulation decreased (Fig. 5), indicating longer donor decay times as the CO₂ pressure increases.

It is important to consider the accuracy possible from the phase-modulation data. There is no single number which characterizes the accuracy because many sensor configurations are possible, and one can obtain various types of data. For instance, a single-phase measurement can be performed at one modulation frequency, one could use both the phase and modulation data at the same frequency, or one could measure phase and modulation at several selected frequencies. The latter would be possible with an acousto-optic-

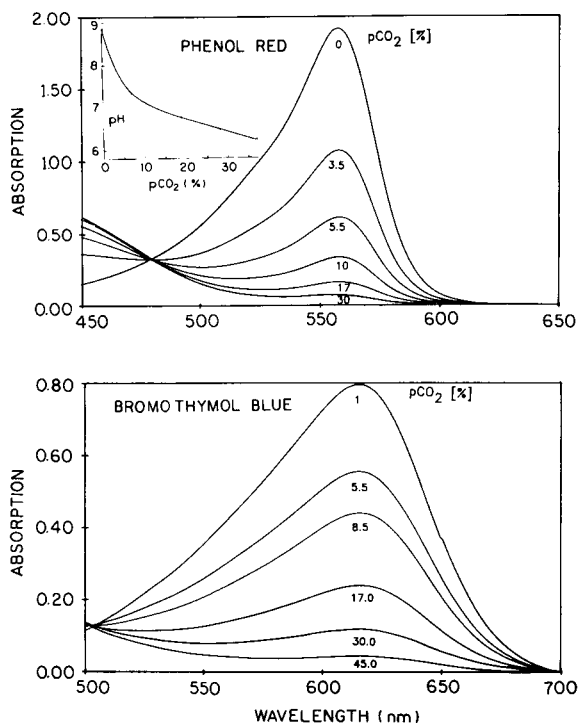


Fig. 2. pH(pCO₂)-dependent absorption spectra of the acceptor Phenol Red and Bromothymol Blue. The inset shows the relationship between pH and pCO₂ for our experimental conditions.

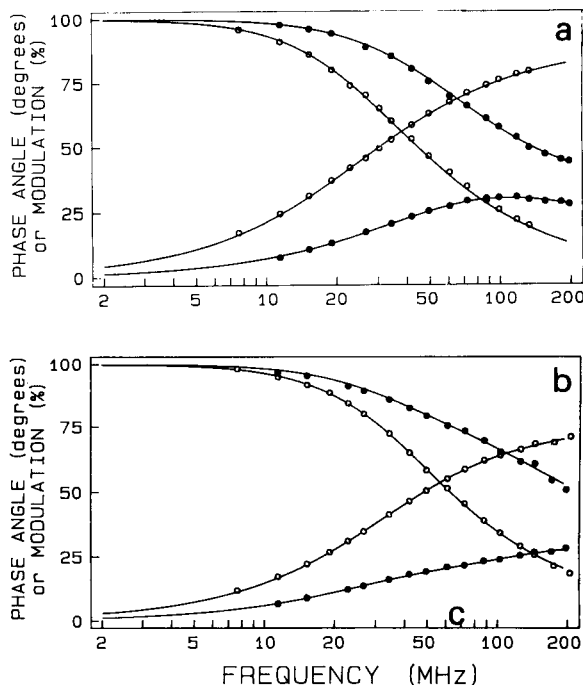


Fig. 3. Frequency response of the donors in the absence and presence of acceptors. Top: (○) Rhodamine alone, $\bar{\tau} = 6.25$ ns; and (●) with 0.004 M Phenol Red, $\bar{\tau} = 2.11$ ns, energy transfer = 0.83. Bottom: (○) Texas Red Hydrazide alone, $\bar{\tau} = 4.30$ ns; and (●) with 0.002 M Bromothymol Blue, $\bar{\tau} = 1.82$ ns, energy transfer = 0.78. $\lambda_{ex} = 568$ nm; $\lambda_{obs} = 600$ nm. $\bar{\tau}$ is the mean lifetime from a multi-exponential analysis [22].

modulated laser source. Based on considerable experience with phase-modulation fluorimetry, we know that phase angles are easily accurate to 0.5° and 0.10° seems possible, particularly with dedicated instrumentation and numerical methods. Assuming an accuracy of 0.5° or 1%, the single-frequency phase and modulation data can provide pCO₂ values accurate to 0.25 Torr. Hence, this sensing scheme appears to have adequate accuracy for clinical use in blood gas determinations.

DISCUSSION

The energy transfer pH(pCO₂) sensors described in this report contained high acceptor concentrations in order to place the acceptors within the Förster distances for energy transfer. There are two disadvantages to this approach.

The first is attenuation of the observed intensity of the donor due to inner-filter effects which attenuate the donor emission and partial absorption of the incident light by the acceptor. The fraction of the incident light absorbed by the donor is approximately given by the fractional absorption of the donor at the excitation wavelength [28]. Hence, the high acceptor concentration results in decreased donor emission due to non-productive absorption by the acceptor.

A second disadvantage of our unlinked donors and acceptors is the dependence of the extent of energy transfer on the acceptor concentration [C]. This dependence is given by

$$I(t) = I^0 \exp \left[-\frac{t}{\tau_0} - 2\gamma \left(\frac{t}{\tau_0} \right)^{1/2} \right] \quad (3)$$

$$[C]_0 = \frac{3000}{2\pi^{3/2}NR_0^3} \quad (4)$$

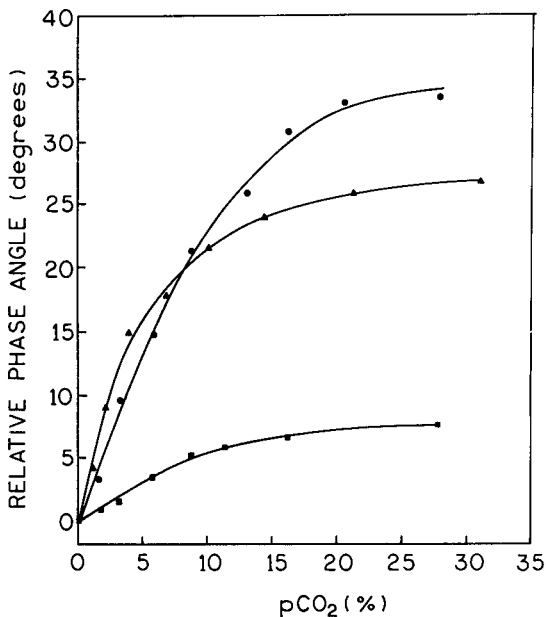


Fig. 4. Dependence of the donor phase angle on $p\text{CO}_2$. The donor-acceptor pairs were in polyHEMA hydrogel, 25°C. (●) Texas Red Hydrazide + Bromothymol Blue (0.002 M), $\lambda_{\text{ex}} = 543$ nm, $\lambda_{\text{obs}} = 600$ nm, 133 MHz; (▲) Eosin + Phenol Red (0.004 M), $\lambda_{\text{ex}} = 543$ nm, $\lambda_{\text{obs}} = 580$ nm, 155 MHz; (■) Rhodamine 6G + Phenol Red (0.004 M), $\lambda_{\text{ex}} = 543$ nm, $\lambda_{\text{obs}} = 600$ nm, 133 MHz.

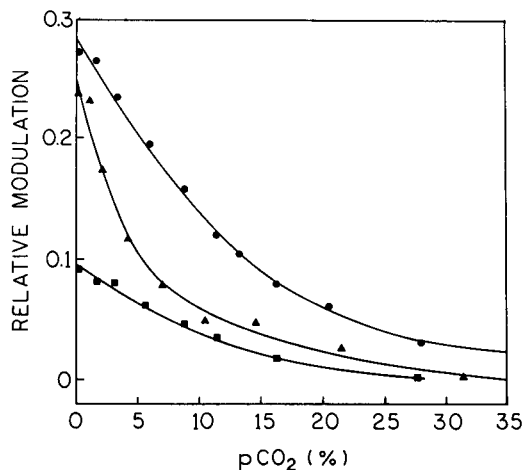


Fig. 5. Dependence of the donor modulation on $p\text{CO}_2$. See Fig. 4 for details.

where τ_0 is the decay time of the donor in the absence of acceptors, $[C]_0$ is the critical concentration of acceptor, $\gamma = [C]/[C]_0$, and R_0 is the Förster distance [29,30]. It is quite possible that the acceptor concentrations can change in a physiological environment due to water evaporation or absorption, or due to osmotic effects. The changes in acceptor concentration will require recalibration of the $\text{pH}(p\text{CO}_2)$ sensor.

The two disadvantages discussed above can be avoided by the use of covalently linked donor-acceptor pairs. Because the acceptor is covalently linked to the donor, both are present in a one-to-one ratio. Hence, there will be minimal non-productive absorption due to the acceptor, and the linked probe can be more dilute to avoid inner-filter effects. Importantly, the linked probes will not be sensitive to dilution effects, so that the sensors will require little if any calibration. This advantage of linked donor-acceptor pairs has been recognized by others [10,11].

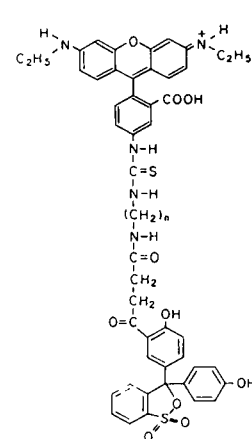
Several additional donor-acceptor pH probes are shown in Fig. 6. A variety of "Gedanken" probes can be imagined with a range of spectral properties. The R6G-PR probe (Fig. 6, upper left) would display properties similar to that described for the R6G-PR hydrogel sensor (above). The use of FRET as the pH-to-lifetime transduction mechanism provides a straightforward path for using other light or laser sources. If desired,

the R6G donor could be replaced with a ruthenium (Ru) or lanthanide complex. These could be excited with electroluminescent lamp [15] or flash lamp sources because of their long decay times. The long Ru or lanthanide decay times could be measured after decay of the prompt autofluorescence, as is now done in the so-called “time-resolved immunoassays” [31]. The Ru complex would be sensitive to oxygen [32,33], but the lanthanides are not quenched by oxygen.

Finally, the use of FRET allows selection of the donor for use with red 633-nm He-Ne or laser diode sources, as shown for the Indocyanine–Thymol Blue probe in Fig. 6 (lower left).

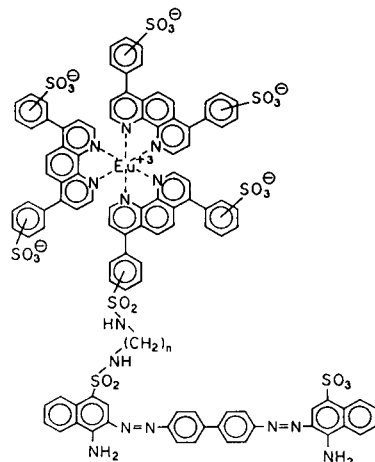
Laser diodes are desirable sources for clinical instrumentation because of their simplicity, reliability and low cost. Also, laser diodes can be electronically modulated which eliminates the need for an external modulator. Designer probes such as those shown in Fig. 6 could have wide applications in analytical chemistry, clinical chemistry and biomedical research.

This work was supported by a grant (DIR-8710401) from the National Science Foundation and grants RR07510 and RR08119 from the National Institutes of Health.



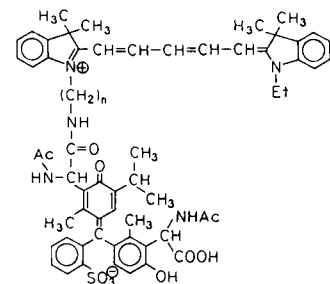
$\lambda_{EX}=525\text{ nm}$, $\lambda_{EM}=550\text{ nm}$, $\tau_0=5.3\text{ ns}$

RHODAMINE 6 G - PHENOL RED



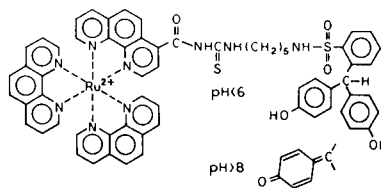
$\lambda_{EX}=365\text{ nm}$, $\lambda_{EM}=615\text{ nm}$, $\tau_0\sim 500\ \mu\text{s}$

Eu^{+3} BATHOCUPROIN - DISULFONYL CONGO RED



$\lambda_{EX}=650\text{ nm}$, $\lambda_{EM}=670\text{ nm}$, $\tau_0\sim 1\text{ ns}$

INDOCYANINE - THYMOL BLUE



$\lambda_{EX}=485\text{ nm}$, $\lambda_{EM}=590\text{ nm}$

$\tau_0=3.25\ \mu\text{s} (\text{N}_2)$, $\tau_0=436\text{ ns} (\text{air})$ in water

TRIS (PHENANTHROLINE) RUTHENIUM - PHENOL RED

Fig. 6. Gedanken pH sensors.

REFERENCES

- 1 O.S. Wolfbeis, *Fiber-Optic Chemical Sensors and Biosensors*, Vol. I, CRC Press, Boca Raton, FL, 1991.
- 2 O.S. Wolfbeis, *Fiber-Optic Chemical Sensors and Biosensors*, Vol. II, CRC Press, Boca Raton, FL, 1991.
- 3 R.W. Murray, R.E. Dessy, W.R. Heineman, J. Janata and W.R. Seitz (Eds.), *Chemical Sensors and Microinstrumentation* (ACS Symposium Series, Vol. 403). American Chemical Society, Washington, DC, 1989.
- 4 L.A. Saari and W.R. Seitz, *Anal. Chem.*, 54 (1982) 821.
- 5 H. Offenbacher, O.S. Wolfbeis and E. Furlinger, *Sensors Actuators*, 9 (1986) 73.
- 6 O.S. Wolfbeis and J.H. Baustert, *J. Heterocycl. Chem.*, 22 (1985) 1215.
- 7 M.-R.S. Fuh, L.W. Burgess, T. Hirschfeld, G.D. Christian and F. Wang, *Analyst*, 112 (1987) 1159.
- 8 N.R. Clement and J.M. Gould, *Biochemistry*, 20 (1981) 1534.
- 9 Z. Zhujun and W.R. Seitz, *Anal. Chim. Acta*, 160 (1984) 47.
- 10 D.M. Jordan and D.R. Walt, *Anal. Chem.*, 59 (1987) 437.
- 11 P. Yuan and D.R. Walt, *Macromolecules*, 23 (1990) 4611.
- 12 P. Yuan and D.R. Walt, *Anal. Chem.*, 59 (1987) 2391.
- 13 G. Gabor and D.R. Walt, *Anal. Chem.*, 63 (1991) 793.
- 14 J.R. Lakowicz, H. Szmecinski and K.W. Berndt, *Proc. SPIE Vol.*, 1648 (1992).
- 15 K.W. Berndt and J.R. Lakowicz, *Anal. Biochem.*, 201 (1992) 319.
- 16 K.W. Berndt, I. Gryczynski and J.R. Lakowicz, *Rev. Sci. Instrum.*, 61 (1990) 1816.
- 17 R.B. Thompson, J.K. Frisoli and J.R. Lakowicz, *Anal. Chem.*, 64 (1992) 2075.
- 18 C. Bojarski and K. Sienicki, *Photochemistry and Photo-physics*, Vol. 1, CRC Press, Boca Raton, FL, 1989, pp. 1–57.
- 19 J.R. Lakowicz, *Principles of Fluorescence Spectroscopy*, Plenum Press, New York, 1983, pp. 81–86.
- 20 E. Gratton and M. Limkeman, *Biophys. J.*, 44 (1983) 665.
- 21 J.R. Lakowicz and B.P. Maliwal, *Biophys. Chem.*, 21 (1985) 61.
- 22 J.R. Lakowicz, G. Laczko and I. Gryczynski, *Rev. Sci. Instrum.*, 57 (1986) 2499.
- 23 C. Bojarski and J. Domsta, *Acta Phys. Hung.*, 30 (1971) 145.
- 24 A. Kawski and H. Szmecinski, *Naturforsch. Teil A*, 37 (1982) 64.
- 25 I. Gryczynski, W. Wicz, M.L. Johnson and J.R. Lakowicz, *Chem. Phys. Lett.*, 145 (1988) 439.
- 26 J.R. Lakowicz, H. Szmecinski, I. Gryczynski and W. Wicz, *J. Phys. Chem.*, 94 (1990) 8413.
- 27 G. Laczko, J.R. Lakowicz, I. Gryczynski, Z. Gryczynski and H. Malak, *Rev. Sci. Instrum.*, 61 (1990) 2331.
- 28 J. Eisinger and J. Flores, *Anal. Biochem.*, 94 (1979) 15.
- 29 R.G. Bennett, *J. Chem. Phys.*, 41 (1964) 3037.
- 30 K.B. Eisenthal and S. Siegel, *J. Chem. Phys.*, 41 (1964) 652.
- 31 T. Lövgren and K. Peterson, in K. Van Dyke and R. Van Dyke (Eds.), *Luminescence Immunoassay and Molecular Applications*, CRC Press, Boca Raton, FL, 1990, pp. 233–253.
- 32 J.R. Bacon and J.N. Demas, *Anal. Chem.*, 59 (1987) 2780.
- 33 E.R. Carraway, J.N. Demas, B.A. DeGaff and J.R. Bacon, *Anal. Chem.*, 63 (1991) 337.

Single drop method for determination of ions using an electrodeless piezoelectric quartz crystal

Toshiaki Nomura, Yukiko Ohno and Yutaka Takaji

Department of Chemistry, Faculty of Science, Shinshu University, Asahi, Matsumoto 390 (Japan)

(Received 5th May 1992; revised manuscript received 29th June 1992)

Abstract

A measuring system was constructed with a horizontal platinum plate, a piezoelectric quartz crystal (quartz plate) on the platinum plate and a platinum wire set vertically above the centre of the platinum plate and at a distance of 0.8 mm from it in the same housing. The platinum plate and the wire were connected to an oscillator. The procedure is as follows: set the quartz plate on the platinum plate, set the recorder to record the frequency, place a single drop of reagent solution containing buffer and electrolyte on the quartz plate, leave for about 7 min to obtain a constant frequency, place a single drop of the ion sample solution containing electrolyte and buffer on the quartz plate along with a platinum wire using a micropipette, read off the frequency shift (ΔF , Hz) between the frequency at the start (when the single drop of the sample solution was placed, F_1) and that at 100 s later (F_2), $\Delta F = F_1 - F_2$, and calculate the concentration of the ion from a calibration graph constructed with a standard solution. Sulphate and potassium ions at levels of 50 μM –0.5 mM can be determined using the barium salt or tetraphenylborate, respectively, with good reproducibility.

Keywords: Piezoelectric sensors; Ion sensors; Potassium; Quartz crystal; Sodium

A piezoelectric quartz crystal (PQC) having evaporated metal electrodes (normal PQC) oscillates in solutions [1] and the frequency shifts with the temperature, density, viscosity and specific conductivity of the solutions and the mass change on the PQC [2]. A quartz plate having no electrodes, but with each side in contact with separate electrolyte solutions and connected via wires immersed in the solutions to the oscillator (electrodeless PQC), oscillates and the frequency changes with changes in the permittivity [3] in addition to changes in the properties of the solutions and the mass change adsorbed on the quartz plate, as with the normal PQC. A quartz plate set between but not in contact with two platinum

plates oscillates in a liquid when the platinum plates are connected to the oscillator (electrode-separated PQC) [4] and the frequency shifts with the permittivity and boiling point [5] in addition to the properties of the liquid and the mass change adsorbed on the quartz plate.

A quartz plate was set on a horizontal platinum plate and a single drop of electrolyte solution was placed on it. A platinum wire inserted in the solution and the platinum plate were connected to the oscillator with wires. The quartz plate oscillated and the frequency shifted with mass change adsorbed on the quartz plate as a precipitate. An ion, e.g., sulphate, which could form a precipitate that would adsorb on the quartz plate, could be determined with this method. A minute amount of cyanide in a single drop of sample solution could also be determined with the normal PQC [6], but because the cyanide

Correspondence to: T. Nomura, Department of Chemistry, Faculty of Science, Shinshu University, Asahi, Matsumoto 390 (Japan).

attacks the platinum, the PQC must be frequently replaced. However, the quartz plate was not consumed with the ion of interest and could be used repeatedly for long periods if washed with solvents to remove the adsorbed precipitate.

EXPERIMENTAL

Apparatus and reagents

A quartz plate (AT cut, $9 \times 9 \text{ mm}^2$) was prepared as follows. The electrodes of a normal PQC, obtained commercially, were dissolved with aqua regia. The quartz plate was rinsed with water, immersed in hot sodium hydroxide solution (2 M) for about 20 min, rinsed with acetone and then water, and dried. PTFE resin was sprayed on the one side of the quartz plate, which was laid horizontally on a filter-paper, and a disc plate (3.3 mm diameter) was placed on its centre. The quartz plate treated with PTFE resin could hold repeatable droplets. The upper cup of a housing (volume ca. 5 ml, Fig. 1) had a hole in it to insert the sample solution. The separate bottom of the housing had a horizontal platinum

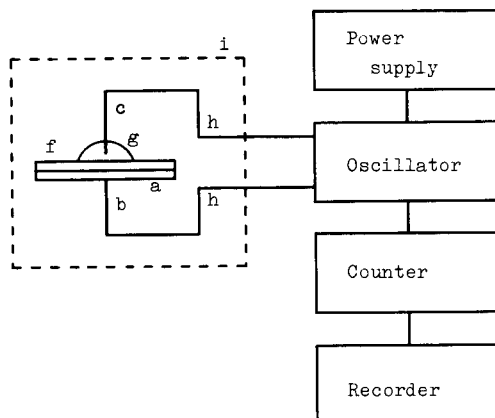


Fig. 2. Schematic diagram of the apparatus. The measuring cell (i) was thermostated with a circulator. a = Platinum plate; b = copper wire; c = platinum wire; f = quartz plate; g = electrolyte solution; h = lead wires.

plate ($9 \times 9 \text{ mm}^2$) soldered on the top of a copper wire (about 1 mm diameter), which was placed on the centre of the bottom vessel, a small pool of water to wet the substrate or to prevent the evaporation of water from solutions, and a platinum wire (1 mm diameter), the tip (about 3 mm) of which was bent downwards in the centre of the house and used to guide the sample solution on to the quartz plate, in addition to the leading wire. The distance between the platinum plate and the top of the platinum wire was adjusted to 0.5–1.0 mm. The platinum wire and the copper wire were insulated from the pool of water and connected to an integrated circuit (IC) oscillator (normal TTL) to which was applied 5.0 V by a power supply (Metronix, 521C). The frequency was recorded with a Toa Denpa FBR-251A recorder via a frequency counter (Advantest, TR-5824) (Fig. 2). The temperature of the housing in a 200-ml beaker was controlled at $25.0 \pm 0.1^\circ\text{C}$ with a circulator (Yamato Kagaku, CTE-22A).

Analytical-reagent grade reagents and deionized water prepared with an autostill (Yamato Kagaku, WG-25) were used. Stock standard solutions (10 mM) of sodium sulphate and potassium chloride were prepared by dissolving 1.420 g of sodium sulphate and 0.746 g of potassium chloride, respectively, in water and diluting to 1 l.

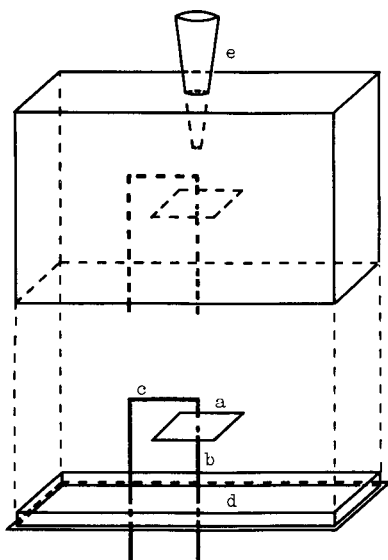


Fig. 1. Measuring cell. a = Platinum plate ($9 \times 9 \text{ mm}^2$); b = copper wire (1 mm diameter); c = platinum wire (1 mm diameter); d = pool of water; e = sample inlet.

These solutions were subsequently diluted as necessary. Electrolyte solution was prepared by mixing equivalent volumes of 0.5 M sodium acetate–acetic acid buffer solution (pH 4.6) and 1 M potassium chloride solution. Barium nitrate solution (10 mM) was prepared from the equivalent volumes of 20 mM barium nitrate solution and the electrolyte solution. Sulphate ion sample solution was prepared from the sulphate solution, 10 ml of the electrolyte solution and water, diluting to 20 ml. Sodium tetraphenylborate solution (10 mM) contained 10 mM sodium tetraphenylborate and 0.5 M sodium chloride. Potassium ion sample solution was prepared from potassium ion solution, 10 ml of sodium chloride solution (1 M) and water, diluting to 20 ml.

Procedure

Set the quartz plate (coated surface upwards) on the platinum plate in the housing with the pool of water, place 5 μ l of barium nitrate (or sodium tetraphenylborate) solution on the quartz plate, put on the cup and record the frequency. When the latter has attained a constant value, drop 5 μ l of the sample solution with a micropipette through the hole in the cup. Read off the frequency shift (ΔF) between the start (F_1) and 100 s later (F_2); $\Delta F = F_1 - F_2$ (Hz). Calculate the concentration of sulphate (or potassium) ion from a calibration graph prepared from the standard solutions using the procedure described above.

Rinse the platinum wire and the quartz plate with EDTA ($\text{Na}_2\text{Y} \cdot \text{H}_2\text{O}$) (or nitric acid for potassium ion) solution (10 mM) to remove the adsorbed precipitate, then with water and acetone.

RESULTS AND DISCUSSION

Sulphate ion reacts with barium ion to form a precipitate of barium sulphate, and adsorption of the precipitate on a piezoelectric quartz crystal changes the frequency. Sulphate ion can therefore be determined from the frequency change [7]. Application of the determination of sulphate by the single drop method is discussed below.

Situation of the precipitating reagent on the quartz plate

Coated as substrate. A 5- μ l volume of barium nitrate solution (10 mM) or barium nitrate solution (10 mM) containing 10 mM sodium chloride as electrolyte was dropped on the quartz plate treated with PTFE resin and dried at 80°C in a vacuum drying oven (Yamato Kagaku, DP22). The coated quartz plate was set in the housing and the cup was put on. The lead wires from the platinum wire and the copper wire were connected to the oscillator and the frequency counter and recorder were switched on. A single drop of the sample solution was placed on the quartz plate with a 5- μ l micropipette through the hole in the cup. The frequency shift between the start and 100 s later was read.

The precision of the determination of sulphate with the coated quartz plate was poor because barium nitrate and sodium chloride crystallized on it with different particle sizes. To achieve good precision the substrate must be coated as a uniform film. The reagent was therefore mixed with a deliquescent compound such as calcium chloride or magnesium chloride. A 5- μ l volume of barium nitrate solution (10 mM) containing 20 mM calcium or magnesium chloride was placed on the quartz plate and dried in an oven at 80°C, followed by the procedure described above. The frequency shift of the quartz plate due to adsorption of the sulphate precipitate was recorded (Fig. 3). The frequency shifts (ΔF) between the start (F_1) and 100 s later (F_2), $\Delta F = F_1 - F_2$, were measured. The reproducibility of the frequency shifts were much better than in the previous procedure. In addition, magnesium chloride as the deliquescent compound was much better than calcium chloride with respect to reproducibility.

Using the same PTFE-treated quartz plate, the calibration graph of frequency shift versus sulphate ion concentration was linear over the range 50–400 μ M for 100 s. The standard deviation was 23.2 Hz (8.8%) for five determinations of 200 μ M sulphate. When five pieces of the quartz plate were sprayed with PTFE resin by the same method and used for the determinations, the standard deviation was 42.6 Hz (10.8%) for 300

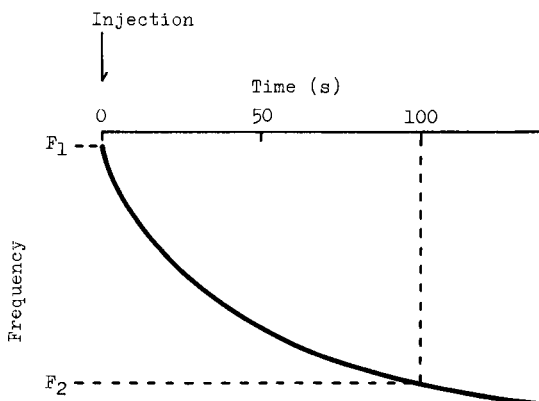


Fig. 3. Frequency shift of the quartz plate treated with the reagent when the sample solution was placed on it.

μM sulphate. It was found that the precipitating species could be determined with a different quartz plate using the same calibration graph.

Injection as reagent solution. A single drop of the reagent solution was placed with a micropipette on the quartz plate, which was set on the platinum plate in the housing. The sulphate sample solution was added to it as described above. The precipitate resulting from the reaction adsorbed on the quartz plate and the frequency shift was measured. A higher sensitivity to the mass of the PQC is obtained nearer to its centre [8]. Hence the solution droplet should be concentrated at the centre of the quartz plate. To obtain a frequency shift caused only by the mass change from adsorption of the precipitate, the properties of the reagent solution should be the same as those of the sample ion solution. Hence the composition of the reagent solution should match that of the sample solution as far as possible.

First, the quartz plate was treated with PTFE resin using a 4.0-mm diameter disc plate. Reagent solution contained barium nitrate (10 mM), sodium acetate–acetic acid buffer (pH 4.6, 0.25 M) and potassium chloride (0.5 M) was placed with a $10\text{-}\mu\text{l}$ micropipette on the quartz plate situated on the platinum plate. The quartz plate oscillated and the cup of the housing was covered. When the frequency had attained a constant value, sulphate sample solution containing sulphate ion, acetate buffer (pH 4.6, 0.25 M) and

potassium chloride (0.5 M) was injected on to the reagent droplet with a $5\text{-}\mu\text{l}$ micropipette through the hole in the cup. The frequency shifted as shown in Fig. 4. The frequency shift caused by the adsorption of the precipitate was measured between the start and 100 s later.

The frequency shifts were proportional to the concentration of sulphate. The standard deviation for five runs using 1.0 mM sulphate solution, however, was 26.4 Hz (13.5%), i.e., the reproducibility was poor, and the determination limit was 0.2 mM. It was considered that the repeatability of the contact area between the quartz plate and the droplets of the reagent solution and then the sample solution was poor, hence the reaction between the species had different speed rates depending on the droplets and the injection conditions.

Second, the quartz plate was treated with PTFE resin using a 3.3-mm diameter disc plate as described above, and the droplets of the barium nitrate and the sulphate ion solutions were each $5\ \mu\text{l}$. The concentration of the barium nitrate in the reagent solution affected the frequency shift, as shown in Fig. 5. The concentration of acetate in the buffer also affected the frequency shift, as shown in Fig. 6, but the reproducibility at 1.5 M decreased.

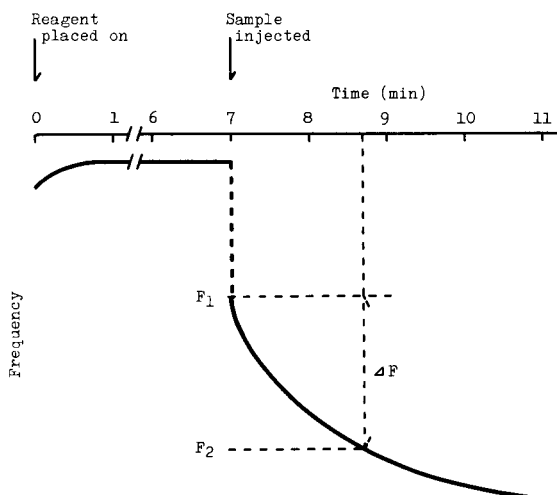


Fig. 4. Frequency shift of the quartz plate on which was placed the reagent solution and then the sample solution.

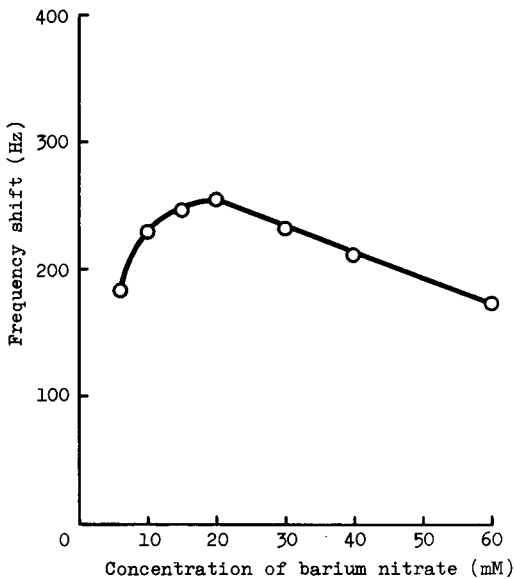


Fig. 5. Dependence of the frequency shift on the concentration of barium nitrate. Sulphate concentration, 1.0 mM; acetate as buffer (pH 4.6), 0.25 M; potassium chloride, 0.5 M; time, 100 s.

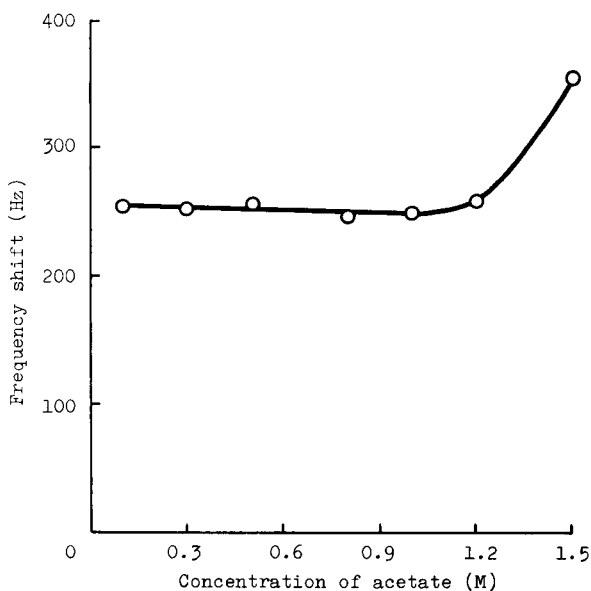


Fig. 6. Dependence of the frequency shift on the concentration of acetate as buffer (pH 4.6). Conditions as in Fig. 5 except the concentration of barium nitrate was 20 mM.

The concentrations of these chemicals in the solutions were then used as described above. The calibration graph of the frequency shifts versus sulphate concentration ($r = 0.999$, $n = 6$) over the range 0–1.0 mM sulphate had better linearity than before. The frequency shift for the blank solution (25 Hz) is due to the difference in the physical properties of the solution before and after the addition of the sample solution. The shift for 1.0 mM sulphate was ca. 250 Hz. The standard deviations for five runs using 0.5 mM sulfate solution were 4.6 Hz (5.3%) for 50 s and 7.6 Hz (6.4%) for 100 s when the same quartz plate was used, and 6.8 Hz (6.6%) for 50 s and 9.4 Hz (6.8%) for 100 s when five different quartz plates were used. The precision of this method was better than that of the coating method described above. The sensitivity of the latter, however, was several times that of the former. Alternatively, a single drop of the sample solution was placed on the quartz plate and then the reagent solution was dropped on to it. The sulphate ion concentrations could be determined with almost the same precision as in the above method using the same quartz plate.

Application to the determination of potassium ion

The single drop method for the determination of a minute amount of precipitating species was applied to potassium ion using tetraphenylborate [9].

Drop 5 μ l of sodium tetraphenylborate solution (10 mM) containing 0.1 M sodium chloride on to the PTFE-treated quartz plate, place it in the housing and leave it for 7 min. Inject 5 μ l of potassium ion sample solution containing 0.1 M sodium chloride. The calibration graph of frequency shift versus potassium ion concentration was linear over the range 50–500 μ M.

The results confirmed that the single drop method could be used for the determination of precipitating species.

Conclusion

An electrodeless PQC was constructed from a platinum plate, a quartz plate and electrolyte solution (sample) and oscillated with mass

changes on the quartz plate, and ions could therefore be determined. This quartz plate with no electrodes could be used as a disposable type because the quartz plate is less expensive than the normal PQC and can be made much smaller for smaller amounts of sample solution. In addition, a higher frequency quartz plate could be used for trace analysis.

REFERENCES

- 1 T. Nomura and A. Minemura, *Nippon Kagaku Kaishi*, 1980 (1980) 1621.
- 2 T. Nomura, M. Watanabe and T.S. West, *Anal. Chim. Acta*, 175 (1985) 107.
- 3 T. Nomura, F. Tanaka, T. Yamada and H. Itoh, *Anal. Chim. Acta*, 243 (1991) 273.
- 4 T. Nomura, T. Yanagihara and T. Mitsui, *Anal. Chim. Acta*, 248 (1991) 329.
- 5 T. Nomura and T. Mitsui, unpublished results.
- 6 T. Nomura, *Anal. Chim. Acta*, 124 (1981) 81.
- 7 T. Nomura, *Bunseki Kagaku*, 36 (1987) 93.
- 8 G. Sauerbrey, *Z. Phys.*, 155 (1959) 206.
- 9 K. Ueno, M. Saito and K. Tamaoki, *Bunseki Kagaku*, 17 (1968) 1548.

Preconcentration of palladium, platinum and rhodium by on-line sorbent extraction for graphite furnace atomic absorption spectrometry and inductively coupled plasma atomic emission spectrometry

M.L. Lee and G. Tölg

Institut für Spektrochemie und angewandte Spektroskopie (ISAS), Bunsen-Kirchhoff-Strasse 11, D(W)-4600 Dortmund 1; and Max-Planck-Institut für Metallforschung, Stuttgart, Laboratorium für Reinststoffanalytik (LRA), Bunsen-Kirchhoff-Strasse 13, D(W)-4600 Dortmund 1 (Germany)

E. Beinrohr¹ and P. Tschöpel

Max-Planck-Institut für Metallforschung, Stuttgart, Laboratorium für Reinststoffanalytik (LRA), Bunsen-Kirchhoff-Strasse 13, D(W)-4600 Dortmund (Germany)

(Received 18th May 1992)

Abstract

A flow system combined with a segmentation technique was used to develop an efficient on-line sorbent extraction preconcentration system for palladium, platinum and rhodium for graphite furnace atomic absorption spectrometry (GFAAS) and inductively coupled plasma atomic emission spectrometry (ICP-AES). The investigated metals were preconcentrated as their bis(carboxymethyl)dithiocarbamate (CMDTC) chelates on a microcolumn packed with XAD-4 after the off-line addition of solid CMDTC to the sample solution containing SnCl_2 and hydrochloric acid. The sample, rinsing and eluent solutions were segmented by air to prevent dispersion. The eluate was collected on-line in a PTFE loop and was forced either into the graphite tube by nitrogen or into the ICP by using a carrier solution. The time duration of one preconcentration cycle was about 10 min. The influence of the acidity of the synthetic sample solution, the concentrations of the complexing reagent and reducing agent, the flow-rate for preconcentration, the efficiency of the desorption and the influence of various matrices were also investigated. The detection limits (3σ) were 0.03, 0.1 and 0.01 ng/ml for Pd, Pt and Rh, respectively, using GFAAS detection. The method was applied for the analysis of polluted biological materials.

Keywords: Atomic absorption spectrometry; Atomic emission spectrometry; Flow system; Inductively coupled plasma spectrometry; Biological samples; Extraction; Palladium; Platinum; Preconcentration; Rhodium

The main advantage of preconcentration procedures is the possibility of determining lower analyte concentrations and avoiding matrix ef-

fects by effective separation of the analyte from interfering matrix components. In this respect flow systems combined with liquid-liquid extraction, ion exchange, sorbent extraction [1–5] and electrochemical deposition [6,7] are of growing interest.

The determination of very low contents of the platinum metals (PM) in environmental samples, arising mainly from the emission of Pt from cata-

Correspondence to: M.L. Lee, Institut für Spektrochemie und angewandte Spektroskopie (ISAS), Bunsen-Kirchhoff-Strasse 11, D(W)-4600 Dortmund 1 (Germany).

¹ On leave from Department of Analytical Chemistry, Slovak Technical University, CS-812 37 Bratislava (Czechoslovakia).

lysts in motor car catalytic converters usually suffers from inadequacies of the analytical methods, e.g., of direct graphite furnace atomic absorption spectrometric (GFAAS) determination [8,9]. The use of direct instrumental methods is also restricted owing to interferences caused by matrix elements and the lack of standard reference materials for the extreme trace concentration range [10]. These difficulties can only be overcome by combination of suitable decomposition, separation, preconcentration and determination steps [11–14].

Recently, the separation and preconcentration of trace elements of PM using ion-exchange columns [15,16] or sorbent extraction [17] has effectively opened up the possibility of on-line procedures. However, common anion-exchange resins do not adsorb negatively charged PM-chloro complexes selectively and, in addition, some of the complexes are adsorbed too strongly to be eluted from the polymeric phase. This drawback also applies to some immobilized chelating ion-exchange resins, although they exert a better selectivity. On the other hand, sorbent extraction based on the reversed-phase adsorption of complexed metals on a hydrophobic polymeric phase has shown promise for overcoming these limitations. An enhancement in selectivity may be expected owing to the different tendency towards complex formation. Moreover, complete and rapid elution can be expected because the complexes are not bound chemically to the sorbent. A problem with these adsorption methods is the low solubility in water of the metal complex, which possibly forms precipitates and may cause clogging of the column. The use of a chelating agent that forms a water-soluble complex could solve this problem.

Some on-line separation or preconcentration procedures for heavy metals from solutions of alkali and alkaline earth elements have recently been investigated by making use of water-soluble complexes, e.g., with bis(carboxymethyl)dithiocarbamate (CMDTC) [18], bis(2-hydroxyethyl)dithiocarbamate (HEDTC) [19], *N*-methylfurohydroxamate (*N*-MFHA) [20] and *N*-(dithiocarbonyl)sarcosine (DTCS) ligands [21,22]. For example, the CMDTC chelates can be adsorbed on a

polystyrene-divinylbenzene resin (XAD-4) in a column from acidic medium and eluted with ammonia solution. This chelating agent can also be utilized for an effective complexing of some PM, e.g., Pd, Pt and Rh, owing to its dithio functional group [23,24].

Unfortunately, the application of a flow system combined with a column preconcentration technique to GFAAS may be hindered by the non-flow-through nature of the graphite furnace detector [3]. This limitation can be overcome by using a segmentation technique with the flow system to elute the adsorbed complexes in a definite volume of eluent solution and transfer it by means of gas pressure into the furnace [5,25–27]. This segmentation technique is useful not only for a discrete non-flow-through detector (GFAAS) but also for a continuous flow-through detector [e.g., inductively coupled plasma atomic emission spectrometric (ICP-AES)] to depress dispersion of the sample zone when transferring it to the detector.

This paper describes an on-line sorbent extraction preconcentration system with a segmentation technique for the determination of Pd, Pt and Rh by accumulation of their CMDTC chelates on XAD-4 resin for GFAAS and ICP-AES measurement.

EXPERIMENTAL

Reagents

The reagents used were of analytical-reagent or Suprapur grade (Merck, Darmstadt, or Johnson Matthey-Alfa Products, Karlsruhe). Dilute noble metal and other metal solutions were all freshly prepared with doubly distilled water from stock standard solutions (Aldrich, Milwaukee, WI, and Titrisol, Merck, 1000 $\mu\text{g ml}^{-1}$). HNO_3 and HCl were purified by sub-boiling distillation and stored in quartz vessels.

The polystyrene-divinylbenzene resin used was Amberlite XAD-4 with 0.3–0.9 mm particle size (Merck). The resin was purified by Soxhlet extraction with methanol for 8 h, then dried, ground and sieved [18–22]. The 50–100- μm fraction was collected and dry packed in the column.

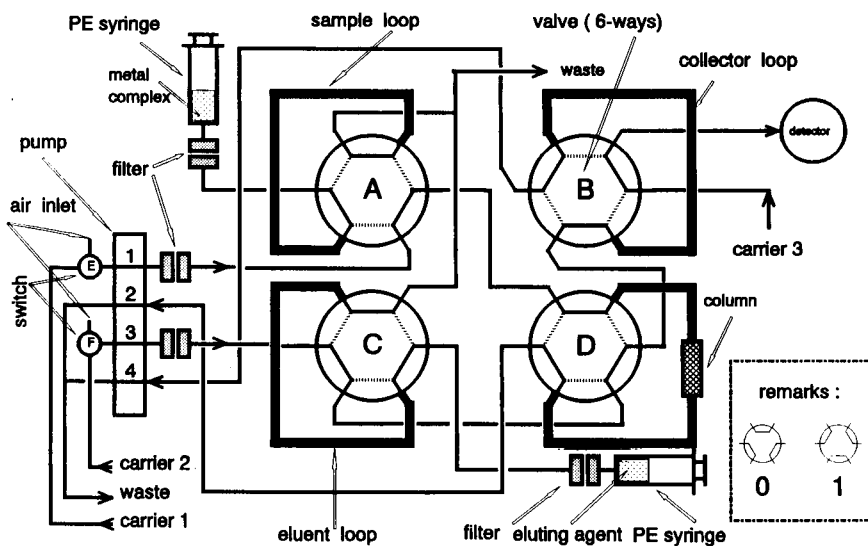


Fig. 1. Flow system manifold for sorbent extraction preconcentration for GFAAS or ICP-AES. Carrier 1, 1 mol l^{-1} HCl; carrier 2, methanol containing 1 mol l^{-1} HNO_3 ; carrier 3, nitrogen (for GFAAS) or 0.5 mol l^{-1} ammonia solution (for ICP-AES). A–D, six-way valves; E and F, three-way switches; 1–4, pump channels.

The procedure for synthesizing the CMDTC reagent was based on that described by Plantz et al. [18].

The eluent solutions were 5 and 0.5 mol l^{-1} NH_4OH for GFAAS and ICP-AES, respectively. To prevent hydrolysis of metals, 1.2% (w/v) CMDTC was also present in the eluent solution.

Tin(II) chloride solution [25% (w/v) SnCl_2] was prepared by dissolving 0.3 g of $\text{SnCl}_2 \cdot y2\text{H}_2\text{O}$ in 0.5 ml of HCl and subsequently diluting to 1 ml

with water. The solution was freshly prepared each day.

Potassium iodide solution containing ascorbic acid was prepared by dissolving 3 g of KI and 0.3 g of ascorbic acid in water and diluting to 10 ml .

Ascorbic acid solution was prepared by dissolving 0.3 g of ascorbic acid in water and diluting to 1 ml .

For liquid–liquid extraction, a dithizone stock solution was prepared according to [28]. The

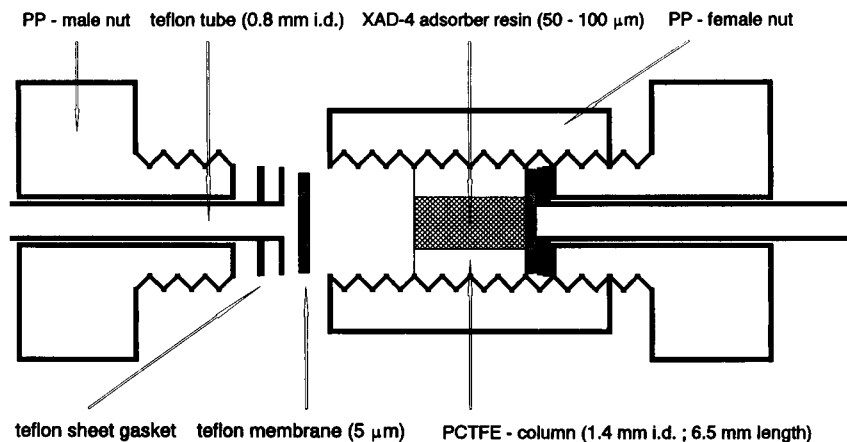


Fig. 2. Design of the microcolumn for the on-line preconcentration system.

dithizone reagent solution was made up by diluting 0.7 ml of the stock solution to 50 ml with isobutyl methyl ketone [8].

Flow system

The on-line sorbent extraction preconcentration system (Fig. 1) consisted of a four-channel peristaltic pump (Minipuls 2, Gilson, Villiers-le-bel, France), four PTFE micro-filters with 5- μm pore size PTFE membranes of 1.4 cm² cross-section, two three-way solvent switches (Sartorius, Göttingen), four six-way PTFE rotary valves (Latek, Eppelheim) and a laboratory-made adsorption column with a total volume of 10 μl . The column (6.5 mm \times 1.4 mm i.d.) (Fig. 2) was made of polychlorotrifluorethylene (PCTFE) and was packed with 50–100- μm XAD-4. The two end parts of the column were sealed with 5- μm PTFE membranes.

Poly(vinyl chloride) pump tubing of 1 mm i.d. was used for all aqueous solutions, but methanol was pumped using solvent-resistant pump tubing of 1 mm i.d. (Abimed, Langfeld, Germany). PTFE tubing (Latek) with of i.d. 0.8 mm was used for all connections. Sample and eluent solutions were filled into the PTFE loops with polyethylene (PE) syringes.

The PTFE micro-filters were set between the top of PE syringes and the entrance part of the loops to remove fine particles from the sample, eluent or carrier solutions which could cause the plugging of the column.

The volume of the sample loop was chosen as 0.60, 1.09, 2.47 or 4.60 ml, depending on the requirements. The volume of the eluent loop was 53.4 μl for GFAAS and 80.9 μl for ICP-AES. All these volumes were calibrated by weighing the water content in the loop and corrected for the density. The PTFE collector was made from PTFE tubing (0.8 mm i.d.) with a volume of about 100 μl .

Instruments

The atomic absorption spectrometer was a Varian SpectrAA 300 with a Zeeman background-correction system. Varian hollow-cathode lamps were used; the wavelengths and lamp currents used were Pd 247.6 nm (5 mA), Pt 265.9 nm

TABLE 1

Temperature programme for the graphite furnace

Step	Time (s)		Temperature (°C)	Gas flow-rate (l min ⁻¹)
	Ramp	Hold		
1	5	0	70	3
2	40	0	95	3
3	20	0	100	3
4	40	0	120	3
5	60	0	160	3
6	40	2	510	3
7	5	3.5	1000 ^b	3
8	0	1.3 ^a	2700 ^c	0
9	0	2	2700 ^c	3

^a For Pt 1.3, for Pd 1.2, for Rh 1.0. ^b For Rh 900. ^c For Pt 2700, for Pd 2500, for Rh 2850.

(8 mA) and Rh 343.5 nm (5 mA). Temperature programmes for the graphite furnace are given in Table 1.

The inductively coupled plasma atomic emission spectrometer used was a Labtest PLS 2000 equipped with a laboratory-made monochromator (Institute of Spectrochemistry and Applied Spectroscopy, Dortmund). A Babington-type nebulizer (G.M.K.-Labtest, Ratingen) was used. The operating conditions and the wavelengths used are given in Table 2.

The UV-visible spectrometer used was a Zeiss Spektralphotometer PMQ II with 1-cm quartz cells.

The high-pressure asher used was from Berghof (Eningen) with a 250-ml PTFE vessel.

TABLE 2

Operating conditions for ICP-AES

Coolant argon flow-rate	20 l min ⁻¹
Sample argon flow-rate	0.5 l min ⁻¹
R.f. incident power	1.2 kW
R.f. reflected power	≤ 50 W
Nebulizer	GMK
Observation height above load coil	14 mm
Wavelengths (nm) used	Pd 229.651, Pt 214.423, Rh 249.077, Ru 245.657, Au 242.795, Co 238.892, Cu 324.754, Ag 328.068

Preparation of synthetic sample solutions and biological materials

Synthetic sample solution containing HCl. To 5 ml of synthetic sample solution in a quartz tube containing 1 mol l^{-1} HCl and $1\text{--}5 \text{ ng ml}^{-1}$ (for GFAAS) or $1\text{--}5 \text{ } \mu\text{g ml}^{-1}$ (for ICP–AES) of the metal ions under study, $50 \text{ } \mu\text{l}$ of SnCl_2 solution were added, followed after 10 min by 60 mg of CMDTC reagent. After waiting for about 60 min for completion of the reaction, one part (0.5–5 ml) of this solution was taken for preconcentration.

Synthetic sample solution containing H_2SO_4 . To 5 ml of synthetic sample solution in a quartz tube containing 1 mol l^{-1} H_2SO_4 , $50 \text{ } \mu\text{l}$ of KI solution containing ascorbic acid were added, followed after 10 min by 60 mg of CMDTC reagent. After waiting for about 120 min, one part (0.5–5 ml) of the solution was taken for preconcentration.

Samples of biological materials. The sample [e.g., 1 g for beans (BH186H) or 0.2 g for tobacco (TH135B) [29], well homogenized, dried substance] was decomposed in a high-pressure asher for 4 h with addition of 10 ml of HNO_3 and 5 ml of HCl in a 250-ml PTFE vessel. However, PTFE vessels are not suitable for extremely low concentrations [14]. After completing the decomposition, the solution was placed under an infrared lamp to remove most of the HNO_3 by simultaneous addition of small portions of HCl. After cooling, the remainder of the solution was transferred into a quartz tube and made up with 1 mol l^{-1} HCl to 25 ml for beans or 50 ml for tobacco sample. To 5 ml of this solution SnCl_2 and

CMDTC reagent were added, following the procedures described above.

Liquid–liquid extraction

To 5 ml of synthetic sample solution $100 \text{ } \mu\text{l}$ of SnCl_2 solution were added. After 10 min, the solution was shaken with 1 ml of dithizone reagent solution for 2 min. Pd, Pt and Rh were determined directly in the organic phase by GFAAS.

Flow-through preconcentration

HCl (1 mol l^{-1}) was used as carrier 1 and methanol containing 1 mol l^{-1} HNO_3 as carrier 2. There were two positions (1 and 0; see Fig. 1) for operation of the valves A, B, C and D and also two positions (1 and 0; 1 = carrier, 0 = air flow) for the solvent switches E and F. The four channels (1, 2, 3 and 4) of the peristaltic pump can be set “on” or “off” individually. The pumping rate can be set manually depending on the requirements. The sequence of the operation is given in Table 3.

Sequence 1. For filling the sample and eluent solutions into the sample and eluent loops by PE syringes, respectively, valve B was set for collection of eluate and valve D for adsorption of complexes. The solvent switches E and F were set at the position for carrier 1 and carrier 2, respectively.

Sequence 2. The valve A was turned to the position for sample loading, which was pushed by carrier 1 through the column at a flow-rate of 0.5 ml min^{-1} . To avoid dispersion, a small section of air was present between sample solution and carrier 1. After completing the preconcentration,

TABLE 3

Sequence of operations for on-line sorbent extraction

No.	Valve				Switch		Pump channel			
	A	B	C	D	E	F	1	2	3	4
1	0	1	0	0	1	1	Off	Off	Off	Off
2	1	1	0	0	1	1	On	On	Off	Off
3	1	1	1	1	1	1	Off	Off	On	On
4	1	0	1	1	1	1	Off	Off	On	On
5	1	1	1	0	1	0	On	On	Off	On
6	1	1	1	1	0	0	Off	On	Off	Off

the column and the sample loop were further washed with carrier 1 for about 1 min to remove the residues of the matrix.

Sequence 3. Valves C and D were simultaneously turned for transportation of the eluent solution and desorption of the complexes. The eluent solution was pushed by carrier 2 counter directionally through the column at a flow-rate of 0.2 ml min^{-1} . A small section of air was placed between eluent solution and carrier 2 to locate the eluate and to prevent its dispersion. The desorbed complexes were then transferred into a small PTFE collector loop. After the desorption process the column can be regenerated by a further 1-min rinse with carrier 2.

Sequence 4. Valve B had to be turned to inject the eluate into the detector before the eluate was passing from the collector.

Sequence 5. The column can be rinsed with carrier 1 for further 1 min in this step and carrier 2 in the loops can be removed by air flowing through switch F. The air in these loops was used for segmentation in the next cycle.

Sequence 6. Pump channel 2 was set at a flow-rate of 2 ml min^{-1} . The carrier 1 in the loops can be removed by air flowing through switch E and air was used for segmentation in the next cycle.

Sequence 7. The valves, switches and pump channels were set to the original positions and the system was ready for the next run.

Owing to the different composition of the sample matrix, the standard addition technique was used for calibration. Otherwise the recovery test was made by comparing the signal area of the sample solution obtained by using the flow-through system with that of a standard solution which was prepared from eluent solution and

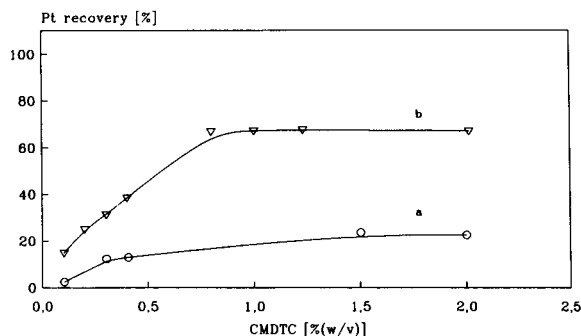


Fig. 3. Effect of CMDTC concentration on the recovery, measured with ICP-AES. $1 \mu\text{g}$ of Pt(IV), 0.60 ml of synthetic sample solution. (a) $1 \text{ mol l}^{-1} \text{ HCl}$; (b) $1 \text{ mol l}^{-1} \text{ H}_2\text{SO}_4$.

introduced directly into the detector by the following process (Table 4).

Sequence 1. The standard solution was filled into eluent loop.

Sequence 2. The standard solution was drawn into the PTFE collector loop at a flow rate of 0.3 ml min^{-1} .

Sequence 3. The standard solution was transferred into the detector.

RESULTS AND DISCUSSION

Effect of CMDTC concentration on the recovery of Pt(IV)

The effect of CMDTC concentration on the recovery of Pt(IV) was investigated in the absence of the reducing agent (e.g., SnCl_2 or KI) by using the ICP spectrometer as a detector. The results are shown in Fig. 3. With a concentration of 1.2% (w/v) of CMDTC the recovery from $1 \text{ mol l}^{-1} \text{ HCl}$ was only ca. 20% (a) and ca. 70% from $1 \text{ mol l}^{-1} \text{ H}_2\text{SO}_4$ (b). The insufficient recovery with

TABLE 4

Sequence of operations for the transportation of standard solutions for direct determination (valve A, switch E, pump channel 1 and 2 are not critical in this case)

No.	Valve				Switch		Pump channel			
	A	B	C	D	E	F	1	2	3	4
1		1	0	0		0			Off	On
2		1	1	0		0			Off	On
3		0	1	0		0			Off	On

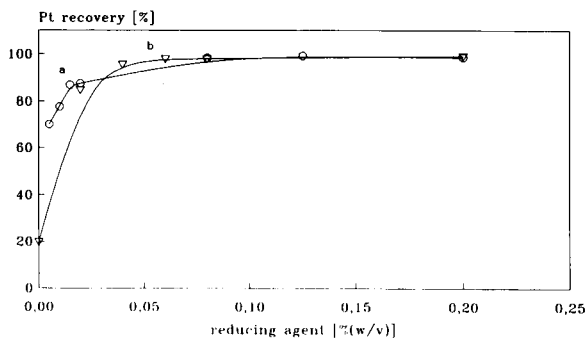


Fig. 4. Effect of reducing agent on the Pt(IV) recovery, measured with ICP-AES. 1 μg of Pt(IV), 0.60 ml of synthetic sample solution containing 1.2% (w/v) CMDTC. (a) With KI in 1 mol l^{-1} H_2SO_4 ; (b) with SnCl_2 in 1 mol l^{-1} HCl.

HCl solution was probably due to the formation of the kinetically inert Pt(IV)–chloro complex in HCl [30]. These results indicated that at least 1% (w/v) CMDTC should be added to the sample solution to ensure a high degree of complexation; 1.2% (w/v) CMDTC was used throughout subsequent experiments.

Effect of reducing agent

The inert Pt(IV) species can be reduced to the more labile Pt(II) form with SnCl_2 in HCl [31] or KI in H_2SO_4 [32] solutions prior to the addition of CMDTC complexing reagent. The results are depicted in Fig. 4. Complete retention of 1 μg of Pt(IV) from 0.6 ml of sample solution was observed at a concentration of the reducing agents above 0.1% using 1.2% (w/v) CMDTC with the ICP spectrometer as a detector. On the other hand, Rh(III) can only be accumulated in the presence of SnCl_2 from HCl solutions. As Pd(II) was more labile than Pt(IV) and Rh(III) [31], the Pd chelate can be formed and concentrated completely in the absence of SnCl_2 or KI. To ensure the complete reduction of Pt(IV) and Rh(III), a concentration of 0.25% (w/v) of the reducing agents was chosen. In the case of KI as reducing agent, 0.03% (w/v) of ascorbic acid was added to the sample solutions to reduce iodine, which was formed when reducing Pt(IV) and which could be also adsorbed on the XAD-4 resin.

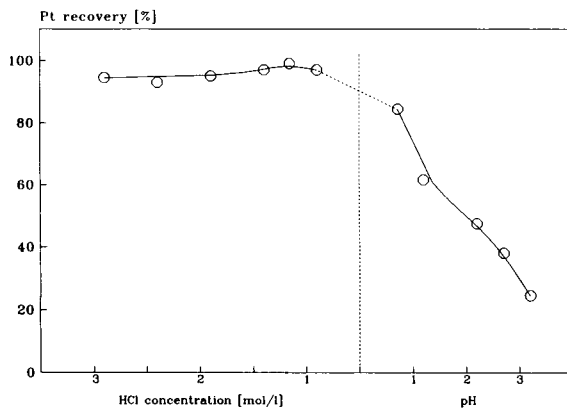


Fig. 5. Effect of acidity of the synthetic sample solution on the recovery, measured with ICP-AES. 1 μg of Pt(IV), 0.60 ml of synthetic sample solution containing 0.25% (w/v) of SnCl_2 , 1.2% (w/v) of CMDTC and corresponding HCl.

Effect of acidity of synthetic sample solution on the recovery of metal ions

The recovery of 1 μg of Pt(IV) was monitored at various HCl concentrations by using the ICP spectrometer as a detector. The results in Fig. 5 show that complete retention occurred in 1–3 mol l^{-1} HCl, whereas at pH 1 and 3 the recoveries were 70 and 30%, respectively. The complete retention in the more acidic solutions has been explained by the protonation of the carboxyl groups of the metal complex in acidic solution and the formation of a neutral metal complex

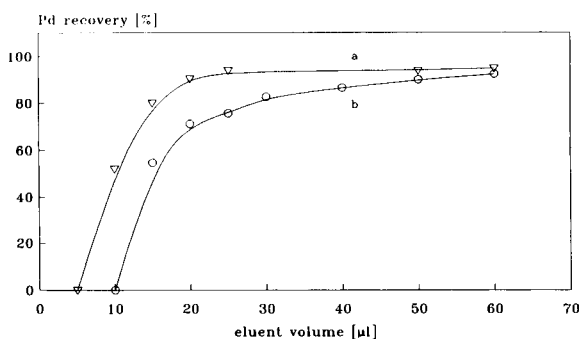


Fig. 6. Effect of volume of eluent solution on the recovery of Pd, measured with GFAAS. (a) 5 mol l^{-1} ammonia solution containing 1.2% (w/v) CMDTC; (b) 0.5 mol l^{-1} ammonia solution containing 1.2% (w/v) CMDTC. 1 ng of Pd, 0.60 ml of 1 mol l^{-1} H_2SO_4 synthetic sample solution containing 1.2% (w/v) CMDTC.

[18,21], which can then be adsorbed by the non-polar XAD-4 resin. By increasing the pH, the carboxyl groups of the metal complexes were charged and therefore removed from the resin. The same adsorption property of the complexes of Pd and Rh was observed in this study.

Desorption properties

Owing to the easy deprotonation of the CMDTC metal complexes in basic solution, it was possible to desorb the adsorbed metal complexes from XAD-4 resin by using a basic eluent, e.g., ammonia solution [18]. To avoid the possibility of dissociation of the chelates during the elution procedure, 1.2% (w/v) CMDTC was also present in the eluent solution. The desorption efficiency was investigated for the example of Pd with the GFAAS detector by using different volumes of the eluent solution (5 or 0.5 mol l⁻¹ ammonia) and the results are depicted in Fig. 6. By utilizing 5 mol l⁻¹ ammonia as eluent solution (a), complete recovery ($\geq 95\%$) can be achieved by using 25 μ l, whereas when using 0.5 mol l⁻¹ ammonia as eluent solution (b), a 93% recovery can only be reached with the use of more than 60 μ l of the eluent solution. Generally, 5 mol l⁻¹ ammonia resulted in better desorption than 0.5 mol l⁻¹.

For the GFAAS measurement, 5 mol l⁻¹ ammonia containing 1.2% (w/v) CMDTC can be applied as the elution solution. However, in ICP-AES measurements, instability of the plasma can be observed after introducing 5 mol l⁻¹ ammonia solution into the plasma source. By using 0.5 instead of 5 mol l⁻¹ ammonia solution as eluent solution, this drawback can be largely eliminated. Hence 53.4 μ l of elution solution containing 5 mol l⁻¹ of ammonia and 1.2% (w/v) CMDTC was chosen for GFAAS measurements and 80.9 μ l of elution solution containing 0.5 mol l⁻¹ ammonia and 1.2% (w/v) CMDTC for ICP-AES measurements.

On account of the hydrophobic properties of the XAD-4 resin, newly packed columns had to be rinsed with methanol, ethanol or acetone before use. After the elution procedure, the column was rinsed with methanol again (sequence 3). HNO₃ (1 mol l⁻¹) was present in the methanol to facilitate the rinsing process. The lifetime for a

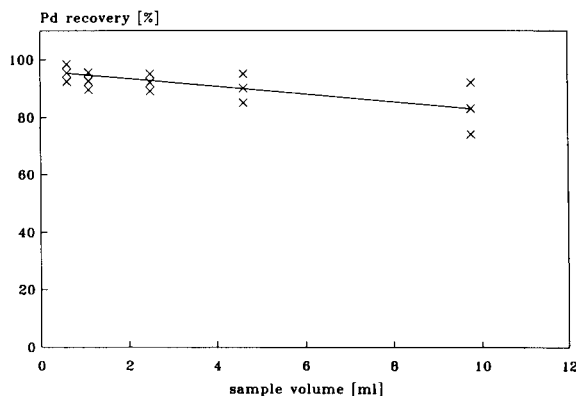


Fig. 7. Effect of sample volume on the recovery of Pd, measured with GFAAS ($n = 4$). 1 ng of Pd, 1 mol l⁻¹ H₂SO₄ synthetic sample solution containing 1.2% (w/v) CMDTC.

such treated column was more than 1 month of daily routine use.

Effect of sample volume and flow-rate

The recoveries of 1 ng of Pd from different sample volumes were tested with GFAAS detection and are shown in Fig. 7. Generally, the recoveries decreased slowly with increasing sample volume. Nevertheless, the yield for accumulation was still satisfactory if the sample volume was lower than 5 ml.

The sample flow-rate in this study was limited first by the back-pressure in the column packed with a fine resin with a particle size of 50–100 μ m and second by the recovery required. The recovery decreased slowly with increasing flow-rate (Fig. 8). The effect of the flow-rate on the adsorption recovery of higher analyte amounts (b) was less significant than that for lower analyte amounts (a). A flow-rate of 0.5 ml min⁻¹ was chosen as a compromise.

Stability of the complexes

Dithiocarbamates decompose rapidly in acidified solutions to carbon disulphide and protonated amine [33]. The rate of decomposition of CMDTC reagent in acidic solutions was studied spectrophotometrically by measuring the decrease in the absorbance of the reagent at 280 nm, as shown in Fig. 9. The half-life of the CMDTC was about 8 min at pH 6 and only about

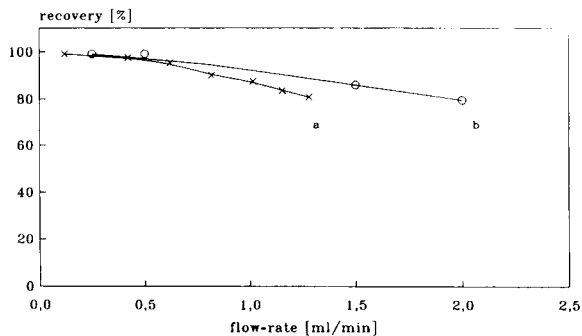


Fig. 8. Effect of flow-rate on recovery. (a) 1 ng of Pd, 0.6 ml of $1 \text{ mol l}^{-1} \text{ H}_2\text{SO}_4$ synthetic sample solution containing 0.3% (w/v) KI, 0.03% (w/v) ascorbic acid and 1.2% (w/v) CMDTC, measured with GFAAS; (b) $1 \mu\text{g}$ Pt(IV) from 2.47 ml, measured with ICP-AES.

1.4 min at pH 4. In contrast, the investigated metal complexes were relatively stable in acidic solutions (Figs. 10 and 11). By using SnCl_2 as reducing agent, the recoveries of Pd, Pt and Rh from sample solutions containing $1 \text{ mol l}^{-1} \text{ HCl}$ (Fig. 10) at first increased with time (time interval between the addition of CMDTC to sample solution and the desorption of complexes from the column), and reached a constant value of about 100% after 60 min which was maintained over 360 min. In contrast, after reaching the maximum value of about 100%, the recovery of Cu decreased dramatically with time, and after 240 min it had dropped to about 20%. This was probably caused by the lower stability of the Cu complex

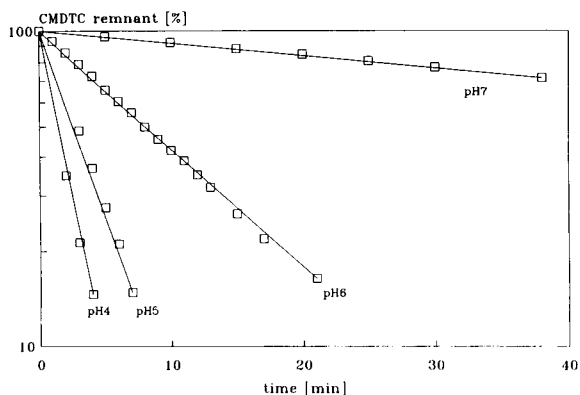


Fig. 9. Effect of pH on the decomposition rate of CMDTC reagent.

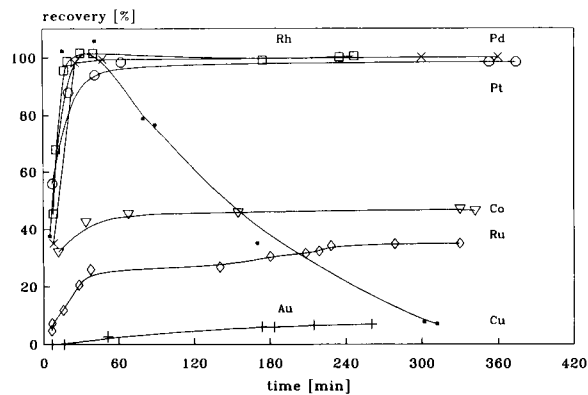


Fig. 10. Effect of time on the recoveries of metal ions, measured with ICP-AES. $1 \mu\text{g}$ of corresponding metal ion, 0.60 ml of $1 \text{ mol l}^{-1} \text{ HCl}$ synthetic sample solution containing 0.25% (w/v) SnCl_2 and 1.2% (w/v) of CMDTC.

with CMDTC than the Pd, Pt and Rh complexes under these conditions. On the other hand, the recoveries of Ru and Co were about 35–45%, which is insufficient for the preconcentration. Moreover, Fe, Ti, V, Al, Zn, Ni, Cd, Ag, Os and Ir were found not to be adsorbed under these conditions.

If KI was used as the reducing agent, the recoveries of Pd and Pt from $1 \text{ mol l}^{-1} \text{ H}_2\text{SO}_4$ (Fig. 11) were also found to increase with time. After 120 min they had reached a constant value of about 100%, which was maintained up to 360

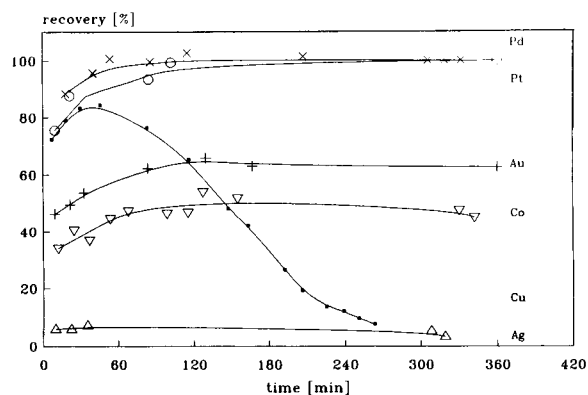


Fig. 11. Effect of the time on the recoveries of metal ions, measured with ICP-AES. $1 \mu\text{g}$ of corresponding metal ion, 0.60 ml of $1 \text{ mol l}^{-1} \text{ H}_2\text{SO}_4$ synthetic sample solution containing 0.3% (w/v) KI, 0.03% (w/v) ascorbic acid and 1.2% (w/v) CMDTC.

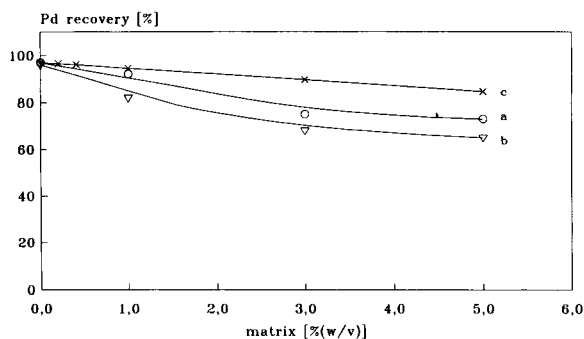


Fig. 12. Effect of matrix compounds on the recovery, measured with GFAAS. 2 ng of Pd, 0.60 ml of 1 mol l⁻¹ HCl synthetic sample solution containing 1.2% (w/v) CMDTC. (a) NH₄Cl; (b) Al; (c) Fe. For Fe, ascorbic acid solution (concentration twice that of Fe) was added.

min. The behaviour of Cu in this system was similar to that in solutions containing HCl. The recoveries of Co and Au were about 45–60% and that of Ag was about 5%. Fe, Ti, Al, Zn, Ni, Cd, Rh, Ru, Os and Ir were not adsorbed in this system.

Matrix effects

Interfering matrices can easily be removed by passing the sample solution through the column while the investigated metal ions remain on the non-polar resin bed as their CMDTC chelates. As an example, Fig. 12a shows the effect of the NH₄Cl matrix on the recovery of 2 ng of Pd using GFAAS detection. The recovery decreased with increasing concentration of the matrix, and at an NH₄Cl concentration of 5% (w/v) the recovery was about 80%. However, this effect may be overcome by the standard addition method.

The matrix effect of Al is shown in Fig. 12(b); at a concentration of 3% (w/v) Al the recovery decreased to about 70%.

The recovery of Pd was significantly affected by the Fe(III) concentration, but this drawback could easily be overcome by reducing Fe(III) to Fe(II) by the addition of ascorbic acid solution prior to the addition of CMDTC to the sample solution. The necessary amount of ascorbic acid was found to be twice that of Fe(III). The influence of the Fe(III) concentration on the recovery of Pd under these conditions is illustrated in Fig. 12c. At a concentration of 5% (w/v) Fe(III), the

recovery of 2 ng of Pd was about 85%. The effect of Fe(III) on the recovery of Pt was also tested by this method. Prior to the addition of SnCl₂, which was necessary to reduce Pt(IV) to Pt(II), ascorbic acid was added. Similar results to those for Pd were obtained.

Cu(II) ions significantly influenced the Pd recovery. The maximum tolerable concentration of Cu(II) in the sample solution was only about 200 μg ml⁻¹.

Reproducibility, accuracy and limits of detection

The analytical performance of the proposed method is illustrated by the results from GFAAS measurements. A 78-fold enhancement in peak area can be obtained by preconcentrating 4.6 ml of the sample solution containing 1 mol l⁻¹ HCl compared with the direct introduction of 53.4 μl of the solution, while achieving a 5% R.S.D. (n = 5) in the case of 0.5 ng ml⁻¹ Pd, 1 ng ml⁻¹ Pt or 0.5 ng ml⁻¹ Rh. The detection limits (3σ) were 0.03, 0.1 and 0.01 ng ml⁻¹ for Pd, Pt and Rh, respectively. The reproducibility by the ICP-AES measurement was also found to be about 5%.

The accuracy of the proposed method was checked with the standard addition method by determining 2 ng ml⁻¹ Pd, 9 ng ml⁻¹ Pt and 2 ng ml⁻¹ Rh in a synthetic sample solution containing 0.5% (w/v) NH₄Cl, 100 μg ml⁻¹ Al, 100 μg ml⁻¹ Fe, 10 μg ml⁻¹ Cu and 1 mol l⁻¹ HCl. The analytical results were compared with those from liquid–liquid extraction method and are given in Table 5. A reagent blank value was not observed under the above conditions and satisfactory agreement between the two methods was achieved.

TABLE 5

Determination of Pd, Pt and Rh in synthetic sample solution containing 0.5% (w/v) NH₄Cl, 100 μg ml⁻¹ Al and Fe, 10 μg ml⁻¹ Cu and 1 mol l⁻¹ HCl

Element	Added (ng ml ⁻¹)	Determined with flow system (ng ml ⁻¹) ^a	Determined by extraction (ng ml ⁻¹) ^a
Pd	2	2.1 ± 0.1	1.9 ± 0.1
Pt	9	9.1 ± 0.4	8.0 ± 1.0
Rh	2	2.1 ± 0.1	2.2 ± 0.1

^a Mean ± S.D. (n = 4).

TABLE 6

Determination of Pt in polluted biotic materials

Sample	Determined with flow system ($\mu\text{g g}^{-1}$) ^a	Determined by extraction ($\mu\text{g g}^{-1}$) [29]
Beans (BH186H)	0.075 ± 0.005	0.07
Tobacco (TH135B)	1.31 ± 0.07	1.5

^a Mean ± S.D. ($n = 4$).*Determination of Pt in biological materials*

Standard additions were used to eliminate the matrix effect. Tobacco and bean samples [29] were decomposed and analysed by the process described under Experimental. The results of Pt determinations were compared with those given by liquid–liquid extraction and are listed in Table 6.

Conclusion

The results of these experiments imply that the interfering matrices for GFAAS or ICP-AES in the determination of Pd, Pt and Rh can be easily removed by passage through the column while the investigated metal ions remain on the non-polar resin bed in the column as their CMDTC chelates. Moreover, the on-line sorbent extraction preconcentration technique combined with segmentation makes the flow system more flexible to be adapted to GFAAS or ICP-AES. Owing to the low detection limits of the GFAAS technique, it is more suitable for the analysis of biological materials.

The financial support for M.L. Lee for this research by the DAAD (Deutscher Akademischer Austauschdienst) of the Federal Republic of Germany is gratefully acknowledged. E. Beinrohr thanks the Alexander von Humboldt Foundation, Bonn, for awarding a research fellowship.

REFERENCES

- G.D. Clark, D.A. Whitman, G.D. Christian and J. Ruzicka, *CRC Crit. Rev. Anal. Chem.*, 21 (1990) 357.
- V. Porta, O. Abollino, E. Mentasti and C. Sarzanini, *J. Anal. At. Spectrom.*, 6 (1991) 119.
- Z. Fang, M. Sperling and B. Welz, *J. Anal. At. Spectrom.*, 5 (1990) 639.
- E. Beinrohr, M. Cakrt, J. Garaj and M. Rapta, *Anal. Chim. Acta*, 230 (1990) 163.
- E. Beinrohr, M. Cakrt, M. Rapta and P. Tarapcik, *Fresenius' Z. Anal. Chem.*, 335 (1989) 1005.
- E. Beinrohr, *Fresenius' Z. Anal. Chem.*, 338 (1990) 735.
- E. Beinrohr, M. Németh, P. Tschöpel and G. Tölg, *Fresenius' Z. Anal. Chem.*, 343 (1992) 566.
- F. Alt, U. Jerono, J. Messerschmidt and G. Tölg, *Mikrochim. Acta*, III (1988) 299.
- R. Eller, F. Alt, G. Tölg and H.J. Tobshall, *Fresenius' Z. Anal. Chem.*, 334 (1989) 723.
- F. Alt, in P. Braetter and P. Schramel (Eds.), *Trace Element Analytical Chemistry in Medicine and Biology*, Vol 5, Walter de Gruyter, Berlin, New York, pp 279–296.
- G. Tölg, *Fresenius' Z. Anal. Chem.*, 320 (1985) 736.
- G. Tölg, *Fresenius' Z. Anal. Chem.*, 317 (1984) 620.
- P. Tschöpel, *Pure Appl. Chem.*, 54 (1982) 913.
- P. Tschöpel and G. Tölg, *J. Trace Microprobe. Tech.*, 1 (1982) 1.
- M. Groto, M. Sandrock and A. Kettrup, *React. Polym.*, 13 (1990) 267.
- J.J. Lih, K.Y. Yeh and C.Y. Liu, *Fresenius' Z. Anal. Chem.*, 336 (1990) 12.
- M. Schuster, *Fresenius' Z. Anal. Chem.*, 342 (1992) 791.
- M.R. Plantz, J.S. Fritz, F.G. Smith and R.S. Houk, *Anal. Chem.*, 61 (1989) 149.
- J.N. King and J.S. Fritz, *Anal. Chem.*, 57 (1985) 1016.
- I.A. Al-Biaty and J.S. Fritz, *Anal. Chim. Acta*, 146 (1983) 191.
- Y. Sakai and N. Mori, *Talanta*, 33 (1986) 161.
- Y. Sakai, *Talanta*, 27 (1980) 1073.
- H. Bode, *Fresenius' Z. Anal. Chem.*, 144 (1954) 165.
- J.T. Pyle and W.D. Jacobs, *Anal. Chem.*, 36 (1964) 1796.
- T.M. Vickrey, M.S. Buren and H.E. Howell, *Anal. Lett.*, 11 (1978) 1075.
- R.A. Stockton and K.J. Iroglic, *Int. J. Environ. Anal. Chem.*, 6 (1979) 313.
- K. Backstrom and L.-G. Danielson, *Anal. Chem.*, 60 (1988) 1354.
- J. Fries and H. Getrost, *Organische Reagenzien für die Spurenanalyse*, Merck, Darmstadt, 1975.
- F. Alt and G. Tölg, *Schlussbericht zum Forschungsvorhaben "Beitrag zur Verbesserung der extremen Spurenanalyse der Platinmetalle in biotischen und umweltrelevanten Materialien"*, Forschungsvorband "Edelmetallemissionen" des Bundesminister für Forschung und Technologie, 07VPT01, Dortmund, 1990.
- S.J. Al-Bazi and A. Chow, *Talanta*, 31 (1984) 815.
- P. Vest, M. Schuster and K.-H. Koenig, *Fresenius' Z. Anal. Chem.*, 339 (1991) 142.
- Z. Marczenko and S. Kus, *Analyst*, 110 (1985) 1005.
- A. Hulanicki, *Talanta*, 14 (1967) 1371.

Automatic apparatus for heterogeneous enzyme immunoassays based on electrocatalytic detection of the enzyme and electrochemical regeneration of the solid phase

Denis Huet and Christian Bourdillon

Laboratoire de Technologie Enzymatique, URA 1442 du CNRS, Université de Compiègne, BP 649, 60206 Compiègne Cedex (France)

(Received 14th August 1992)

Abstract

A glassy carbon electrode, anodized for a short time at about 2.2 V vs. SCE, is a very convenient regenerable solid phase for the successive stages of an automated enzyme-linked immunosorbent assay. The anodized surface adsorbs the primary antibody and the blocking proteins in a similar manner to classical polystyrene solid phases; the detection of the immobilized glucose oxidase used as the label can be obtained from an electrocatalytic process occurring directly on the electrode; and the protein stacking, accumulated during the assay, can be eliminated by a simple re-anodization at the end of the cycle, allowing the adsorption of a new primary antibody. An automatic apparatus has been developed round an electrochemical flow cell fed with samples and reagents according to the principles of flow-injection analysis. Using rabbit IgG as analyte and glucose oxidase as label, series of 150 successive assays were conducted on the same electrode before it was polished again. The overall time of one assay, including the time for primary antibody adsorption and electrode regeneration, was 55 min.

Keywords: Enzymatic methods; Immunoassay; Electrocatalytic detection; Enzyme electrodes; Enzyme-linked immunosorbent assay; Glucose oxidase; Immunoglobulin G; Solid-phase regeneration

An important parameter for the reliability of heterogeneous enzyme immunoassays is the quality of the solid-phase support for the primary antibody or antigen. This problem, well known with polystyrene microtitre plates, is generally solved by the manufacturers, who treat and optimize the surface of the disposable plates. The situation is more complex in the framework of an automatic procedure as the solid phase cannot be exchanged to conduct successive assays. Two basic choices can be made to regenerate the solid

phase at the end of the assay: either the re-use of the primary antibody already linked on the support, or the immobilization of a new antibody after complete cleaning of the support.

In the former instance, a washing solution, containing chaotropic ions or buffers at low pH and high ionic strength, is used to break the antibody–antigen bond. This method, which is the most commonly employed, especially in the development of immunosensors, has been tested, apparently with success, with different kinds of solid phases including polysaccharide gels [1–3], electrode or membrane interfaces [4,5] and fiberoptic interfaces [6]. However, as pointed out in reviews in the affinity chromatography field [7,8],

Correspondence to: C. Bourdillon, Laboratoire de Technologie Enzymatique, Université de Compiègne, BP 649, 60206 Compiègne Cedex (France).

successful regeneration including the negligible irreversible denaturation of the immobilized antibodies needs a relatively low level of affinity between antigen and antibody. This is in contradiction with the high affinity constants required for good sensitivity of enzyme-linked immunosorbent assay (ELISA) [9] and no commercial device, to the author's knowledge, has been developed based on this washing concept.

In the latter instance, the strategy is to completely eliminate the immunological stacking by unhooking the primary antibody. A possible solution is to use a reversible covalent linkage such as a disulphide bond between the solid phase and this primary antibody and a dithiothreitol washing at the end of the assay [10]. A more drastic method is to attack the solid phase surface itself. A small thickness of the solid phase, a glassy carbon electrode in this experiment, can be destroyed by electrochemical corrosion in such a way that all the molecules adsorbed on the surface are removed [11]. A new primary antibody can then be adsorbed for the next assay.

Electrochemical detection for enzyme immunoassays has been developed largely to take advantage of the ease with which small amounts of the enzyme-generated products can be amperometrically detected (for reviews, see [12,13]). For heterogeneous assays, the main strategies depend on the relative position between the immunological solid phase and the detector surface. The electrode can be completely separated as in the simple electrochemical detection of the product after normal assay on microtitre plates [14] or, if the electrochemical detection is performed "on-line", behind an immunological reactor [2,3]. The solid phase can be more intimately associated with the electrode as with a membrane-covered sensor [15] or when the antibody is directly linked to the electrode surface [4,11,16].

This last case represents a real integration at a molecular level between the role of analyte capture devoted to the solid phase and the role of product detection obtained from the electrochemical surface. The kinetic coupling between the enzyme reaction immobilized at the electrode surface and the electrode kinetics itself has already been described [17] and the amount of

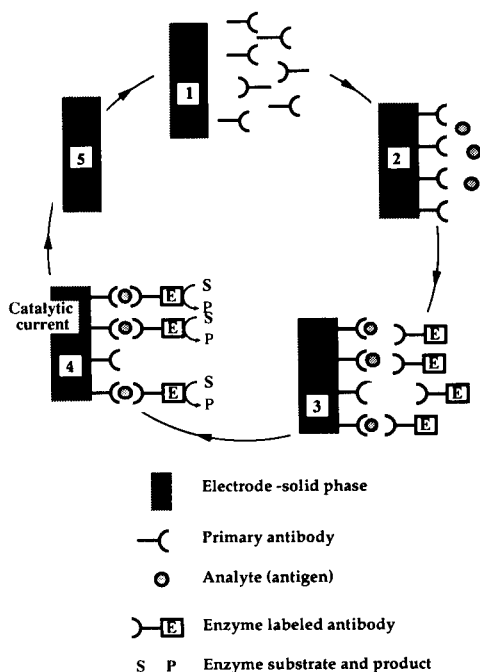


Fig. 1. Cycle of events for a heterogeneous enzyme immunoassay using a carbon electrode as regenerable solid phase. Five main steps: 1 = adsorption of the primary antibody on carbon electrode; 2 = capture of the analyte molecules; 3 = saturation of analyte with the labelled antibody; 4 = electrocatalytic measurement of the immobilized enzyme activity; 5 = regeneration of the solid phase by electrochemical cleaning.

analyte molecules captured in a sandwich assay can be calculated from the catalytic current with some reasonable assumptions [11,16].

In this context, the electrochemical cleaning of the electrode–solid phase appears to be logical means to regenerate both the capability of the solid phase to adsorb a new primary antibody and the reactivity of the electrode to detect the electroactive product of the enzymatic reaction. The principle of the overall cycle of measurement, including the regeneration step, is summarized in Fig. 1.

In this work, the ability of electrochemical corrosion to clean the solid phase for a large number of regenerations was studied and this principle was applied to the development of an automatic apparatus. The experimental model was the ELISA determination of rabbit IgG on a glassy carbon electrode. The label, glucose oxi-

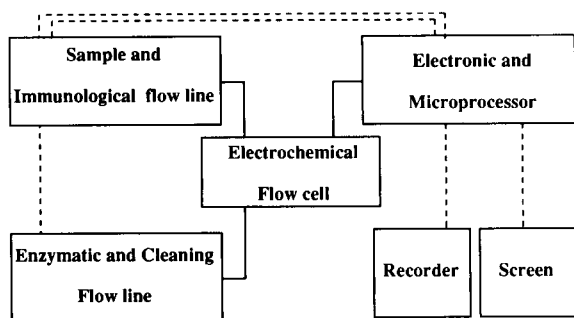


Fig. 2. Schematic diagram of the electrochemical enzyme immunoassay apparatus.

dase, was measured by the catalytic current produced during the coupling between the enzymatic reduction of benzoquinone and the electrochemical regeneration of benzoquinone [11].

EXPERIMENTAL

Reagents

Affinity-purified goat antirabbit IgG and rabbit IgG were obtained from Jackson Immuno-research Laboratories (West Grove, PA). Glucose oxidase-labelled goat antirabbit IgG was supplied by Cappel (Organon Teknika, West Chester, PA). Gelatin (O.C., 250 bloom) was from Rousselot (Isle sur Sorgue, France). Bovin serum albumin, grade V, casein and *p*-benzoquinone were obtained from Sigma (St. Louis, MO).

Apparatus

A prototype automatic electrochemical immunoassay analyser was developed by SERES (Les Milles, France) and is shown in Fig. 2. The electrochemical cell was a thin-layer flow cell made of PTFE. The thickness of the PTFE spacer was 200 μm and the total dead volume of the cell was 21 μl . The working electrode was a glassy carbon disc (Tokai grade GC-A), 3 mm in diameter. The carbon electrode was polished mechanically with alumina of decreasing size down to 0.05 μm , the alumina powder being carefully removed during the 5 min between each treatment with an ultrasonic bath (Branson 1200). This polishing

was repeated after each series of about 150 measurements.

Two counter electrodes, both platinum discs 3 mm in diameter, were mounted in the cell. One, used as regular counter electrode for amperometric detection, was 10 mm downstream of the working electrode in the flow system. The other, set directly in front of the working electrode, was used only during the electrochemical cleaning step. This position was required to minimize the ohmic drop, as the current level was high during this stage (ca. 10 mA).

Two separate lines alternatively fed the cell. The first was used for the introduction of analyte samples and immunological reagents. A motorized valve (Pharmacia MV-8 channels), a sampler (SERES) and a peristaltic pump injected successively the primary antibody solution, the blocking buffer, the sample solution, the labelled antibody solution and the rinsing buffer solution. The flow-rates were about 2 $\text{cm}^3 \text{h}^{-1}$. This circuit was built with a 0.3-mm diameter PTFE tube in such a way that the dead volumes were small (20–30 μl per reagent). The second flow line was not so optimized from the dead volume point of view. Two peristaltic pumps and a double-channel valve (Sirai) allowed the successive injection of the benzoquinone and the glucose-benzoquinone solutions for the enzyme activity determination and the acidic solution used for the electrochemical cleaning of the carbon electrode. The flow-rate was 96 $\text{cm}^3 \text{h}^{-1}$ for each step.

The electronic equipment, including the microprocessor for automation, allowed the following main functions: control and timing of pumps and valves for the two flow lines; automatic sample processing; control of the three-electrode potentiostat for amperometric detection and of the two-electrode amperostat for electrode cleaning. The A/D converter for the current and the digital data treatment was not included in this prototype.

Immunoassay procedures

Phosphate-buffered saline (PBS buffer) [0.02 mol l^{-1} phosphate buffer (pH 7.4) + 0.25 mol l^{-1} NaCl] was used as a diluting solution for the

immunological reagents. The blocking solution was 0.1% gelatin solution in PBS buffer.

Step 1: adsorption of the primary antibody. The carbon electrode was cleaned and conditioned from the preceding cycle of measurement. The anti-rabbit IgG solution, typically $200 \mu\text{g cm}^{-3}$ in PBS buffer, was introduced for 10 min for adsorption on the electrode. The electrode surface was then saturated with a protein such as gelatin with 10 min of the blocking solution at a flow-rate of $1.8 \text{ cm}^3 \text{ h}^{-1}$.

Step 2: capture of the analyte molecules. The analyte, here rabbit IgG solution, was introduced from the sampler through the electrochemical cell at a flow-rate of $1.8 \text{ cm}^3 \text{ h}^{-1}$ and then stopped for 5 min. The real time of extraction was only 6 min, given a relatively low analyte capture ratio.

Step 3: saturation of the immobilized analyte with the labelled antibody. The glucose oxidase-labelled goat anti-rabbit IgG solution ($20 \mu\text{g cm}^{-3}$ in PBS) was introduced at a flow-rate of $1.8 \text{ cm}^3 \text{ h}^{-1}$ for 10 min.

Step 4: electrocatalytic detection. Amperometric measurement of the immobilized glucose oxidase activity was performed with the carbon electrode poised at 700 mV vs. SCE. The catalytic current was due to the successive introduction (flow-rate $96 \text{ cm}^3 \text{ h}^{-1}$) of a $5 \times 10^{-3} \text{ mol l}^{-1}$ solution of benzoquinone in 0.25 M phosphate buffer (pH 6.8) for 2 min followed by a solution of 0.1 mol l^{-1} glucose + $5 \times 10^{-3} \text{ mol l}^{-1}$ benzoquinone in the same buffer for 2 min. Including the final rinsing with the first solution, the total time for this step was 6 min.

Step 5: electrochemical cleaning. The special counter electrode in front of the working electrode was used during this stage. The acidic solution ($1.6 \text{ mol l}^{-1} \text{ HNO}_3$) was introduced at a flow-rate of $96 \text{ cm}^3 \text{ h}^{-1}$ for 1 min and a current of 10 mA was then maintained for 12 s (the resulting working potential was $2.20 \pm 0.05 \text{ V}$ vs. SCE). The electrochemical cell was then rinsed with PBS buffer at a flow-rate of $96 \text{ cm}^3 \text{ h}^{-1}$ for 5 min.

The time for a complete cycle of measurement for a sandwich assay, including the adsorption of the first antibody, was typically 55 min.

RESULTS AND DISCUSSION

Electrochemical detection of the enzymatically produced hydroquinone

We used the principle of electrocatalytic detection described previously [11,17]. The catalytic current measured at a controlled potential under steady-state conditions is the result of the enzymatic production of hydroquinone just at the interface of the electrode. For a high electrochemical rate constant, this current is only kinetically controlled by the enzymatic activity [18]. However, if this rate constant decreases as a result of electrode fouling, the catalytic current may be partially limited by the electrochemical efficiency.

It is well known that quinone–hydroquinone solutions are not very stable near neutral pH and above, the adsorption of the by-products often being involved in the electrode passivation (e.g., [19]). Thus, before starting the study of any electrode fouling due to protein adsorption, it was necessary first to check the efficiency of the electrochemical corrosion to restore the amperometric hydroquinone detection itself. For this purpose, a carefully polished carbon electrode was settled in the thin-layer cell and submitted to numerous cycles of measurement with a standard solution of hydroquinone [$2.5 \times 10^{-5} \text{ mol l}^{-1}$ in 0.1 mol l^{-1} phosphate buffer (pH 6.8) at a flow-rate of $84 \text{ cm}^3 \text{ h}^{-1}$] with or without electrochemical cleaning between each cycle. The result is shown in Fig. 3.

Despite the fact that at 0.7 V vs. SCE for this redox couple on a carbon electrode the current was mainly controlled by diffusion–convection phenomena, electrode fouling was apparent after about ten measurements (ca. 20% of the hydrodynamic current after 60 cycles). The electrochemical cleaning restored correctly the initial current and repetitive anodizations were able to stabilize this current for a large number of cycles (relative standard deviation less than 5% for 100 detections). This result was expected as numerous procedures for cleaning and activating carbon electrodes have already been optimized (for a review, see [12]) and include plasma treatment [21], electrochemical cycling [20,22–24] and laser activa-

tion [19,25]. However, the technical simplicity and the short duration of this “in situ” procedure should be noted.

Protein adsorption on the anodized carbon electrode

As on polystyrene microtitre plates, the carbon surface must be able to adsorb correctly the primary antibody and the blocking proteins used to minimize undesirable non-specific binding. The adsorption isotherm of the primary antibody was measured by using the half-sandwich method. The clean electrode was first incubated with dilutions of the antibody for 5 min. After washing for 10 min with the blocking solution (1 g l^{-1} gelatin), the adsorbed antibody molecules were recognized by the glucose oxidase-labelled antibody ($20 \mu\text{g cm}^{-3}$) for 10 min. The final amount of immobilized glucose oxidase was then electrochemically detected (see step 4 of the procedure) and the carbon electrode was electrochemically cleaned (see step 5). This experiment was automatically repeated on the apparatus with random order for introduction of primary antibody concentrations (up to $500 \mu\text{g cm}^{-3}$ including blanks). The results are shown in Fig. 4.

The first and major observation is the efficiency of cleaning the electrode surface between

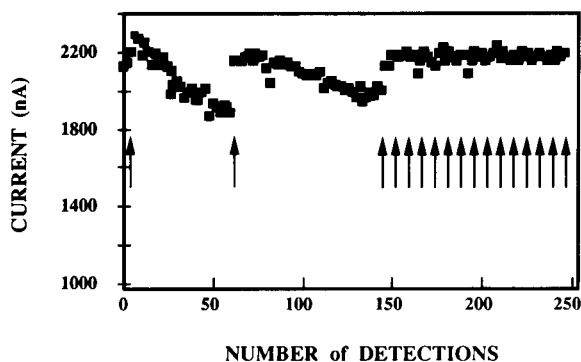


Fig. 3. Repetitive detection of hydroquinone on a glassy carbon electrode (0.07 cm^2) with or without electrochemical cleaning. Arrows indicate the cleaning at measurements numbers 1, 60, 145 and between each detection up to 248. Conditions of detection, hydroquinone $2.5 \times 10^{-5} \text{ mol l}^{-1}$ in phosphate buffer at a flow-rate of $84 \text{ cm}^3 \text{ h}^{-1}$; working potential, 0.7 V vs. SCE. Conditions of cleaning, anodization with a current of 10 mA for 12 s in $1.6 \text{ mol l}^{-1} \text{ HNO}_3$.

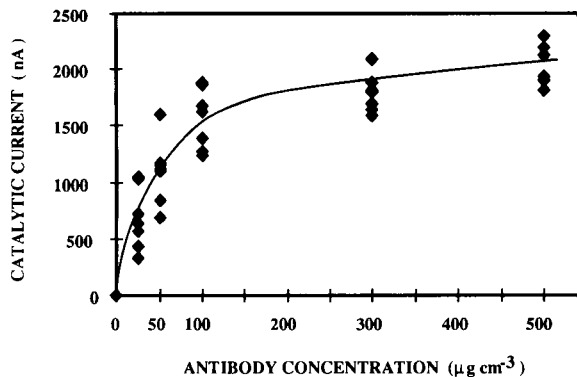


Fig. 4. Repetitive measurements of the primary antibody adsorption at various antibody concentrations. The electrochemical cleaning of the glassy carbon electrode was realised by anodization between each experiment. The adsorbed antibody was revealed by the half-sandwich method using glucose oxidase as label. Coating time, 5 min. Ambient temperature. Electrode surface area, 0.07 cm^2 . The currents due to non-specific binding (average value 200 nA) have been subtracted.

each measurement, because there was no accumulation of glucose oxidase activity in 42 successive experiments. This efficient cleaning allowed a reasonable reproducibility (20%) of the current at the isotherm plateau.

Adsorption of antibodies on the carbon electrode was previously studied quantitatively by using an electrocatalytic procedure [11,16]. The amount of adsorbed protein at the isotherm plateau was found to be ca. $1.8 \times 10^{-12} \text{ mol cm}^{-2}$, close to the value measured on polystyrene plates [26]. These calculations were made using the measurement of the catalytic current carried out on rotating disc electrodes, i.e. under easily modelled hydrodynamic conditions. The hydrodynamic conditions are not so simple with the thin-layer flow cell used in this work, and no specific effort was made to calculate the antibody coverage. However, as the measured current range was the same (100–2500 nA) and the only variant was the introduction of the solutions by pumping, it is estimated that the primary antibody coverage was of the same order of magnitude.

Anodized carbon surfaces are thus convenient for antibody adsorption and the coating concentration for the complete ELISA was chosen to be

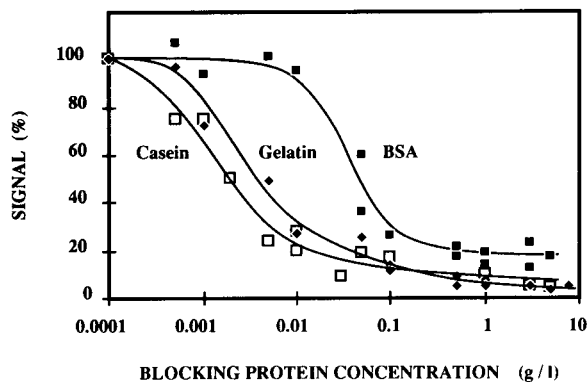


Fig. 5. Inhibition of non-specific binding on the anodized glassy carbon after 10 min of incubation with blocking proteins. Automatic electrochemical cleaning of the electrode between each experiment. Labelled antibody concentration $20 \mu\text{g cm}^{-3}$.

$200 \mu\text{g cm}^{-3}$, at the beginning of the plateau. This concentration is relatively high compared with classical coating concentrations for microtitre plates, but a disadvantage is the short duration of this adsorption step (5 min instead of several hours for polystyrene wells), included here in the overall cycle of the assay.

Another important point linked to the use of carbon electrode as an immunological solid phase is the inhibition of non-specific binding (NSB) by a preventive coating with inert proteins. Three classical blocking molecules were studied here: bovin serum albumin (BSA), gelatin and casein. The anodized carbon electrode was first coated with the blocking protein for 10 min and incubated for 10 min with the labelled antibody. After a standard detection (step 4) and an electrochemical cleaning (step 5), the cycle was repeated automatically with various concentrations of the three proteins (Fig. 5).

All the proteins tested on the anodized carbon surface exhibited a sigmoidal inhibition curve similar to those obtained on polystyrene surfaces [27]. Moreover, the concentrations of each protein required for 50% inhibition of NSB are similar for the two surfaces (e.g., $9 \times 10^{-2} \text{ g l}^{-1}$ on polystyrene and $6 \times 10^{-2} \text{ g l}^{-1}$ on carbon for BSA, or $6 \times 10^{-4} \text{ g l}^{-1}$ on polystyrene and $12 \times 10^{-4} \text{ g l}^{-1}$ on carbon for casein). With carbon, the best results of inhibition were obtained for

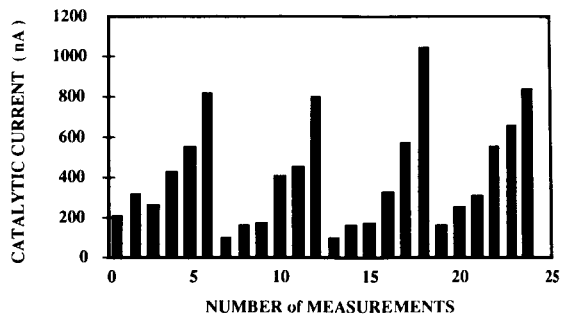


Fig. 6. Typical results for automatic ELISA determinations on a carbon electrode. The set of six standard solutions was repeated four times. The concentrations of the analyte solutions (rabbit IgG) were successively 0 (NSB determination), 3.3×10^{-9} , 6.7×10^{-9} , 1.3×10^{-8} , 1.7×10^{-8} and 3.3×10^{-8} M. Extraction time, 5 min. Ambient temperature. Each measurement took 55 min including the electrochemical cleaning and the adsorption of a new primary antibody.

both casein and gelatin (93% and 95% inhibition, respectively) after incubation for 10 min with 1 g l^{-1} solutions. A 1 g l^{-1} gelatin solution in PBS was chosen as the blocking solution for subsequent experiments.

Automation of the complete sandwich assay

The reliability of the apparatus was studied with dilutions of rabbit IgG used as analyte standards, the main question being the stability of the glassy carbon surface after numerous cycles of regeneration. The result in Figs. 6 and 7 were obtained after about 100 cycles at various analyte concentrations, without any additional treatment

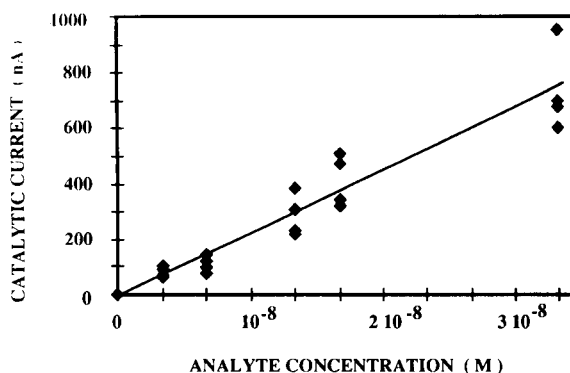


Fig. 7. Calibration graph for the automatic determination of rabbit IgG concentrations. Conditions as in Fig. 6. The results were corrected for NSB.

of the working electrode. Despite a dispersion of the catalytic currents around the calibration graph (regression coefficient 0.91 for 24 points), it is clear that the repetitive electrochemical cleaning was efficient and did not induce any hysteresis in the behaviour in the regenerable solid phase. The maximum number of re-uses of the same carbon surface between polishing was about 150. After this number we found that the signal decreased irreversibly for the conditions of anodization used (see Discussion).

A major source of error and dispersion of results was identified as being due to a lack of temperature control. As the aim was to conceive the simplest possible apparatus, the role played by the temperature in some key points of the assay had been underestimated: adsorption of the primary antibody, analyte capture and enzyme activity determination. As the duration of the 24 assays of this set needed 1 day, successive assays were done at variable room temperatures. This situation is different to the classical ELISA performed simultaneously on microtitre plates as the temperature fluctuations act identically on every well.

The apparatus was then placed in a thermostated room and the precision studied for the maximum capacity of the sampler (36 samples). Figure 8 shows that the quality of the results has clearly improved, the relative standard deviation

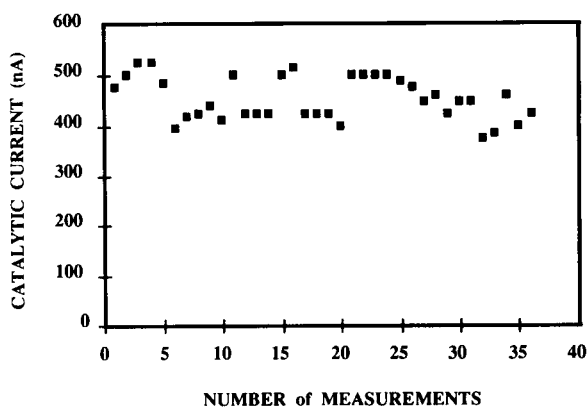


Fig. 8. Repetitive assays at constant analyte concentration (6.7×10^{-9} M). Conditions as in Fig. 6 except that the apparatus and reagents were placed in a thermostated room at $26 \pm 1^\circ\text{C}$.

(9% for this set) being of the same order of magnitude as those measured, in general, for enzyme immunoassays [28].

DISCUSSION

The regeneration of the glassy carbon surface by anodization appears to be especially convenient for the different roles played by an immunological solid phase in an automatic apparatus: the regeneration process is technically simple and very short (less than 2 min, including the pumping time of the cleaning solution); the adsorption of the primary antibody and blocking protein on the clean surface is easy and reproducible; there is no electrode fouling for the electrocatalytic detection of the enzyme product; and the proteins coated on the electrode surface can be completely eliminated at the end of each assay. Hence it is possible to exchange the primary antibody if the assay of a different analyte molecule is needed.

However, owing to the alteration of the catalytic current after 150 cycles, the total number of measurements is limited. The limiting parameter has not yet been clearly identified and it is of interest to discuss how to improve this number in the future. First, the final aspect of the electrode surface after 150 anodizations was not drastically different to that after one or two anodizations. Optical microscopy has shown some free particles on the surface, which were easily removed by wiping the surface with a paper tissue, but the pitting corrosion was found to be relatively low and the surface still brittle. This is in agreement with the experimental observation that the amount of adsorbed primary antibody did not increase in the successive anodizations, which is an indication that the actual surface area was not increased. Many investigators have considered the possibility of surface roughening and the associated increase in surface area during anodization [20,23,29]. Their studies did not show a large increase in surface area, at least for moderate anodization potentials (≤ 1.8 V vs. SCE). Although our treatment was applied at a higher potential (10 mA, giving about 2.2 V vs. SCE), the

result was identical. However, the potential measurement was perhaps altered by the ohmic drop in our small volume cell (ca. 20 μ l) and the actual potential was certainly lower.

Another observation is the intense production of gas on the electrode surface during the anodization. This forbids comparisons between the charge passed in our anodizations and those in other experiments [20,23], as a large part of the charge was used to produce gas. This bubble formation perhaps plays a role in the efficient elimination of the molecules adsorbed on the interface and this parameter will have to be studied in detail.

Anyway, part of the charge was used to modify the carbon interface itself. Kopley and Bard [20] have demonstrated, by ellipsometric measurements, that repetitive anodizations coincided with the growth of a graphite oxide layer. Graphite oxide is a rather poorly characterized material, composed of a disordered carbon layer and C–O bonds. As this material exhibits a low conductivity [20], the growth of this layer during our experiments could produce the alteration in the catalytic current that was measured after 150 cycles.

It is clear that, if it is required to increase the number of successive assays, there must be better understanding of the effects of the formation of this layer on the immunoassay parameters. These aspects and especially the influence of the potential and time values for anodization will be studied with the help of a second-generation prototype currently in preparation. This new apparatus includes temperature control of the cell to increase the long-term accuracy of the results.

This study was supported by a grant "Aliment 2002" from the Ministère de la Recherche et de la Technologie. The assistance of SERES (Les Milles) with the technical development of the automatic system is gratefully acknowledged.

REFERENCES

- 1 B. Mattiason, C. Borrebaeck, B. Sanfridson and K. Mosbach, *Biochim. Biophys. Acta*, 483 (1977) 221.
- 2 W.U. De Alwis and G.S. Wilson, *Anal. Chem.*, 57 (1985) 2754.
- 3 W.U. De Alwis and G.S. Wilson, *Anal. Chem.*, 59 (1987) 2786.
- 4 G.A. Robinson, V.M. Cole, S.J. Rattle and G.C. Forrest, *Biosensors*, 2 (1986) 45.
- 5 P. Battaillard, F. Gardies, N. Jaffrezic-Renault, C. Martelet, B. Colin and B. Mandrand, *Anal. Chem.*, 60 (1988) 2374.
- 6 F.V. Bright, T.A. Betts and K.S. Litwiler, *Anal. Chem.*, 62 (1990) 1065.
- 7 T. Kristiansen, in O. Hoffman, M. Breitenbach, F. Koller, O. Kraft and O. Scheiner (Eds.), *Affinity Chromatography*, Pergamon, Oxford, 1978, pp. 191–206.
- 8 G.C. Calton, *Methods Enzymol.*, 104 (1984) 381.
- 9 M.E. Devey and M.W. Steward, in D.M. Kemeny and S.J. Challacombe (Eds.), *ELISA and Other Solid Phase Immunoassays*, Wiley, New York, 1988, pp. 135–1153.
- 10 J.L. Boitieux, R. Groshemy and D. Thomas, *Anal. Chim. Acta*, 197 (1987) 229.
- 11 C. Gyss and C. Bourdillon, *Anal. Chem.*, 59 (1987) 2350.
- 12 W.R. Heineman and H.B. Halsall, *Anal. Chem.*, 57 (1985) 1321A.
- 13 T.T. Ngo (Ed.), *Electrochemical Sensors in Immunological Analysis*, Plenum, New York, 1987.
- 14 S.H. Jenkins, W.H. Heineman and H.B. Halsall, *Anal. Biochem.*, 168 (1988) 292.
- 15 M. Aizawa, A. Morioka and S. Suzuki, *Anal. Chim. Acta*, 115 (1980) 61.
- 16 D. Huet and C. Bourdillon, *J. Immunol. Methods*, 135 (1990) 33.
- 17 C. Bourdillon, J.P. Bourgeois and D. Thomas, *J. Am. Chem. Soc.*, 102 (1980) 4231.
- 18 R.M. Mège and C. Bourdillon, *J. Biol. Chem.*, 260 (1985) 14701.
- 19 M. Poon and R.L. McCreery, *Anal. Chem.*, 59 (1987) 1615.
- 20 L.J. Kopley and A.J. Bard, *Anal. Chem.*, 60 (1988) 1459.
- 21 J.F. Evans and T. Kuwana, *Anal. Chem.*, 49 (1977) 1632.
- 22 W.J. Blaedel and R.A. Jenkins, *Anal. Chem.*, 46 (1974) 1952.
- 23 R.C. Engstrom, *Anal. Chem.*, 54 (1982) 2310.
- 24 F.G. Gonon, C.M. Fombarlet, M.J. Buda and F.J. Pujol, *Anal. Chem.*, 53 (1981) 1386.
- 25 M. Poon and R.L. McCreery, *Anal. Chem.*, 58 (1986) 2745.
- 26 L.A. Cantarero, J.E. Butler and J.W. Osborne, *Anal. Biochem.*, 105 (1980) 375.
- 27 R.F. Vogt, D.L. Phillips, L.O. Henderson, W. Whitfield and F.W. Spierto, *J. Immunol. Methods*, 101 (1987) 43.
- 28 A. Hubbuch, E. Debus, R. Linke and W.J. Schrenk, *Prog. Clin. Biochem.*, 4 (1986) 109.
- 29 R.C. Engstrom and V.A. Strasser, *Anal. Chem.*, 56 (1984) 136.

Amperometric enzyme immunoassay for urinary human serum albumin using plasma-treated membrane

Shigeki Kaku, Setsuko Nakanishi¹ and Kazuo Horiguchi

Research Laboratory, Susumu Co., Ltd., 14 Kamitobaumawashi-cho, Minami-ku, Kyoto 601 (Japan)

Masanori Sato

Faculty of Textile Science, Kyoto Institute of Technology, Kyoto (Japan)

(Received 7th July 1992)

Abstract

A partial modification was made to a microporous hydrophobic polypropylene film by water vapour plasma glow discharge treatment. The modified part, a spot 6 mm in diameter, became hydrophilic so that water could penetrate easily. By treating this "plasma spot membrane" with octamethylenediamine and glutaraldehyde, a membrane for immobilization of proteins was obtained. As immobilization of the antibody and the immunoreaction could be performed in the limited spot area, only small amounts (10 μ l) of reagents and sample were required. Using this plasma spot membrane and a Pt–AgCl electrode, an amperometric enzyme immunoassay system was established for the measurement of urinary human serum albumin. In this system, non-specific adsorption of enzyme-labelled antigen to the membrane was only 4.4% of specific binding. The range of measurement was 0.5–200 mg l⁻¹ of human serum albumin, which is satisfactory for the diagnosis of human kidney function.

Keywords: Amperometry; Enzymatic methods; Immunoassay; Albumin; Human serum albumin; Plasma-treated membrane; Serum; Urine

Plasma treatment and plasma polymerization are new techniques for modifying the surfaces of polymers and inorganic materials. This dry process has been applied in various industrial fields [1–3], and has made it possible to introduce various functional groups or to deposit thin films (a few nanometres thick) on the surface in order to change its characteristics. This technique has been applied in biochemistry to obtain biocompatible materials and substrates for the immobilization of proteins [4–7].

To perform an amperometric enzyme immunoassay, a membrane made of polypropylene film having partially hydrophilic properties obtained by plasma treatment was developed. A system to determine insulin in serum using this modified membrane has been reported [8], in which the sensitivity was comparable to that of radioimmunoassay (RIA).

In this work, the plasma-treated membrane was applied to measure human serum albumin (HSA) and the characteristics of this membrane for an amperometric biosensor were established. HSA is a marker for the detection of renal disease. Recently, much interest has been directed to the measurement of concentrations of HSA in the range of tens of mg l⁻¹. The excretion of urinary albumin at this level is defined as mi-

Correspondence to: S. Kaku, Research Laboratory, Susumu Co., Ltd., 14 Kamitobaumawashi-cho, Minami-ku, Kyoto 601 (Japan).

¹ Present address: Pharmaceutical Basic Research Laboratories, Japan Tobacco Inc., Yokohama (Japan).

croalbuminuria [9]. The detection of microalbuminuria has a high prognostic value for diabetic patients with no symptoms of clinical nephropathy [10–12]. This range of HSA is largely measured by RIA [10]. Various non-isotopic assays of HSA such as immunoturbidimetric assay [13], enzyme-linked immunosorbent assay (ELISA) [14] and solid-phase luminescent catalyst immunoassay [15], and immunoelectrodes [16], fibre-optic immunosensors [17] and piezoelectric crystal sensors [18], have been developed as alternative methods to RIA. The present amperometric immunoassay using a plasma-treated membrane provides a method with a satisfactory range of measurement of urinary HSA. The plasma-treated membrane can be utilized as an inexpensive substrate for immobilization of proteins and mass production is feasible.

EXPERIMENTAL

Materials and reagents

As the substrate membrane for immobilization of proteins, microporous polypropylene film (Celgard No. 2500, 25 μm thick and 45% porosity, from Celanese, USA) was used. Protein A was purchased from UCB Bioproducts (Belgium) and monoclonal antibody against human serum albumin (derived from mouse, protein concentration 68.7 mg ml^{-1}) from Cedarlane Labs. (Canada). Human serum albumin (HSA, globulin-free), glucose oxidase (GOD type VII, from *Aspergillus niger*), bovine serum albumin (BSA, fraction V, RIA grade), Tween 20 (polyoxyethylene sorbitan monolaurate), 2-mercaptoethylamine, concanavalin A (type IV) and 4,4'-dithiodipyridine were obtained from Sigma (USA). *N*-(ϵ -Maleimidocaproyloxy)succinimide (EMCS) was obtained from Dojindo Labs. (Japan), octamethylenediamine (1,8-diaminooctane) from Aldrich (USA) and β -D-glucose from Wako (Japan). Glutaraldehyde (grade for electron microscopy) and other chemicals of analytical-reagent grade were supplied by Nacalai Tesque (Japan). Sephadex G-25 and cyanogen bromide-activated Sepharose 4B were obtained from Pharmacia (Sweden).

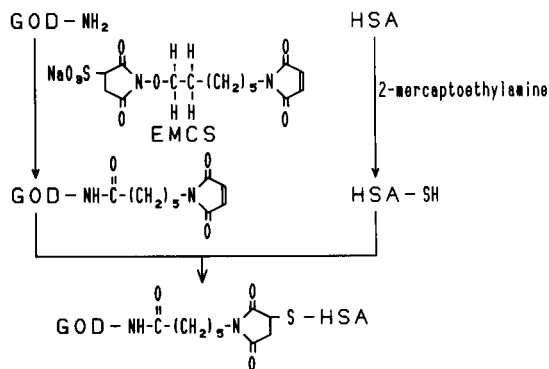


Fig. 1. Preparation of GOD-HSA conjugate. GOD maleimidized by EMCS and thiol-containing HSA were conjugated.

Equipment

GOD activity was measured by amperometry with a P-8 polarograph (Yanaco, Japan) and a Pt-AgCl electrode (Horiba, Japan). Observation and characterization of the membrane were accomplished with an S-2400 scanning electron microscope (SEM) (Hitachi, Japan) and a JIR-5500 Fourier transform infrared spectrometer (JEOL, Japan).

Preparation of glucose oxidase-labelled HSA

GOD-labelled HSA was prepared by the maleimide method [19,20] as shown in Fig. 1. Maleimide groups were introduced into GOD using EMCS. A solution of 10 mg of GOD dissolved in 1.0 ml of 0.1 M phosphate-buffered saline (PBS) (pH 7.0) was incubated with a solution of 1.32 mg of EMCS dissolved in 0.7 ml of *N,N*-dimethylformamide at 30°C for 30 min. The maleimidized GOD was purified by gel filtration with a Sephadex G-25 column using 0.1 M phosphate buffer (pH 6.0). The quantification of maleimide groups was carried out with 2-mercaptoethylamine, EDTA and 4,4'-dithiodipyridine [19]. Three or four maleimide groups were introduced into one GOD molecule.

A thiol group was introduced into HSA as follows. A solution of 20 mg of HSA dissolved in 2 ml of 0.1 M PBS (pH 6.0) and 300 μl of 0.1 M 2-mercaptoethylamine were incubated at 37°C for 90 min. By analysis with 4,4'-dithiodipyridine [19],

it was confirmed that one thiol group was introduced into one molecule of HSA.

GOD-HSA was prepared by mixing maleimide-GOD and thiol-containing HSA in a molar ratio of 1:4 at 4°C for 18 h. The unreacted maleimide groups of GOD-HSA were blocked with 2-mercaptoethylamine. The conjugate was purified to separate free HSA by affinity chromatography using concanavalin A, which binds specifically to the sugar chain of GOD. Although the conjugate obtained contained not only GOD-HSA but also free GOD after the purification, free GOD did not affect the immunoreaction. Gel filtration and gel electrophoresis studies showed that the binding ratio of GOD to HSA was 1:1 and the molecular weight of the GOD-HSA conjugate was about 230 000. The absorbance of the conjugate at 280 and 450 nm was 0.423 and 0.043, respectively. The activity of GOD-HSA as an HSA antigen was confirmed by crossed immunoelectrophoresis.

Preparation of the plasma spot membrane

The surface of Celgard microporous polypropylene film was hydrophobic and there were no functional groups to interact with protein. To immobilize proteins, functional groups were introduced on the surface as follows.

The film was made partially hydrophilic with a low-temperature plasma glow discharge. A diagram of the equipment for plasma treatment is shown in Fig. 2. Celgard film was sandwiched between two pieces of aluminium plate (18 × 18 cm) having 64 holes of 6 mm in diameter arranged at regular intervals. These plates served as masks to make the film partially hydrophilic and also as electrodes for plasma glow discharge. Celgard film sandwiched between the aluminium plates was placed at the centre of two parallel rectangular aluminium electrodes (20 × 20 cm) in the vacuum chamber. The mask and electrodes were connected to a 5 kHz power supply and matching network. After evacuating the chamber to less than 10^{-3} Torr by an oil diffusion pump and rotary pump, water vapour was introduced into the chamber. The pressure was adjusted to 0.5 Torr by regulating the flow-rate of the water vapour. Plasma discharge was carried out at 0.1 A

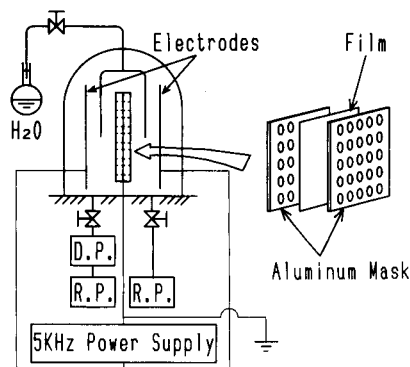


Fig. 2. Schematic diagram of the equipment for plasma treatment. Celgard film was sandwiched between two aluminium masks with holes. R.P. = rotary oil pump and D.P. = oil diffusion pump.

and 420 V for 5 min. The temperature of the aluminium mask was below 40°C during discharge, and there was no damage to the film by heat. After plasma treatment, the film was removed from the aluminium mask.

When the film was floated on water, the unmasked part (6 mm in diameter) affected by the plasma became hydrophilic and the water permeated through it. The masked part remained hydrophobic. Each region with a hydrophilic spot was called a “plasma spot membrane”.

Preparation of antibody-immobilized plasma spot membrane

The film was treated so as to immobilize proteins on its hydrophilic part. After the plasma treatment, the film was dipped into 0.05% octamethylenediamine solution for 5 min at room temperature. The film was then taken out of the solution and sandwiched between filter-papers (No. 2, Toyo, Japan) to remove excess of solution on the surface. After drying the film in air at 25°C for 15 min, it was dipped into 5% glutaraldehyde solution at 4°C overnight. It was then washed thoroughly with distilled water to remove excess of glutaraldehyde. The 64 hydrophilic spots in a Celgard film then became ready to immobilize proteins.

This film was handled as a whole sheet without being cut into 64 pieces with individual spots until amperometric measurement. The film was

set on a perforated table having 64 holes of 12 mm diameter and then the protein solution was dropped on to each spot. The reactions were carried out under a humid atmosphere so as not to concentrate the protein solution.

Antibody fixation was conducted as follows. A solution of 10 μl of protein A [0.05 mg ml^{-1} in 0.1 M phosphate buffer (pH 7.0)] was dropped on to each spot and incubated for 2 h at 25°C. Part of the solution soaked into the spot and the drop kept its hemispherical shape without flowing out during the incubation. Then, a solution of 10 μl of 3% BSA dissolved in 0.15 M PBS (pH 7.2) was applied for 2 h at 25°C as a blocking treatment to suppress the non-specific adsorption of HSA-containing sample and GOD–HSA on the spots. A solution of 10 μl of antibody diluted 200-fold in 0.1 M phosphate buffer (pH 7.0) was dropped and incubated at 4°C for 18 h. Following each of these steps, the plasma spot membrane was washed with 0.15 M PBS (pH 7.0) and then air-dried.

Protein A binds specifically to the Fc region of antibody and is thus useful by orienting the antibody so that the antigen-recognition sites are directed away from the surface of membrane [21,22]. This makes it possible for antigen-recognition sites to bind effectively with antigens.

Immunoreaction on the plasma spot membrane

To measure HSA, a competitive binding assay was adopted. The standard HSA sample [$0.5\text{--}200 \text{ mg l}^{-1}$ in 0.15 M PBS (pH 7.0)] and 10-fold diluted GOD–HSA were mixed in a ratio of 1 : 1. A solution of 10 μl of each mixture was dropped on the antibody-immobilized plasma spot membrane and incubated for 2 h at 25°C. Ten spots were used for one concentration of HSA. The immunoreaction was stopped by washing the plasma spot membrane with 0.15 M PBS (pH 7.0) containing 0.05% Tween 20. The film was cut into 64 squares, each containing one spot.

Amperometric determination of HSA

GOD is specific for glucose, according to the following equation:

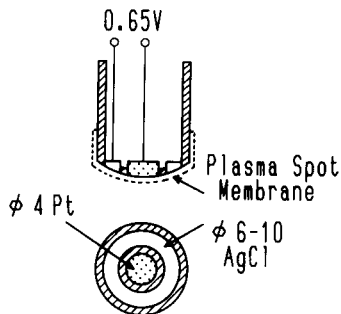


Fig. 3. Design of the H_2O_2 electrode for amperometric measurement with the plasma spot membrane. The membrane was adapted to the electrode with a Teflon ring.

After the immunoreaction, the GOD activity of each spot was measured by amperometry using a hydrogen peroxide electrode system consisting of Pt and AgCl ($\Delta E = 0.65 \text{ V}$) as shown in Fig. 3. The sensitivity of the electrode may change during the measurement owing to contamination of its surface by protein adsorption [23]. To avoid such a problem, the electrode was pretreated before amperometric measurement as follows: the electrode was immersed in 5% BSA solution for 1 h, washed with distilled water, treated with 5% glutaraldehyde solution at 25°C for 30 min and then rinsed with water.

The hydrophilic part of the plasma spot membrane was then closely adapted to the centre of the Pt electrode with a Teflon ring. It was inserted in a vessel containing 5 ml of 0.15 M PBS (pH 5.8) with stirring at 450 rpm at 25°C, then 0.1 ml of $\beta\text{-D-glucose}$ solution (200 mg ml^{-1}) was added to the vessel. The current due to hydrogen peroxide generated by the enzymatic reaction was recorded.

RESULTS AND DISCUSSION

Observation of the surface of the plasma spot membrane by SEM

The Celgard film was microporous. Figure 4a shows a schematic illustration of this pore. The maximum size of a micropore was $0.04 \times 0.4 \mu\text{m}$. A scanning electron micrograph of the surface of the intact Celgard film is shown in Fig. 4b. Figure

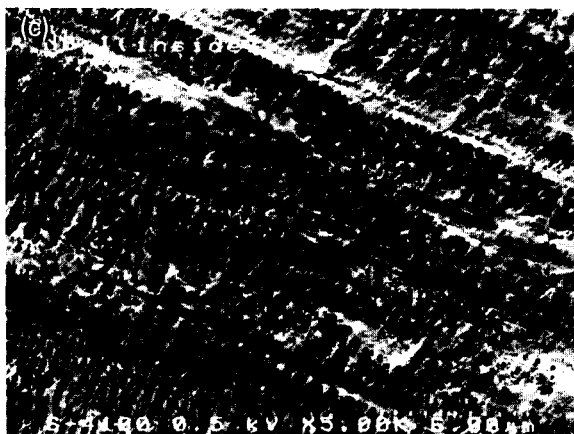
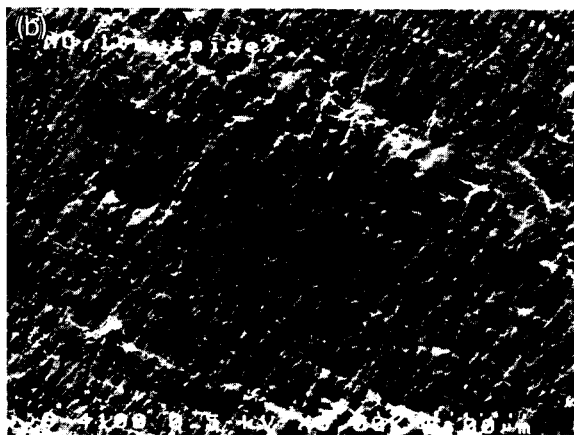
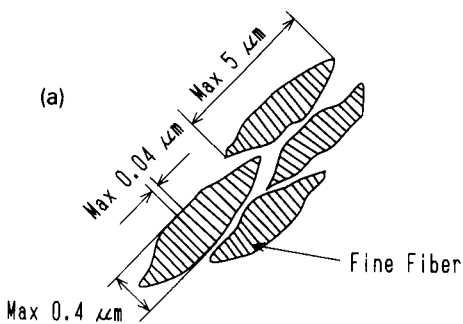


Fig. 4. (a) Schematic illustration of the pores of Celgard film. (b) Scanning electron micrograph of intact Celgard film. (c) Scanning electron micrograph of plasma-treated Celgard film. Fine fibres which separated the pores were partially etched by the plasma glow discharge.

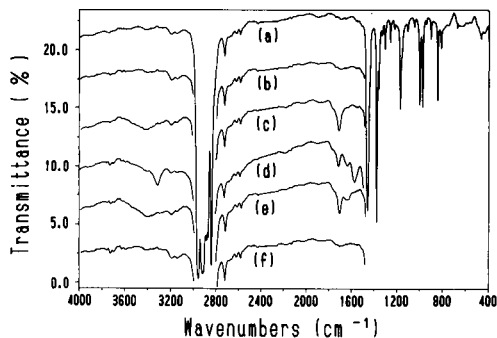


Fig. 5. Infrared spectra of Celgard film before and following plasma treatment and pretreatment for immobilizing proteins. (a) Intact film; (b) masked part of film after plasma treatment; (c) unmasked part of film, a spot of 6 mm diameter, after plasma treatment; (d) a spot after treatment with octamethylenediamine; (e) a spot after treatment with octamethylenediamine and glutaraldehyde; (f) masked part of film after treatment with octamethylenediamine and glutaraldehyde.

4c shows the surface of the plasma-treated spot. Fine fibres which separated the pores were partially etched, so that the pore was enlarged.

Analysis of the plasma spot membrane by infrared spectrometry

To immobilize proteins covalently, functional groups should be introduced on the hydrophobic surface of the membrane. After the plasma treatment and each step of the pretreatment for immobilizing proteins, the surface of the plasma spot membrane was examined by Fourier transform infrared transmission spectrometry. The intact film showed a typical polypropylene spectrum as shown in Fig. 5a. After water vapour plasma treatment, the masked part showed the same spectrum as the intact Celgard, as shown in Fig. 5b. A spot of 6 mm diameter affected by the plasma discharge showed absorption maxima at 3400 cm^{-1} (OH stretching vibration) and 1710 cm^{-1} (C=O stretching vibration), indicating the formation of hydroxyl, carboxyl and/or aldehyde groups, as shown in Fig. 5c.

After being dipped in octamethylenediamine solution and dried, the spot showed two new peaks at 3340 cm^{-1} (NH stretching vibration) and 1570 cm^{-1} (NH in-plane deformation) due to amino groups, as shown in Fig. 5d. After the

treatment with glutaraldehyde and washing with distilled water, the absorption at 3340 and 1570 cm^{-1} diminished and peaks at 3400 and 1710 cm^{-1} appeared as shown in Fig. 5e. By this treatment, octamethylenediamine and glutaraldehyde formed a Schiff's base and aldehyde groups were introduced on the membrane surface. Glutaraldehyde forms polymers in its solution and cyclopolymerization is possible [24]. A three-dimensional complex might be formed between polymeric glutaraldehyde and octamethylenediamine on the inner surface of the microporous membrane. Protein was immobilized by the reaction between its amino groups and aldehyde groups on the membrane surface.

After the pretreatment, the hydrophobic part masked during plasma treatment showed the same spectrum as the intact membrane, as shown in Fig. 5f.

Characteristics of the plasma spot membrane for an amperometric biosensor

In amperometric measurements, the membrane should be permeable to electrically active substances. A thinner membrane gives a more rapid response. The plasma spot membrane seemed to satisfy this requirement. Non-permeability of an intact film to hydrogen peroxide was confirmed using the electrode covered with Celgard film by amperometry. In contrast, when the plasma spot membrane was set on the electrode, a rapid response with hydrogen peroxide was observed. The current was saturated within 30 s.

To confirm the applicability of the plasma spot membrane as a substrate for an amperometric biosensor, GOD was immobilized on it and its activity was measured with the electrode. Figure 6 shows the GOD activity of the plasma spot membranes treated with various concentrations of octamethylenediamine following 5% glutaraldehyde, and immobilized with different concentrations of GOD solution. The amount of immobilized protein could be adjusted easily by changing the concentration of octamethylenediamine solution.

The reproducibility and stability of the plasma spot membrane for an amperometric biosensor were examined as follows. When 20 μl of GOD

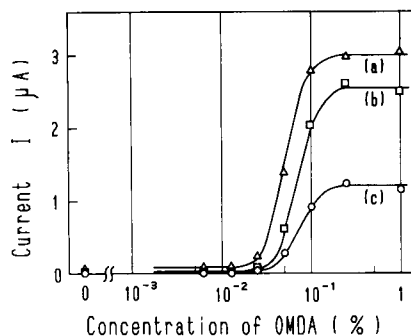


Fig. 6. Dependence of the immobilized GOD activity on octamethylenediamine (OMDA) concentration at different GOD concentrations. Concentration of the applied solution of 20 μl of GOD (a) 0.8, (b) 0.2 and (c) 0.04 $\mu\text{g} \mu\text{l}^{-1}$.

solution (0.2 $\mu\text{g} \mu\text{l}^{-1}$) were immobilized on the plasma spot membrane treated with 3% octamethylenediamine solution, the range of measurement was 0–5 mg ml^{-1} of glucose. The relative standard deviation (R.S.D.) among the spots was 4.3% ($n = 10$). In addition, continuous measurement of glucose over 100 times using such a GOD-immobilized membrane gave an R.S.D. of 6.4%.

Determination of HSA

Using the plasma spot membrane pretreated with a 0.05% solution of octamethylenediamine, HSA was determined. The current data obtained by amperometry were expressed as B/B_0 according to the following equation:

$$B/B_0 (\%) = (I_x/I_0) \times 100$$

where I_x is the current due to $x \text{ mg l}^{-1}$ of HSA and I_0 is the current in the absence of HSA.

A typical calibration graph obtained by a competitive immunoreaction is shown in Fig. 7, with a measurement range of 0.5–200 mg l^{-1} HSA. The R.S.D. among the spots applied with the same concentration of HSA was 8.6% ($n = 10$).

For a practical enzyme immunoassay, non-specific adsorption of antigen and enzyme-labelled antigen on the substrate should be avoided as far as possible. Non-specific adsorption in the present system was examined by applying GOD–HSA to the plasma spot membrane on which there was no anti-HSA antibody. This

membrane gave only 4.4% of the current I_0 . Hence the substrate used in the present system was almost free from non-specific adsorption of antigen or labelled antigen. The range of measurement coincided with that required for examination of human kidney functions. In a normal body, the HSA level in urine is 1.5–17 mg l⁻¹ in 24 h urine collections [10]. In cases of abnormality in the glomerulus, HSA is several tens of mg l⁻¹. The present measurement system is therefore useful for measuring urinary HSA without dilution even at the high concentrations possible in an abnormal case.

Recent industrial plasma techniques can treat polymer film continuously by winding the latter from a roll of the film in a plasma discharge. Therefore, the present plasma-treated membrane can be prepared by mass production, with low cost and uniformity.

In addition, in an attempt at semi-automatic measurement, a system was made using a commercial 24-well micro-plate for culture vessels as shown in Fig. 8. The GOD-immobilized plasma spot membranes were attached to the perforated bottom of the wells. For measuring the GOD activity by amperometry, a Pt–AgCl electrode was attached lightly to the membrane on the underside. In this way, troublesome procedures of setting and removing the membrane are unnecessary. In this system, the accuracy of the measurement of glucose was acceptable with 3.3% R.S.D. ($n = 40$). The plasma spot membrane made this measurement system possible.

In conclusion, the partially hydrophilic spot membrane, prepared by treatment with a plasma

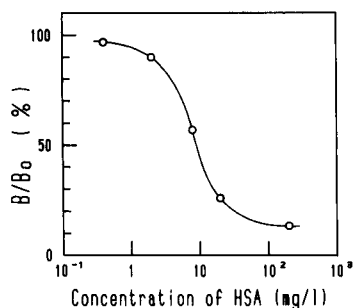


Fig. 7. Calibration graph for human serum albumin measurements with the plasma spot membrane.

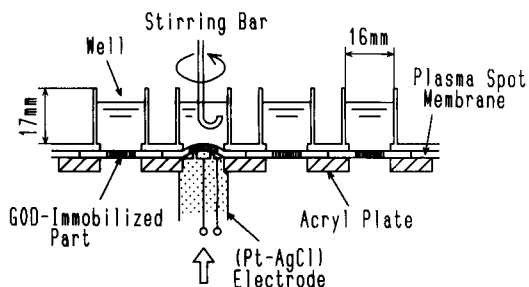


Fig. 8. Semi-automatic amperometric measurement system using the plasma spot membrane and a 24-well micro-plate.

glow discharge, made possible the amperometric measurement of HSA with an enzyme immunoelectrode. The range of measurement conformed with that required for clinical use. The plasma spot membrane was applicable in amperometric enzyme immunoassays requiring minimum amounts of reagents and sample with minimum non-specific adsorption. The present plasma technique may produce uniform membranes for immobilization of proteins on a large scale.

The authors are grateful to Mr. M. Wada and Mr. K. Ueda of the Application Technology Department, Technoresearch Laboratory, Hitachi Instrument Engineering, Japan, for scanning electron microscopy.

REFERENCES

- H. Yasuda and C.E. Lamaze, *J. Appl. Polym. Sci.*, **17** (1973) 201.
- K.S. Chen, N. Inagaki and K. Katsuura, *J. Appl. Polym. Sci.*, **27** (1982) 4655.
- N. Inagaki, T. Nishio and K. Katsuura, *J. Polym. Sci., Polym. Lett. Ed.*, **18** (1980) 765.
- Y. Ishikawa, S. Sasakawa, M. Takase and Y. Osada, *Thromb. Res.*, **35** (1984) 193.
- B.D. Ratner, N.B. Mateo, S.I. Ertel and T.A. Horbett, *Polym. Mater. Sci. Eng.*, **62** (1990) 250.
- Y. Osada, Y. Iino and Y. Iriyama, *Chem. Lett.*, (1982) 171.
- Y. Ishikawa, S. Sasakawa, M. Takase, Y. Iriyama and Y. Osada, *Makromol. Chem., Rapid Commun.*, **6** (1985) 495.
- S. Kaku, S. Nakanishi and K. Horiguchi, *Anal. Chim. Acta*, **225** (1989) 283.
- G.C. Vivreti, M. Wiseman and S. Redmond, *Diabetic Nephropathy*, **3** (1984) 79.
- U. Di Mario, P. Pietravalle, A. Napoli, S. Morano, M. Mancuso, S. Gambardella and D. Andreani, *Horm. Metab. Res.*, **18** (1986) 689.

- 11 G.C. Viverti, H. Keen, J.C. Pickup and R.W. Bilous, *Acta Endocrinol., Suppl.*, 242 (1981) 59.
- 12 G.C. Vibeti, R.D. Hill, R.J. Jarret, A. Argyropoulos, U. Mahmud and H. Keen, *Lancet*, i (1982) 1430.
- 13 A.M. Teppo, *Clin. Chem.*, 28 (1982) 1359.
- 14 A. Puri, R. Casburn-Budd, V. Eisen and J.D.H. Slater, *Clin. Chem.*, 31 (1985) 1214.
- 15 Y. Ikariyama and S. Suzuki, *Anal. Chim. Acta*, 156 (1984) 24.
- 16 B. Mattiasson and H. Nillson, *FEBS Lett.*, 78 (1977) 251.
- 17 T. Hara, K. Tsukagoshi, A. Arai and Y. Imashiro, *Bull. Chem. Soc. Jpn.*, 62 (1989) 2844.
- 18 E. Prusak-Sochaczewski and J.H.T. Luong, *Anal. Lett.*, 23 (1990) 401.
- 19 E. Ishikawa, M. Imagawa, S. Hashida, S. Yoshitake, Y. Hamaguchi and T. Ueno, *J. Immunoassay*, 4 (1983) 209.
- 20 K. Kusai, I. Sekuzu, B. Hagihara, K. Okunuki, S. Yamauchi and M. Nakai, *Biochim. Biophys. Acta*, 40 (1960) 555.
- 21 L.J. Kricka, in M.K. Schwartz (Ed.), *Ligand-Binder Assays (Clinical Biochemical Analysis, Vol. 17)*, Dekker, New York, 1985, p. 78.
- 22 U. Jönsson, M. Malmqvist, I. Rönnerberg and L. Berghem, *Prog. Colloid Polym. Sci.*, 70 (1985) 96.
- 23 C.A. Broyles and G.A. Rechnitz, *Anal. Chem.*, 58 (1986) 124.
- 24 D. Hopwood, in P.J. Stoward (Ed.), *Fixation in Histochemistry*, Chapman and Hall, London, 1973, p. 47.

Polarographic study of the Eu(III)–triethylenetetraaminehexaacetic acid complex and determination of europium by oscillopolarography

Xiao-Tai Fu

Centre of Microcosm Analysis, Da Qing Petroleum College, Anda City (China)

Chun-Ming Wang and Yu-Xiang Zhang

Department of Chemistry, Lanzhou University, Lanzhou 730000 (China)

(Received 31st March 1992; revised manuscript received 23rd September 1992)

Abstract

The single-sweep polarographic behaviour of Eu(III)–TTHA (triethylenetetraaminehexaacetic acid) complex was studied. In $0.1 \text{ mol l}^{-1} \text{ NH}_4\text{Cl} + 0.1 \text{ mol l}^{-1} \text{ NH}_3$ solution, the electrode reaction of the complex is $[\text{Eu(III)L}]^{3-} + e \rightarrow \text{Eu(II)} + \text{L}^{6-}$ and the polarographic current is controlled by the diffusion process of the complex. The method can be used to determine trace Eu concentrations in the range 2.5×10^{-6} – $5.0 \times 10^{-4} \text{ mol l}^{-1}$ in solution.

Keywords: Polarography; Europium; Oscillopolarography

In some inorganic salt supporting electrolyte systems [1–3], the sensitivity of the determination of europium is unsatisfactory and many coexisting transition metal ions interfere. Some amine–carboxylic acid chelating agents such as EDTA have been used to improve the method for the determination of europium, but changes in pH strongly influence the peak height of the complex [4]. Li and Gao [5] proposed the Eu(III)–diethylenetriaminepentaacetic acid (DTPA) complex and showed that DTPA is better than EDTA for determining europium. In this paper it is demonstrated that most of the interferences can be removed by using the triethylenetetraaminehexaacetic acid (TTHA)– NH_4Cl – NH_3 system, because the stability constant of the Eu(III)–TTHA complex ($\log K > 23$) is much greater than that of

most transition metal ions with TTHA [6], and the half-wave potential of Eu(III)–TTHA is more negative than that of transition metal ion–TTHA and oxygen. The characteristics of the polarographic wave of Eu(III)–TTHA and the optimum conditions for the determination of europium were also studied.

EXPERIMENTAL

Apparatus

A JP-1A single-sweep oscilloscopic polarograph with three electrodes, a PAR-384A polarographic analyser with a Model 303A static mercury electrode, an HDV-7 potentiostat with a DCD-1 signal generator as a cyclic voltammetric analyser and a PHS-2 acidimeter were used. All potentials are given vs. SCE.

Correspondence to: C.-M. Wang, Department of Chemistry, Lanzhou University, Lanzhou, 730000 (China).

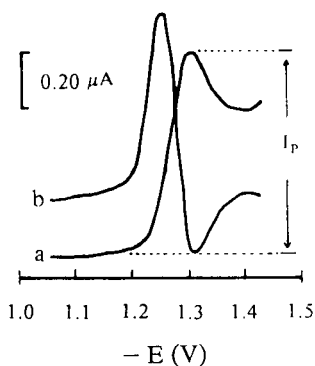


Fig. 1. Single-sweep oscillopolarogram. $0.1 \text{ mol l}^{-1} \text{ NH}_4\text{Cl} + 0.1 \text{ mol l}^{-1} \text{ NH}_3 + 4.0 \times 10^{-3} \text{ mol l}^{-1} \text{ TTHA} + 5.0 \times 10^{-5} \text{ mol l}^{-1} \text{ Eu(III)}$; $\text{pH} = 9.2$. (a) Normal wave; (b) derivative wave. Scan rate 250 mV s^{-1} .

Reagents

A standard solution of $1.0 \times 10^{-2} \text{ mol l}^{-1}$ Eu(III) was prepared by dissolving 175.9 mg of Eu_2O_3 in 5 ml of HCl (1 + 1) and diluting to 100 ml with water. Solutions of $2.0 \times 10^{-2} \text{ mol l}^{-1}$ TTHA, $0.5 \text{ mol l}^{-1} \text{ NH}_4\text{Cl}$ and $0.5 \text{ mol l}^{-1} \text{ NH}_3$ were prepared in the normal way with water. All other reagents were of analytical-reagent grade and doubly distilled water was used throughout.

Procedure

A 10-ml volume of the analytical solution (containing $4.0 \times 10^{-3} \text{ mol l}^{-1}$ TTHA, $0.1 \text{ mol l}^{-1} \text{ NH}_4\text{Cl}$ and $0.1 \text{ mol l}^{-1} \text{ NH}_3$ and a suitable amount of Eu^{3+}) was added to the cell and deoxygenated with nitrogen for 2 min. The potential scan was then performed in the range -1.0 to -1.5 V . The polarogram obtained is shown in Fig. 1.

RESULTS AND DISCUSSION

Choice of supporting electrolyte

The complex gives a polarographic wave in various supporting electrolytes such as KCNS, NH_4OAc , NH_4Cl , LiCl, NaNO_3 , NaClO_4 , HOAc-NaOAc , $\text{Na}_2\text{B}_4\text{O}_7$ and $\text{NH}_4\text{Cl-NH}_3$, but their wave shapes and sensitivity are different. The best wave shape and I_p was obtained in 0.1

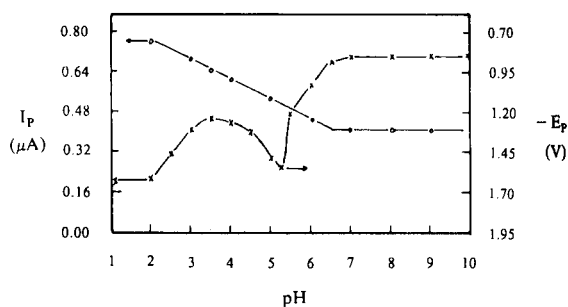


Fig. 2. Effect of pH on I_p and E_p . $5.0 \times 10^{-5} \text{ mol l}^{-1} \text{ Eu(III)}$ in the supporting electrolyte.

$\text{mol l}^{-1} \text{ NH}_4\text{Cl} - 0.1 \text{ mol l}^{-1} \text{ NH}_3$. Because many metallic ions can form complexes with TTHA, the concentration of TTHA in solution should be greater than the total concentration of all metal ions. The best results for determining europium in samples were obtained in $4.0 \times 10^{-3} \text{ mol l}^{-1}$ TTHA. In fact, a range of $5 \times 10^{-4} - 4 \times 10^{-2} \text{ mol l}^{-1}$ TTHA is satisfactory for determining Eu(III) alone.

Effect of pH

It can be seen from Fig. 2 that I_p and E_p are constant at $\text{pH} > 7$, which indicates that Eu(III) forms a stable complex with TTHA under these conditions. At $\text{pH} < 2$, $E_p = -0.75 \text{ V}$, which is near the half-wave potential of Eu(III) in HCl

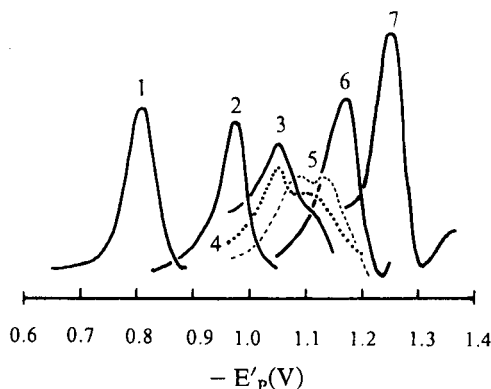


Fig. 3. Effect of pH on E'_p and derivative wave shape. $5.0 \times 10^{-5} \text{ mol l}^{-1} \text{ Eu(III)}$ in the supporting electrolyte. pH: (1) 3.5; (2) 4.6; (3) 5.0; (4) 5.2; (5) 5.4; (6) 5.7; (7) 8.2.

medium. This result showed that Eu(III)–TTHA does not exist in strongly acidic medium. The pH range 3–8 is of interest, where apparently two kinds of complexes can be formed under different pH conditions. Figure 3 shows the effect of pH on the derivative peak potential (E'_p) and the derivative peak shape. The peak shape undergoes a transformation from a single peak (curves 1 and 2) into a double peak (curves 3, 4 and 5) and then into a single peak (curves 6 and 7) again. The double peak probably corresponds to the reduction of $[\text{Eu(III)HL}]^{2-}$ and $[\text{Eu(III)L}]^{3-}$ ($\text{L}^{6-} = \text{TTHA}$ anion). Because a change in the acidity of the solution must cause a change in the conditional formation constants of both complexes [7,8], the fraction of both complexes in the solution would change. Each of them would react at different potentials at a dropping mercury electrode (DME) and produce two peaks [9] (according to Masuda et al. [6], $\log K_{\text{EuHL}} = 16.56$ and $\log K_{\text{EuL}} = 23.28$). This is why the derivative wave becomes wider and lower when the pH is increased from 3.5 to 5.7. At $\text{pH} > 7$, $[\text{Eu(III)L}]^{3-}$ would be the main species in solution so that the wave shape shows a single peak (Fig. 3) that does not change with further increase in pH (Fig. 2).

Linear range

Under the optimum conditions, there is a linear relationship between I_p and the concentration of Eu(III) over the range 2.5×10^{-6} – $5.0 \times$

10^{-4} mol l^{-1} . The regression equation derived from the calibration graph by the least-squares method is $I_p = 12581.0C + 0.0098$ with a regression coefficient of 0.9995 (where C is the molar concentration of europium).

Interference from coexisting ions

Under the optimum experimental conditions, many different metal ions do not interfere with the determination of Eu(III). Several interfering ions such as Bi(III), Fe(III), Se(IV) and As(III) can be removed by precipitation. Hydroxide and oxalic acid are effective precipitants. Table 1 shows the effect of coexisting ions.

Temperature coefficient

The temperature coefficient of I_p is 1.46% $^{\circ}\text{C}^{-1}$ in the range 13–30 $^{\circ}\text{C}$ and 0.45% $^{\circ}\text{C}^{-1}$ in the range 30–42 $^{\circ}\text{C}$. The positive temperature coefficient is indicative of the diffusion-limited character of the complex wave.

Effect of the height of the mercury reservoir on I_p

By d.c. polarography, I_p was found to be proportional to the square root of the height of the mercury reservoir. According to logarithmic analysis of the diffusion wave, the number of electrons transferred in the electrode reaction is $n = 1.04$ and $E_{3/4} - E_{1/4} = -52$ mV. These data show that the d.c. polarographic wave is a reversible diffusion wave.

TABLE 1
Effect of coexisting ions on peak height [5.0×10^{-5} mol l^{-1} Eu(III)]

Coexisting ion	Added (mg)	Relative error (%)	Coexisting ion	Added (mg)	Relative error (%)
Cu(II)	1.0	+3.6	Ca(II)	1.0	+1.9
Pb(II)	1.0	-7.1	Mg(II)	1.0	0.0
Zn(II)	1.0	0.0	Sr(II)	1.0	0.0
Cd(II)	1.0	-1.4	Ba(II)	1.0	+7.1
Sb(III)	1.0	+4.6	Al(III)	1.1	0.0
Ni(II)	1.0	-1.4	Ag(I)	0.1	0.0
Co(II)	1.0	-5.4	Fe(III)	1.0	-11.4
Th(IV)	1.0	+1.9	La(III)	1.4	+3.7
Zr(IV)	1.0	+1.9	Bi(III)	1.0	-70.4
Mo(VI)	0.2	+1.9	As(III)	0.1	-4.1
Mn(II)	0.22	+1.9	Se(IV)	0.01	-9.1

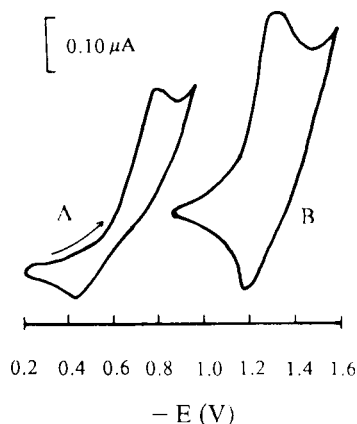


Fig. 4. Cyclic voltammograms: (A) $0.2 \text{ mol l}^{-1} \text{ NH}_4\text{Cl} + 1.0 \times 10^{-5} \text{ mol l}^{-1} \text{ Eu(III)}$; (B) $0.1 \text{ mol l}^{-1} \text{ NH}_4\text{Cl} + 0.1 \text{ mol l}^{-1} \text{ NH}_3 + 4.0 \times 10^{-3} \text{ mol l}^{-1} \text{ TTHA} + 5.0 \times 10^{-5} \text{ mol l}^{-1} \text{ Eu(III)}$. Scan rate 50 mV s^{-1} .

Cyclic voltammetry

The cyclic voltammogram is shown in Fig. 4. The reversibility of the complex wave is better than that of the simple ion wave.

Reduction mechanism of the complex

The electrochemical behaviour of the complex was studied by d.c. polarography, single-sweep polarography and cyclic voltammetry. The reduction process of the complex is different in acidic and alkaline media. The reduction process is accompanied by uptake of hydrogen ions in an acidic medium; the plot of E_p vs. pH is a straight line with the equation $E_p = -0.58 - 0.116\text{pH}$. The results show that two protons are added to TTHA. Hence the electrode reaction is $[\text{Eu(III)HL}]^{2-} + 2\text{H}^+ + e \rightarrow \text{Eu(II)} + \text{H}_3\text{L}^{3-}$. In the solution ($\text{pH} > 7$) E_p remains constant with

TABLE 2
Analytical results for Eu

Parameter	Experiment No.								
	1	2	3	4	5	6	7	8	9
Eu ₂ O ₃ content ($\mu\text{g g}^{-1}$)	228.0	220.0	228.0	228.0	228.0	211.2	211.3	220.0	211.2
Average Eu ₂ O ₃ content ($\mu\text{g g}^{-1}$)	221.0								
Standard deviation ($\mu\text{g g}^{-1}$)	8.2								
Relative standard deviation (%)	3.7								
Eu ₂ O ₃ content by ICP-AES ($\mu\text{g g}^{-1}$)	218.4								

TABLE 3

Recovery of Eu from a 50-mg sample

Sample No.	Eu ₂ O ₃ added	Eu ₂ O ₃ found (μg)	Amount recovered (μg)	Recovery (%)
1	0	11.0	–	–
2	0	10.8	–	–
3	17.6	29.0	18.1	102.8
4	35.2	44.0	33.1	94.0
5	70.4	77.7	66.8	94.9

increasing pH and the electrode reaction can be written as $[\text{Eu(III)L}]^{3-} + e \rightarrow \text{Eu(II)} + \text{L}^{6-}$. The reversibility of the electrode reaction in alkaline medium is better than that in acidic medium.

Determination of Eu in rare earth oxide

A small amount of sample (about 0.05 g) was dissolved in 5 ml of $6 \text{ mol l}^{-1} \text{ HCl}$ and several drops of H_2O_2 and 0.1 g of NH_4Cl were added. The solution was heated nearly to dryness, then 2 ml of water were added and the mixture was heated nearly to dryness again. After cooling, the residue was dissolved with water and the solution was transferred into a 25-ml flask. A small amount of the solution (1–5 ml, depending on the europium content in the sample) can be used to determine europium under the optimum conditions. The results are given in Table 2 and the recovery of europium is shown in Table 3.

REFERENCES

- W. Noddack and A. Bruckl, *Angew. Chem.*, 50 (1937) 362.
- L. Holleck., *Z. Elektrochem.*, 46 (1940) 69.

- 3 H.A. Laitinen and W.A. Ziegler, *Ind. Eng. Chem., Anal. Ed.*, 13 (1941) 852
- 4 E.I. Onstott, *J. Am. Chem. Soc.*, 74 (1952) 3773.
- 5 R.-L. Li and X.-X. Gao, *Chem. J. Chin. Univ.*, 2 (1981) 25.
- 6 Y. Masuda, T. Nakamori and E. Sekido, *Nippon Kagaku Kaishi*, 74 (1978) 199.
- 7 W.L. Masterton and E.J. Slowinski, *Chemical Principles*, Beijing University Press, Beijing, 1980.
- 8 Laitinen and Harris, *Chemical Analysis*, McGraw-Hill, New York, 2nd ed., 1975 pp. 27–216.
- 9 X.-X. Gao, *Polarographic Catalytic Wave* (in Chinese), Science Press, Beijing, 1991.

Simultaneous determination of copper, nickel, lead, cobalt and cadmium by adsorptive voltammetry

Zheng-Qi Zhang, Sheng-Zong Chen, Hui-Min Lin and Hong Zhang

Department of Chemistry and Chemical Engineering, Hunan University, Changsha 410082 (China)

(Received 22nd April 1992; revised manuscript received 24th September 1992)

Abstract

The synthesis of 1-(2-pyridylazo)-2,7-dihydroxynaphthalene (2,7-PADN) and the electroanalytical characteristics of its metal complexes are reported. In pH 9.80 buffer solution the complexes of copper, nickel, lead, cobalt and cadmium with 2,7-PADN give sensitive adsorption polarographic waves at -0.35 , -0.45 , -0.49 , -0.60 and -0.67 V, respectively, which can be used to determine trace amounts of these elements, the detection limits being 8.0, 5.0, 2.5, 0.5 and 5.0 nM, respectively.

Keywords: Polarography; Voltammetry; Cadmium; Cobalt; Copper; Lead; Nickel

Anodic stripping voltammetric procedures for copper, cadmium, lead and zinc have been reported [1–7]. These elements have also been determined by potentiometric stripping analysis [8]. In recent years, adsorptive voltammetry and adsorptive stripping voltammetry have attracted much attention for the determination of trace and ultratrace components [9–11]. In these two techniques the adsorption of a metal chelate at a mercury electrode, as an effective preconcentration step, is related to the structure of the ligand. Hence the synthesis of new organic chelating agents is desirable for increasing the sensitivity of adsorptive stripping voltammetry [12,13].

Recently, the azo compound 1-(2-pyridylazo)-2,7-dihydroxynaphthalene (2,7-PADN), which had not been described previously, was synthesized, and was used to determine lead at levels down to 10^{-11} M in the presence of 0.0011% Triton X-100

by adsorptive voltammetry [14]. A great advantage of 2,7-PADN, compared with 4-[2-(5-bromopyridyl)azo]-1,3-dihydroxynaphthalene (5-Br-PADN) [12] and 5-[(*p*-methylphenyl)azo]-8-aminoquinoline (*p*-MPAQ) [13], is the possibility of simultaneously determining several metal ions by adsorptive voltammetry. This paper describes a sensitive adsorptive voltammetric procedure for the simultaneous determination of trace amounts of copper, nickel, lead, cobalt and cadmium.

EXPERIMENTAL

Apparatus

Single-sweep polarograms were recorded on a JP-1A polarograph (Chengdu Instrumental Factory). The polarographic cell has a three-electrode system: a dropping mercury electrode (DME) as the working electrode, a saturated calomel electrode as the reference electrode and a platinum wire auxiliary electrode. The pulse polarograms and cyclic voltammograms were

Correspondence to: Z.-Q. Zhang, Department of Chemistry and Chemical Engineering, Hunan University, Changsha, 410082 (China).

recorded on an M270 electrochemical analysis system (EG&G PAR), using a Model 303 static mercury drop electrode (EG&G PAR) as the working electrode.

Reagents and solutions

Reagents were of analytical-reagent grade. Water, redistilled in a fused-silica apparatus, was used throughout. Stock solutions of copper(II), nickel(II), lead(II), cobalt(II) and cadmium(II) were prepared by dissolving 0.250 g of copper sulphate [$\text{CuSO}_4 \cdot 5\text{H}_2\text{O}$], 0.290 g of nickel nitrate [$\text{Ni}(\text{NO}_3)_2 \cdot 6\text{H}_2\text{O}$], 0.331 g of lead nitrate [$\text{Pb}(\text{NO}_3)_2$], 0.238 g of cobalt chloride [$\text{CoCl}_2 \cdot 6\text{H}_2\text{O}$] and 0.258 g of cadmium sulphate [$3\text{CdSO}_4 \cdot 8\text{H}_2\text{O}$] in 50 ml of 0.5 M hydrochloric acid and diluting to 1000 ml. The solutions were standardized volumetrically with EDTA. Solutions of lower concentration were prepared by serial dilution. A standard mixture was prepared by mixing the stock solutions of the metal ion. An ethanolic solution of 2,7-PADN was prepared by dissolving 0.226 g of 2,7-PADN in 1000 ml of absolute ethanol.

Synthesis of 2,7-PADN

n-Butyl nitrite was prepared according to Noyes [15] and dried with magnesium carbonate. 2-Aminopyridine was dissolved in sodium ethylate and mixed with *n*-butyl nitrite in a 1:1 molar ratio. The mixture was refluxed on a water-bath. After cooling, the light yellow diazotate was isolated by adding diethyl ether. The diazotate was mixed with 2,7-dihydroxynaphthalene in absolute ethanol in a 1:1.1 molar ratio and the mixture was stirred for 24 h at room temperature. The dark-red precipitate was isolated by addition of water. The dried precipitate was recrystallized from aqueous ethanol (1 + 1) (yield about 80%). The reagent was purified for electroanalytical purposes by chromatography on a column of Polyamide 6 (Beijing Chemical). The purity of the reagent was checked and it was ensured that only the polarographic wave of 2,7-PADN was present in single-sweep polarograms. Elemental analysis: $\text{C}_{15}\text{H}_{11}\text{N}_3\text{O}_2$ requires C 67.92, H 4.18, N 15.84 and O 12.06; found, C 67.85, H 4.22, N 15.88, O 12.05%.

Adsorptive voltammetry of the pure metal ion solution

A 0.25-ml volume of 1.0×10^{-3} M 2,7-PADN solution, 2.0 ml of ammonia–ammonium chloride buffer solution (pH 9.80) and a suitable volume of the standard mixture were mixed, and set aside for 7 min for complete complex formation. After diluting to 10 ml with redistilled water, the solution was transferred into the polarographic cell and purged with oxygen-free nitrogen for 10 min. A flow of nitrogen over the cell was maintained throughout the analysis to prevent interference from oxygen. The derivative polarogram was recorded.

Analysis of samples

A 0.2–0.4-g amount of human hair was weighed and washed with acetone, chloroform and shampoo, then thoroughly with deionized water. The samples were digested in perchloric acid at 200°C until the sample was colourless. Tea samples were digested with $\text{HNO}_3\text{--HClO}_4\text{--H}_2\text{SO}_4$. An appropriate amount of the digested hair or treated tea sample was placed in a 10-ml volumetric flask, then analysis was performed as described above for pure metal ion solution.

Recovery experiments

A standard mixture containing copper, nickel, lead, cobalt and cadmium ions was placed in a 50-ml beaker containing the sample. The mixture was then treated and analysed as described above.

RESULTS AND DISCUSSION

Single-sweep polarography

The reagent 2,7-PADN gives a polarographic reduction wave. The peak potential shifts in the negative direction with increasing pH of the test solution. In a weakly basic solution 2,7-PADN reacts with copper(II), nickel(II), lead(II), cobalt(II) and cadmium(II) to form purple–red complexes which give new polarographic reduction waves.

Figure 1 shows the derivative single-sweep polarograms of these metal complexes. In pH 9.80 buffer solution the peak potential of 2,7-PADN is

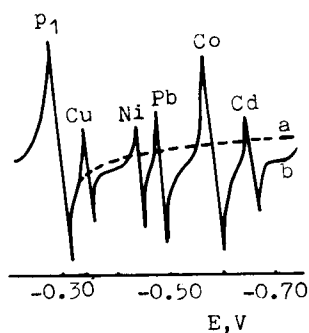


Fig. 1. Derivative polarograms. (a) pH 9.80; [2,7-PADN] = 2.5×10^{-5} M; (b) as (a) + 1.0×10^{-7} M metal ions.

–0.30 V and those of the complexes are –0.35, –0.45, –0.49, –0.60 and –0.67 V, respectively. These polarographic reduction waves can be used to determine trace amounts of copper, nickel, lead, cobalt and cadmium.

Adsorptive characteristics of the Pb(II)–2,7-PADN complex

The electrochemical characteristics of the complex of lead with 2,7-PADN were investigated. The adsorption of this complex at the mercury electrode was demonstrated by constructing electrocapillary curves and by carrying out medium-exchange experiments.

The electrocapillary curve of a buffer solution containing 2,7-PADN is lower than that of the pure buffer, and the electrocapillary curve of the solution containing the Pb(II)–2,7-PADN complex was lower still than that of the 2,7-PADN solution, indicating that 2,7-PADN and its lead(II) complex are both adsorbed at the mercury drop electrode.

For medium-exchange studies, the hanging mercury drop electrode used as a working electrode was kept in contact with a stirred solution containing the Pb(II)–2,7-PADN complex for 5 min. Subsequently, the electrode was cleaned carefully and transferred into the measuring cell containing the background solution only. The reduction process shown in the voltammogram obtained in the measuring cell closely resembled those in the preconcentration cell.

The normal-pulse polarogram of the Pb(II)–2,7-PADN complex has a maximum, indicating

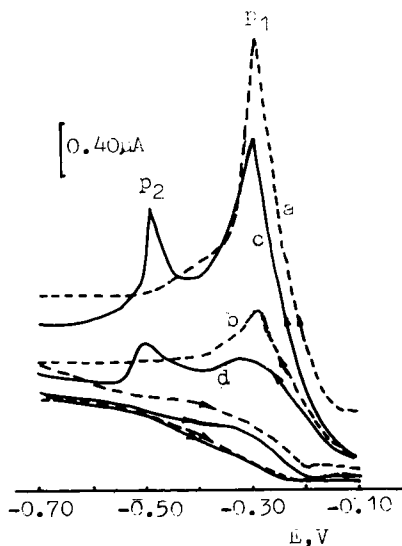


Fig. 2. Cyclic voltammograms. pH 9.80; scan rate, 100 mV s^{-1} . Dashed lines, [2,7-PADN] = 2.5×10^{-5} M; solid lines, [2,7-PADN] = 2.5×10^{-5} M and $[\text{Pb}^{2+}] = 5.0 \times 10^{-7}$ M. (a, c) First scan; (b, d) second scan. reference electrode, SCE; electrode area, 0.020 cm^2 .

that the adsorption process of the complex was essentially reactant adsorption [16].

Cyclic voltammetry

The cyclic voltammograms of the Pb(II)–2,7-PADN system are shown in Fig. 2. Over the range from –0.10 to –0.70 V there is no cathodic or anodic peak of lead(II) in ammonia–ammonium chloride solution (pH 9.80). In this solution, starting the first scan (Fig. 2 curve c), resulted in two distinct cathodic peaks due to the reduction of the adsorbed dye (at –0.30 V) and the adsorbed complex (at –0.49 V). No oxidation

TABLE 1

Molar ratio between the analytes in test solution ($[\text{co-existing ion}]/[\text{analyte}]$)

Analyte	Coexisting ion				
	Cu ²⁺	Ni ²⁺	Pb ²⁺	Co ²⁺	Cd ²⁺
Cu ²⁺	–	30	30	30	40
Ni ²⁺	30	–	50	30	40
Pb ²⁺	40	40	–	30	50
Co ²⁺	80	80	50	–	50
Cd ²⁺	100	80	60	40	–

TABLE 2
Simultaneous determination of Cu, Ni, Pb, Co and Cd in tea and hair samples

Sample	Added ($\mu\text{g g}^{-1}$)					Found ($\mu\text{g g}^{-1}$) ^a					Recovery (%)					Content ($\mu\text{g g}^{-1}$) ^b		
	Cu	Ni	Pb	Co	Cd	Cu	Ni	Pb	Co	Cd	Cu	Ni	Pb	Co	Cd	Cu	Pb	Cd
Tea No. 1	0	0	0	0	0	9.80	2.43	2.03	0.95	0.12								
No. 2	0	0	0	0	0	7.12	1.58	1.12	0.76	0.085								
No. 3	0	0	0	0	0	10.3	1.40	1.67	0.88	0.098								
	5.00	5.00	1.00	1.00	0.50	15.0	6.15	2.60	1.80	0.63	94.0	95.0	93.0	92.0	106	11.5	1.63	0.090
	10.0	10.0	5.00	5.00	1.00	20.5	11.1	6.60	5.90	1.06	102	97.0	98.0	100	96.2			
	25.0	20.0	10.0	10.0	5.00	35.0	21.6	11.5	10.6	5.07	98.8	102	98.3	97.2	99.4			
Hair	0	0	0	0	0	31.7	3.64	23.1	0.98	0.60						31.5	23.5	0.58
	15.0	1.00	10.0	0.50	0.50	46.0	4.68	32.6	1.42	1.13	95.3	104	95.0	88.0	106			
	30.0	5.00	20.0	1.50	3.00	62.0	8.56	42.8	2.43	3.66	101	98.0	98.5	96.7	102			
	60.0	15.0	40.0	5.00	8.00	91.2	18.3	63.5	5.90	8.50	99.2	97.7	101	98.4	98.7			

^a Mean of three parallel determinations. ^b Determined by the method described in the literature [11].

peak of the dye and the complex is observed on the anodic branch, which indicates that the reduction of 2,7-PADN and its lead complex is irreversible. Subsequent repetitive scans yielded significantly smaller (but stable) cathodic peaks corresponding to the reduction of dissolved species. This behaviour indicates that the dye and complex are adsorbed at the mercury electrode [17]. The width at half-height of peak p_2 was determined (curve c) and found to be 40 mV, so the value of αn_α can be calculated to be 1.56 [18].

Optimum conditions

Preliminary experiments were performed with a solution containing 50 nM each of Cu^{2+} , Ni^{2+} , Pb^{2+} , Co^{2+} and Cd^{2+} . The experiments showed that the main factors affecting the peak current of the complexes include the pH, the amount of 2,7-PADN added, the volume fraction of ethanol in the test solution and the standing time of the test solution. The composition of the background solution of this system was optimized by using a modified simplex procedure. The initial simplex was set up with the aid of homogenetic experimental designs [19]. The optimum background solution composition found was as follows: pH 9.80, 2.5×10^{-5} M 2,7-PADN and 2.5% (v/v) ethanol; the optimum standing time was 7 min. Under these optimum conditions, the peak height of the complexes is stable for 10 h.

The detection limits, taken as the concentration that gave a signal equal to three times the standard deviation of the blank signal, calculated from the calibration slopes, for the simultaneous determination of copper, lead, cobalt, nickel and cadmium, were 8.0, 2.5, 0.5, 5.0 and 5.0 nM, respectively. The reproducibility was evaluated by fifteen repetitive measurements on a solution containing 20 nM each of copper, nickel, lead and cadmium and 10 nM cobalt. The relative standard deviations were 1.5, 2.7, 1.8, 2.5 and 2.8%, respectively.

Interference from coexisting ions

The simultaneous determination of five metal ions by adsorptive voltammetry requires careful attention to the concentration ratio at which the metal ions are present. A large excess of one

metal ion may affect the response of the others via competition for the complexing ligand and a change in the coverage of the electrode surface. Table 1 shows the molar ratio between analytes in a test solution which do not interfere in the determination of the analyte.

The effect of other metal ions such as Fe^{3+} , Mn^{2+} , Al^{3+} , Ca^{2+} , Mg^{2+} , Ba^{2+} and Zn^{2+} was investigated by adding the appropriate amounts of the metal ion solutions to 10 ml of solution containing 50 nM each of copper(II), nickel(II), lead(II), cobalt(II) and cadmium(II). Interference was taken as the level causing an error in excess of 10%. The amounts that did not interfere were 2.0 mg each of Ca^{2+} , Mg^{2+} and Ba^{2+} , 0.50 mg of Al^{3+} , 0.10 mg of Mn^{2+} , 50 μg of Zn^{2+} and 10 μg of Fe^{3+} .

Application

The method was applied to the simultaneous determination of copper, nickel, lead, cobalt and cadmium in human hair and tea samples.

Calibration graphs were constructed by treating the standard mixture according to the procedure described for the analysis of samples. The regression equations for the calibration lines were as follows for copper, $y = 8.12x - 0.053$ ($r = 0.999$); for nickel, $y = 4.00x - 0.009$ ($r = 0.998$); for lead, $y = 1.32x - 0.007$ ($r = 0.996$); for cobalt, $y = 3.74x - 0.011$ ($r = 0.999$); and for cadmium, $y = 2.57x - 0.004$ ($r = 0.997$), where y is the peak current in μA and x is the concentration of the metal ion in $\mu\text{g ml}^{-1}$. There was linearity between peak current and concentration in the concentration ranges 0.6–64 ng ml^{-1} for copper, 0.5–60 ng ml^{-1} for nickel, 2.0–200 ng ml^{-1} for lead, 0.05–60 ng ml^{-1} for cobalt and 1.0–100 ng ml^{-1} for cadmium. The results for the determination of the metals and the recovery of added metal ions by using the recommended method are summarized in Table 2.

REFERENCES

- 1 T.M. Karadakhli, F.M. Najib and F.A. Mohammed, *Talanta*, 34 (1987) 995.

- 2 E. Casassas, A.M. Perez-Vendrell and L. Puignou, *Int. J. Environ. Anal. Chem.*, 45 (1991) 55; C.A.116 (1992) 65952v.
- 3 A. Cardo Alberola and C. Mongay Fernandez, *Quim. Ind.*, 34 (1988) 339; C.A., 112 (1990) 164607k.
- 4 Y.H. Cui, Z.-Y. Zhang and Q.-O. Wang, *Zhonghua Yixue Jianyan Zazhi*, 14 (1991) 9.
- 5 S.-Z. Yao, L.-P. He, B.-H. Zhu and Y.-X. Wu, *Fenxi Huaxue*, 18 (1990) 65.
- 6 Y. Cai, *Huanjing Baohu*, (1989) 30; C.A.111 (1989) 201243r.
- 7 W.-Z. Chen and J.-H. Chen, *Fenxi Huaxue*, 9 (1991) inside back cover; C.A.116 (1992) 50439j.
- 8 L. Almestrand, D. Jagner and L. Renman, *Talanta*, 33 (1986) 991.
- 9 J. Wang, in A.J. Bard (Ed.), *Electroanalytical Chemistry*, Vol. 16, Wiley, New York, 1989, p.1.
- 10 T.-G. Wu and J.L. Wong, *Anal. Chim. Acta*, 246 (1991) 301.
- 11 F.-C. Meng and Z.-F. Zhao, *Fenxi Huaxue*, 13 (1985) 167.
- 12 Z.-Q. Zhang, *Mikrochim. Acta*, I (1991) 89.
- 13 Z.-Q. Zhang, Z.-P. Chen, S.-Z. Cheng and G.-F. Yang, *Talanta*, 38 (1991) 1487.
- 14 H.-M. Li, Thesis, Hunan University, 1991.
- 15 W.A. Noyes, *Org. Synth.*, Collect. Vol. 2, 1955, p.108.
- 16 M. Lovric, *J. Electroanal. Chem.*, 170 (1984) 143.
- 17 S. Dong, *Fenxi Yiqi*, No. 1 (1984) 1.
- 18 E. Laviron, *J. Electroanal. Chem.*, 52 (1974) 355.
- 19 X. Wang, B. Deng and J. Qin, *Fenxi Shiyanshi*, No. 4 (1986) 46.

Determination of colloidal electrolytes: conductimetric titration of hydroxyzine hydrochloride with ammonium molybdate

Ryszard Mikulski and Brunon Dembiński

Institute of Chemistry, N. Copernicus University, ul. Gagarina 7, PL-87 100 Toruń (Poland)

(Received 15th June 1992; revised manuscript received 29th September 1992)

Abstract

A solution containing 1–30 mg of hydroxyzine hydrochloride can be titrated conductimetrically with ammonium molybdate. The proposed method was checked by the determination of hydroxyzine hydrochloride in a Hydroxyzinum preparation.

Keywords: Conductimetry; Titrimetry; Colloidal electrolytes; Hydroxyzine hydrochloride; Pharmaceuticals

Colloidal electrolytes are widely used in the pharmaceutical industry, which has led to the need for methods for the determination of such compounds, especially when present in low concentrations. Hydroxyzine hydrochloride (2-(2-[4-(*p*-chloro- α -phenylbenzyl)-1-piperazinyl]ethoxy) ethanol dihydrochloride, applied, e.g., in Atarax, Hydroxyzinum, Masmoran or Vistaril preparations) is used as a psychotropic drug that acts on the nervous system, lessening its irritability. An aqueous solution of hydroxyzine hydrochloride exhibits colloidal properties and forms a poorly soluble compound with ammonium molybdate. Ammonium molybdate was used earlier with success to determine dodecylquinolinium bromide by amperometric titration [1]. Gravimetry, titrimetry and some instrumental techniques (spectrophotometry, polarography, amperometry, potentiometry) are the methods most often used to determine psychotropic drugs [2–6].

The conductance titration of substances is possible if a reaction occurs in which one ion is substituted for a second ion of different mobility either before or after the equivalence point. The conductance method is well suited for the determination of the end-points in precipitation titrations. The shape of the titration curve can be predicted by summing the ionic conductances of the various species at any point during the course of titration. The solubility of the precipitate that has been formed will affect the titration curve. Whereas this effect will make gravimetric analysis impossible, it can be tolerated in conductimetric titration, the only effect being that appreciable solubility of the precipitate leads to a rounding off of the intersection of the branches of the graph.

EXPERIMENTAL

Materials

Hydroxyzine hydrochloride was obtained from Polfa (Poland). The purity of the compound, pre-

Correspondence to: R. Mikulski, Institute of Chemistry, N. Copernicus University, ul Gagarina 7, PL-87 100 Toruń (Poland).

viously dried at 378 K for 2 h, was determined by titrating the base content after extraction with 0.1 M perchloric acid in chloroform [7]. The content of ammonium molybdate, $(\text{NH}_4)_6\text{Mo}_7\text{O}_{24} \cdot 4\text{H}_2\text{O}$, was determined titrimetrically according to the literature [8]. Molybdates [Mo(VI)] were quantitatively reduced in 2 M hydrochloric acid solution at 333–353 K by silver to Mo(V) and the latter was titrated with standard cerium (IV) sulphate solution using ferroin of *N*-phenylanthranilic acid as indicator. All solutions serving for measurements were prepared by dissolving the appropriate amount of compound in 15 ml of triply distilled water. The measurements were done with a type E315A automatic conductivity meter (Meratronik, Poland) and a type OK 0907P conductimetric bell-shaped electrode (Radelkis, Hungary).

Procedure

Measurements were made in aqueous medium below the critical micelle concentration (the CMC at 298 K is $4.17 \times 10^{-4} \text{ mol l}^{-1}$) [9]. After each addition of 0.1 ml of titrant the solution was stirred for 2 min and left for 2 min in order to attain equilibrium. Titration was performed at 298 K. The concentration of the titrant reagent was 5–6 times higher than that of the titrant. The determination was repeated five times and mean values were calculated. Considering the change in

volume, the values observed were corrected by multiplication by a factor $(V + v)/V$, where V is the volume of the original solution and v is the volume of titrant added. This correction can be minimized by using a titrant that is much more concentrated than the sample solution. If the ratio of molarities is at least 20:1 the correction can be neglected for most systems.

RESULTS AND DISCUSSION

On the addition of ammonium molybdate, a precipitate is formed in the solution. With the formation of this precipitate, a longer period of time is required for the solution to equilibrate so that the conductance can be measured. On the titration curve an end-point is seen that corresponds to a 1:5 mole ratio. The precipitate that is formed consists of $(\text{C}_{21}\text{H}_{27}\text{ClN}_2\text{O}_2)_5(\text{NH}_4)\text{Mo}_7\text{O}_{24}$. The shape of the conductimetric titration curve in the investigated range of concentrations shown in Fig. 1 is typical of this type of determination.

The end-point was obtained by extrapolation of the two linear branches of the plot. The maximum difference between the lowest and the highest results in a separate series of determinations at concentrations up to 0.5 mmol l^{-1} was < 8%. During the titration of solutions of concentra-

TABLE 1

Results of conductimetric titration of hydroxyzinum hydrochloride with ammonium molybdate

Concentration of hydroxyzinum hydrochloride (mmol l^{-1})	Amount of hydroxyzinum hydrochloride taken (y) (mg)	Amount of hydroxyzinum hydrochloride found (y_m) (mg)	Standard deviation ^a , S_r ^b (mg)	Error, S_m ^c (%)
0.146	0.982	1.001	0.040	+1.96
0.231	1.554	1.568	0.044	+0.92
0.567	3.806	3.823	0.095	+0.44
1.020	6.855	6.838	0.110	-0.25
1.147	7.704	7.695	0.155	-0.12
1.554	10.44	10.45	0.19	+0.16
2.032	13.65	13.63	0.22	-0.10
3.484	23.40	23.45	0.24	+0.25
4.474	30.05	30.21	0.28	+0.52

^a $n = 5$. ^b $S_r^2 = (\sum_{i=1}^m S_r^2)/m$. The standard error (S_e) of the conductimetric method (where $m = 9$), as found on the basis of the sampling distribution, is 0.173 mg. ^c $S_m = 100(y_m - y)$.

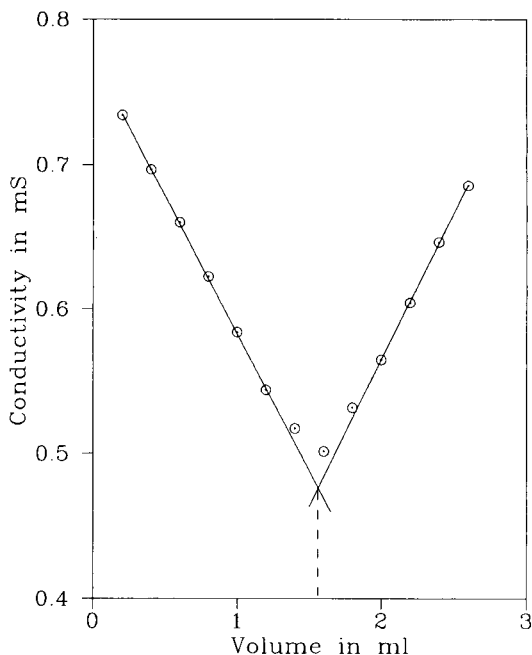


Fig. 1. Conductimetric titration curve for hydroxyzine hydrochloride (11.14 mg in a 15-ml sample) with ammonium molybdate (4.434 mg ml^{-1}).

tions $> 0.5 \text{ mmol l}^{-1}$, the variation in the results reached a maximum of 4%. The bias in the analytical results in the investigated range of concentrations did not exceed 2%. The mean results of measurements for several concentrations of titrations are presented in Table 1.

In order to prove the usefulness of the elaborated method, the determination of hydroxyzine hydrochloride in Hydroxyzinum dragées was carried out. Hydroxyzinum dragées (Polfa) with a declared content of 10 mg were used for the determinations. Before dissolution the dragées were powdered in an agate mortar. Four solutions were prepared in volumetric flasks (100 ml), containing 4, 8, 12 and 16 dissolved dragées.

TABLE 2

Conductimetric determination of hydroxyzine hydrochloride in Hydroxyzinum dragées

Sample No. of dragées	Hydroxyzine content (mg in 15 ml)	Hydroxyzine found (mg)	Standard deviation ^a (mg)
4	6.0	5.94	0.11
8	12.0	11.85	0.20
12	18.0	18.20	0.24
16	24.0	24.6	0.30

^a $n = 5$.

Volumes of 15 ml of the prepared solutions were taken for analysis. The further procedure was as described above. The results of the determinations are given in Table 2.

It can be concluded that the proposed conductimetric titration method is rapid and accurate, and does not need an expensive reagent for the determination of hydroxyzine hydrochloride. It has been confirmed by the analysis of a Hydroxyzinum preparation that the method is useful for small amounts of the compound and suitable for use in drug-checking laboratories.

REFERENCES

- 1 R. Mikulski, *Anal. Chim. Acta*, 236 (1990) 325.
- 2 M. Lopes, and A.M. Leal, *Rev. Pharm. Port.*, 8 (1958) 14; *C.A.*, 53 (1959) 14421.
- 3 A. Danek, *Diss. Pharm.*, 13 (1961) 149.
- 4 B. Dembiński, *Chem. Anal. (Warsaw)*, 32 (1987) 763.
- 5 J. Blažek, V. Spinkova and Z. Strijskol, *Pharmazie*, 17 (1962) 487; 22 (1967) 130.
- 6 G. Dusinsky, *Pharmazie*, 12 (1957) 309.
- 7 *Pharmacopeia USPC No. 22*, Inc. 12061, United States Pharma. Copeial Convention, 1990, p. 674.
- 8 A.J. Vogel, *Text Book of Quantitative Inorganic Analysis*, Longman, London, 4th ed., 1978, p. 367.
- 9 R. Mikulski, in preparation.

Determination of chemical oxygen demand by a flow-injection method using cerium(IV) sulphate as oxidizing agent

Takashi Korenaga, Xiaojing Zhou, Kimiko Okada and Tosio Moriwake
Faculty of Engineering, Okayama University, 3-1-1 Tsushima-naka, Okayama 700 (Japan)

Sumio Shinoda

Faculty of Pharmaceutical Sciences, Okayama University, 1-1-1 Tsushima-naka, Okayama 700 (Japan)

(Received 12th September 1992)

Abstract

A method based on flow injection was developed for the automated determination of chemical oxygen demand (COD) that provided a number of possibilities for improvement of the limitations of the standard manual methods. The strong oxidizing agent used is cerium(IV) sulphate, which resulted in a high degree of sample oxidation under mild operating conditions. The reaction between samples and cerium(IV) ion produced a sensitive and reproducible signal, i.e., a decrease in absorbance. The detection limit and relative standard deviation of the method were 0.5 mg l^{-1} and 0.6% ($n = 10$), respectively, for a standard sample consisting of L-glutamic acid and lactose in a ratio of 5:1. When $50\text{-}\mu\text{l}$ samples were injected at a frequency of 20 h^{-1} , the determination range was $0.5\text{--}130 \text{ mg l}^{-1}$ COD. Chloride was tolerated up to a concentration of 30 g l^{-1} without any masking agents. COD values for various types of wastewater samples correlated well with those obtained by standard manual methods.

Keywords: Flow injection; UV-Visible spectrophotometry; Cerium(IV) sulphate; Chemical oxygen demand; Waters

Chemical oxygen demand (COD) refers to the oxygen required for complete oxidation of a water sample, and is a widely used parameter in controlling the degree of pollution in water and managing effluent quality. The conventional method for COD determination is manual and is based on titration of the samples with a toxic reagent such as potassium permanganate or potassium dichromate. This type of standard manual method is time consuming and its accu-

racy depends on operator skill. Much effort has been devoted to the improvement and alteration of the standard manual methods [1–7]. In 1980, the first flow-injection analyser for continuous monitoring of COD was developed by Korenaga [1]. Appleton and Tyson [5] investigated an automated method with a commercial flow-injection system. These methods applied to COD determination are capable of maintaining a consistently high sample throughput in a reproducible manner. However, the main problems still to be resolved are the toxic effluent produced during the COD determination and the complicated operating conditions necessary to obtain a high degree of sample oxidation.

Correspondence to: T. Korenaga, Faculty of Engineering, Okayama University, 3-1-1 Tsushima-naka, Okayama 700 (Japan).

This paper describes an attempt to utilize less hazardous cerium(IV) sulphate as the oxidizing agent for the determination of COD employing the flow-injection method. Ce(IV) is not only non-toxic, but also has a higher redox potential than Mn(VII) and Cr(VI). The determination of COD by this means can be carried out under milder and simpler conditions than other published flow-injection methods, without the need for any catalyst. A double-plunger micropump adopted in this flow system features very short strokes (1 mm) and small plunger diameter (2.5 mm) to provide constant reciprocal feeding of very small amounts ($4.9 \mu\text{l}$) of solution with a characteristic phase shift of 180° . Such a micropump can facilitate sample/reagent homogenization, leading to an increase in the degree of sample oxidation.

EXPERIMENTAL

Reagents

All chemicals were of analytical-reagent grade.

Standard solution for COD determination. The aqueous standard solution contained various concentrations of L-glutamic acid and lactose, which were mixed in weight proportions of 5 + 1.

Cerium(IV) sulphate-sulphuric acid solution. A 0.0997 g amount of cerium (IV) sulphate was dissolved in 1 l of distilled water containing 60 ml of sulphuric acid. The final concentrations in the reagent solution were 3.0×10^{-4} M Ce(IV) and 6% (v/v) sulphuric acid.

Apparatus and procedure

A schematic diagram of the flow system is shown in Fig. 1. The flow system should be built from parts that are resistant to oxidizing agents in order to ensure long-term operation. A Sanuki Model SR-3000 double-plunger micropump with a linear cam mechanism was used for stable delivery at low flow-rates. The reagent solution and carrier (distilled water) were both delivered by the micropump at a flow-rate of 0.2 ml min^{-1} . Sample solutions ($50 \mu\text{l}$) were injected into the carrier stream by an automatic sample injector. The two streams were merged, and mixing and

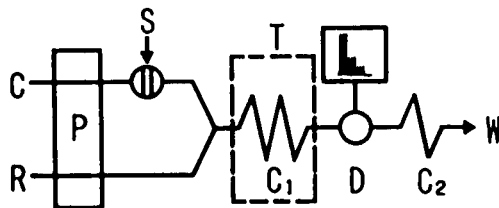


Fig. 1. Schematic diagram of the flow-injection system for COD determination. R = 3.0×10^{-4} M $\text{Ce}(\text{SO}_4)_2$ solution containing 6% sulphuric acid; C = carrier (distilled water); P = double-plunger pump; S = automatic sample injector ($50 \mu\text{l}$); T = thermostat (100°C); C₁ = reaction tube ($20 \text{ m} \times 0.5$ mm i.d.); C₂ = back-pressure tubing ($3 \text{ m} \times 0.25$ mm i.d.).

reaction occurred in a coiled reaction tube ($20 \text{ m} \times 0.5$ mm i.d.) the temperature of which was maintained at 100°C by an oil-bath. The absorbance change caused by a decrease in Ce(IV) concentration was measured by a spectrophotometric detector equipped with a flow-through cell (10-mm light path, $8\text{-}\mu\text{l}$ inner volume) and operated at 320 nm. The absorbance was continuously recorded.

RESULTS AND DISCUSSION

Oxidizing agent for COD determination

Extensive work on automatic COD determination has been accomplished using the flow-injection method with potassium dichromate or potassium permanganate as an oxidizing agent. However, this method necessitates complicated operating conditions such as high temperature and high acid concentration [5]; milder conditions than those employed in the standard manual method gave low results because there were stable compounds in the samples that resisted oxidation. Consequently, an alternative method for COD determination, if it can result in a high degree of sample oxidation under milder conditions, is most desirable. To achieve this, cerium (IV) sulphate was chosen as a suitable candidate and appears to have great promise.

Figure 2 illustrates the absorption spectra of Ce(IV) and Ce(III); maximum absorption of Ce(IV) is found at 320 nm. At this wavelength, the absorption of Ce(III) is negligible compared with

that of Ce(IV). This, combined with the highly efficient oxidation of samples, results in a detection limit that is considerably lower (0.5 mg l^{-1} COD) than that with the flow-injection method using potassium dichromate or potassium permanganate (5 mg l^{-1} COD) [1,3] as oxidizing agent. According to the half-reactions and thermodynamic data shown below, a major advantage of the present method is that the redox parameter of Ce(IV) is not as dependent on the pH values of solutions as are those of Cr(VI) and Mn(VII):

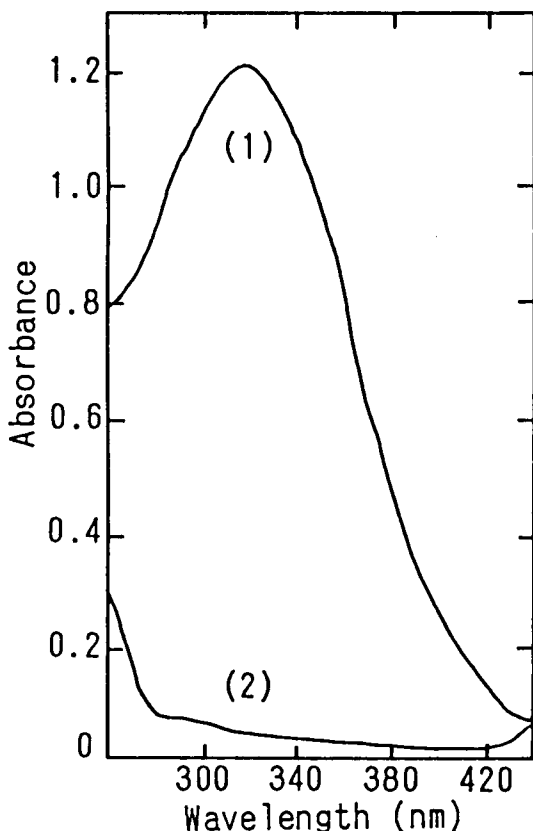
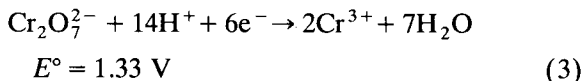
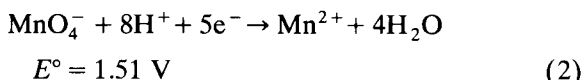
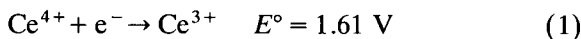


Fig. 2. Absorption spectra of (1) $2.0 \times 10^{-4} \text{ M Ce(IV)}$ and (2) $2.0 \times 10^{-4} \text{ M Ce(III)}$ in 3% sulphuric acid solution.

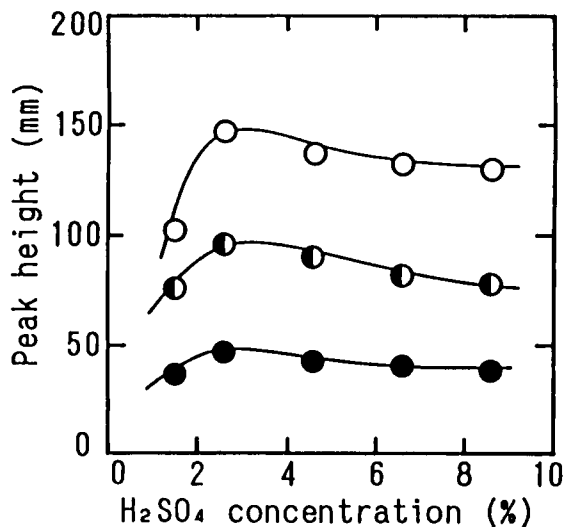


Fig. 3. Relationship between sulphuric acid concentration and response of flow-injection system to COD. $\circ = 100$; $\bullet = 50$; $\bullet = 20 \text{ mg l}^{-1}$ COD.

The experimental results shown in Fig. 3 confirmed this theoretical evaluation. When standard solutions with 20, 50 and 100 mg l^{-1} COD were individually injected into the carrier stream, and the concentration of sulphuric acid in the cerium(IV) sulphate solution exceeded 6%, the peak heights remained constant. In contrast to the flow-injection method using potassium dichromate or potassium permanganate, which requires a high acid concentration and leads to large blank peaks owing to the difference between the viscosities of the reagent stream and carrier stream, the present method has not only milder operating conditions, but also a stable baseline and very few blank peaks. Specifically, this method is not seriously impaired by impurities normally found in wastewater samples, and is free from interference from chloride because the use of low acid concentration inhibits the reactions of the interfering compounds with oxidizing agents. In acidic solutions, the solubility of cerium(IV) sulphate increased with decreasing sulphuric acid concentration, whereas its stability simultaneously decreased. A sulphuric acid concentration of 6% was therefore selected as the optimum to obtain a stable cerium(IV) sulphate solution with sufficiently high concentration.

At any possible range of solubility, the concentration of oxidizing agent was investigated to obtain rapid and effective oxidation of the samples, and to control the response (a transient negative departure from the steady-state absorbance) over a range that could be accurately determined. The optimum concentration for the oxidizing agent was found to be 3.0×10^{-4} M. After merging with the carrier stream, the reagent stream of this concentration showed an absorbance value of about 0.76.

Recent interest in the use of the present method is centred on continuous monitoring for diverse applications such as process control of wastewater treatment. Unfortunately, the technique does not lend itself to continuous monitoring when unattended over a long period, because the gradual self-decomposition of cerium(IV) sulphate solution may be more rapid than expected and its concentration should be checked every other day.

Development of instrument

To ensure the durability and reliability of the flow-injection systems, various types of pumping systems were tested with respect to various parameters. Peristaltic pumps are unsuitable for pumping strong oxidizing agents, especially when operating at high temperatures. The pump tubes quickly become fatigued and the flow-rate may be unstable, leading to excessive baseline drift and unreliable responses. Complete mixing between streams is vital for a high degree of sample oxidation and high reproducibility; however, syringe pumps are seriously lacking in their ability to intermix adjacent streams [8].

As demonstrated by previously published studies [8,9], the double-plunger micropump has a robust and exceptionally stable propulsion system that is more suitable for operations against a higher than normal back-pressure and for handling aggressive liquids such as organic solvents, strong acids and bases and oxidizing agents. This type of micropump appropriate for use in the determination of COD is based on slow reaction, because it can achieve complete mixing between the samples and the reagents and ensure great

smoothness of the flow-injection profiles and high reproducibility of the sample zone dispersion.

In the determination of COD, the reaction temperature has a strong influence on the response profiles. Heating the reaction tube usually results in higher sensitivity and better reproducibility, in addition to higher selectivity towards chloride owing to the reduced reaction time. A high-quality thermostat was employed for the precise control of reaction temperature. This thermostat can give thermal stability to better than $\pm 0.5^\circ\text{C}$ over a wide range of temperature. Further, back-pressure PTFE tubing (3 m \times 0.25 mm i.d.) was connected behind the flow cell to inhibit the formation of bubbles in the streams.

Optimization of operating conditions

Flow-injection systems for COD generally utilize a reagent solution containing a high concentration sulphuric acid. Merely mixing the reagent solutions and carrier streams thus generates a stream temperature of about 100°C even without heating [5], so that the precise control of reaction temperatures becomes difficult. This problem has been resolved here by the use of dilute sulphuric acid. The effect of temperature on the reaction between the samples and oxidizing agent was studied over the range $90\text{--}120^\circ\text{C}$, employing the thermostat. The results showed that a temperature of 100°C was most suitable for samples with a high COD value (Fig. 4A). On the other hand, when the temperature was higher than 110°C , the sensitivity of the samples with low COD values may be suitable but, as might be expected, the signal was very noisy. For this study the reaction tube was therefore immersed in an oil-bath at 100°C .

A low flow-rate is effective for gaining achieving reaction times with minimum sample dispersion. The effects of flow-rate on the sensitivity for COD determination and the residence time were investigated over the range $0.1\text{--}1.5$ ml min^{-1} , and a flow-rate of 0.2 ml min^{-1} was chosen as a compromise between the sensitivity and sampling frequency. Obviously, a low flow-rate results in a reduction in reagent consumption. At a flow-rate of 0.2 ml min^{-1} , the consumption of reagent

solution was less than 300 ml day⁻¹, causing few problems in the wastewater treatment.

the diameter and length of reaction tube are also important factors affecting reaction times and response profiles. The effect of reaction tube length was examined using PTFE tubing of 0.5 mm i.d. and injecting standard solutions with COD values of 20, 50 and 100 mg l⁻¹. As shown in Fig. 4B, a reaction tube of length 20 m gave

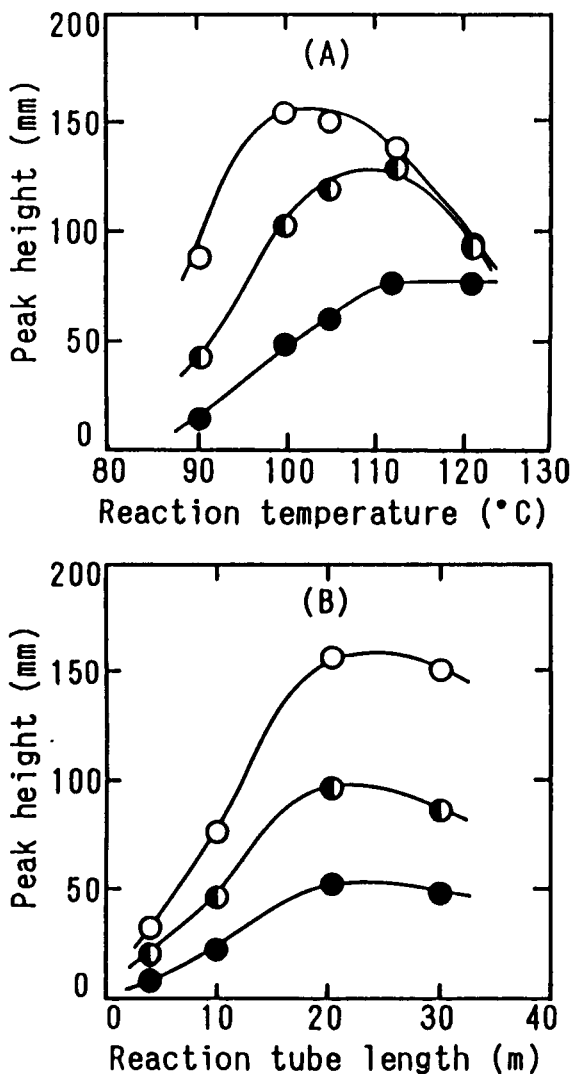


Fig. 4. Effect of (A) reaction temperature and (B) reaction tube length on sensitivity for COD. ○ = 100; ◐ = 50; ● = 20 mg l⁻¹ COD.

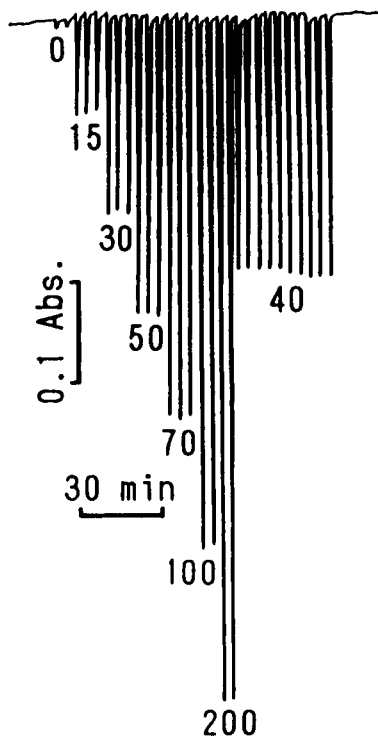


Fig. 5. Representative flow-injection peak profiles obtained with standard solution. The numbers on the peaks correspond to COD in mg l⁻¹.

maximum response. With a reaction tube of 20 m × 0.5 mm i.d. and a total flow-rate of 0.4 ml min⁻¹, a sufficiently high sampling frequency (20 h⁻¹) is easily obtainable.

An attempt was made to improve the sensitivity for COD determination by injecting various volumes of standard solutions. Increasing the sample volume led to increased sensitivity and a reduced linear calibration range, but a sample volume of 50 μl gave a better response despite a slightly shorter linear calibration range.

Linearity, reproducibility and sensitivity

Typical responses to the standard solutions with various COD values are shown in Fig. 5, and were obtained by injecting a sample volume of 50 μl. A sample throughput rate of 20 h⁻¹ was chosen as a convenient frequency that showed no apparent carryover between samples and good recorder traces. Reproducible performance is usually restricted to a certain extent by baseline

instability. The traces with a stable baseline showed good reproducibility and precision. Statistical analysis gave a relative standard deviation of 0.6% for ten injections of standard solutions containing 40 mg l⁻¹ COD. The precision of the analytical results appears to be better than that attainable by other flow-injection methods.

Using 3.0 × 10⁻⁴ M cerium(IV) sulphate solution and a sample volume of 50 μl, the calibration graph was linear over the range 0–130 mg l⁻¹ and the detection limit was 0.5 mg l⁻¹ COD, although the determination of COD was based on mild conditions.

Determination of COD in wastewater samples

The organic pollutants in wastewater are complex, and achieving the same degree of oxidation for different types of samples is very difficult. Particularly compounds containing an aromatic nucleus may be only partly and irreproducibly oxidized by Cr(VI) ion or Mn(VII) ion. Unless stronger oxidizing agents are used, the choice of standard substances is also important for a good correlation with standard manual methods. A mixture of L-glutamic acid and lactose (5 + 1) was selected and tested. As indicated, the mixture was a suitable standard substance for the determination of COD in various wastewater samples, and gave good recorder traces and good correlation with the standard manual methods.

For application of the flow-injection methods using potassium dichromate or potassium permanganate to the determination of COD in various environmental water samples, the chloride interference has been discussed in detail by Korenaga and Ikatsu [1–3] and Appleton and Tyson [5]. These studies demonstrated serious chloride interference in the determination of COD when no mercury(II) sulphate and/or silver sulphate is added, and a definite error caused by oxidation of chloride to chlorine. Here, the interference from chloride was investigated using the standard solutions (40 mg l⁻¹ COD) containing chloride levels between 0 and 30 g l⁻¹. The results summarized in Table 1 show that the present method can tolerate chloride up to 30 l⁻¹ without the need for the addition of mercury(II) sulphate and/or silver sulphate.

TABLE 1

Effect of chloride concentration on the determination of COD

COD (mg l ⁻¹)	Chloride (mg l ⁻¹)	Peak height (mm)	Error (%)
40	0	85.0	–
40	10	81.0	–5
40	50	78.5	–8
40	100	75.0	–12
40	500	75.5	–11
40	1000	78.0	–8
40	5000	87.0	+2
40	10000	89.0	+5
40	30000	89.5	+5

In the usual case, the filtration of samples such as those used here would be unnecessary, as these samples were almost clear solutions. When the sample contains a high concentration of suspended solid components, however, filtration is essential and great care is required to avoid altering the composition of the oxidizable organic substances. The effect of filtration on the COD determination was studied using a filter with a pore size of 0.45 μm serial wastewater samples. As shown in Table 2, the filtered samples gave lower results than non-filtered samples. Consequently, injecting directly into the flow system as soon as possible after collection, rather than filtering, will provide more reliable results.

Real samples taken from various types of wastewater and effluent were analysed by the present method. Good agreement was obtained between COD values given by this method and the flow-injection method using potassium permanganate (Table 3). The results were checked

TABLE 2

Effect of filtering wastewater samples on the determination of COD

Samples	Peak height (mm)		Error (%)
	Non-filtered	Filtered	
1	105.8	92.0	–13
2	90.1	75.8	–16
3	75.5	62.0	–18
4	52.6	50.7	–4
5	34.2	26.9	–21

TABLE 3

Results obtained with the present method and other flow-injection methods

Sample	COD values (mg l ⁻¹)		
	This method	COD _{Mn} ^a	COD _{Cr} ^b
Wastewater	A	4.5	4.8
	B	7.0	7.4
	C	16.0	17.0
	D	5.5	–
	E	3.2	–
Effluent	F	90	96
	G	218	179
	H	140	113
	I	290	238
	J	160	103
	K	131	116
	L	111	79
	M	143	90
	N	83	65

^{a,b} Flow-injection methods using potassium permanganate and potassium dichromate, respectively.

by incorporating known amounts of a standard substance in the wastewater samples and determining the COD values. Good recoveries (94–102%) of the standard substance added were confirmed. In Fig. 6, the results for fourteen wastewater samples from a food factory are compared with those obtained by the standard manual method using potassium permanganate, and

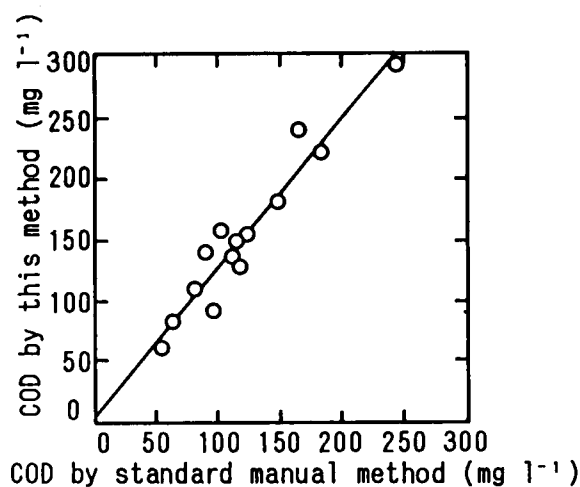


Fig. 6. Representative correlation results between the standard manual method and the present method.

the correlation was satisfactory. The regression equation and correlation coefficient were $y = 1.24x + 6.1$ and 0.95 respectively, where y and x denote the COD values obtained by the present method and the standard manual method, respectively.

Conclusions

A series of feasibility studies indicated that the present method is rapid, simple and as effective as standard manual methods in oxidizing wastewater samples. The results obtained are encouraging in comparison with other published flow-injection methods, even though a lower acid concentration is used and masking agents for chloride interference and catalysts for a high degree of sample oxidation are omitted. The flexibility of the operating conditions and standard substances makes this approach broadly applicable to various types of wastewater samples; this is a great advantage and allows its use in the process control of wastewater treatment and the quality management of environmental water. The reaction proceeds without the formation of bubbles, owing to the low acid concentration used and to the high-quality micropump which efficiently prevents local overheating and the penetration of bubbles from the sampling head. The stable baseline and high oxidation of samples led to both very good reproducibility and a low detection limit.

Cerium(IV) sulphate is, however, unsuitable for continuous monitoring over long periods because its self-decomposition results in a baseline drift and a gradual variation of the degree of sample oxidation. This problem remains to be resolved.

REFERENCES

- 1 T. Korenaga, *Bunseki Kagaku*, 29 (1980) 22.
- 2 T. Korenaga and H. Ikatsu, *Analyst*, 106 (1981) 653.
- 3 T. Korenaga and H. Ikatsu, *Anal. Chim. Acta*, 142 (1982) 301.
- 4 M. Goto, *Trends Anal. Chem.*, 2 (1983) 92.
- 5 J.M.H. Appleton and J.F. Tyson, *Anal. Chim. Acta*, 179 (1986) 269.

- 6 T. Korenaga, T. Takahashi, T. Moriwake and S. Sanuki, in R. Briggs (Ed.), *Advances in Waste Pollution, Instrumentation, Control and Automation of Water and Wastewater Treatment and Transport system*, Pergamon, Oxford, 1990.
- 7 M.L. Balconi, M. Borgarello, R. Ferraroli and F. Realini, *Anal. Chim. Acta*, 261 (1992) 295.
- 8 T. Korenaga, M. Izawa, T. Fujiwara, T. Takahashi, H. Muraki and S. Sanniki, *Anal. Sci.*, 7 (1991) 515.
- 9 T. Korenaga, X. Zhou, M. Izawa, T. Takahashi and T. Moriwake, *Anal. Chim. Acta*, 261 (1992) 67.

Determination of bromide in sodium chloride matrices by flow-injection analysis using blank peak elimination and kinetic discrimination

W.J.M. Emaus and H.J. Henning

Department of Analytical Chemistry, Akzo Salt and Basic Chemical Division, P.O. Box 25, 7550 GC Hengelo (Netherlands)

(Received 7th July 1992; revised manuscript received 9th October 1992)

Abstract

Flow-injection analysis was applied to the determination of bromide in a sodium chloride matrix. The method is based on oxidation of bromide with chloramine-T to bromine, followed by reaction with phenol red to form bromophenol blue, the absorbance of which is measured spectrophotometrically. The interference of chloride, forming chlorinated reaction products at a much slower rate than the reaction with bromophenol blue, is prevented in flow-injection analysis because of the short reaction times. The influence of blank peaks, which appear because of the difference in the refractive indices of the aqueous carrier solution and the sample solution, is eliminated by use of a large sample injection volume. The limit of quantification of bromide in sodium chloride is 1.0 mg kg^{-1} . The relative standard deviation at a level of $30\text{--}50 \text{ mg Br}^{-1} \text{ kg}^{-1}$ is better than 1%. The repeatability and reproducibility were determined in a round-robin test. The characteristics of the method such as calibration, selectivity and ruggedness are described. The sample throughput is about 60 h^{-1} .

Keywords: Flow injection; UV-Visible spectrophotometry; Bromide; Sodium chloride

In the chlor-alkali industry, sodium chloride is the basic chemical for the production of chlorine and sodium hydroxide by electrolysis. Concentrated brine as feedstock in the electrolytic process must have an acceptable level of purity to ensure the quality of the products. The presence of bromide in the feed brine results in chlorine contaminated with bromine, which can pose problems for the chlorine processing industry in maintaining the quality of chlorine-containing intermediates or derived industrial products. To support the production process of an electrolysis salt with a low level of bromide, methods were inves-

tigated for the determination of bromide in sodium chloride and brine. The prerequisites for an analytical method were a low limit of quantification (LOQ) [mg kg^{-1} level with a relative standard deviation (R.S.D.) of 10%] and a short time of analysis (minutes).

Different approaches can be followed for the determination of bromide. The traditional method [1,2] is based on oxidation of Br^{-} by hypochlorite. The resulting bromate is determined iodimetrically by volumetric or coulometric titration. The lowest concentration to be determined (LOQ) with an R.S.D. of 10% for this method is 0.5 mg kg^{-1} . The determination of total bromine in NaCl by x-ray fluorescence spectrometry [3] yields an LOQ of 5 mg kg^{-1} . However, both the classical titration and x-ray fluorescence methods are time

Correspondence to: W.J.M. Emaus, Department of Analytical Chemistry, Akzo Salt and Basic Chemical Division, P.O. Box 25, 7550 GC Hengelo (Netherlands).

consuming. By ion chromatography with electrochemical detection only bromide levels greater than 15 mg kg^{-1} in NaCl can be determined [4].

Spectrophotometric methods for the determination of bromide have been reported using rosaniline [5,6] or phenol red [7]. Using phenol red, the bromide is oxidized to bromine, by peroxomonosulphate [8] or chloramine-T [9], followed by reaction with phenol red to form bromophenol blue. Thiosulphate is added to decompose the excess of chloramine-T, preventing the bleaching of bromophenol blue.

With this spectrophotometric method using phenol red, chloride has been identified as an important interferent at levels as low as 100 mg l^{-1} . Correction curves can be used to compensate for this positive interference of up to 5 g l^{-1} of chloride [10]. The interference depends on the reaction time and on the concentration of reagents [7,9]. However, various levels of chloride that do not interfere with the phenol red method have also been reported [11,12].

Flow-injection analysis (FIA) permits the reproducible handling of solutions and strict control of the timing [13]. Kinetic discrimination is one of the fundamental FIA approaches [14] in which the difference in reaction rates between reagent and analyte and between reagent and interferences is exploited. Utilizing FIA for enhancing the selectivity of the phenol red method for the determination of Br^- in NaCl has been

reported [15,16]. None of these papers, however, dealt with NaCl concentrations up to 300 g l^{-1} .

In FIA, blank peaks appear where there is a difference in refractive index between the carrier and the sample solution [17]. A way to compensate for this problem is to make the matrix of the carrier the same as the matrix of the sample solution. Owing to its bromide content, NaCl of commercially available quality is not suitable for the carrier solution. In this work, these problems were overcome by using water as the carrier solution combined with injection of a large volume of sample.

The flow-injection phenol red method was used for determining $0.5\text{--}10 \text{ mg l}^{-1}$ of bromide in NaCl solutions containing 300 g l^{-1} or less of NaCl. The side-reactions of chloramine-T (CAT) with phenol red and of CAT with chloride forming eventually chlorophenol blue and chlorobromophenol blue were prevented by the very short time of reaction. The method was applied to the determination of bromide in NaCl and brine.

EXPERIMENTAL

Instrumentation

The FIA system was a Tecator FIAstar 5010 analyser with a Tecator Chemifold I, shown schematically in Fig. 1. The detector was a Tecator 5023 spectrophotometer. Polyethylene tubing

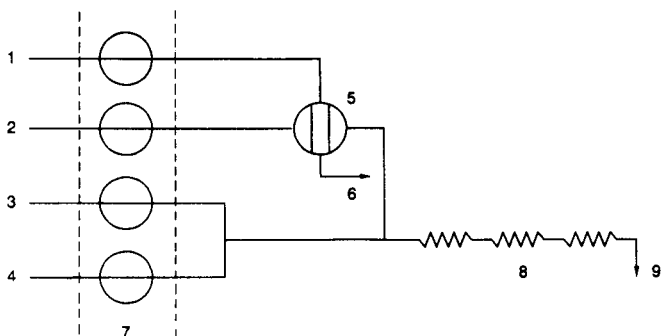


Fig. 1. FIA manifold for the determination of bromide in brine. 1 = Calibration or test sample solution, flow-rate 1.2 ml min^{-1} ; 2 = carrier (water), flow-rate 1.2 ml min^{-1} ; 3 = CAT solution, flow-rate 2 ml min^{-1} ; 4 = buffered phenol red solution, flow-rate 2 ml min^{-1} ; 5 = injection valve with 0.4-ml sample loop; 6 = drain; 7 = tubing pump; 8 = mixing coils (three), length 60 cm, diameter 0.5 mm; 9 = to spectrophotometer, 1-cm cell, wavelength 590 nm.

was used throughout. The absorbance of bromophenol blue was monitored at 590 nm with a 1-cm path length flow cell. The peak-height maximum between 15 and 25 s after injection was related to the bromide concentration. The data were analysed with the software packages Tecator Superflow II, STATCAL [18] and SAS [19].

Reagents

All chemicals were of analytical-reagent grade. The reagents were degassed by vacuum aspiration.

Bromide standard solution was prepared by dissolving 148.9 mg of KBr in 1 l of water. CAT solution was prepared by dissolving 0.4 g of CAT in 1 l of water containing 10 ml of bromide standard solution. Buffered phenol red solution contained per litre of water 40 g of sodium acetate, 25 ml of acetic acid ($\geq 99\%$) and 10 ml of phenol red solution consisting of 0.2 g of phenol red in 100 ml of 0.01 M sodium hydroxide solution.

RESULTS AND DISCUSSION

Kinetic discrimination

To illustrate the effect of the side-reaction of chloride forming chlorinated reaction products, the stopped-flow option of the FIA system was used. At a level of $8 \text{ mg Br}^- \text{ l}^{-1}$ in the presence of 0 and $300 \text{ g NaCl l}^{-1}$, the pump was stopped at the steady state, 23 s after injection. At this moment the absorbances were still the same. After 125 s the pump was started again. In Fig. 2 the difference in the absorbance versus time curves, due to the formation of chlorinated reaction products in the presence of NaCl, is shown.

Investigation on the matrix of the carrier

With FIA the matrix of the carrier and the sample should be similar to prevent a noisy signal due to differences in refractive index. The main condition that the carrier must not contain any analyte cannot be fulfilled, however, because commercially available NaCl contains $4\text{--}10 \text{ mg kg}^{-1}$ of bromide, which was investigated by the

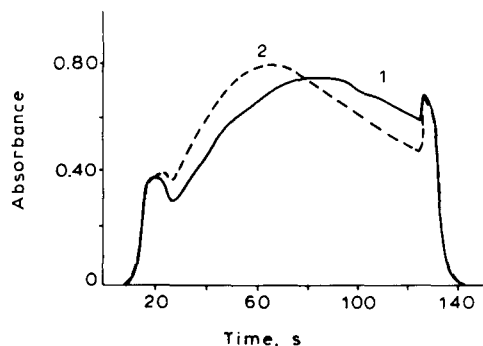


Fig. 2. Influence of NaCl on the absorbance–time curves after reaching the steady state using stopped flow. (1) no NaCl; (2) $300 \text{ g NaCl l}^{-1}$.

method described in this paper. Also, NaCl crystallized by addition of 500 ml of acetone to 1 l of saturated brine to prepare a “bromide-free” salt still contains 2 mg kg^{-1} of bromide (Table 1).

Because of the presence of Br^- in NaCl, it was decided to use water as the carrier. The effects of differences in the refractive indices of the carrier and sample solutions could be eliminated by installation of a 0.4-ml sample loop in combination with three reaction coils in the FIA manifold, so that the steady state is reached between the disturbing blank peaks for every concentration of bromide in the calibration range (Fig. 3). The parameters of the Superflow II software are adjusted to measure the peak height at this plateau.

The use of water as carrier and aqueous calibration solutions requires that the signal measured should be independent of the NaCl concentration. With NaCl samples spiked with bromide, the influence of the NaCl concentration in the

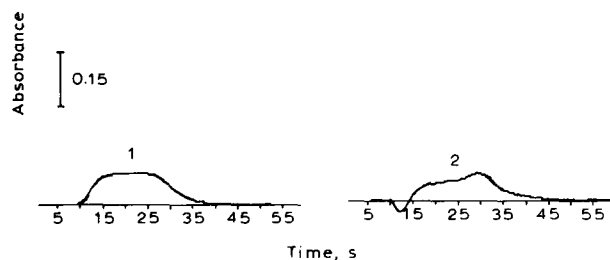


Fig. 3. Blank peak elimination by measuring at the steady state between 15 and 25 s after injection. (1) $2 \text{ mg Br}^- \text{ l}^{-1}$ in water; (2) $1.3 \text{ mg Br}^- \text{ l}^{-1}$ in brine containing $300 \text{ g NaCl l}^{-1}$.

TABLE 1

Bromide contents of NaCl of different qualities

NaCl quality	Bromide content (mg kg ⁻¹)
Baker p.a. ^a	10
Baker p.a. ^a	7
Merck Suprapur	5
Merck Ultrex	4
Purified ^b	2

^a Different charges. ^b Crystallized from saturated brine (Merck Suprapur)–acetone (2+1, v/v).

injected sample was investigated at levels of 100 and 300 g l⁻¹. The calibration explained below was used for this. Figure 4 shows that the influence of the NaCl concentration at the different bromide levels investigated is negligible.

Calibration

Calibration was performed by using six equispaced calibration solutions in the range 0.5–10 mg of bromide per litre of water. The calibration solutions were prepared by volumetric dilution of the bromide standard solution. The calibration graph obtained was curved, despite the standard addition of bromide via the CAT solution and the simultaneous addition of the CAT and the

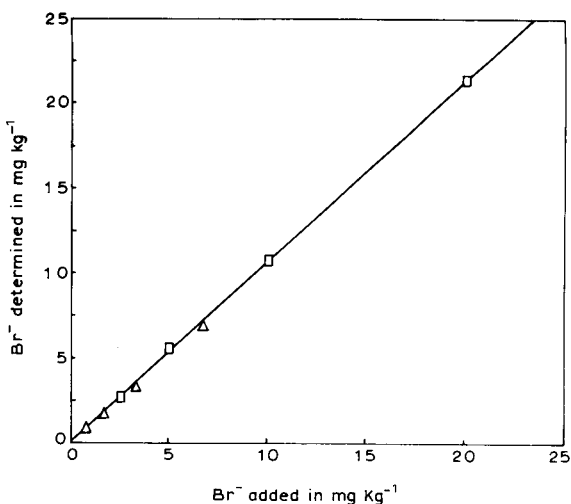


Fig. 4. Influence of the NaCl concentration in the injected sample: □ = 100; △ = 300 g l⁻¹.

TABLE 2

Influence of other components

Component	Maximum amount per test portion (μg)	Nature of the interference and possible treatment
Nitrite	100	Does not interfere
	> 100	Results too low; interference cannot be eliminated by addition of amido sulphonic acid
Iodide	100	In the presence of 300 g NaCl l ⁻¹
	20	In the absence of NaCl; results too high when iodide > 20 μg
K ₄ Fe(CN) ₆	1000	Does not interfere
	> 1000	Results too low
Bromate	1000	Does not interfere
	> 1000	Not tested

buffered phenol red solution in the FIA manifold. The simultaneous addition was done to overcome the effect of bromination of impurities in the reagents. The lower limit of the calibration range corresponds to the LOQ. The higher limit of the calibration graph corresponds with the amount of bromophenol blue that can be produced with the prescribed reagents. The regression equation is $y = -7(\pm 1.3) + 36.4(\pm 0.6)x + 0.72(\pm 0.05)x^2$, where y is absorbance and x is bromide concentration (mg l⁻¹). The residual standard deviation is 1.2 absorbance at 590 nm (mg Br⁻ l⁻¹)⁻¹.

Analytical characteristics

To investigate the selectivity, the interference of bromate, the possible salt additives nitrite and iodide and the anti-caking agent potassium hexacyanoferrate(II) was tested. The results are given in Table 2.

Information on the ruggedness of the method was obtained by investigating the influence of the concentration of CAT and the amount of phenol red added. The concentration of CAT solution was the less rugged parameter. The blank value using 0.4 g l⁻¹ CAT solution was adjusted to zero. Increasing the CAT concentration to 0.8

TABLE 3

Comparison of the results of the FIA and two other methods

Sample	Bromide (mg kg ⁻¹) ^a		
	FIA	Titration	XRF
NaCl-I	37.1 ± 0.10	36.6 ± 0.24	38.8 ± 0.58
NaCl-II	51.6 ± 0.50	50.3 ± 0.26	53.0 ± 0.82
Brine-I	20.6 ± 0.11	– ^b	22.2 ± 0.75
Brine-II	139.4 ± 0.41	140.3 ± 0.38	144.4 ± 1.43
Brine-III	350.8 ± 0.48	– ^b	352.4 ± 2.59

^a Mean values and standard deviations of five replicates.^b Not determined.

and 1.6 g l⁻¹ resulted in blank values of 0.08 and 0.38, respectively, and decreasing the concentration to 0.2 g l⁻¹ yielded a blank value of –0.01. The effect of the consumption of CAT for the oxidation of bromide was therefore minimized by using a CAT concentration of 0.2–0.4 g l⁻¹. The 0.4 g l⁻¹ solution was preferred, giving a greater measuring range. Increasing the amount of phenol red resulted in an incomplete formation of bromophenol blue and decreasing the amount resulted in a smaller measuring range.

Because of the absence of suitable reference materials, the trueness of the FIA results was established by comparison with the results obtained by iodimetric titration and x-ray fluorescence (XRF) spectrometry. These experiments were performed in a single laboratory. The methods were applied to two electrolysis salt samples (NaCl-I, a fine salt; and NaCl-II, an undried clotty salt) and three brine samples from a production process (brine-I, untreated brine; brine-II, a brine enriched with bromide; and brine-III, a brine with a high bromide content from an evaporator). The results are given in Table 3. The SAS procedure [19] TTEST was used for comparing pairs of means. This test both provides the exact two-sample *t*-test, which assumes equal variances, and is an approximate test that is used if the assumption of equal variances is not met. The probability values are given in Table 4. A *p* value of < 0.05 indicates a significant difference at the 5% significance level. For instance, for sample NaCl-I, a Δ of only 0.3 mg Br⁻ kg⁻¹ between the means of the FIA and the titration methods is significant at this 5% level. The overall conclu-

TABLE 4

p Values as result of the two-sample *t*-test

Sample	FIA vs. titration	FIA vs. XRF	XRF vs. titration
NaCl-I	0.0020	0.0026	0.0001
NaCl-II	0.0008	0.0125	0.0001
Brine-I	– ^a	0.0075	– ^a
Brine-II	0.0062	0.0001	0.0003
Brine-III	– ^a	0.2571	– ^a

^a Not determined.

sion is that, especially owing to the high precision of the FIA method, the small differences in the mean values are statistically significant.

The repeatability (*r*) and the reproducibility (*R*) of the FIA method were determined by means of an inter-laboratory test conforming to ISO 5725 [20]. Three laboratories participated, each analysing the samples five times. Outliers (1% significance level) were removed, stragglers (5% significance level) were not. The results are presented in Table 5. The discrepancy in the repeatability and reproducibility between NaCl-I and NaCl-II is related to inhomogeneity of the undried clotted sample NaCl-II. This sample had a reproducibility of 4 mg kg⁻¹ at the 50 mg kg⁻¹ level of bromide.

The LOQ was determined by establishing the standard deviation, analysing ten times an NaCl sample with a bromide content near the expected LOQ level. At a level of about 4 mg Br⁻ kg⁻¹ the standard deviation *s*₁₀ was 0.10 mg kg⁻¹. Using an R.S.D. of 10%, the LOQ is 1.0 mg kg⁻¹.

TABLE 5

Repeatability and reproducibility (ISO 5725 [20])

Sample	Bromide (mg kg ⁻¹)	
	Repeatability (<i>r</i>)	Reproducibility (<i>R</i>)
NaCl-I	0.3	1
NaCl-II	1	4
Brine-I	0.2	1
Brine-II	1	6
Brine-III	5	18

Conclusions

The FIA method developed for the determination of bromide in sodium chloride matrices has a limit of quantification of $1.0 \text{ mg Br}^- \text{ kg}^{-1}$ and an R.S.D. of better than 1% at a level of 30–50 mg kg^{-1} . The time of analysis is about 60 s, which permits the processing of 60 samples per hour.

The FIA method employs kinetic discrimination to prevent the interference of chloride. The bromide content in commercially available NaCl is too high to use this NaCl for preparing the carrier. Water can be used as the carrier by injecting a large volume of the brine samples and measuring the absorbance at the steady state. In this way the effect of blank peaks, caused by differences in refractive indices between the carrier and sample solution, is eliminated. Owing to the ability to process large series of samples in a standardized way, this FIA method is ideally suited for industrial applications.

REFERENCES

- 1 J.H. van der Meulen, *Chem. Weekbl.*, 28 (1931) 82.
- 2 G. Hunter and A.A. Goldspink, *Fresenius' Z. Anal. Chem.*, 79 (1954) 467.
- 3 M. Iwatsuki, Y. Niino and T. Fukasawa, *Nippon Kaisui Gakkaishi*, 44 (1990) 119.
- 4 R.D. Rocklin and E.L. Johnson, *Anal. Chem.*, 55 (1983) 4.
- 5 E.F. Joy, J.D. Bonn and A.J. Barnard, *Anal. Chem.*, 45 (1973) 856.
- 6 G. Hunter and A.A. Goldspink, *Analyst*, 79 (1954) 467.
- 7 A. Pèron and J. Courtot-Coupez, *Analisis*, 6 (1978) 389.
- 8 H.F. Dobolyi, *Anal. Chem.*, 56 (1984) 2961.
- 9 D.R. Jones, *Talanta*, 36 (1989) 1243.
- 10 C.L. Basel, J.D. Defreese and D.O. Whittemore, *Anal. Chem.*, 54 (1982) 2090.
- 11 F. Khalili and M. Fayyad, *Dirasat*, 13 (1986) 179.
- 12 M. Archimbaud and M.R. Bertrand, *Chim. Anal. (Paris)*, 52 (1970) 531.
- 13 J. Ruzicka and E.H. Hansen, *Anal. Chim. Acta*, 78 (1975) 145.
- 14 G. Gordon, K. Yoshino, D.G. Themelis, D. Wood and G.E. Pacey, *Anal. Chim. Acta*, 224 (1989) 383.
- 15 P.I. Anagnostopoulou and M.A. Koupparis, *Anal. Chem.*, 58 (1986) 322.
- 16 T. Anfält and S. Twenström, *Anal. Chim. Acta*, 179 (1986) 453.
- 17 T. Yamane and M. Saito, *Talanta*, 39 (1992) 215.
- 18 J. Kragten, *Anal. Chim. Acta*, 241 (1990) 1.
- 19 S.D. Schlotzhauer and R.C. Littell, *SAS System for Elementary Statistical Analysis*, SAS Institute, Cary, NC, 1987, p. 191.
- 20 International Standard ISO 5725, International Organization for Standardization, Geneva, 2nd edn., 1986.

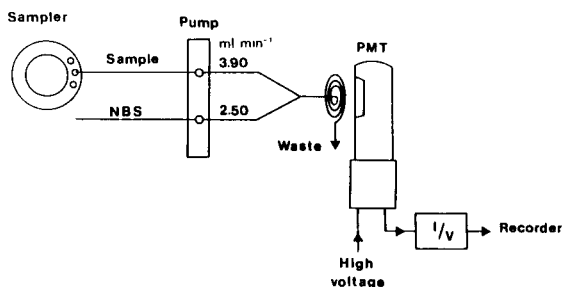


Fig. 1. Schematic diagram of the continuous-flow CL analyser (not to scale).

attributed to hypobromous acid which is produced by its hydrolysis. NBS is more stable than hypobromite and has been used extensively as a brominating and oxidizing agent.

Hydralazine and dihydralazine, which contain one and two hydrazine groups, respectively, are

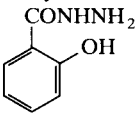
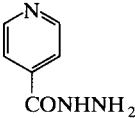
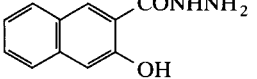
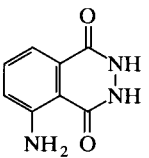
well known antihypertensive compounds. Hydralazine has been determined by chromatographic [8], chemiluminescence [9], fluorescence [10] and classical titrimetric [11] methods. The titrimetric agent was NBS and the reaction involved oxidation of the hydrazino group to the keto group. Colorimetry [12], polarography [13], enthalpimetry [14] and potentiometry [15] have been proposed for the determination of dihydralazine.

Rifampicin and rifamycin SV are antibiotics of the rifamycin family (Table 1), with excellent therapeutic action. The available methods for the determination of rifamycins are restricted to spectrometry [16], differential spectrometry [17] and liquid chromatography [18].

This work is concerned with the study of the CL observed during the reaction of NBS with some hydrazides and the products of dihydrala-

TABLE 2

Analytical characteristics for the determination of some hydrazide compounds

Compound ^a	Linear range (M)	Slope (\pm S.D.)	Intercept (\pm S.D.)	Correlation coefficient	n ^b
Hydrazide of salicylic acid 	$(1.00-6.50) \times 10^{-4}$	$(1.67 \pm 0.03) \times 10^4$	-0.48 ± 0.09	0.9994	7
Isoniazid 	$(5.00-50.0) \times 10^{-5}$	$(9.38 \pm 0.14) \times 10^4$	-1.92 ± 0.40	0.9994	7
Hydrazide of 3-hydroxy-2-naphthoic acid 	$(1.00-50.0) \times 10^{-5}$	$(4.88 \pm 0.05) \times 10^5$	-3.27 ± 1.37	0.9996	9
Luminol 	$(0.60-60.0) \times 10^{-9}$	$(4.10 \pm 0.05) \times 10^8$	0.60 ± 0.14	0.9996	8

^a $C_{\text{NaOH}} = 2.0$ M (optimum for the determination of isoniazid [7]). ^b Number of standard solutions, each measured three times.

zine, rifampicin (rifampin) and rifamycin SV (rifocin) after alkaline degradation. The emission intensity and the sensitivity are greatly enhanced when ammonia is also present in the reaction medium. The CL methods developed were applied successfully to the determination of dihydralazine and rifamycins in pharmaceutical dosage forms.

EXPERIMENTAL

Apparatus

A schematic diagram of the continuous-flow CL analyser is shown in Fig. 1. It consisted of two basic units, the detector housing and the flow-through system.

The detector housing included a coiled glass flow cell situated in front of the photomultiplier tube (PMT). The cell consisted of 3.5 turns of glass tubing (i.d. 2 mm) and its total height was 22 mm. The coil volume was 300 μl . The distance of the coil from the PMT was 2 mm for greatest sensitivity. The coil was backed by a mirror for maximum light collection by the PMT. High voltage (-720 V) was supplied to the PMT (EMI 9783R, S-5 response) by two Heath Universal power supplies (0–500 V) connected in series. The output of the PMT was connected to an

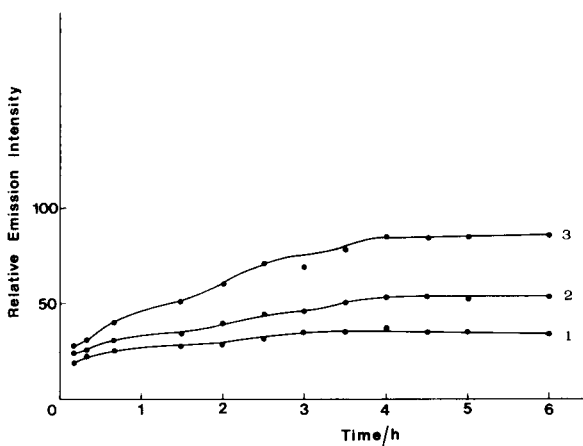


Fig. 2. Effect of degradation time on the CL intensity from (1) 0.0200, (2) 0.0500 and (3) 0.100 $\mu\text{g ml}^{-1}$ of rifampicin. $C_{\text{NaOH}} = 1.00\text{ M}$ and $C_{\text{NH}_3} = 5.0 \times 10^{-4}\text{ M}$.

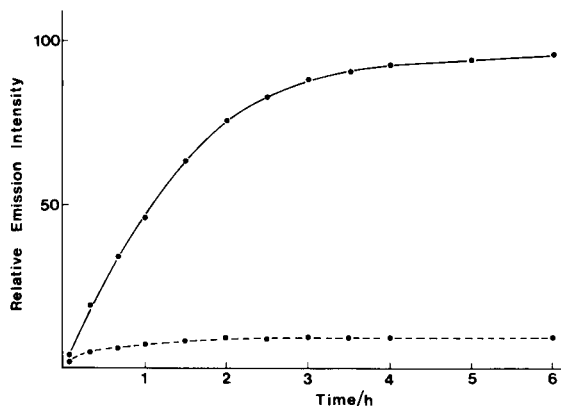


Fig. 3. Effect of degradation time on the CL intensity from (broken line) 5.00 and (solid line) 15.0 $\mu\text{g ml}^{-1}$ of dihydralazine. $C_{\text{NaOH}} = 0.0030\text{ M}$ and $C_{\text{NH}_3} = 0.050\text{ M}$.

operational amplifier (RCA CA 3140) which served as a current-to-voltage (I/V) converter. The PMT, coil, mirror and I/V converter were housed in a metal, light-tight casing, 30 cm long, 20 cm high and 20 cm wide. Damping was provided by inserting an RC circuit between the output of the I/V converter and the recorder. The output of the CL analyser was recorded with a Knauer Model 73341 chart recorder.

The solutions of reactants were supplied by a Technicon proportioning pump III and were mixed at a Y-junction, 20 mm before entering the flow cell. The final solution was carried into the flow cell by a Tygon tube of 2 mm i.d. Samples were supplied to the manifold by a Technicon sampler II with a 40-sample capacity.

Reagents

All solutions were prepared from analytical-reagent grade materials with deionized, distilled water.

N-Bromosuccinimide stock solution (0.0500 M) was prepared daily by dissolving 2.225 g of NBS (Serva) in water and diluting to 250 ml. The solution was kept at 4°C in an amber-coloured bottle in the dark.

Stock solutions (100.0 $\mu\text{g ml}^{-1}$) of rifampicin and rifamycin SV sodium salt were prepared daily by dissolving 0.1000 g of each compound (Elpen, Athens) in water and diluting to 1 l.

TABLE 3

Analytical characteristics for the determination of rifampicin, rifamycin SV and dihydralazine by the proposed CL method

Analyte	Linear range ($\mu\text{g ml}^{-1}$)	LOD ^a ($\mu\text{g ml}^{-1}$)	Slope (\pm S.D.)	Intercept (\pm S.D.)	Correlation coefficient	n ^b
Rifampicin	0.020 – 1.00	0.0017	154.9 \pm 1.1	6.57 \pm 0.50	0.9998	12
Rifamycin SV (sodium salt)	0.0050– 1.00	0.0005	292.3 \pm 1.9	12.51 \pm 0.79	0.9998	12
Dihydralazine ^c (sulphate)	2.00 –30.0	1.23 ^d	1.96 \pm 0.02	0.016 \pm 0.023	0.9993	12

^a LOD = limit of detection (blank plus three times its standard deviation). ^b Number of standard solutions, each measured three times. ^c Log I /log C calibration graph. ^d LOD: signal-to-noise ratio = 3.

Dihydralazine sulphate stock solution (100.0 $\mu\text{g ml}^{-1}$) was prepared by dissolving 0.1000 g of dihydralazine sulphate (Ciba-Geigy, Athens) in water and diluting to 1 l. The solution was stable for at least 1 week.

All other chemicals were of the best grade available and were used as received.

Measurement procedure

Initiate the instrument under the optimized flow conditions of 3.90 ml min⁻¹ for the sample and 2.50 ml min⁻¹ for the NBS. Keep the sampling needle always in the “wash” position until the baseline is established on the recorder. Adjust the sampler to allow 15 s for sample and 18 s for washing water to enter the manifold when rifampicin and rifamycin SV are determined. The corresponding times for the determination of dihydralazine were 19 s for the sample and 15 s for the washing water. Once the sampler is activated, the analysis proceeds automatically. Construct a calibration graph of emission intensity [I (mV)]

versus concentration [C ($\mu\text{g ml}^{-1}$)] of rifampicin or rifamycin, or log I versus log C for dihydralazine, and determine the content of each compound in the sample solution. Include a standard solution for every twelve sample solutions.

Determination of rifampicin or rifamycin SV

Transfer 25.00 ml of 4.0 M sodium hydroxide solution and 10.00 ml of 0.010 M ammonia solution into a volumetric flask with the appropriate volume of stock rifampicin or rifamycin solution and dilute to 100 ml with water. The final solution should contain 0.0200–1.00 $\mu\text{g ml}^{-1}$ of rifampicin or 0.00500–1.00 $\mu\text{g ml}^{-1}$ of rifamycin SV in 1.0 M sodium hydroxide and 0.0010 M ammonia.

Determination of dihydralazine

Transfer 15.00 ml of 0.020 M sodium hydroxide solution and 5.00 ml of 1.00 M ammonia solution into a volumetric flask with the appropriate volume of stock dihydralazine and dilute to

TABLE 4

Results for the measurement of rifampicin, rifamycin SV and dihydralazine in aqueous solutions

Analyte	Concentration range ($\mu\text{g ml}^{-1}$)	Error (%)		Correlation coefficient	n ^a	Concentration ($\mu\text{g ml}^{-1}$)	R.S.D. (%, $n = 10$)
		Range	Average				
Rifampicin	0.0200 – 1.00	0.2–3.5	1.7	0.9997	10	0.0200 0.200	2.1 1.1
Rifamycin SV (sodium salt)	0.00500– 1.00	0 –1.2	0.5	0.99997	11	0.0100 0.100	4.0 1.5
Dihydralazine (sulphate)	2.00 –30.0	0 –4.1	1.5	0.9996	10	5.00 30.0	1.1 0.4

^a Number of samples, each measured three times.

100 ml with water. The final solution should contain 2.00–30.0 $\mu\text{g ml}^{-1}$ of dihydralazine in 0.0030 M sodium hydroxide and 0.050 M ammonia.

Determination of analytes in pharmaceutical preparations

Tablets. Not less than twenty tablets were weighed and finely powdered. A sample equivalent to ca. 200 mg of analyte was weighed accurately, transferred into a 1-l volumetric flask and diluted to volume with water. The powder was sonicated for 10 min to aid dissolution and then filtered. Working solutions were prepared from this sample solution by appropriate dilution so that the final analyte concentration was within the working range.

Capsules. Ten capsules were weighed, emptied and the procedure for tablets was followed.

Injections. The content of each injection was diluted with water appropriately so that the final analyte concentration was within the working range.

RESULTS AND DISCUSSION

Recent investigations [7] have shown that NBS is an efficient reagent for CL reactions. The main advantage of NBS over other organic and inorganic oxidants used in CL procedures is the absence of an absorption band and the lack of side-reactions.

Relationship between the CL and the structure of the hydrazides

The capability of NBS to participate in a CL reaction was further demonstrated by studying its

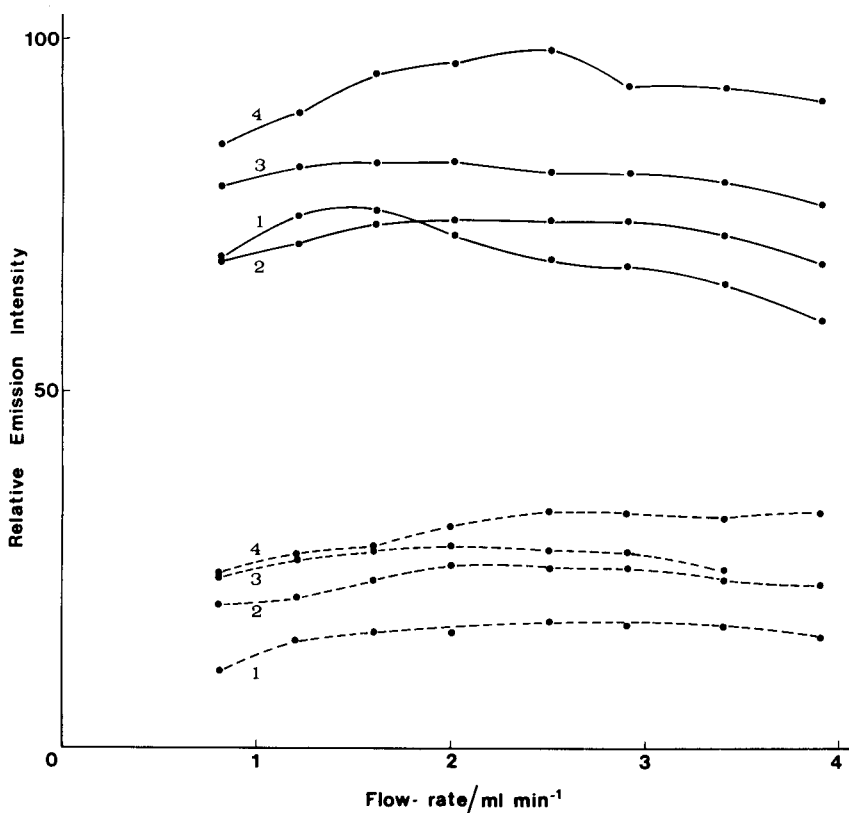
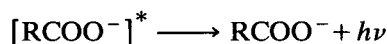
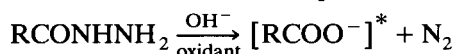


Fig. 4. Effect of flow-rate of 0.0150 M NBS in 0.050 M sodium hydroxide on the CL intensity from (broken lines) 5.00 and (solid lines) 20.0 $\mu\text{g ml}^{-1}$ of rifampicin supplied to the manifold at (1) 2.00, (2) 2.50, (3) 2.90 and (4) 3.90 ml min^{-1} .

reactions with some hydrazides. These substances are known for their chemiluminescent reactivity, which is probably due to the considerable energy released by the oxidation of the hydrazinocarbonyl group and the simultaneous formation of nitrogen and carbonyl groups. The general scheme of the reaction can be simplified to [19]



The energy released can be as high as 135 kcal mol⁻¹ and this exothermicity fulfils the main requirement for the occurrence of chemiluminescence [20]. An additional factor for the observation of CL from this reaction is the production of carboxylate anion in the excited singlet state with fluorescent properties [19,21]. Thus, the CL efficiency is related to the structure of the reaction product, i.e., its ability to fluoresce.

Table 2 summarizes the analytical parameters of some hydrazides. For comparison purposes, the study was carried out under the same experimental conditions as with isoniazid [7]. From these results, it can be concluded that the CL

efficiency is increased by the presence of electron-releasing substituents in the molecule, provided that there is no steric hindrance of resonance that might affect the reaction site. Thus, the CL intensity increases with increase in the number of aromatic rings within the molecule of the analyte. Further, the CL efficiency of isoniazid is higher than that of the hydrazide of salicylic acid because of the presence of nitrogen in the aromatic ring. The heteroatom acts more favourably for electron distribution than the hydroxyl group which is attached to the ring. The oxidation of luminol therefore shows intense CL, as would be expected from the high fluorescence capability of the 3-aminophthalate anion, which is the emitting species.

CL from dihydralazine and rifamycins

Further investigations showed that the oxidation of dihydralazine and rifampicin by NBS produced CL. Preliminary experiments also showed that the emission intensity increased on increasing the delay time of solution introduction into the manifold. A series of experiments were conducted to establish the optimum analytical condi-

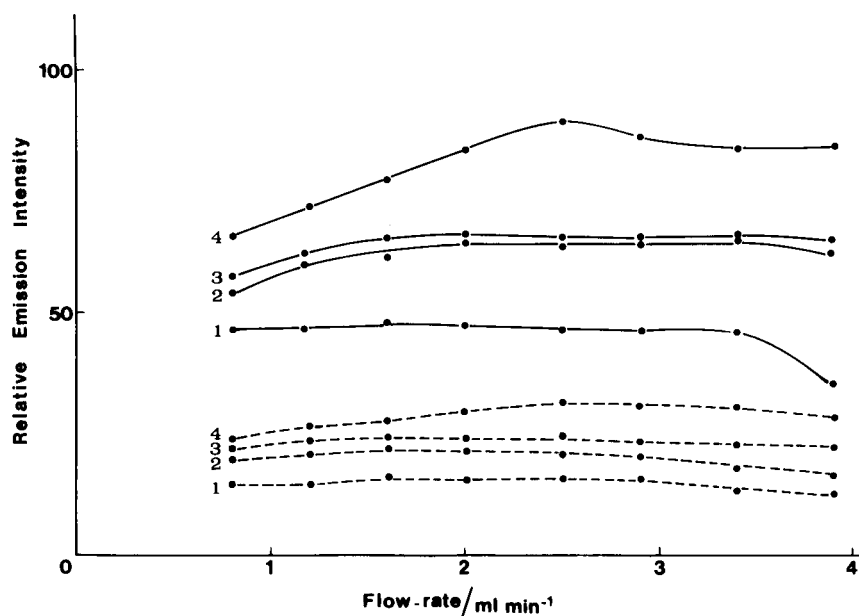


Fig. 5. Effect of flow-rate of 0.0150 M NBS in 0.0050 M sodium hydroxide on the CL intensity from (broken lines) 20.0 and (solid lines) 50.0 μg ml⁻¹ of dihydralazine supplied to the manifold at (1) 2.00, (2) 2.50, (3) 2.90 and (4) 3.90 ml min⁻¹.

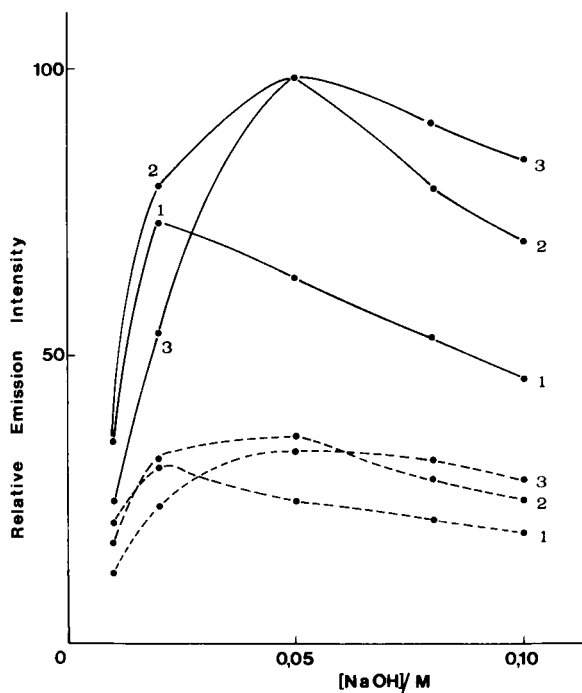


Fig. 6. Effect of sodium hydroxide concentration on the CL intensity from (broken lines) 5.00 and (solid lines) 20.0 $\mu\text{g ml}^{-1}$ of rifampicin with (1) 0.0050, (2) 0.0200 and (3) 0.050 M NBS.

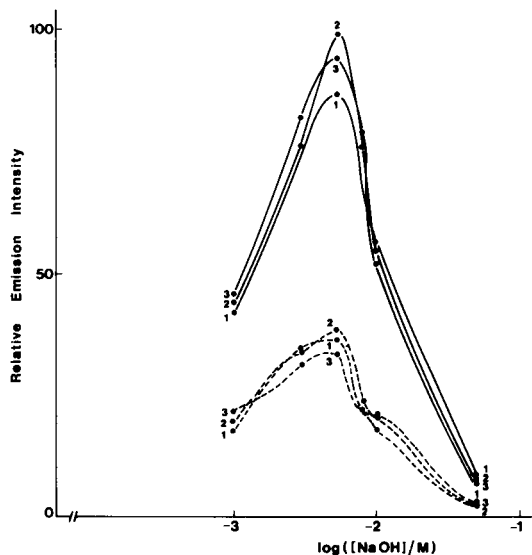


Fig. 7. Effect of sodium hydroxide concentration on the CL intensity from (broken lines) 20.0 and (solid lines) 50.0 $\mu\text{g ml}^{-1}$ of dihydralazine with (1) 0.0050, (2) 0.0150 and (3) 0.050 M NBS.

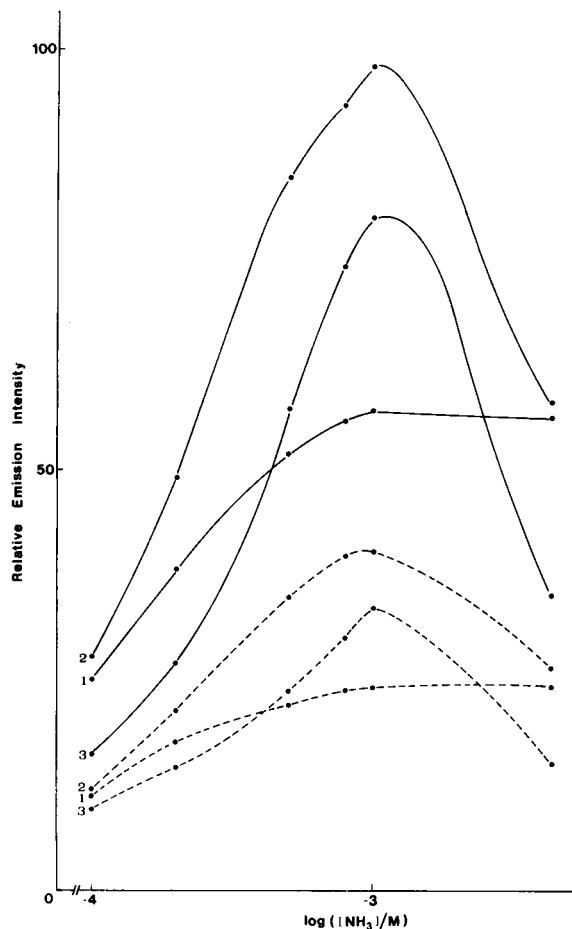


Fig. 8. Effect of ammonia concentration on the CL intensity from (broken lines) 0.400 and (solid lines) 1.00 $\mu\text{g ml}^{-1}$ of rifampicin at (1) 0.50, (2) 1.00 and (3) 2.00 M sodium hydroxide.

tions for the chemiluminescent oxidation of rifampicin and dihydralazine by NBS. The parameters studied were time of degradation in alkaline medium to chemiluminogenic products, reagent and sample flow-rates and oxidant and alkali concentrations. The optimum values of these parameters used for the determination of rifampicin were used also for the determination of the rifampicin SV sodium salt.

Degradation time in alkaline medium

The concentration of the final products that participate in CL reactions with NBS at ambient

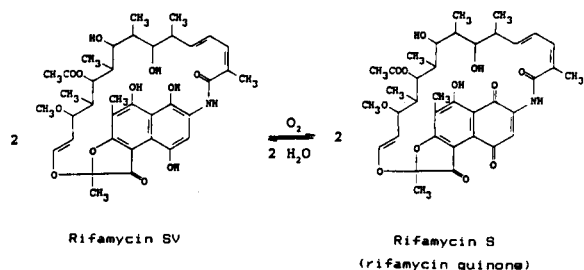
TABLE 5

Recovery of rifampicin and dihydralazine from solutions with a tenfold concentration of various additives used as excipients

Additive	Mean recovery ($n = 3$) (%)	
	Rifampicin ($0.100 \mu\text{g ml}^{-1}$)	Dihydralazine (sulphate) ($5.00 \mu\text{g ml}^{-1}$)
Glucose	95.4	99.6
Galactose	99.8	95.8
Lactose	100.4	99.4
Sugar	100.3	99.8
Starch	98.3	98.8
Carbopol ^a	97.7	100.2
Carbowax ^b	100.0	98.4
Talc	100.5	98.8
Cellulose acetate		
hydroxyphthalate	99.9	102.4
Magnesium stearate	96.8	99.0
CaSO ₄	104.6	101.4
EDTA	102.4	99.8
Sorbitol	99.0	100.4
Sodium citrate	102.7	101.0
Sodium lauryl sulphate	100.3	98.6

^a Carboxypolymethylene. ^b Polyethylene glycol 4000.

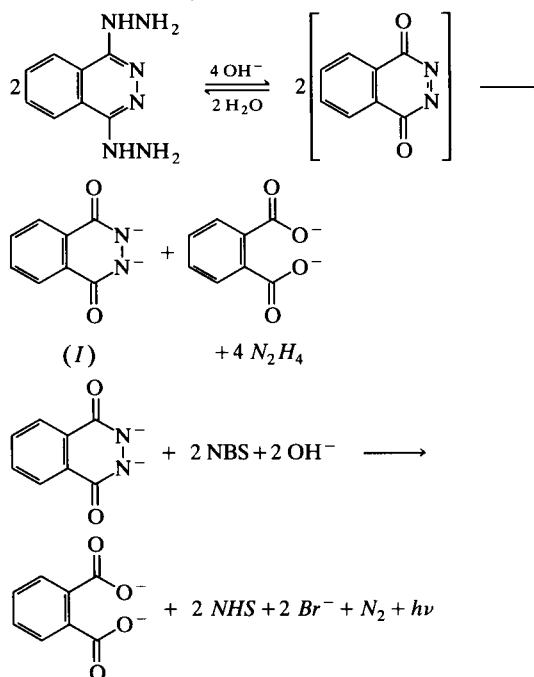
temperature were greatly affected by the degradation time. Figures 2 and 3 show that if the analytes are allowed to stand for about 4 h in alkaline medium, the emission intensity attains a constant maximum value. Hence the analysis must be carried out after a 4-h delay to ensure completion of degradation and repeatability of measurements. The degradation scheme for rifamycin SV is [22]



Rifampicin is similarly degraded to rifampicin quinone [23].

Dihydralazine reacts with NBS to produce CL only after alkaline degradation, probably to give

2,3-dihydrophthalazine-1,4-dione (I) [15], which is then oxidized by NBS:



The phthalate radical (intermediate) is the emitting species of the above reaction. The reac-

TABLE 6

Recovery of rifampicin ($0.0200 \mu\text{g ml}^{-1}$) and dihydralazine ($5.00 \mu\text{g ml}^{-1}$) from solutions with co-existing compounds

Analyte	Co-existing compound	Concentration ratio (compound to analyte)	Recovery ($n = 3$) (%)
Rifampicin	25-Desacetyl-rifampicin	10	904.9
		1	190.2
	Rifampicin <i>N</i> -oxide	0.1	97.6
		10	988.2
	Rifampicin quinone	1	186.0
		0.1	102.9
Ascorbic acid	10	1314	
	1	169.6	
	0.1	99.6	
Dihydralazine	Reserpine	10	98.1
		1	98.4
	Hydrochlorothiazide	10	112.8
		1	103.0
	Ascorbic acid	10	77.4
		1	94.8
	0.1	99.6	

tion is similar to the chemiluminogenic oxidation of luminol, which generates the aminophthalate radical. The presence of the 3-amino group is responsible for the more intense CL generated by luminol than by 2,3-dihydrophthalazine-1,4-dione. However, the CL reactions of rifamycin quinone (rifamycin S) and rifampicin quinone with NBS and the nature of the emitting species are not clear.

Effect of flow-rate

The effect of flow-rate on the emission intensity is shown in Figs. 4 and 5 for rifampicin and

dihydralazine, respectively. The optimum values for the reagent and sample flow-rates were 2.50 and 3.90 ml min⁻¹, respectively, for both compounds. These flow-rates allow the solutions to react for about 0.6 s before entering the cell, depending on the manifold configuration.

Effect of NBS and alkali concentrations

The effect of sodium hydroxide concentration in the range 0.010–0.10 M on 5.00 and 20.0 µg ml⁻¹ of rifampicin and in the range 0.0010–0.050 M on 20.0 and 50.0 µg ml⁻¹ of dihydralazine is shown in Figs. 6 and 7, respectively. Concentra-

TABLE 7

Recovery experiments on rifampicin, rifamycin SV and dihydralazine added to sample solutions of commercial formulations

Analyte	Formulation	Analyte (µg ml ⁻¹)			Recovery (n = 3) (%)
		Initially present	Added	Recovered	
Rifampicin	Rifadin Capsules, 150 mg	0.0488	0.0500	0.0508	101.6
			0.1000	0.0996	99.6
			0.1500	0.1521	101.4
	Capsules, 300 mg	0.0497	0.0500	0.0491	98.2
			0.1000	0.1003	100.3
			0.1500	0.1498	99.9
	Tablets, 600 mg	0.0476	0.0500	0.0507	101.4
			0.1000	0.1025	102.5
			0.1500	0.1550	103.3
	Suspension, 100 mg in 5 ml	0.0571	0.0500	0.0497	99.4
			0.1000	0.0966	96.6
			0.1500	0.1498	99.9
	Rifampicine Capsules, 300 mg	0.0490	0.0500	0.0496	99.2
			0.1000	0.0999	99.9
			0.1500	0.1447	96.5
Tablets, 600 mg		0.0485	0.0500	0.0487	97.4
			0.1000	0.0997	99.7
			0.1500	0.1524	101.6
Mean: 99.9					
Rifamycin SV	Rifocin Injection, 250 mg in 3 ml	0.0526	0.0485	0.0484	99.8
			0.0969	0.0992	102.4
			0.1454	0.1503	103.4
			Mean: 101.9		
Dihydralazine	Nepresol Tablets, 25 mg	2.46	2.00	1.92	96.0
			6.00	6.02	100.3
			7.50	7.59	101.2
			Mean: 99.2		

tions of 0.0200 M for NBS and 0.050 M for sodium hydroxide were determined to be optimum for the determination of rifampicin. Correspondingly, the optimum concentrations for dihydralazine were 0.0150 M for NBS and 0.0050 M for sodium hydroxide. (These are not the optimum alkaline concentrations in the presence of ammonia; see below.) At higher concentrations of NBS the emission intensity decreases slightly. The chosen concentrations of NBS ensure that the emission intensity depends only on the concentration of rifampicin and dihydralazine. However, the effect of sodium hydroxide concentration is critical, because at higher concentrations of alkali the CL emission intensity was reduced or eliminated, probably for kinetic reasons. The rate increases and the reaction proceeds to completion before entry of the solution into the measuring cell.

Effect of ammonia

The reaction of ammonia with NBS was found to produce CL [7,24]. When ammonia was added to the rifampicin or dihydralazine solution, the CL emission was more intense than the sum of the intensities from each of the components of the mixture. This observation is probably due to oxidation of ammonia by NBS to excited nitrogen [25], which then chemiexcites the emitting species produced by each CL reaction studied. As the addition of ammonia allows the determination of very low concentrations of analyte, its effect on the emission intensity at various concentrations of sodium hydroxide was investigated. Figure 8 shows that 0.0010 M ammonia and 1.0 M sodium hydroxide were the optimum concentrations for maximum intensity for the determination of rifampicin. Correspondingly, Fig. 9 shows that the optimum concentrations for dihydralazine were 0.050 M ammonia and 0.0030 M sodium hydroxide. It must be noted that no blank emission intensity was observed for the determination of dihydralazine using the above optimum concentrations of alkali and ammonia, in contrast to the rifampicin measurement. This must be attributed to the low concentration of sodium hydroxide, which is 100 times lower than optimum for the reaction between NBS and ammonia [24].

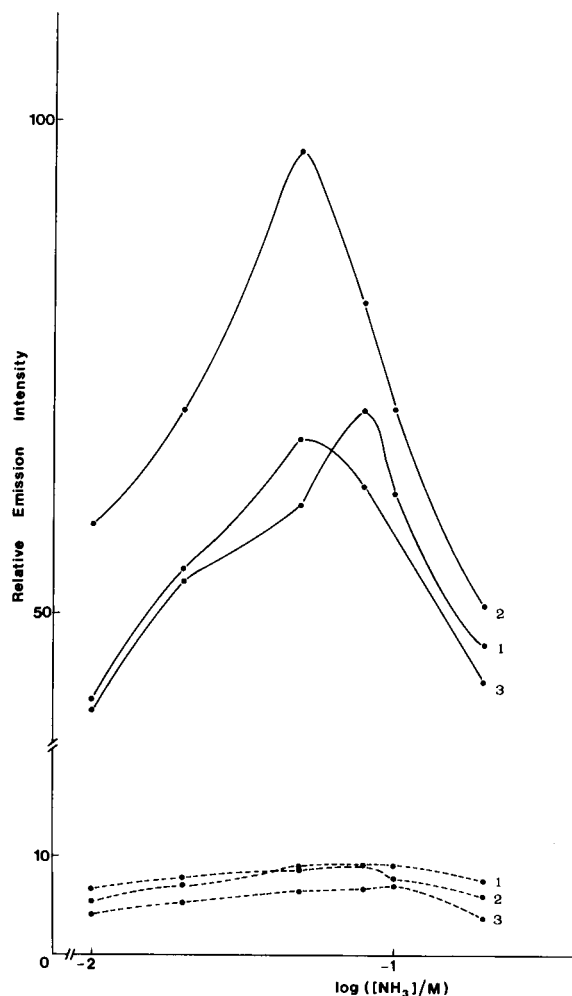


Fig. 9. Effect of ammonia concentration on the CL intensity from (broken lines) 5.00 and (solid lines) 15.0 $\mu\text{g ml}^{-1}$ of dihydralazine at (1) 0.0010, (2) 0.0030 and (3) 0.0050 M sodium hydroxide.

Analytical parameters

Figures 10 and 11 show typical recordings for a series of rifampicin and dihydralazine standards, respectively, obtained using the corresponding proposed procedures. Solutions can be introduced into the manifold at a rate of about 105 h^{-1} , for all analytes. Table 3 summarizes the analytical characteristics for the compounds studied. Results for the determination of analytes in aqueous solutions are given in Table 4.

The slopes of the log–log calibration graphs

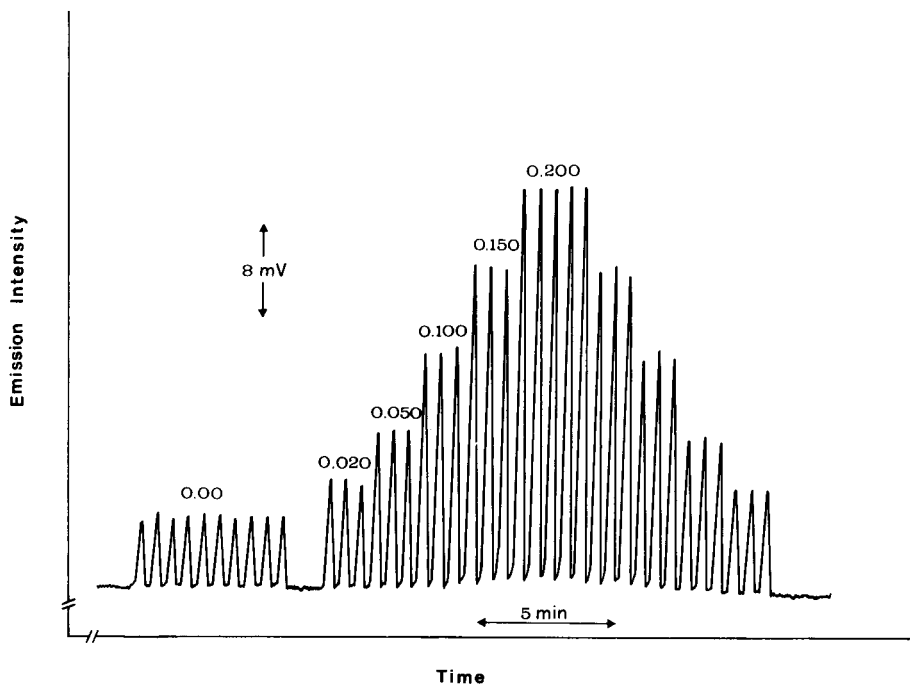


Fig. 10. Typical recording output for the NBS-rifampicin reaction under the recommended conditions. The numbers above each set of peaks are $\mu\text{g ml}^{-1}$ rifampicin.

show that the emission intensity is proportional to the dihydralazine concentration to the power 1.96, indicating that two molecules of dihydrala-

zine are required to produce one photon. Rifampicin and rifamycin SV generate one photon per analyte molecule.

TABLE 8

Determination of rifampicin, rifamycin SV and dihydralazine in commercial formulations with the proposed CL method and official methods [8,26]

Analyte	Formulation	Analyte (mg)			Relative difference (CL – official) (%)
		Amount	Found		
			By CL (\pm S.D. ^a)	By official methods	
Rifampicin	Rifadin (capsule)	150	150 \pm 2	153	-2.0
		300	310 \pm 6	307	+1.0
	Rifampicine (capsule)	300	302 \pm 1	300	+0.7
	Rifadin (tablet)	600	584 \pm 1	601	-2.8
	Rifampicine (tablet)	600	586 \pm 6	590	-0.7
Rifadin (5-ml suspension)	100	113 \pm 1	116	-2.6	
					Mean: 1.6
Rifamycin SV	Rifocin (3-ml injection) ^b	250	263 \pm 4	262	+0.4
Dihydralazine	Nepresol (tablet)	25	24.8 \pm 0.4	25.2	-1.6

^a Each sample measured three times. ^b The sample also contains 10 mg of lidocaine hydrochloride, polyvinylpyrrolidone and preservatives.

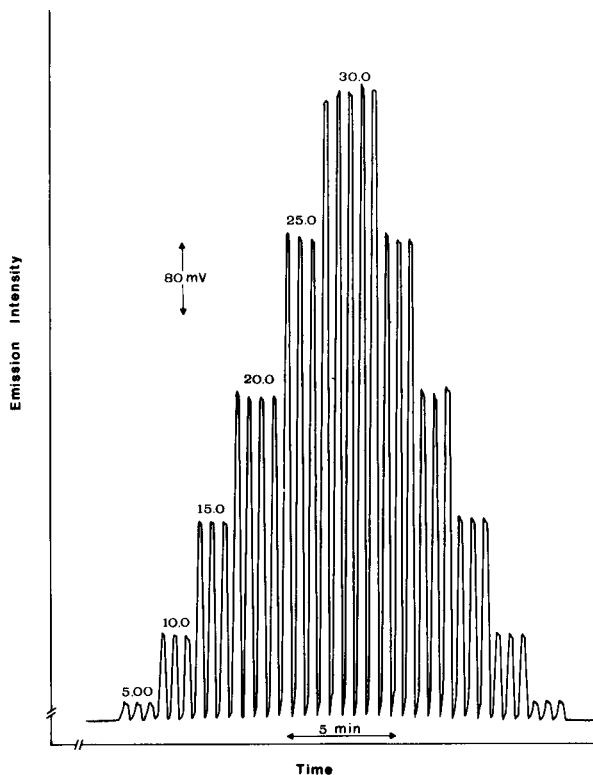


Fig. 11. Typical recording output for the NBS–dihydralazine reaction under the recommended conditions. The numbers above each set of peaks are $\mu\text{g ml}^{-1}$ dihydralazine.

Interference studies

In order to assess the possibility of applying the proposed continuous CL methods to assays of commercial formulations, the effect of some common excipients used in pharmaceutical preparations was studied by analysing synthetic sample solutions containing $0.100 \mu\text{g ml}^{-1}$ of rifampicin or $5.00 \mu\text{g ml}^{-1}$ of dihydralazine and a tenfold concentration of each excipient. The undissolved material, if any, was filtered before measurement. The recovery results are given in Table 5. No interference was observed from any of the excipients tested, which showed recoveries in the range 95.4–104.6% for rifampicin and 95.8–102.4% for dihydralazine.

The effect of some common co-existing compounds on the recovery of 0.0200 and $5.00 \mu\text{g ml}^{-1}$ of rifampicin and dihydralazine, respectively, was studied by analysing synthetic samples,

as for excipients, but with various amounts of each co-existing compound (Table 6). 25-Desacetyl-rifampicin, rifampicin quinone and rifampicin *N*-oxide are the degradation products of rifampicin and they also give CL reactions with NBS. Hence the present method cannot be applied for stability studies.

Reserpine and hydrochlorothiazide are two common co-existing compounds with dihydralazine, with antihypertensive and diuretic action, respectively. Reserpine does not interfere even when present in a tenfold excess. Hydrochlorothiazide interferes when present at a concentration ratio > 1 , probably owing to a sensitization effect. The reactions of both compounds with NBS under the experimental conditions used did not produce CL.

Ascorbic acid is a common co-existing compound used as an antioxidant for preservation. When rifampicin is determined, ascorbic acid does not interfere, even when present in a tenfold excess, because of its oxidation by dissolved oxygen in alkaline solution. However, when dihydralazine is determined, the alkali concentration is very low and the oxidation of ascorbic acid is not complete. The unreacted amount of ascorbic acid reacts with NBS, reduces the concentration and, therefore, decreases the emission intensity.

It should be noted that the method cannot be applied to samples containing rifampicin and isoniazid, because the latter reacts in alkaline medium with NBS producing CL emission [7]. However, the CL detector might be used for the analysis of rifampicin and isoniazid mixtures after liquid chromatographic separation.

Accuracy

The accuracy of the proposed continuous-flow CL methods was examined by performing recovery experiments on solutions prepared from analyte formulations. The mean recoveries found for rifampicin, rifamycin SV and dihydralazine were 99.9% (range 96.5–103.3%), 101.9% and 99.2%, respectively (Table 7).

The proposed methods were also evaluated by analysing commercial formulations and comparing the results with those obtained by official methods [8,26]. Satisfactory agreement between

the results was obtained (Table 8) with a mean relative difference of 1.5%.

Conclusions

The capability of NBS as an organic CL oxidizing reagent was confirmed and its application in pharmaceutical analysis was extended. However, the nature of the emitting species has not been clearly established.

The proposed CL methods for the determination of dihydralazine, rifampicin and rifamycin SV are simple, accurate and precise. The results are reproducible and show that the methods can be applied to the sensitive analysis of pharmaceutical preparations without severe interferences.

The authors are grateful to Professor G.D. Christian and Professor A.C. Calokerinos for helpful discussions. One of the authors (S.A.H.) thanks the University of Athens for financial support.

REFERENCES

- 1 R.W. Abbott, A. Townshend and R. Gill, *Analyst*, 111 (1986) 635.
- 2 I.I. Koukli, A.C. Calokerinos and T.P. Hadjiioannou, *Analyst*, 114 (1989) 711.
- 3 N. Grekas and A.C. Calokerinos, *Talanta*, 37 (1990) 1043.
- 4 N.L. Malavolti, D. Pilosof and T.A. Nieman, *Anal. Chim. Acta*, 170 (1985) 199.
- 5 R.L. Veazey and T.A. Nieman, *J. Chromatogr.*, 200 (1980) 153.
- 6 S. Kobayashi and K. Imai, *Anal. Chem.*, 52 (1980) 424.
- 7 S.A. Halvatzis, M.M. Timotheou-Potamia and A.C. Calokerinos, *Analyst*, 115 (1990) 1229.
- 8 United States Pharmacopeia 1985, Mack, Easton, PA, 21st edn., 1985, p. 495.
- 9 W.K. Nonidez and D.E. Leyden, *Anal. Chim. Acta*, 96 (1978) 401.
- 10 D.V. Naik, B.R. Davis, K.M. Minnet and S.G. Schulman, *J. Pharm. Sci.*, 65 (1976) 274.
- 11 N.K. Mathour and C.K. Narang (Eds.), *The Determination of Organic Compounds with N-Bromosuccinimide and Allied Reagents*, Academic, London, 1975, p. 81.
- 12 W. Kitzing, *Pharmazie*, 16 (1961) 401; *C.A.*, 62 (1965) 403.
- 13 F. Zbigniew and S. Edmund, *Acta Pol. Pharm.*, 39 (1982) 395; *Anal. Abstr.*, 45 (1983) 3E60.
- 14 F. Trischler, *Fresenius' Z. Anal. Chem.*, 292 (1978) 141.
- 15 S. Pinzauti, V. Dal Piaz and E. La Porta, *J. Pharm. Sci.*, 63 (1974) 1446.
- 16 G.R. Rao, S.S.N. Murty and E.V. Rao, *Indian Drugs*, 22 (1985) 484; *Anal. Abstr.*, 48 (1986) 2E31.
- 17 C.R. Pasqualucci, A. Vigevani, P. Radaelli and G.G. Gallo, *J. Pharm. Sci.*, 59 (1970) 685.
- 18 N. Awata, I. Iwane, H. Nakagawa and I. Sugimoto, *Yukuzaigaku*, 38 (1978) 145; *Anal. Abstr.*, 38 (1980) 4E29.
- 19 E.H. White, M.M. Bursey, D.F. Roswell and J.H.M. Hill, *J. Org. Chem.*, 32 (1967) 1198.
- 20 F. McCapra, *Prog. Org. Chem.*, 8 (1973) 231.
- 21 K.D. Gundermann, *Angew. Chem., Int. Ed. Engl.*, 4 (1965) 566.
- 22 S. Furesz, *Antibiot. Chemother.*, 16 (1970) 316.
- 23 J.K. Seydel, *Antibiot. Chemother.*, 16 (1970) 380.
- 24 S.A. Halvatzis and M.M. Timotheou-Potamia, *Talanta*, submitted for publication.
- 25 H. Jurgensen and J.D. Winefordner, *Talanta*, 31 (1984) 777.
- 26 *European Pharmacopoeia*, Maisonneuve, Paris, 2nd edn., 1983, p. 52 and 1985, p. 432.

Flow-injection chemiluminometric determination of sodium cyclamate¹

Ioannis M. Psarellis, Evangelos G. Sarantonis and Antony C. Calokerinos

Laboratory of Analytical Chemistry, University of Athens, Panepistimiopolis, Zografou, 157 71 Athens (Greece)

(Received 27th July 1992)

Abstract

The sensitizing effect of sodium cyclamate on the chemiluminogenic oxidation of sulphite by cerium(IV) in sulphuric acid allows the determination of the artificial sweetener in the range 1.00–50.0 $\mu\text{g ml}^{-1}$. The flow-injection method developed is rapid and precise and allows measurements on up to 100 solutions per hour. Acetonitrile does not alter significantly the analytical characteristics of the method, which can therefore be proposed for the determination of the analyte after liquid chromatographic separation from other sweeteners and possible metabolites.

Keywords: Chemiluminescence; Flow injection; Sodium cyclamate; Sweeteners

Sodium cyclamate (sodium cyclohexylsulphamate) is an artificial non-nutritive sweetener, about 30 times sweeter than sucrose [1]. It can be determined by titration with perchloric acid in acetic acid [2], with a cyclamate-selective electrode [3] and by UV absorption after normal- [4] or reversed-phase [5] separation by liquid chromatography (LC) from other sweeteners. No chemiluminescent procedure for the determination of sodium cyclamate seems to have been reported.

The oxidation of sulphite by cerium(IV) exhibits weak chemiluminescence (CL) [6], which is enhanced by the presence of 3-cyclohexylamino-propanesulphonic acid (CAPS) [7]. CAPS also

enhances the intensity from the CL reaction between sulphite and permanganate in acidic medium [8]. CAPS is not a fluorophore, and so cannot participate in an energy transfer mechanism; its sensitizing action on the CL emission is not fully understood. Other examples of compounds with a cyclohexyl structure showing sensitizing effects similar to that of CAPS are 3-cyclohexylaminoethanesulphonic acid (CHES), 3-cyclohexylamino-2-hydroxy-1-propanesulphonic acid (CAPSO) and sodium cyclamate [9].

It was decided to investigate the possibility of using the sensitizing action of sodium cyclamate on the cerium(IV)–sulphite CL reaction and to evaluate the analytical usefulness of this intriguing property.

Correspondence to: A.C. Calokerinos, Laboratory of Analytical Chemistry, University of Athens, Panepistimiopolis, Zografou, 157 71 Athens (Greece).

¹ Presented at SAC 92, the 10th International Conference on Analytical Chemistry, Reading, UK, 20–26th September, 1992.

EXPERIMENTAL

Apparatus

The flow manifold used (Fig. 1) was similar to that used previously [10] and consisted of a peri-

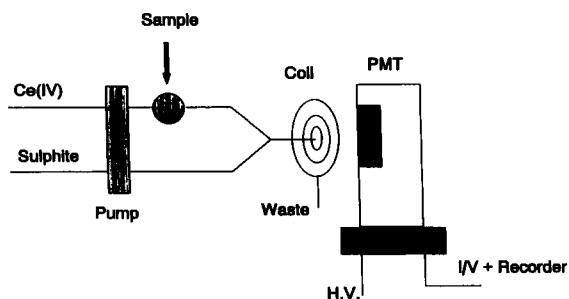


Fig. 1. Schematic diagram of the flow-injection chemiluminescence (not to scale).

static pump (Ismatec Mini-S 820) which pumped both reagent solutions at equal flow-rates (6.0 ml min^{-1}) through PTFE flow tubes, a low-pressure PTFE injection valve (Rheodyne Model 5020, Anachem) manually operated and provided with a $50\text{-}\mu\text{l}$ sample loop through which the sample was injected into the stream of oxidant, and a Y-shaped mixing element for mixing the two streams, positioned in front of the flow cell inlet.

The detector consisted of a glass coil with 3.5 turns of glass tubing (2 mm i.d.) with a total height of 22 mm accommodated in a Heath sample cell module (EU-701-11). The coil was placed 2 mm from the photomultiplier tube window and was backed by a mirror for maximum light collection by the photomultiplier (PMT). The PMT (RCA 931A, S-4 response) was housed in a Heath photomultiplier module (EU-701-30) and was operated at -700 V . The output was fed to a current-to-voltage (I/V) converter based on an RCA CA 3140 operational amplifier. Damping was provided by inserting an RC circuit between the converter and the multi-speed variable-span recorder (Perkin-Elmer Model 56).

Reagents

All solutions were prepared from analytical-reagent grade materials in deionized, distilled water.

A $1.00 \times 10^{-2} \text{ M}$ stock solution of sulphite was prepared by dissolving 0.630 g of sodium sulphite (Merck) in water and diluting with water to 500 ml.

A $5.00 \times 10^{-3} \text{ M}$ stock solution of cerium(IV) was prepared by dissolving 0.2022 g of cerium(IV)

sulphate tetrahydrate (Ferak) in 0.10 M sulphuric acid and diluting to 100 ml with the same acid.

A $100.0 \mu\text{g ml}^{-1}$ solution of sodium cyclamate was prepared by dissolving 0.1000 g of the compound (Sigma) in water and diluting with water to 1 l.

Procedure

Cerium(IV) ($2.5 \times 10^{-4} \text{ M}$ in 0.10 M sulphuric acid) and $1.00 \times 10^{-3} \text{ M}$ sulphite were continuously pumped into the manifold. Volumes of 50 μl of solutions of sodium cyclamate were injected into the stream of oxidant.

RESULTS AND DISCUSSION

The principle of the determination of cyclamate is that it increases the weak radiation emitted during the CL oxidation of sulphite by cerium(IV) in sulphuric acid medium. The two reactants are continuously mixed and introduced into the flow cell and the weak CL emission is continuously recorded as the baseline. When cyclamate is injected into the oxidant stream, the intensity is enhanced in proportion to its concentration.

Effect of flow-rate

The solutions of cerium(IV) and sulphite were introduced into the manifold at equal flow-rates. Sodium cyclamate was injected into the stream of oxidant, as with this configuration the emission was about 20 times more intense than when it was injected into the stream of $1.00 \times 10^{-2} \text{ M}$ sulphite.

The effect of flow-rate on the emission intensity is shown in Fig. 2. High flow-rates were required for increased sensitivity, as was expected from the increased reaction rate. It was decided to supply the oxidant and the sulphite solution each at 6.0 ml min^{-1} to avoid extensive consumption of reagents without a pronounced increase in sensitivity. The weak emission generated from sulphite in the absence of cyclamate (blank emission) was continuously recorded as the baseline.

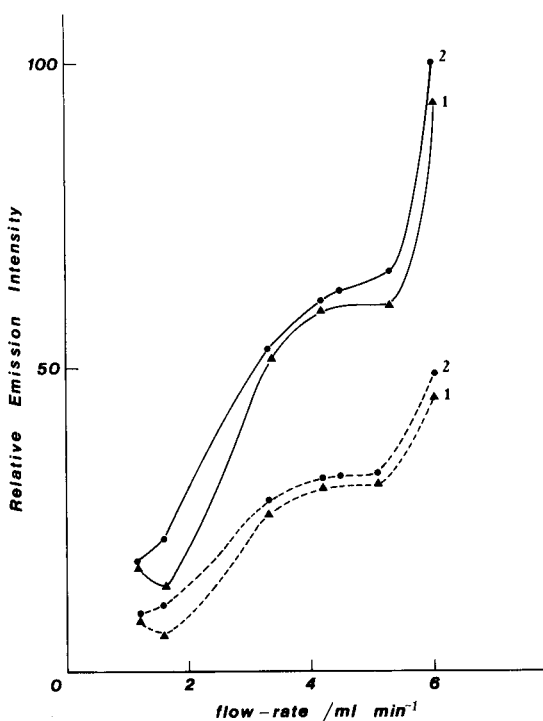


Fig. 2. Effect of flow-rate on the emission intensity from 10.00 (solid line) and 5.00 (dashed line) $\mu\text{g ml}^{-1}$ sodium cyclamate injected in (1) 1.0×10^{-3} and (2) 2.5×10^{-4} M cerium(IV) in 0.10 M sulphuric acid; $[\text{SO}_3^{2-}] = 1.00 \times 10^{-3}$ M.

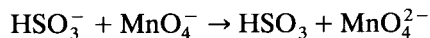
Effect of concentration of cerium(IV) and sulphuric acid

The effect of the concentration of cerium(IV) in 0.10 M sulphuric acid is shown in Fig. 3. The optimum concentrations for the oxidant are 5.0×10^{-4} and 2.5×10^{-4} M when 1.00×10^{-2} and 1.00×10^{-3} M sulphite is used, respectively. Nevertheless, the difference in emission intensity between these two oxidant concentrations is not significant. This observation allowed the use of 2.5×10^{-4} M cerium(IV) to minimize the absorption of radiation generated by concentrations of the analyte at the upper part of the calibration graph.

Cerium(IV) is a strong oxidant in sulphuric acid solutions [11] and the concentration of the acid affects the CL intensity (Fig. 4). The optimum concentration used was 0.20 M.

Effect of concentration of sulphite

Excited sulphur dioxide has been proposed as the emitting species during the oxidation of sulphite by permanganate [12] and cerium(IV) [13]. The mechanism proposed by Meixner and Jaeschke [14] for the CL reaction with permanganate is



Thus, sulphite acts as the reductant and the energy released from the chemical reaction chemiexcites the unreacted sulphur dioxide, which emits radiation with wavelengths > 300 nm [15]. Therefore, the concentration of sulphite is important, as shown in Fig. 4, from which it was decided to use 1.00×10^{-3} M for all further work.

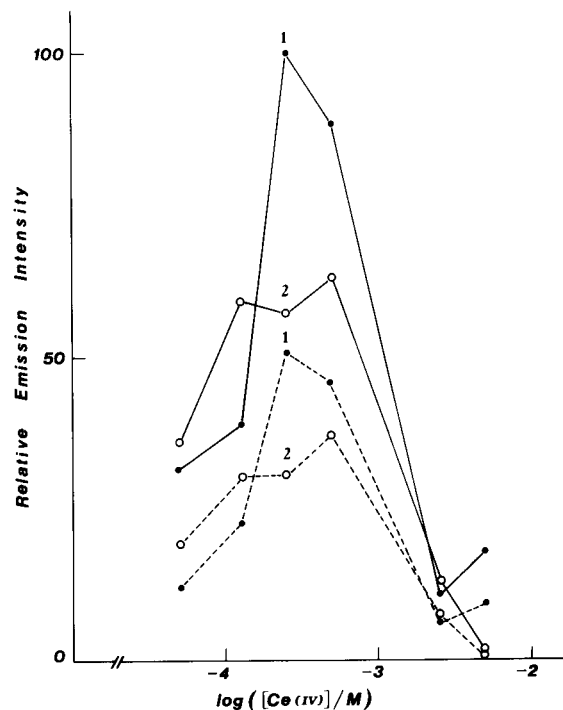


Fig. 3. Effect of cerium(IV) concentration in 0.10 M sulphuric acid on the emission intensity from (1) 1.00×10^{-3} and (2) 1.00×10^{-2} M sulphite in the presence of 10.00 (solid line) and 5.00 (dashed line) $\mu\text{g ml}^{-1}$ sodium cyclamate.

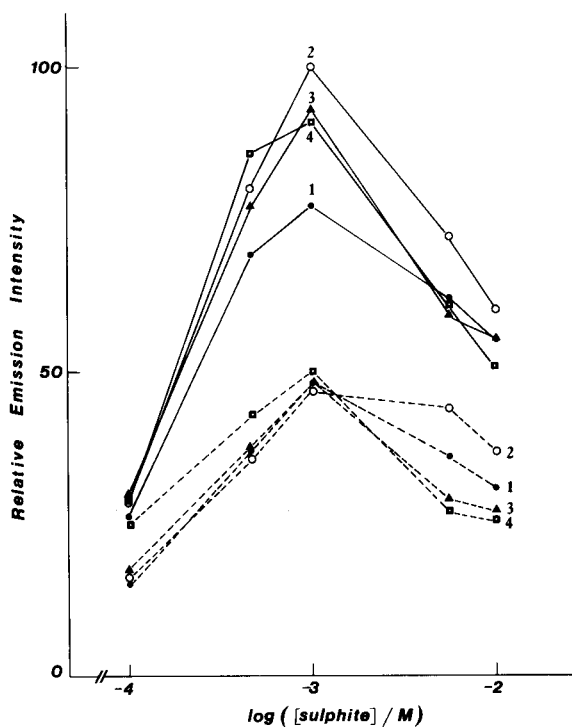


Fig. 4. Effect of sulphite concentration on the emission intensity from 10.00 (solid line) and 5.00 (dashed line) $\mu\text{g ml}^{-1}$ sodium cyclamate injected in 2.5×10^{-4} M cerium(IV) dissolved in (1) 0.10, (2) 0.20, (3) 0.50 and (4) 1.0 M sulphuric acid.

Analytical parameters

Figure 5 shows a typical recording for a series of sodium cyclamate standards carried out using the proposed procedure. The calibration graph is linear in the range 1.00–50.0 $\mu\text{g ml}^{-1}$ of sodium cyclamate (Table 1) and the relative standard deviations for 5.00 and 20.0 $\mu\text{g ml}^{-1}$ are 2.8 and 1.0%, respectively ($n = 8$).

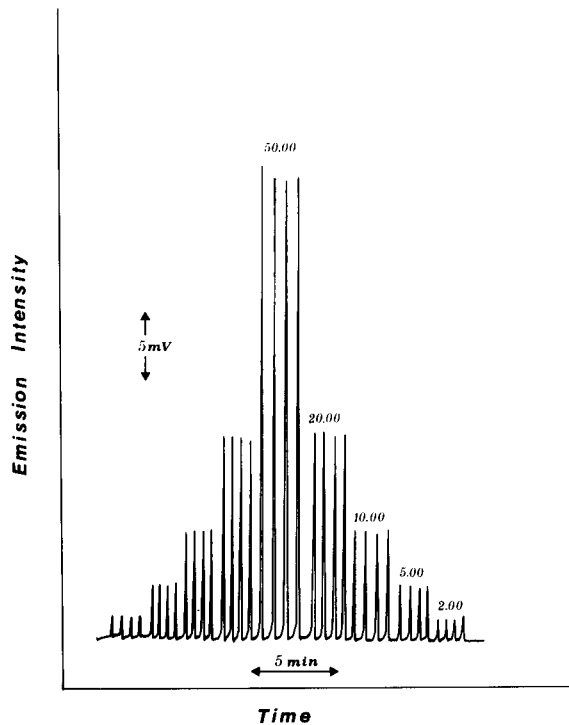


Fig. 5. Typical recorder outputs for the cerium(IV)–sulphite CL reaction sensitized by various concentrations of cyclamate ($\mu\text{g ml}^{-1}$, shown above each set of peaks).

Interference studies

In order to assess the possible analytical applications of this CL method, the effect of some common sweeteners was studied by analysing synthetic sample solutions containing 10.0 $\mu\text{g ml}^{-1}$ of sodium cyclamate with various excess amounts of each sweetener. The undissolved material, if any, was filtered before measurement. The re-

TABLE 1

Analytical characteristics for the determination of sodium cyclamate by its sensitizing effect on the cerium(IV)–sulphite CL reaction and the effect of acetonitrile

Acetonitrile (%, v/v)	Concentration ($\mu\text{g ml}^{-1}$)		Calibration graph		
	Linear range	LOD ^a	Slope	Intercept	r ($n = 5$)
0–10	1.00–50.0	0.40	0.426	0.43	0.9990
20	5.00–50.0	1.80	0.335	0.0043	0.9998
30	5.00–50.0	2.20	0.219	0.11	0.9998

^a Limit of detection (signal-to-noise ratio = 3).

TABLE 2

Effect of various sweeteners on the CL emission intensity from $10.0 \mu\text{g ml}^{-1}$ of sodium cyclamate

Sweetener	Decrease in CL intensity (%)		
	S/C ^a = 100	S/C = 10	S/C = 1
Aspartame	86.5	72.7	45.5
Fructose	71.4	42.9	16.7
Galactose	60.0	42.0	0
Glucose	91.4	76.9	53.8
Sorbitol	76.4	68.1	55.3
Sugar	87.8	46.7	17.9

^a Concentration ratio (sweetener to cyclamate).

sults (Table 2) show severe interference from equal concentrations of sorbitol, glucose and aspartame, whereas sugar and fructose interfere to a lesser extent. Galactose leaves the intensity unaffected when present at the same concentration as sodium cyclamate. The interference can be attributed to the reaction of cerium(IV) with each sweetener and to the complexity of the chemiluminogenic solution, which reduces the efficiency of the energy transfer and the chemi-excitation processes.

The effect of fructose and aspartame on the CL measurement of sodium cyclamate was further investigated by keeping the oxidant and reductant concentrations constant and changing the concentration of sulphuric acid. The results (Table 3) show that as the concentration of acid is lowered, the interference is decreased. This is due to the decrease in the reaction efficiency and, therefore, cerium(IV) reacts with the interferences to a lesser extent. This is accompanied by

TABLE 3

Effect of sulphuric acid on the interference from aspartame and fructose on the CL intensity from $10.0 \mu\text{g ml}^{-1}$ of sodium cyclamate

Sulphuric acid (M)	Decrease in CL intensity (%)					
	Aspartame			Fructose		
	S/C ^a = 100	S/C = 10	S/C = 1	S/C = 100	S/C = 10	S/C = 1
0.050	44.4	20.6	0	44.4	26.7	6.7
0.10	53.3	36.7	3.3	43.0	21.4	7.2
0.50	87.9	59.3	24.4	48.2	25.0	16.7
1.0	86.5	72.7	45.3	71.4	42.9	22.5

^a Concentration ratio (sweetener to cyclamate).

a decrease in the sensitivity of the method, which is pronounced at 0.050 M sulphuric acid. Therefore, 0.10 M sulphuric acid is the best concentration as a compromise between low sensitivity and reduced interference from other sweeteners.

Effect of acetonitrile

As acetonitrile is a common solvent used in the LC separations of sodium cyclamate from other sweeteners and possible metabolites, its effect on the CL intensity was investigated. The effect of aqueous solutions of acetonitrile on the analytical parameters of the proposed CL method are shown in Table 1. From the results, it is seen that up to 30% (v/v) acetonitrile in water does not affect the linear range severely, but a decrease in the slope of the regression line is observed. The decrease in sensitivity due to quenching by the presence of organic solvents is a common observation in CL detection after LC separation [16]. Nevertheless, the method can be used for the determination of sodium cyclamate after LC separation from other compounds by using aqueous acetonitrile as the mobile phase.

Conclusions

Although the mechanism of the CL reaction is not fully understood, sodium cyclamate can be determined by its sensitizing action on the cerium(IV)–sulphite chemiluminescent reaction. Other sweeteners interfere to various extents but separation can be used as acetonitrile does not interfere severely with the determination.

REFERENCES

- 1 T.H. Grenby, *Chem. Br.*, 27 (1991) 342.
- 2 M.V. Rao, A.G. Krishnamacharyulu, O.P. Kapur and C.S.P. Sastry, *J. Food Sci. Technol.*, 20 (1983) 205.
- 3 D. Feng and C. Chen, *Fenxi Huaxue*, 16 (1988) 738; *Anal. Abstr.*, 51 (1989) 5J159.
- 4 A. Herrmann, E. Damawandi and M. Wagemann, *J. Chromatogr.*, 280 (1983) 85.
- 5 J.F. Lawrence and C.F. Charbonneau, *J. Assoc. Off. Anal. Chem.*, 71 (1988) 934.
- 6 K. Takeuchi, T. Nakada and S. Suzuki, *Anal. Chim. Acta*, 174 (1985) 359.
- 7 I.I. Koukli, E.G. Sarantonis and A.C. Calokerinos, *Analyst*, 113 (1988) 603.
- 8 S.A. Al-Tamrah, A. Townshend and A.R. Wheatley, *Analyst*, 112 (1987) 883.
- 9 I.I. Koukli, E.G. Sarantonis and A.C. Calokerinos, *Anal. Lett.*, 23 (1990) 1167.
- 10 A.B. Syropoulos, E.G. Sarantonis and A.C. Calokerinos, *Anal. Chim. Acta*, 239 (1990) 195.
- 11 I.M. Kolthoff and R. Belcher, *Volumetric Analysis*, Vol. III, Interscience, New York, 1957.
- 12 J. Stauff and W. Jaeschke, *Atmos. Environ.*, 9 (1975) 1038.
- 13 K. Takeuchi and T. Ibusuki, *Anal. Chim. Acta*, 174 (1985) 359.
- 14 F. Meixner and W. Jaeschke, *Fresenius' Z. Anal. Chem.*, 317 (1984) 343.
- 15 R.W.B. Pearse and A.G. Gaydon, *The Identification of Molecular Spectra*, Chapman and Hall, London, 4th edn., 1976.
- 16 R.W. Abbott, A. Townshend and R. Gill, *Analyst*, 112 (1987) 397.

Liquid chromatographic assay of microbially derived phloroglucinol antibiotics for establishing the biosynthetic route to production, and the factors affecting their regulation

P. Shanahan and J.D. Glennon

Analytical Chemistry, University College, Cork (Ireland)

J.J. Crowley, D.F. Donnelly and F. O'Gara

Microbiology Department, University College, Cork (Ireland)

(Received 13th July 1992; revised manuscript received 6th October 1992)

Abstract

A preparative chromatographic isolation method involving thin-layer and liquid chromatography (LC) is described for the microbially derived antibiotic monoacetylphloroglucinol (MAPG). Isolation of MAPG along with the previously described 2,4-diacetylphloroglucinol (DAPG) confirms the production of two antimicrobial metabolites from *Pseudomonas* sp. strain F113. A gradient LC assay was developed for the determination of these compounds in growth culture media. A sample pretreatment procedure involving solid phase extraction on octadecylsilica is utilised prior to sample injection onto the LC column. This assay is used to monitor production of the two antibiotic metabolites from the strain of *Pseudomonas*. A range of nitrogen sources in the growth culture medium was tested for their ability to affect antibiotic production. A carbon source, such as galactose promotes high yields of antibiotics when the growth medium contains a nitrogen source in the form of ammonium ions, and produces low yields when the nitrogen source is added as nitrate ions. The LC assay is further applied to monitor the enzymatic acetylation of MAPG to DAPG, through an enzymatic activity named MAPG acetyltransferase which provides the final step in the elucidation of the biosynthesis of DAPG.

Keywords: Liquid chromatography; Antibiotics; Diacetylphloroglucinol; Monoacetylphloroglucinol; Phloroglucinol

Microbial cells synthesise a variety of compounds ranging from relatively simple sugars, amino acids and fatty acids to more complex antibiotics, pigments, proteins and polysaccharides [1]. Microbial cells are ideal for the production of many industrial chemicals, due to the ease of their mass-production, and the catalytic activi-

ties of the enzymes they contain. Modern microbial technology is targeted towards the exploitation of these enzymes for the production of useful chemicals in so-called bioreactors [2]. The potential appears limitless. For example, conservative estimates put the amount of enzymes identified to date, at only 10% of the total that occur in nature [1], and it is envisaged that in the future many beneficial chemicals will be synthesised using enzyme reactions.

High on the list of desirable microbial metabo-

Correspondence to: J.D. Glennon, Analytical Chemistry, University College, Cork (Ireland).

lites are antibiotics. Although the antibiotic era was initiated almost 50 years ago, the mass production of these compounds still remains the greatest success story in microbial biosynthesis. The vast majority of antibiotics have been detected by screening “wild type” microorganisms isolated from their natural habitats [3,4]. To date there are over 50 different antibiotic substances attributed to the species of *Pseudomonas fluorescens* alone, however only two of these, pyocyanine and pyrrolnitrin, have been produced on a commercial basis. With respect to this disappointing number Zahner [5] remains optimistic that microorganisms will provide a rich source for new products. None the less it is recognised that there is a great need to screen a larger diversity of microorganisms with more sensitive metabolite detection systems.

In the biosynthesis of antibiotics, and any other secondary metabolites, the coordinated cooperation of several enzymes is usually required. The performance of a particular enzyme depends on the concentration of several components of the medium (substrates, products, inductors, repressors, inhibitors and activators) [2]. Thus in order to achieve the full biological potential of the cells the optimal production conditions must be maintained at least with respect to the most important key parameters.

We previously reported on *Pseudomonas* sp. strain F113 isolated from the rhizosphere of sugar beet, that can inhibit a range of plant root pathogens through production of the antibiotic compound 2,4-diacetylphloroglucinol (DAPG) [6]. Recent studies in our laboratory on the same microbial strain have revealed the production of a second phloroglucinol compound monoacetylphloroglucinol (MAPG) which also possesses antibiotic properties. We describe here a liquid chromatographic (LC) method for the isolation of the monoacetyl compound and also the development of a gradient LC assay for quantitative detection of both phloroglucinols in growth culture media. This assay was used to monitor the enzymatic acetylation of MAPG to DAPG and also to show how different nutrients in the growth medium effect the production of one or both of these antifungal compounds.

EXPERIMENTAL

Preparative liquid chromatography

The preparative liquid chromatography system consisted of two Shimadzu LC-8A preparative liquid chromatography pumps which can operate up to 320 kgf cm^{-2} and supply flow-rates up to 100 ml min^{-1} . The pumps are controlled by a Shimadzu SCL-8A system controller. The solvents were mixed using a preparative mixing chamber before reaching the column. The sample was applied using a 1-ml loop attached to a Rheodyne injection valve. The column used was a BioRad preparative LC column ($250 \times 21.5 \text{ mm}$ i.d.) packed with Hi-Pore RP-318 material with particle size of $10 \mu\text{m}$. The mobile phase consisted of methanol–water (35:65, v/v). UV detection was carried out using a Shimadzu SP6-6A spectrophotometric detector at 254 nm equipped with a preparative flow-through cell. The output signal was recorded on a Shimadzu computerised data bank (C-R4A Chromatopac). All fractions were collected using an automatic fraction collector (Shimadzu FCV-100B).

Isolation of monoacetylphloroglucinol (MAPG) using preparative LC

Isolation of the crude antibiotic compound from the *Pseudomonas* species (code named F113) was carried out as described previously [6]. This crude isolate was then streaked on thin-layer plates coated with silica gel G.F. (Sigma) and developed in dichloromethane–hexane–methanol (50:40:10, v/v). A broad band ($R_f = 0.48$) was scraped from the plate and assayed for biological activity as before [6]. The acetone was removed by rotary evaporation at 30°C and the residual material was dried under high vacuum for 12 h. The residue was reconstituted in methanol, filtered and applied to the preparative column for final purification. Repeated fractions of the purified compound were collected and the purity was checked using analytical LC, where it gave a single peak. An elemental analysis was also performed and the experimental values of C 57.8%, H 4.81% and N 0% compared favourably with the theoretical values of 57.1%, 4.76% and 0% for C, H and N, respectively. The 270 MHz ^1H

and ^{13}C NMR spectra were obtained on a Jeol Gix FT NMR spectrophotometer in deuterated acetone, with TMS as internal standard. A mass spectrum was obtained from the mass spectrometry laboratory, University College, Dublin, on a VG analytical 70E apparatus.

Analytical LC apparatus

The analytical LC system consisted of a Beckman System Gold programmable solvent pump (module 126) attached to a Beckman autosampler with a 20- μl loop. The column used was a Spherisorb ODS-2 analytical column (particle size 5 μm , 250 \times 4.6 mm i.d. \times 6 mm o.d.). A guard column was inserted before the main column (45 \times 4.6 mm i.d. \times 6 mm o.d.) packed with Hypersil ODS (particle size 5 μm). The detector used was a UV spectrophotometric detector (Beckman System Gold module 166). The pump and detector were controlled using an IBM computer (personal system/2 Model 50). Data acquisition and manipulation were also performed using this computer.

LC Assay for MAPG and DAPG

Isocratic elution conditions necessary for the separation of MAPG and DAPG resulted in a broad DAPG peak and overall reduced sensitivity, however a three-step gradient elution programme provided excellent separation of these compounds. Solvent A contained 100% water and solvent B contained methanol–THF (3:1). The initial conditions required isocratic flow at 92% B and 8% A for 6 min. During the following 3 min the organic content in the mobile phase was raised to 45% B and this composition was maintained isocratically for a further 1 min. During the next minute, the solvent system was changed to 45% A, 55% B and maintained isocratically for a further 15 min. Finally the eluent composition was returned to the initial condition over 1 min, which was maintained for 8 min, giving a total gradient time of 35 min. Solvents for mobile phase preparation were of LC grade and all mobile phases were filtered and degassed on a Millipore LC filtration system using 0.45- μm filters. Before chromatographic analysis, all in vitro and enzyme extract samples were pretreated by solid

phase extraction using SepPak ODS cartridges (Waters) [7].

Monitoring in vitro antibiotic production

The ability of a number of nitrogen sources to induce antibiotic production was investigated. The cells were first cultured in 10 ml of Luria Bertani (LB) [8] medium, (overnight, at 28°C, shaking on a gyrotory G10 shaker at 150 rpm). The cells were washed twice in quarter strength ringers (Oxoid), added into 10 ml of the test medium, and incubated under stationary conditions in 100-ml Erlenmeyer flasks at 12°C. After four days a count on the number of colony forming units (cfu)^a was obtained, before antibiotic production was monitored using the outlined LC assay.

Preparation of cell-free extract

Bacterial cells were harvested by centrifugation (Denley BS 400) at 4500 rpm for 10 min after overnight growth in 200 ml LB medium. The supernate was discarded and the cells resuspended and washed in a sodium phosphate buffer (pH 6.8) and chilled in an ethanol/ice bath. The cells were disrupted by subjecting them to three pulses of sonic oscillation (15 s) on an MSE Soniprep 150 sonic oscillator with intervals of 60 s between each pulse. Cell debris was removed by centrifugation [8000 rpm (2000 g) for 4 min at 4°C]. The supernate was retained, stored on ice, and termed the cell-free extract for the purposes of this study.

Enzymatic transformation of MAPG to DAPG

Reaction mixtures (3.5 ml) consisted of 71.53% (v/v) of a 0.025 M solution of MAPG and 0.03% (v/v) 0.1 M Tris–HCl (pH 6.8). The volumes of distilled water and cell-free extract added varied from 28.47% (v/v) to 0% (v/v) depending on the final concentration of cell-free extract required. The controls employed were boiled cell-free extract or water in lieu of cell-free extract. The various reaction mixtures were equilibrated in 5 ml glass screw top bottles for 1 h at 23°C. The

^a cfu is the cell count unit providing a representation of the number of viable bacterial cells present in a culture, normally expressed per ml of that culture.

reactions were terminated by placing the reaction vessels in boiling water for 5 min.

RESULTS AND DISCUSSION

For many years, failure to detect antibiotic production in soils, unmodified by sterilisation or nutrient amendment left open the possibility that antibiotics are not actually produced by microorganisms in a natural environment [9,10]. Recently Thomashow et al. [11] devised an LC assay for the detection of phenazine-1-carboxylic acid in an untreated soil. This antibiotic compound is a metabolite of some pseudomonads and production of this compound is directly related to a suppression of the fungal disease "Take-all" in wheat. On this basis it is arguable that amongst the many antibiotics that are already known, some may have a greater role to play in plant biocontrol than initially thought. This highlights the need for more sensitive methods to monitor antibiotic production, and for more information on the mechanistic background to the microbial production of these bioactive compounds. In fact many chemical industries seeking to commercialise microbial mediated processes, have embarked on major studies in this area [12].

The antifungal compound 2,4-diacetylphloroglucinol (DAPG) was isolated from a strain of *Pseudomonas* [6], and the chromatographic isolation was optimised using medium pressure liquid chromatography [7]. Further study of the secondary metabolites of the organism, revealed the presence of a second bioactive compound. This compound was isolated using preparative LC on fractions removed from the thin layer plates (Fig. 1). It was crystallised from methanol–water and identified as 2,4,6-trihydroxyacetophenone (monoacetylphloroglucinol) MAPG, on the basis of direct comparison with the NMR and mass spectra of an authentic sample (Aldrich). The experimental melting point (218–220°C) compared favourably with the literature value of 218°C [13]. High-resolution mass spectrometry calculated a molecular weight for $C_8H_8O_4$ of 168.0422; this compares with the experimental value of 168.0420. Base peak: m/e 153.0184 ($M - CH_3$)⁻. To our

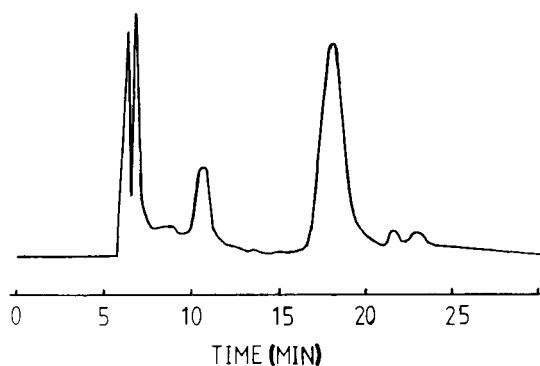


Fig. 1. Chromatogram obtained for the preparative LC isolation of MAPG ($t_R = 17.98$).

knowledge neither the preparative LC isolation of MAPG nor an LC assay which chromatographically separates this compound from the diacetyl form when produced in vitro has yet been reported in the literature. A typical gradient chromatogram showing the separation of MAPG and DAPG is shown in Fig. 2. This assay proved invaluable in studies carried out on the biosynthetic pathway and on the conditions necessary for optimum production of these metabolites. Some of the conditions for DAPG production by

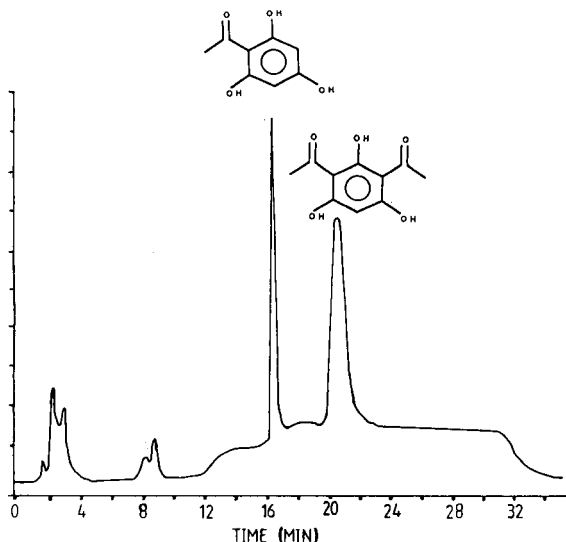


Fig. 2. Chromatogram obtained from supernates of the pseudomonad grown on LB medium showing separation of MAPG and DAPG.

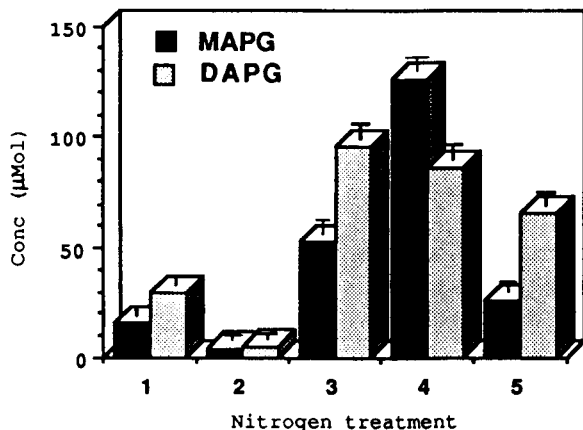


Fig. 3. Effect of nitrogen substrates on MAPG and DAPG production (1 = potassium nitrate; 2 = sodium nitrate; 3 = ammonium chloride; 4 = ammonium sulphate; 5 = urea). Cell counts are standardised at approximately 10^9 cfu ml⁻¹ of each test mixture.

this strain have already been studied in our laboratory. For example the effect of pH, oxygen availability, incubation temperature, and some carbon sources [6]. However this work is further expanded to incorporate a study on nitrogen sources while monitoring simultaneously both antibiotic metabolites.

Like many antimicrobial secondary metabolites DAPG and MAPG have been shown to occur only after the organisms have reached the stationary phase of growth, i.e. no further increase in cell number. MAPG accumulation was seen to be regulated by the composition of the growth medium as shown previously with other antibiotics [14]. When stationary phase bacterial cells were presented with various nitrogen sources in the presence of galactose as the sole carbon source, a variation in the levels of MAPG and DAPG was observed (Fig. 3). Antibiotic production was stimulated when the available nitrogen source was in the form of ammonium ions, while poor production was observed when the nitrogen source was supplied in the form of nitrate ions. From colony counts recorded prior to the LC assay the number of cfu remained at approximately 10^9 cfu ml⁻¹, and thus the changes in antibiotic levels are not attributed to a variation in biomass. The LC assay provides the basis for further study on the regulatory effect of a broad

range of substrates on antibiotic production. For example carbon sources, nitrogen sources, ions, minerals and vitamins, and the concentrations of these substrates can be determined to produce optimal antibiotic production.

Along with the need for a complete understanding of the metabolic substrates necessary for optimum antibiotic production, an understanding of the biosynthetic route of the compound is desirable in the design of an efficient biocontrol agent. In this work, we report for the first time on the isolation of an enzyme activity in crude cell extract which converts MAPG to DAPG. Unlike many enzymatic reactions, enzymatic conversion of MAPG to DAPG cannot be monitored continuously by UV as there is no significant difference in the UV profiles of either compound. However many enzyme assays which employ LC in a “stop and sample” or discontinuous assay procedure have been described previously [15]. The technique adopted here involves stopping the reaction by immersing the reaction vessel in a bath of boiling water to denature the enzyme. The sample was then pretreated in the usual manner and passed through the LC system. A major factor which determines the initial velocity of an enzyme catalysed reaction is enzyme concentration. A linear relationship between the velocity of the reaction and enzyme concentration (ml of crude cell extract) was established using the LC assay (Fig. 4). Such a relationship is generally applicable to enzyme catalysed reactions [16]. Additions

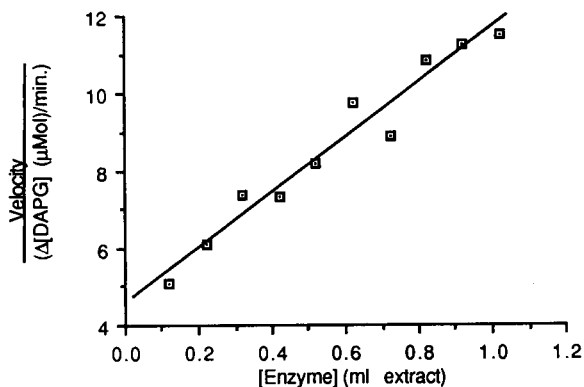


Fig. 4. Plot showing the reaction velocity (change in DAPG per min) versus enzyme concentration (volume of extract). Linear regression coefficient ($R = 0.9795$).

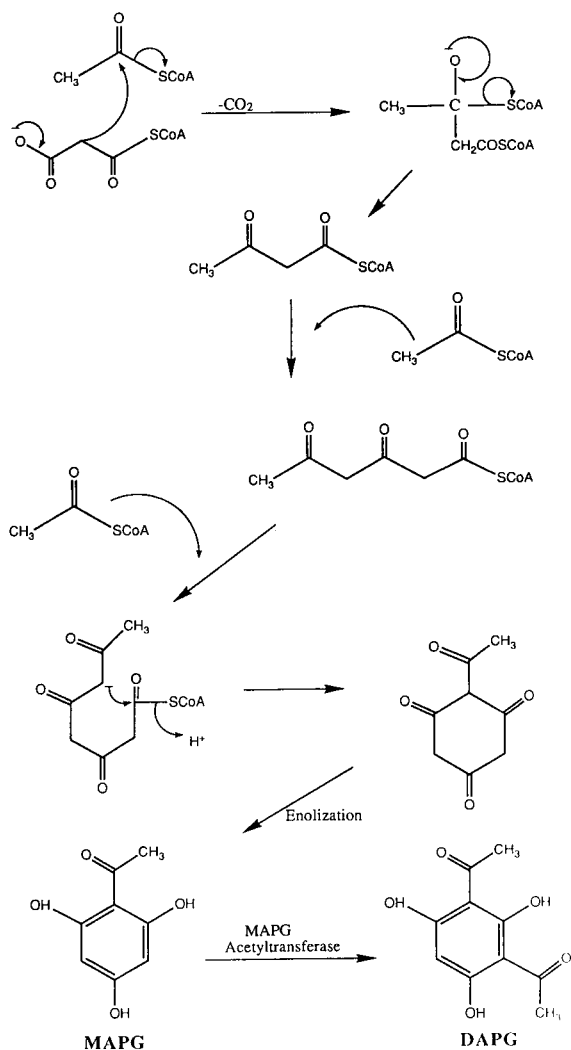


Fig. 5. The biosynthetic route to MAPG as outlined by Mann [18] and the subsequent acetylation of MAPG to DAPG via MAPG acetyltransferase.

of excess acetyl-S-CoA to the reaction mixture did not alter the velocity of the reaction. In accordance with the systematic nomenclature of enzymes [17], this enzymatic activity associated with cell-free extracts of *Pseudomonas* sp. strain F113 has been named MAPG acetyltransferase. The scheme shown by Mann [18] outlines the biosynthetic route to MAPG via a Claisen type condensation reaction (Fig. 5). Therefore, based on the work in this article it is consistent to suggest that the biosynthesis of DAPG from MAPG is catal-

ysed by the novel enzymatic activity of MAPG acetyltransferase in *Pseudomonas* strain F113.

Conclusions

The advent of more sensitive detection methods and recombinant DNA technology have conclusively shown that antibiotics are produced in natural environments, and through their production, microorganisms can function as biocontrol agents against plant pathogenic fungi [4,11]. The isolation of MAPG from the *Pseudomonas* sp. strain F113 adds an additional compound to the spectrum of antibiotic compounds produced by this organism. To access the biocontrol potential of this strain, there is a need to determine the conditions under which metabolic production of these compounds can be maximised in vitro. Such studies were made possible by the development of a gradient LC assay for the simultaneous analysis of MAPG and DAPG. The enzymatic transformation of MAPG to DAPG can also be studied with this assay. This reaction, in conjunction with information from the literature [18] provides a possible biosynthetic route to DAPG. The enzymatic acetylation of MAPG to DAPG also has the practical application of converting a readily supplied chemical (MAPG) to a compound which involves an elaborate chemical synthesis (DAPG). From a microbial viewpoint the acetylation reaction generates a compound which is over five times more toxic to plant pathogenic fungi than MAPG [13], thus increasing the strain's ability to survive in the competitive environment of the rhizosphere. The understanding of how the microbe functions at a molecular level and the manipulation of these functions are desirable prerequisites for the development of any successful biocontrol agent.

We thank Michael O'Shea and Pat Higgins for their technical assistance, Dr. Peter Caplin, University College Dublin, for running the mass spectrum, Dr. Peter Stephens and Don Cronin for their helpful assistance and advice. This work was supported in part by the contract No. EC AGRE 0019 under the ECLAIR programme and the contract No. BIOT CT91-0283 under the EC BRIDGE programme to F. O'Gara.

REFERENCES

- 1 S.L. Neidleman, *Genet. Eng. Biotechnol.*, 11 (1991) 20–22.
- 2 K. Schugerl, *Anal. Chim. Acta*, 213 (1988) 1–9.
- 3 L.K. Fredrickson, L.F. Elliott, and J.C. Engibous, *Soil Biol. Biochem.*, 19 (1987) 127–134.
- 4 C.R. Howell and R.D. Stipanovic, *Phytopathology*, 70 (1980) 712–715.
- 5 H. Zahner, *Pestic. Sci.*, 16 (1985) 424–425.
- 6 P. Shanahan, D.J. O'Sullivan, P. Simpson, J.D. Glennon, and F. O'Gara, *Appl. Environ. Microbiol.*, 58 (1992) 353–358.
- 7 P. Shanahan, A. Borro, F. O'Gara and J.D. Glennon, *J. Chromatogr.*, 606 (1992) 171–177.
- 8 T. Maniatis, E.F. Fritsch and J. Sambrook, *Molecular Cloning: A Laboratory Manual*, Cold Spring Harbor Laboratory, Cold Spring Harbor, New York, 1982.
- 9 D. Gottlieb, *J. Antibiot.*, 29 (1976) 987–1000.
- 10 S.T. Williams, *Pedobiologia*, 23 (1982) 427–435.
- 11 L.S. Thomashow, D.M. Weller, R.F. Bonsall and L.S. Pierson, *Appl. Environ. Microbiol.*, 56 (1990) 908–912.
- 12 H. Malmos, *Chem. Ind.*, 6 (1990) 183–186.
- 13 T.K.K. Reddi, Y.P. Khudyakov and A.V. Borovkov, *Mikrobiologiya*, 38 (1969) 776–780.
- 14 W.J. Douglas and N.I. Gutterson, *Appl. Environ. Microbiol.*, 52 (1986) 1183–1189.
- 15 D.B. Drucker, *Microbiological Applications of High Performance Liquid Chromatography*, Cambridge University Press, Cambridge, 1987.
- 16 M. Dixon, E.C. Webb, C.J.R. Thorne and K.F. Tipton, *Enzymes*, Longman, London, 3rd edn., 1979.
- 17 E.C. Webb, *Enzyme Nomenclature*, Academic Press, New York, 1984.
- 18 J. Mann, *Secondary Metabolism*, Clarendon Press, Oxford, 1987.

Substoichiometric ion-pair extraction and determination of barium(II) with macrocyclic crown ether and cryptand

Tomoko Fukaya, Hisanori Imura¹ and Nobuo Suzuki

Department of Chemistry, Faculty of Science, Tohoku University, Sendai 980 (Japan)

(Received 4th June 1992; revised manuscript received 25th September 1992)

Abstract

Barium(II) is extracted with macrocyclic ligands (18-crown-6 or cryptand-2.2.2) in various organic solvents as the ion pair with picrate ion. The extraction with both ligands increased in the order benzene < 1,2-dichloroethane < nitrobenzene. Barium(II) is substoichiometrically extracted into 1,2-dichloroethane or 1,2-dichloroethane–nitrobenzene (1 + 1) with $(0.5-1) \times 10^{-4}$ M 18-crown-6 or cryptand-2.2.2 in the presence of $(1-2) \times 10^{-2}$ M picrate at pH 4–10 or 7–11, respectively. The 18-crown-6 system was superior to the cryptand-2.2.2 system in selectivity toward other alkaline earth and alkali metals. The substoichiometric process combined with isotope dilution was successfully applied to the accurate determination of barium in a Y–Ba–Cu–O superconducting oxide ceramic.

Keywords: Isotope dilution methods; Barium; Ceramics; Crown ethers; Cryptands; Extraction; Superconductors

Substoichiometry combined with the isotope dilution principle is an accurate and precise method and has the advantage that quantitative separation and recovery of an element from a sample matrix are not required and the element can be determined by measuring only the radioactivity of the substoichiometric extract without any calibration standards. This method has been applied to the determination of various elements, but not barium [1–4].

The substoichiometric extraction of Sr^{2+} with macrocyclic ligands (18-crown-6 and cryptand-2.2.2) and its application in the determination of strontium in a seaweed sample has been reported previously [5]. The Ba^{2+} ion forms stable complexes with these macrocyclic ligands, because the ionic diameter of Ba^{2+} (2.70 Å) [6] is very close to

the cavity diameters of 18-crown-6 (2.68–2.86 Å) [7] and cryptand-2.2.2 (2.8 Å) [8].

In this work, the extraction of Ba^{2+} with 18-crown-6 and cryptand-2.2.2 into benzene, 1,2-dichloroethane and nitrobenzene was studied by using picrate as a counter anion at an ionic strength of 0.10 M (HCl–LiCl). Then the substoichiometric extraction of Ba^{2+} with a substoichiometric amount of 18-crown-6 and cryptand-2.2.2 in the presence of an excess of picrate was studied in detail. Substoichiometry combined with isotope dilution was applied to the accurate determination of barium in a Y–Ba–Cu–O superconducting oxide ceramic.

EXPERIMENTAL

Reagents and apparatus

A radioisotope, ^{131}Ba , was produced from caesium chloride (Merck, Suprapur) by the (p,3n) reaction with 36-MeV protons from a cyclotron in

Correspondence to: N. Suzuki, Department of Chemistry, Faculty of Science, Tohoku University, Sendai 980 (Japan).

¹ Present address: Department of Chemistry, Faculty of Science, Ibaraki University, Mito 310 (Japan).

the Tohoku University Cyclotron and Radioisotope Centre. The bombarded target was dissolved in 10 M hydrochloric acid and fed into a cation-exchange column (Dowex 50W-X8). After elution of the caesium fraction containing the radioactive byproduct of ^{132}Cs with 10 M hydrochloric acid, carrier-free ^{131}Ba was eluted with 6 M hydrochloric acid. The ^{131}Ba fraction was evaporated to dryness and the residue dissolved in 0.01 M hydrochloric acid. The radiochemical purity was checked by γ -ray spectrometry with a germanium detector connected with a multi-channel analyser.

A carrier solution of Ba^{2+} was prepared by dissolving high-purity barium carbonate (Johnson Matthey, Specpure, 99.999% purity) in hydrochloric acid. Radioactive Ba^{2+} working standard solution was prepared by adding a few drops of the carrier-free ^{131}Ba solution to an aliquot of the carrier solution. 18-Crown-6 (Merck, 98% purity) was recrystallized from hexane. Cryptand-2.2.2 (Merck, 99% purity) and picric acid (Wako, guaranteed reagent grade) were used as received. Other reagents were of analytical-reagent grade and were used as received.

General extraction procedure

A 5-ml portion of an aqueous solution containing 1×10^{-6} – 0.03 M Ba^{2+} labelled with ^{131}Ba and 0.001 – 0.1 M picrate was shaken for 30 min with a 5-ml portion of an organic solution of 5×10^{-5} – 0.001 M 18-crown-6 or cryptand-2.2.2. After centrifugation, the γ -activity of each phase was measured with a well-type NaI(Tl) scintillation counter. The distribution ratio (D) of Ba^{2+} was calculated as the ratio of the γ -counts in the two phases. The pH of the aqueous phase was adjusted with lithium hydroxide solution. The equilibrium pH was measured with a combination glass electrode. All procedures were done in a thermostated room at 25°C .

Recommended procedure for the substoichiometric isotope dilution method

A sample of Y–Ba–Cu–O superconducting oxide ceramic was dissolved in 4 M hydrochloric acid, mixed with a radioactive spike solution containing a known amount of Ba^{2+} (M_s) labelled with ^{131}Ba and evaporated to dryness. The residue

was dissolved in water. Lithium hydroxide solution (0.25 M) was added to separate yttrium(III) and copper(II) as precipitates of the hydrated oxides. After centrifugation, the supernatant solution (sample solution) was used for substoichiometric extraction. Equal amounts of Ba^{2+} were extracted from the sample and the spike solution with a substoichiometric amount of the macrocyclic ether and their γ -activities (A and A_s , respectively) were measured. The Ba^{2+} content in the sample was calculated from the equation $M = M_s(A_s/A - 1)$.

RESULTS AND DISCUSSION

Extraction behaviour of barium(II) with macrocyclic ligands

Extraction of $(0.10\text{--}1.0) \times 10^{-5}$ M Ba^{2+} with a 0.0010 M macrocyclic ligand into organic solvents such as benzene, 1,2-dichloroethane and nitrobenzene was studied in the presence of 0.011 M picrate. The ionic strength of the aqueous phase was maintained at 0.10 M with hydrochloric acid and lithium chloride. The extraction curves for 18-crown-6 and cryptand-2.2.2 are shown in Figs 1 and 2, respectively. The distribution ratios of Ba^{2+} in the 18-crown-6 system

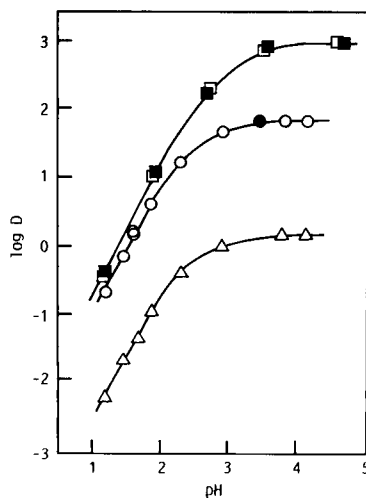


Fig. 1. Extraction of Ba^{2+} with 0.0010 M 18-crown-6 and 0.011 M picrate. Δ = Benzene; \circ , \bullet = 1,2-dichloroethane; \square , \blacksquare = nitrobenzene. Open symbols, 1.0×10^{-5} M Ba^{2+} ; solid symbols, 1.0×10^{-6} M Ba^{2+} .

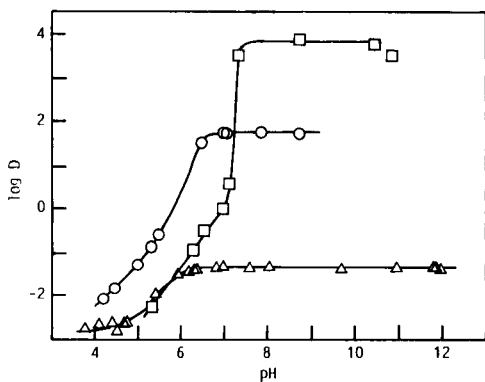
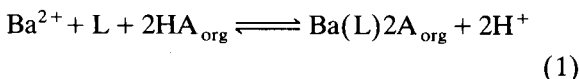


Fig. 2. Extraction of Ba^{2+} (1.0×10^{-5} M) with 0.0010 M cryptand-2.2.2 and 0.011 M picrate. Δ = Benzene; \circ = 1,2-dichloroethane; \square = nitrobenzene.

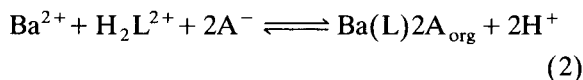
increase with increase in pH and become constant for each solvent. In the lower pH region, the $\log D$ vs. pH plots are straight lines with a slope of 2. Such behaviour can be readily explained by considering the following extraction equilibrium,



where L and HA denote the macrocyclic ligand and picric acid, respectively and the subscript org indicates the organic phase. Taking account of the acid dissociation constant of picric acid ($\text{p}K_{\text{a}} = 0.38$) [9] and its partition coefficient ($\log P = 2.03$ for benzene and 2.63 for nitrobenzene) [10], the distribution ratio of Ba^{2+} ($D = [\text{Ba}(\text{L})2\text{A}]_{\text{org}} / [\text{Ba}^{2+}]$) is proportional to the square of the proton concentration in the aqueous phase at low pH. Above pH 4, as all of the picric acid added dissociates in the aqueous phase, the distribution ratio of Ba^{2+} is independent of the proton concentration. The extraction of the ion-pair complex, $\text{Ba}(\text{L})2\text{A}$, is strongly dependent on the organic solvent and increases in the order benzene < 1,2-dichloroethane < nitrobenzene, which agrees with the increase in polarity of the solvents, e.g., dipole moment, dielectric constant and solubility parameter. Polar solvents such as 1,2-dichloroethane and nitrobenzene are expected to be preferred for the substoichiometric extraction of Ba^{2+} .

Cryptand-2.2.2 shows a different behaviour to 18-crown-6. As shown in Fig.2, the $\log D$ vs. pH plots in the lower pH region are curved for all the solvents. Additionally, the profile of these curves changed with the shaking time. In the extraction by 1,2-dichloroethane, the $\log D$ values at pH 4–6 were increased by longer shaking for 48 h and the plot was a straight line with a slope of 2. In nitrobenzene, although the $\log D$ values at pH 4–7 were raised considerably by shaking for 72 h, the plots were still slightly curved. These results show the slow extraction of Ba^{2+} with cryptand-2.2.2 below pH 7, ascribed to the slow complexation in the aqueous phase. As cryptand-2.2.2 is a diamine and has $\text{p}K_{\text{a}}$ values of 7.28 and 9.60 [8], it exists in the protonated form in such a pH region. Further, in the complexation of Ba^{2+} with cryptand-2.2.2, the metal ion has to enter the cavity of the ligand through specific sites owing to its three-dimensional structure.

The extraction equilibrium with cryptand-2.2.2 at pH 4–6 can be written as



Therefore, the distribution ratio of Ba^{2+} is proportional to the square of the proton concentration in the aqueous phase, as observed in the 1,2-dichloroethane system. The effect of solvents on the extraction of Ba^{2+} was similar to that for 18-crown-6, i.e., the distribution ratio increased in the order benzene < 1,2-dichloroethane < nitrobenzene.

Substoichiometric extraction of barium(II) with macrocyclic ligands

The extraction of Ba^{2+} with a substoichiometric amount of 18-crown-6 (4.8×10^{-5} M) and cryptand-2.2.2 (4.7×10^{-5} M) into 1,2-dichloroethane was examined in the presence of an excess of picrate (0.010 M). The total concentration of the macrocyclic ligand was about one third of the total Ba^{2+} concentration. Figure 3 shows that a constant amount of Ba^{2+} is extracted with 18-crown-6 at pH 3.5–10 and with cryptand-2.2.2 at pH 7.5–11.5. The amount of Ba^{2+} extracted at the plateau region is in good agreement with that

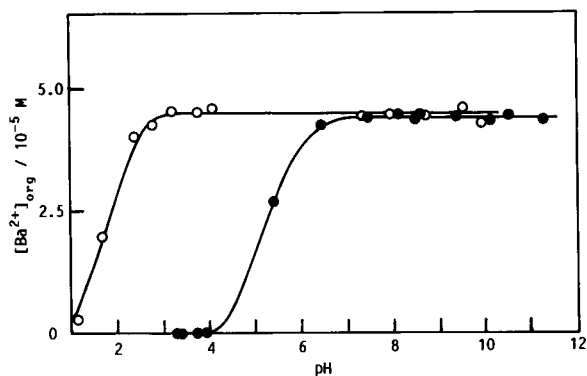


Fig. 3. Effect of pH on the substoichiometric extraction of Ba^{2+} with the macrocyclic ligand in 1,2-dichloroethane in the presence of an excess of picrate. Conditions: 1.5×10^{-4} M Ba^{2+} , 0.010 M picrate. $\circ = 4.8 \times 10^{-5}$ M 18-crown-6; $\bullet = 4.7 \times 10^{-5}$ M cryptand-2.2.2.

expected from a 1:1 reaction of Ba^{2+} with a substoichiometric amount of the macrocyclic ligands. Extraction equilibrium was achieved within 30 min under the given substoichiometric conditions, at $\text{pH} > 3$ for 18-crown-6 and $\text{pH} > 7$ for cryptand-2.2.2.

Figure 4 shows the effect of picrate concentration on the substoichiometric extraction of Ba^{2+} with a fixed amount of 18-crown-6 in some organic solvents. A constant amount of Ba^{2+} is extracted over a wide range of picrate concentra-

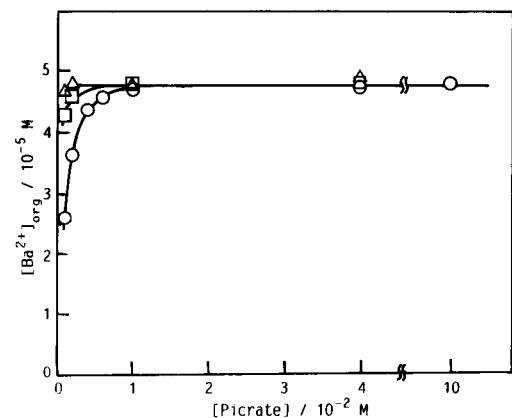


Fig. 4. Effect of picrate concentration on the substoichiometric extraction of Ba^{2+} with 18-crown-6. Conditions: 2.0×10^{-4} M Ba^{2+} , 4.8×10^{-5} M 18-crown-6, pH 8.6-8.8. $\circ = 1,2$ -Dichloroethane; $\square = 1,2$ -dichloroethane-nitrobenzene (1 + 1); $\triangle =$ nitrobenzene.

tion and agrees well with the amount expected from the substoichiometric amount of 18-crown-6. Substoichiometric extraction by different solvents can be achieved with a lower concentration of picrate according to the increase in the polarity of the solvent, i.e., 1,2-dichloroethane < 1,2-dichloroethane-nitrobenzene (1 + 1) < nitrobenzene. In nitrobenzene, however, extraction of Ba^{2+} with picrate occurred slightly without 18-crown-6 and could not be ignored, especially with a high concentration of Ba^{2+} in the aqueous phase. Therefore, 1,2-dichloroethane-nitrobenzene (1 + 1) is to be preferred as a solvent in the substoichiometric extraction of Ba^{2+} , but 1,2-dichloroethane is also useful at higher concentrations of Ba^{2+} .

The effects of the picrate concentration and the solvent on substoichiometric extraction with cryptand-2.2.2 were also examined in the same way as for 18-crown-6. Almost the same results as in Fig. 4 were obtained.

Reproducibility of substoichiometric extraction

Substoichiometric extractions with 5.0×10^{-5} M 18-crown-6 and 5.1×10^{-5} M cryptand-2.2.2 in 1,2-dichloroethane-nitrobenzene (1 + 1) in the presence of 0.020 M picrate was applied to a series of solutions containing different amounts of radioactive Ba^{2+} . Figure 5 shows that the γ -counts of the organic phase increase with in-

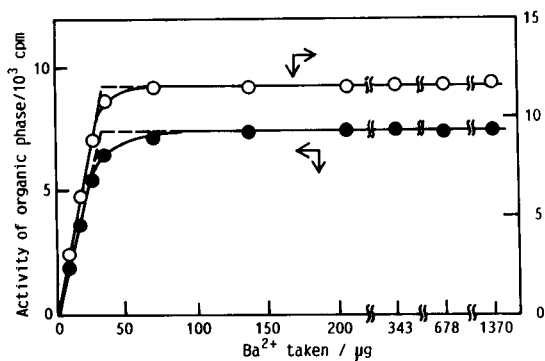


Fig. 5. Reproducibility of the substoichiometric extraction of Ba^{2+} into 1,2-dichloroethane-nitrobenzene (1 + 1) from aqueous solutions containing various amounts of Ba^{2+} and 0.020 M picrate. $\circ = 5.0 \times 10^{-5}$ M 18-crown-6, pH 8.3-8.4; $\bullet = 5.1 \times 10^{-5}$ M cryptand-2.2.2, pH 9.5-9.7.

TABLE 1
Reproducibility of the substoichiometric extraction^a

Ba taken (mg)	γ -Counts of organic phase (cpm)	
	9.9×10^{-4} M 18-crown-6 ^b	9.8×10^{-4} M cryptand-2.2.2 ^c
2.06	6350	5539
2.75	6358	5527
3.43	6345	5539
4.81	6331	5503
6.87	6353	5521
13.7	6353	5519
20.6	6330	
Average \pm s	6345 \pm 11	5525 \pm 14
R.S.D.	0.18%	0.25%

^a Conditions: 0.020 M picrate, 1,2-dichloroethane. ^b pH 8.3–8.4. ^c pH 9.5–9.8.

crease in the amount of Ba²⁺ up to the equivalence point corresponding to a 1 : 1 mole ratio of Ba²⁺ to the macrocyclic ligand. The composition of the extracted species is confirmed to be Ba(L)2A, as expected. Beyond the equivalence point, i.e., under substoichiometric conditions, a constant amount of Ba²⁺ is extracted. The reproducibility of the substoichiometric extraction is high; the relative standard deviation (R.S.D.) for the γ -counts of the organic extracts was 0.64% ($n = 6$) in 18-crown-6 and 0.74% ($n = 5$) in cryptand-2.2.2. Barium at the 10- μ g level can be determined accurately by combining the present substoichiometric extraction and isotope dilution analysis.

The reproducibility of the substoichiometric extraction of Ba²⁺ at the mg level is given as the standard deviation (s) of the average of γ -counts and the R.S.D. in Table 1. The R.S.D. values for the γ -counts of the organic extracts are as low as 0.18% ($n = 7$) in the 18-crown-6 system and 0.25% ($n = 6$) in the cryptand-2.2.2 system. As these R.S.D. values are mainly derived from the statistical error in the activity measurement (ca. 0.2% in the present experiment), it is possible to improve the precision using radioactive Ba²⁺ with higher specific activity.

Effect of diverse ions

The effect of diverse ions on the substoichiometric extraction was investigated by adding vari-

ous amounts of non-active ions to 5 ml of aqueous solutions containing radioactive Ba²⁺. The γ -counts obtained in the presence and absence of the diverse ions were compared and the results are summarized in Table 2. It is obvious that the selectivity in the substoichiometric extraction of Ba²⁺ with 18-crown-6 is higher than that with cryptand-2.2.2. No significant interference from large amounts of sodium, magnesium and calcium occurs in the 18-crown-6 system but serious interference occurs in the cryptand-2.2.2 system. Potassium and strontium show large interferences in both systems. The important elements commonly used in superconducting oxide ceramics, copper(II), lanthanum(III) and yttrium(III), showed no interference.

Determination of barium by the substoichiometric isotope dilution method

Substoichiometric extraction with 18-crown-6 was combined with the isotope dilution method and applied to the accurate analysis of a superconducting oxide. The accuracy of the method was evaluated by determining barium in a synthetic mixture containing known amounts of barium, yttrium and copper. The results are given in

TABLE 2
Effect of diverse ions on the substoichiometric extraction of barium^a

Other ion	Amount added (μ g)	Interference (%) ^b	
		18-Crown-6	Cryptand-2.2.2
Na ⁺	23	+0.9	-13.2
	230	-0.2	-68.1
K ⁺	39	-10.4	-65.5
	390	-52.3	-96.0
Mg ²⁺	24	+1.5	-3.2
	240	-1.4	-14.1
Ca ²⁺	40	0.0	-6.1
	400	+1.0	-49.8
Sr ²⁺	88	-9.0	-18.9
	880	-48.1	-68.4
Cu ²⁺	64	+0.5	+1.3
La ³⁺	140	+0.1	-0.6
Y ³⁺	89	+0.6	-1.6

^a Conditions: 5.1×10^{-5} M 18-crown-6 or 5.0×10^{-5} M cryptand-2.2.2 in 1,2-dichloroethane–nitrobenzene (1 + 1), 2.0×10^{-2} M picrate. Ba²⁺ taken, 140 μ g in 5 ml. ^b Calculated as $100(a - a_s)/a_s$, where a is the γ -count of ¹³¹Ba in the presence of the diverse ions and a_s is that in its absence.

TABLE 3

Substoichiometric determination of barium in a synthetic mixture ^a

Active Ba in spike (M_s) (mg)	γ -Counts from spike (A_s) (cpm)	γ -Counts from sample (A) (cpm)	Ba found (M) (mg) ^b
8.303	21106	9123.7	$\bar{x} = 10.92$
	21084	9081.6	$s = 0.05$
	21027	9102.7	
8.303	20232	8698.7	$\bar{x} = 11.02$
	20173	8666.7	$s = 0.07$
	20132	8641.7	

^a Ba, 10.92 mg; Y, 4.4 mg; Cu, 3.2 mg. ^b Calculated from $M = M_s(A/A_s - 1)$. Overall average = 10.97 mg; $s = 0.09$ mg; R.S.D. = 0.78%; deviation from Ba taken = 0.48%.

Table 3. The average value of 10.97 mg is in good agreement with the added amount (10.92 mg), the relative difference being only 0.48%.

The method was applied to the determination of barium in a superconducting material of general composition $YBa_2Cu_3O_x$. About 1 g of a pellet sample (10 mm diameter) was broken and dried at 110°C. A small piece (30–40 mg) was dissolved in 4 M hydrochloric acid in the presence of a known amount of Ba^{2+} labelled with ¹³¹Ba. Yttrium and copper were removed as pre-

TABLE 4

Substoichiometric determination of barium in a superconducting oxide sample ^a

Sample taken (mg)	Active Ba in spike (mg)	γ -Counts ^b from spike (cpm)	γ -Counts ^b from sample (cpm)	Ba found (%) ^c
31.3520	8.303	5180.0	2033.3	$\bar{x} = 41.13$
		5190.1	2037.5	$s = 0.18$
		5205.9	2030.0	
38.6064	11.07	4661.5	1910.0	$\bar{x} = 41.32$
		4654.0	1905.9	$s = 0.12$
		4656.1	1911.4	
31.8364	11.07	4192.0	1914.0	$\bar{x} = 41.30$
		4189.6	1911.4	$s = 0.23$
		4196.5	1923.7	

^a Y–Ba–Cu–O ceramic. ^b Per 1-g portion of the organic phase.

^c Overall average = 41.25%; $s = 0.32\%$; R.S.D. = 0.76%.

^d Successive substoichiometric extraction.

cipitates of hydrated oxides. In this pre-separation, the procedure can be substantially simplified as quantitative separation and recovery of Ba^{2+} are not required. After the substoichiometric extraction, an aliquot of the organic phase was taken with a pipette and weighed to improve the accuracy and precision.

The results for the superconducting oxide sample are shown in Table 4. The R.S.D.s for each of the three samples are 0.31, 0.28 and 0.62%, respectively. The result obtained from substoichiometric extractions done successively from the same aqueous solution is consistent. These data show that the analytical result is very accurate and does not involve any error due to co-existing elements. The overall mean value for the barium content is $41.3 \pm 0.3\%$ and the R.S.D. is as low as 0.8%.

The proposed substoichiometric isotope dilution analysis method for barium with macrocyclic ligands is simple, highly accurate and precise and can be applied to the determination of barium at μg –mg levels.

The authors are grateful to Professor Y. Shono, Institute for Material Research, Tohoku University, for kindly supplying the superconducting oxide ceramic.

REFERENCES

- 1 K. Kudo and N. Suzuki, *J. Radioanal. Chem.*, 59 (1980) 605.
- 2 K. Kudo and N. Suzuki, *Trends Anal. Chem.*, 3 (1984) 20.
- 3 G.N. Bilimovich, *J. Radioanal. Nucl. Chem.*, 88 (1984) 171.
- 4 N. Suzuki and H. Imura, *Bunseki*, (1987) 106.
- 5 N. Suzuki, T. Fukaya and H. Imura, *Anal. Chim. Acta*, 194 (1987) 261.
- 6 R.D. Shannon, *Acta Crystallogr., Sect. A*, 32 (1976) 751.
- 7 R.M. Izatt, J.S. Bradshaw, S.A. Nielsen, J.D. Lamb and J.J. Christensen, *Chem. Rev.*, 85 (1985) 271.
- 8 J.M. Lehn and J.P. Sauvage, *J. Am. Chem. Soc.*, 97 (1975) 6700.
- 9 R.C. West (Ed.), *CRC Handbook of Chemistry and Physics*, CRC Press, Cleveland, OH, 1979.
- 10 C. Hansch and A. Leo, *Substituent Constants for Correlation Analysis in Chemistry and Biology*, Wiley, New York, 1979.

Influence of ring substituents and matrix on lithium/sodium selectivity of 14-crown-4 and benzo-13-crown-4 compounds

Richard A. Bartsch and Mi-Ja Goo

Department of Chemistry and Biochemistry, Texas Tech University, Lubbock, TX 79409 (USA)

Gary D. Christian and Xiaowen Wen

Department of Chemistry, University of Washington, Seattle, WA 98195 (USA)

Bronislaw P. Czech, Eddy Chapoteau and Anand Kumar

Miles Incorporated, Tarrytown, NY 10591 (USA)

(Received 27th July 1992; revised manuscript received 29th September 1992)

Abstract

Binding of Li^+ and Na^+ by a series of ten benzo-13-crown-4 compounds and a series of fifteen 14-crown-4 derivatives has been assessed by picrate extraction and the response of polymeric membrane electrodes. Variation in cation selectivity was observed when different groups were attached to the central carbon atom of the three-carbon bridges in the ionophores. For the benzo-13-crown-4 series, only weak cation binding and low selectivity was observed in both the picrate extraction and polymeric membrane electrode systems. For the 14-crown-4 series, 6,13-dimethylenyl-14-crown-4 exhibited the highest Li^+ selectivity in picrate extraction. In polymeric membrane electrodes, considerably higher Li^+ selectivity was observed with 6,6,13-tribenzyl-14-crown-4 and 6,6,13,13-tetraethyl-14-crown-4 than with the commercially available Li^+ ionophore 6,6-dibenzyl-14-crown-4. Lack of correlation for the Li^+ selectivities of the 14-crown-4 compounds in the picrate extraction and polymeric membrane electrode systems reveals a profound influence of the matrix on ionophore selectivity.

Keywords: Flow injection; Potentiometry; Crown ethers; Lithium; Picrate extraction; Polymeric membrane electrodes; Ring substituents; Sodium

Small-sized, 12- to 16-membered crown ethers with four oxygen atoms in the ring are potential binders for Li^+ and Na^+ . In the search for selective Li^+ complexing agents, a variety of small-ring crown ethers have been studied. Most attention has been focused upon 14-crown-4 derivatives

which possess good Li^+ binding abilities and may be used in polymeric membrane electrodes [1–10]. Crown ethers with 13-membered rings for which the cavities are only slightly smaller have received much less attention [2,9,11].

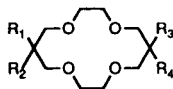
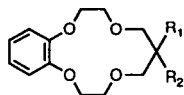
Two frequently utilized methods for the determination of cation binding by crown ether compounds are extraction of metal picrates into organic media and the response of polymeric membrane electrodes in contact with aqueous metal ion solutions. Only very infrequently have the

Correspondence to: Richard A. Bartsch, Department of Chemistry and Biochemistry, Texas Tech University, Lubbock, TX 79409-1061 (USA).

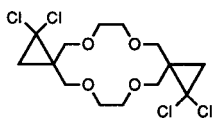
selectivities obtained by the two techniques been compared. To determine if results obtained in one matrix can be extrapolated to the other, an investigation of picrate extraction and polymeric membrane electrode response for two series of crown-4 compounds was undertaken.

Through recent synthetic efforts [12,13], 14-crown-4 and benzo-13-crown-4 compounds with a variety of substituents on the central carbon(s) of the propano bridge(s) have become available. By examination of the Li^+/Na^+ selectivities for these two series of crown-4 compounds in both picrate extract and polymeric membrane electrodes, the

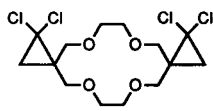
influence of substituents for a single matrix as well as the effect of matrix variation may be assessed. In this paper, we compare Li^+ and Na^+ binding abilities for nine new benzo-13-crown-4 derivatives 2–10 which bear various substituents attached to the central carbon atom of the three-carbon linkage with that of the parent benzo-13-crown-4 (1) [11]. We also report Li^+ and Na^+ binding properties for a series of twelve new (13–20, 22–25) and three previously known 11 [6], 12 [4] and 21 [10,14]) 14-crown-4 derivatives which bear various substituents attached to the central carbon atom(s) of the three-carbon linkage(s).



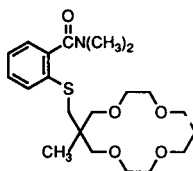
	R ₁	R ₂		R ₁	R ₂	R ₃	R ₄
1	H	H	11	H	H	H	H
2	=CH ₂		12	Bzl	Bzl	H	H
3	—CH ₂ CCl ₂ —		13	Bzl	H	Bzl	H
4	Ph	H	14	Bzl	H	Bzl	Bzl
5	Bzl	H	15	Bzl	Bzl	Bzl	Bzl
6	Bzl	Bzl	16	BzIOCH ₂	CH ₃	H	H
7	BzIOCH ₂	CH ₃	17	BzIOCH ₂	CH ₃	BzIOCH ₂	CH ₃
8	BzIOCH ₂	BzIOCH ₂	18	BzIOCH ₂	BzIOCH ₂	BzIOCH ₂	BzIOCH ₂
9	Et	Et	19	3-CH ₃ OBzl	H	3-CH ₃ OBzl	H
10	PhC(O)NH	CH ₃	20	Et	Et	Et	Et
			21	=CH ₂		=CH ₂	
			22	=CH ₂		Bzl	Bzl



23



24



25

EXPERIMENTAL

Apparatus

Visible spectra were recorded with a Perkin-Elmer Lambda 5 UV–visible spectrophotometer. For the potentiometric study, the carrier and reference solutions were pumped with an Alitea C-4 peristaltic pump (Alitea, Medina, WA). The potential of two indicating electrodes in series relative to the reference electrode was monitored by a Beckman 3500 digital pH meter and a Corning 145 pH meter coupled with a two-pen chart recorder.

Reagents

Benzo-13-crown-4 compounds **1–10** [12] and 14-crown-4 derivatives **11–25** [13] were available from earlier work. Reagent grade chemicals and solvents were used as received. Chlorides of lithium and sodium were used for the potentiometric studies. Deionized water was used for preparing all aqueous solutions. High molecular weight poly(vinyl chloride) (PVC) was obtained from Fluka. The *o*-nitrophenyl octyl ether (NPOE) and potassium tetrakis(*p*-chlorophenyl) borate were purchased from Specialty Organics, Irwindale, CA.

Picrate extraction study. Crown ether solutions (1.5×10^{-2} M) were prepared in deuteriochloroform, which does not contain the stabilizing ethanol present in ordinary chloroform. By use of the reported procedure [2], extractions were conducted by addition of 0.50 ml of a 1.5×10^{-2} M crown ether solution in deuteriochloroform to 0.50 ml of a 1.5×10^{-2} alkali metal picrate solution in a centrifuge tube. The mixture was agitated with a vortex mixer for 1 min. Five identical samples were run concurrently. The mixtures were centrifuged for 10 min to assure complete layer separation. Precisely measured aliquots were removed from each layer with microsyringes and diluted with acetonitrile. Visible spectra of these solutions were measured in the region of 340–550 nm. Extraction constants, K_{ex} , were calculated by the literature methods [15,16].

Potentiometric selectivity study. A flow cell and the FIA system similar to those reported previously were utilized [17]. A set of silver–silver

chloride electrodes was prepared by anodically polarizing silver wire electrodes in 0.1 M HCl for 30 sec [17]. The PVC membrane solutions were prepared by dissolving 1.5 mg of ionophore, 65 mg of plasticizer (NPOE), 33 mg of PVC and 0.5 mg of potassium tetrakis(*p*-chlorophenyl)borate in 500 μ l of THF. A typical membrane electrode was prepared by applying 1 μ l of the membrane solution to a silver–silver chloride electrode surface and allowing the solvent to evaporate completely. This coating operation was repeated twice more than the electrode was conditioned in 140 mM NaCl for several hours before use. A silver–silver chloride electrode in the reference stream was used as the reference electrode.

A 140 mM NaCl solution prepared from deionized water was used as both the carrier solution and the reference stream solution in the FIA system. Both streams were pumped at 0.56 ml/min. The injected sample volume was 200 μ l. All sample solutions were prepared in a 140 mM NaCl solution matrix. Standard LiCl solutions with concentrations from 0.08 to 200 mM were used to construct calibration curves. Signals for 100 mM NaCl solution (i.e., total Na^+ concentration of 240 mM) were recorded for the selectivity study. Each sample was injected twice to verify the reproducibility. Selectivity coefficients were determined by the matched potential method [18].

RESULTS AND DISCUSSION

Picrate extraction study

Binding abilities of the ten benzo-13-crown-4 compounds **1–10** were assessed by solvent extraction of aqueous solutions of lithium and sodium picrates with deuteriochloroform solutions of the crown ethers at room temperature. Extraction constants, K_{ex} , were determined in the customary manner [2] and extraction selectivities, $K_{\text{ex}}(\text{Li}^+)/K_{\text{ex}}(\text{Na}^+)$, were calculated from the extraction constants for the two ionic species. The data are presented in Table 1.

Overall, the extraction constants for both lithium and sodium picrate are quite low for benzo-13-crown-4 compounds **1–10**. Extraction selectivity as assessed from the K_{ex} values may

TABLE 1

Extraction constants, K_{ex} , and extraction selectivities, $K_{\text{ex}}(\text{Li}^+)/K_{\text{ex}}(\text{Na}^+)$, for lithium and sodium picrate extractions by benzo-13-crown-4 compounds **1–10** into deuteriochloroform at 22–23°C

Compound	log K_{ex}		$K_{\text{ex}}(\text{Li}^+)/K_{\text{ex}}(\text{Na}^+)$
	Li ⁺	Na ⁺	
1	1.26 ± 0.04	1.30 ± 0.04	0.9
2	1.32 ± 0.04	1.81 ± 0.05	0.3
3	1.45 ± 0.07	1.72 ± 0.04	0.5
4	1.20 ± 0.14	1.23 ± 0.09	0.9
5	1.34 ± 0.09	1.53 ± 0.07	0.6
6	1.08 ± 0.10	1.23 ± 0.07	0.7
7	0.60 ± 0.18	0.95 ± 0.05	0.4
8	1.46 ± 0.03	0.95 ± 0.05	3.2
9	1.34 ± 0.09	1.48 ± 0.07	0.7
10	1.20 ± 0.14	1.32 ± 0.08	0.8

be divided into three classes: (i) equal binding for Li⁺ and Na⁺; (ii) some preference for Na⁺ over Li⁺ complexation; (iii) some preference for Li⁺ over Na⁺ binding. Essentially equal complexation of Li⁺ and Na⁺ is noted for the parent benzo-13-crown-4 (**1**) and substituted benzo-13-crown-4 compounds **4–6**, **9**, **10**. Some preference for Na⁺ over Li⁺ binding is observed for compounds **2**, **3**, **7** with the largest difference in K_{ex} values being observed for **2** in which an sp²-hybridized carbon atom has been introduced into the crown ether ring. Only for the di(benzyloxymethyl)-substituted compound **8** was preference for Li⁺ over Na⁺ extraction found. Examination of CPK space-filling models indicates that the oxygen atom in one benzyloxymethyl group in **8** may be suitably oriented to provide additional coordination with Li⁺ which is perched on the four ring oxygens.

The Li⁺ and Na⁺ binding abilities of the fifteen 14-crown-4 compounds **11–25** were assessed in the same manner. Extraction and selectivity data for twelve new 14-crown-4 compounds **13–20** and **22–25**, as well as the known crown ethers **11**, **12** and **21** are presented in Table 2. Crown ether amide **25** was the strongest cation binder, but showed no differentiation between Li⁺ and Na⁺. Somewhat unexpectedly, the highest extraction selectivity for Li⁺ over Na⁺ was exhibited by 6,13-dimethylenyl-14-crown-4 (**21**). Earlier, it has been observed that introduction of rigidity into a

flexible crown ether framework can enhance the cation binding ability [19]. The Li⁺/Na⁺ extraction selectivity ratio exceeding 40 indicates that under extraction conditions the presence of two sp²-hybridized carbon atoms facilitates Li⁺ binding. It is suggested that hydrated Li⁺ is hydrogen bonded to the π -electrons of both methylenyl groups. In agreement when one of the methylene functions is replaced by the two benzyl groups, the observed Li⁺ selectivity for the monomethylenyl crown ether **22** plummets to 1.8.

The parent 14-crown-4 (**11**) and 6,13-dibenzyl-14-crown-4 (**13**) also exhibit substantial Li⁺ extraction selectivity. Interestingly 6,6-dibenzyl-14-crown-4 (**12**), which is a positional isomer of compound **13**, shows slightly lower Li⁺ extraction and somewhat stronger Na⁺ extraction which produces a significant decrease in Li⁺ selectivity. The tri- and tetrabenzyl-substituted crown ethers **14** and **15**, respectively, 6,13-di(benzyloxymethyl)-14-crown-4 (**17**) and 6,6,13,13-tetraethyl-14-crown-4 (**20**) exhibit Li⁺ extraction preferences similar to that found for the commercially available Li ionophore 6,6-dibenzyl-14-crown-4 (**12**). The remaining crown ethers discriminate Li⁺ from Na⁺ only weakly.

TABLE 2

Extraction constants, K_{ex} , and extraction selectivities, $K_{\text{ex}}(\text{Li}^+)/K_{\text{ex}}(\text{Na}^+)$, for lithium and sodium picrate extractions by 14-crown-4 compounds **11–25** into deuteriochloroform at 22–23°C

Compound	log K_{ex}		$K_{\text{ex}}(\text{Li}^+)/K_{\text{ex}}(\text{Na}^+)$
	Li ⁺	Na ⁺	
11	2.75 ± 0.01	1.51 ± 0.05	17
12	2.03 ± 0.02	1.32 ± 0.06	5.0
13	2.15 ± 0.05	1.00 ± 0.08	14
14	1.77 ± 0.04	1.04 ± 0.07	5.4
15	1.81 ± 0.02	1.00 ± 0.08	6.4
16	2.33 ± 0.03	2.14 ± 0.03	1.6
17	1.75 ± 0.04	0.93 ± 0.10	7.0
18	1.82 ± 0.02	1.78 ± 0.03	1.1
19	2.23 ± 0.02	1.72 ± 0.04	3.2
20	1.69 ± 0.04	0.95 ± 0.09	5.4
21	2.69 ± 0.03	1.08 ± 0.10	41
22	1.49 ± 0.07	1.32 ± 0.08	1.5
23	2.54 ± 0.03	2.39 ± 0.04	1.4
24	2.74 ± 0.02	2.53 ± 0.04	1.6
25	4.19 ± 0.01	4.13 ± 0.01	1.1

Potentiometric selectivity study

Selectivities of the ten benzo-13-crown-4 **1–10** and fifteen 14-crown-4 compounds **11–25** toward Li^+ and Na^+ were also determined by an emf method in a FIA system [17]. Each crown ether compound was incorporated into a PVC membrane electrode containing potassium tetrakis(*p*-chlorophenyl)borate to reduce electrical resistance and NPOE as plasticizer. The selectivity coefficient, $K_{\text{Li,Na}}^{\text{pot}}$, is defined as the preference of the polymeric membrane for Li^+ over Na^+ . The smaller the $K_{\text{Li,Na}}^{\text{pot}}$ value, the higher is the selectivity for Li^+ . The reciprocal, $1/K_{\text{Li,Na}}^{\text{pot}}$, is termed the Li^+/Na^+ selectivity ratio. The selectivity coefficients for polymeric membranes containing compounds **1–10** and **11–25** were determined by the matched-potential method [18] and are listed in Tables 3 and 4, respectively.

Lithium response curves for polymeric membrane electrodes incorporating the ten benzo-13-crown-4 compounds are shown in Fig. 1. The responses for Li^+ were generally poor with slopes less than 25 mV/decade and only at concentrations above 10^{-2} M. For the benzo-13-crown-4 compounds, the parent benzo-13-crown-4 (**1**) and substituted benzo-13-crown-4 compounds **2–4** and **9** are slightly Na^+ selective. 9-Benzyl-2,3-benzo-13-crown-4 (**5**) exhibits the best (albeit slight) Na^+ selectivity. Compound **7** does not differenti-

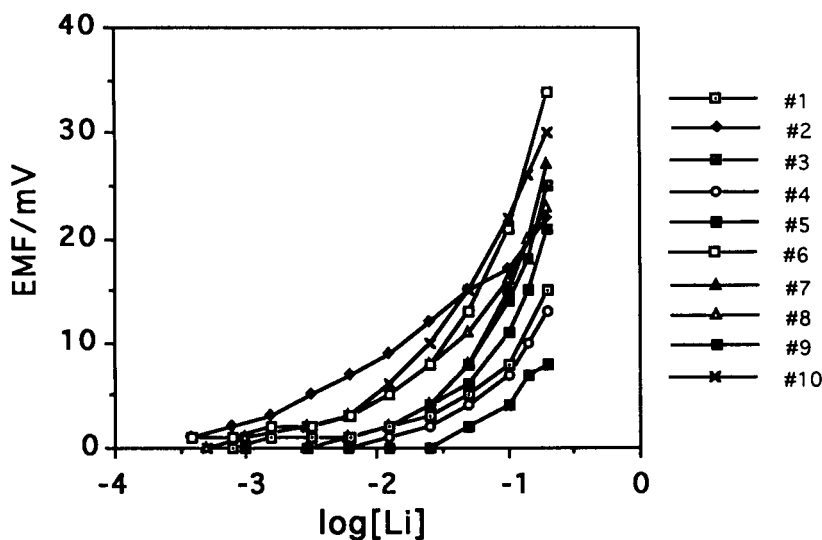


Fig. 1. Lithium response curves of polymeric membrane electrodes incorporating benzo-13-crown-4 ionophores **1–10**.

TABLE 3

Selectivity coefficients^a and their reciprocals for Li^+ with respect to Na^+ for polymeric membrane electrodes incorporating benzo-13-crown-4 compounds **1–10**

Compound	$K_{\text{Li,Na}}^{\text{pot}}$ ^b	$(K_{\text{Li,Na}}^{\text{pot}})^{-1} =$ Li^+ selectivity
1	1.60	0.6
2	1.10	0.9
3	1.18	0.8
4	2.54	0.4
5	4.76	0.2
6	0.59	1.7
7	1.00	1.0
8	0.50	2.0
9	1.18	0.8
10	0.33	3.0

^a Determined by the matched potential method. ^b Reproducibility of the selectivity coefficient value was demonstrated (see Experimental).

ate between Li^+ and Na^+ at all. Some Li^+ selectivity is observed for compounds **6**, **8** and **10**. These three benzo-13-crown-4 derivatives contain bulky substituents (in **6**) or additional binding sites for Li^+ (in **8** and **10**) which have been shown to enhance Li^+ selectivity for membranes containing 14-crown-4 compounds.

Results for polymeric membrane electrodes for compounds **11–25** are presented in Table 4.

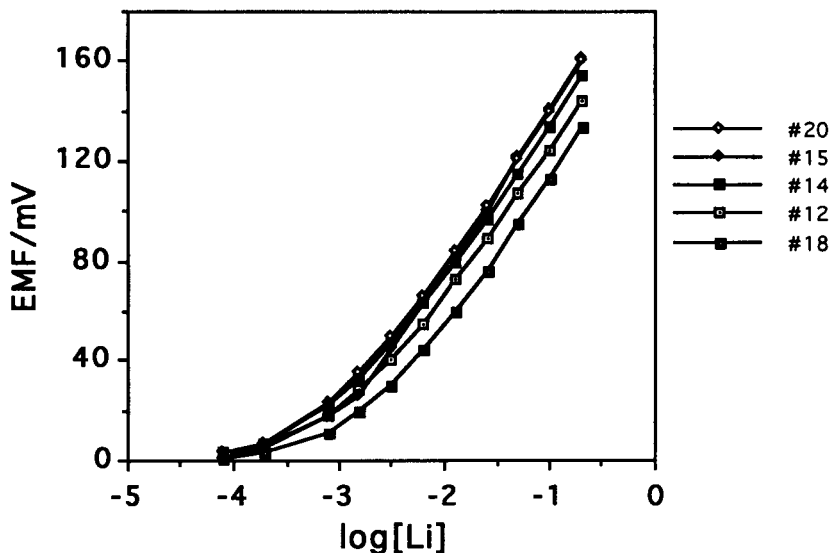


Fig. 2. Lithium response curves of polymeric membrane electrodes incorporating 14-crown-4 ionophores **12**, **14**, **15**, **18** and **20**.

Lithium response curves for polymeric membrane electrodes containing substituted 14-crown-4 ionophores **12**, **14**, **15**, **18** and **20** are shown in Fig. 2. Fig. 3 shows plots for the same ionophores when the membrane contains one percent of trioctylphosphine oxide (TOPO). TOPO often has an enhancing effect on lithium selectivity [20,21].

Clearly, ionophore **14** exhibits superior selectivity when TOPO is present.

The performance of Li^+ selective electrodes containing 14-crown-4 compounds is dependent on several sensitive factors and may vary significantly [8,22,23]. For example, selectivity coefficients ($1/K_{\text{Li,Na}}^{\text{pot}}$) as disparate as 229 [4] and 769

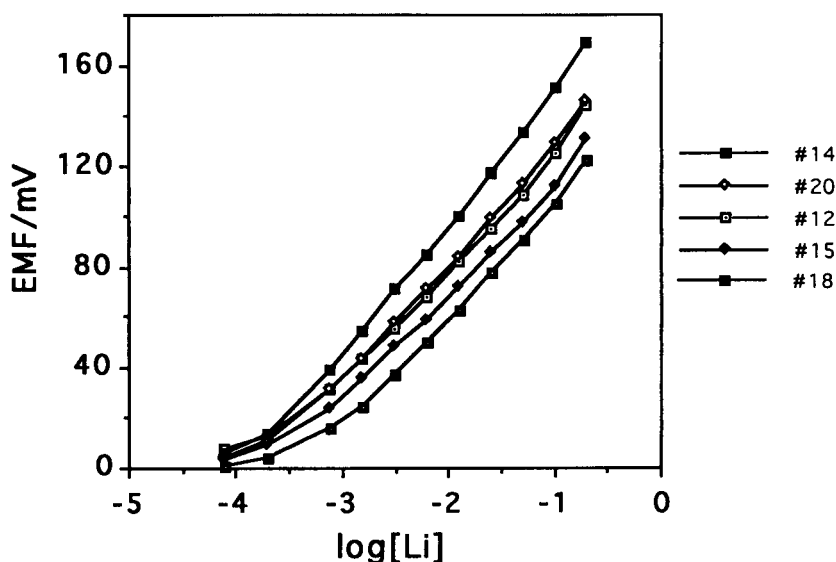


Fig. 3. Lithium response curves of polymeric membrane electrodes containing 1% TOPO and ionophores **12**, **14**, **15**, **18** and **20**.

TABLE 4

Selectivity coefficients^a and their reciprocals for Li⁺ with respect to Na⁺ for polymeric membrane electrodes incorporating 14-crown-4 compounds **11–25**

Compound	$K_{Li,Na}^{pot}$ ^b	$(K_{Li,Na}^{pot})^{-1} =$ Li ⁺ selectivity
11	0.016	62
12	0.010	100
13	0.019	53
14	3.39×10^{-3}	295
15	4.58×10^{-3}	218
16	0.025	40
17	0.011	91
18	8.10×10^{-3}	123
19	0.018	56
20	3.58×10^{-3}	279
21	0.50	2
22	5.50×10^{-3}	182
23	0.037	27
24	0.063	16
25	7.07×10^{-3}	141

^a Determined by the matched potential method. ^b Reproducibility of the selectivity coefficient value was demonstrated (see Experimental).

[24] have been reported for the commercially available lithium ionophore 6,6-dibenzyl-14-crown-4 (**12**). In the present polymeric membrane electrode system, the selectivity coefficient for crown ether **12** was 100; however the matched potential method often gives smaller selectivity coefficient values than the conventional separate solution or fixed interference methods. For the series of 14-crown-4 compounds **11–25**, the best Li⁺ selectivities were observed with 6,6,13-tribenzyl-14-crown-4 (**14**), 6,6,13,13-tetraethyl-14-crown-4 (**20**) and 6,6,13,13-tetrabenzyl-14-crown-4 (**15**) which exhibited $1/K_{Li,Na}^{pot}$ values of 295, 279 and 218, respectively. In addition, 6,6-dibenzyl-13-methylenyl-14-crown-4 (**22**) showed a high relative selectivity coefficient of 182, while the dimethylenyl-substituted compounds **21** showed only a very poor preference for Li⁺. 6,13-Di(benzyloxymethyl)-14-crown-4 (**17**), 6,6,13,13-tetra(benzyloxymethyl)-14-crown-4 (**18**) and crown ether amide (**25**) gave selectivity coefficients of 91, 123 and 141, respectively, which are of similar magnitude to that observed for the commercially available Li⁺ ionophore **12**. Both the *trans* and

cis isomers of 6,13-di(chlorocyclopropyl)-14-crown-4, **23** and **24**, respectively, exhibited rather poor Li⁺ selectivity, with the *trans* isomer being twice as selective as its *cis* counterpart.

Conclusions

The benzo-13-crown-4 compounds **1–10** are found to be weak Li⁺ and Na⁺ binders in both the picrate extraction and polymeric membrane electrode systems. Moreover little differentiation between Li⁺ and Na⁺ is observed. The 14-crown-4 compounds **11–25** generally exhibit stronger complexation of Li⁺ and Na⁺ than the benzo-13-crown-4 compounds in both the picrate extraction and polymeric membrane electrode systems. The Li⁺ selectivity of the 14-crown-4 compounds in both systems is quite sensitive to the introduction of substituents on one or both of the propano bridges of the crown ether. However, there is no correlation between the Li⁺ selectivities of individual members of the ionophore series in the two systems. Thus, 6,13-dimethylenyl-14-crown-4 (**21**) which gives the highest Li⁺ selectivity for picrate extraction into deuteriochloroform exhibits the lowest Li⁺ selectivity in the polymeric membrane system. Thus matrix-dependent factors are demonstrated to exert a profound influence upon ionophore selectivities. The potentiometric system is probably more dependent on reversibility.

6,6,13-Tribenzyl-14-crown-4 (**14**) and 6,6,13,13-tetraethyl-14-crown-4 (**20**) are found to have Li⁺ selectivities in polymeric membrane electrodes which markedly surpass that of the commercially available Li⁺ ionophore 6,6-dibenzyl-14-crown-4 (**12**) and therefore possess potential for the practical determination of Li⁺.

Portions of this research conducted at Texas Tech University were supported by Grant D-775 from the Robert A. Welch Foundation.

REFERENCES

- 1 U. Olsher, J. Am. Chem. Soc., 104 (1982) 4006.
- 2 B.P. Czech, D.A. Babb, B. Son and R.A. Bartsch, J. Org. Chem., 49 (1984) 4805.

- 3 S. Kitazawa, K. Kimura, H. Yano and T. Shono, *J. Am. Chem. Soc.*, 106 (1984) 6978.
- 4 K. Kimura, H. Yano, S. Kitazawa and T. Shono, *J. Chem. Soc., Perkin Trans. 2*, (1986) 1945.
- 5 K. Kobiro, T. Matsuoka, S. Takeda, K. Kakiuchi, Y. Tobe and Y. Odaira, *Chem. Lett.*, (1986) 713.
- 6 K. Kobiro, T. Hiro, T. Matsuoka, K. Kakiuchi, Y. Tobe and Y. Odaira, *Bull. Chem. Soc. Jpn.*, 61 (1988) 4164.
- 7 G.W. Buchanan, R.A. Kirby and J.P. Charland, *J. Am. Chem. Soc.*, 110 (1988) 2477.
- 8 R. Katak, P.E. Nicholson and D. Parker, *J. Chem. Soc., Perkin Trans 2*, (1990) 321.
- 9 R. Wakita, M. Yonetani, Y. Nakatsuji and M. Okahara, *J. Org. Chem.*, 55 (1990) 2752.
- 10 U. Olsher, K.E. Krakowiak, N.K. Dalley and J.S. Bradshaw, *Tetrahedron*, 47 (1991) 2947.
- 11 U. Olsher and J. Jagur-Grodzinski, *J. Chem. Soc., Dalton Trans.*, (1981) 501.
- 12 B.P. Czech, W. Zazulak, A. Kumar, K.N. Dalley, J. Weiming and R.A. Bartsch, *J. Heterocycl. Chem.*, 28 (1991) 1387.
- 13 B.P. Czech, W. Zazulak, A. Kumar, U. Olsher, H. Sheshinski, S. Cohen, Shoham, N.K. Dalley and R.A. Bartsch, *J. Heterocycl. Chem.*, 29 (1992) in press.
- 14 F. Nerdel, M. Mamluk and P. Weyerstahl, *Liebigs Ann. Chem.*, 736 (1970) 75.
- 15 A. Sadakane, T. Iwachido and K. Toei, *Bull. Chem. Soc. Jpn.*, 48 (1975) 60.
- 16 S.S. Moore, T.L. Tarnowski, M. Newcomb and D.J. Cram., *J. Am. Chem. Soc.*, 99 (1977) 6398.
- 17 R.Y. Xie, V.P.Y. Gadzekpo, A.M. Kadry, Y.A. Ibrahim, J. Ruzicka and D. Christian, *Anal. Chim. Acta*, 184 (1986) 259.
- 18 V.P.Y. Gadzekpo and G.D. Christian, *Anal. Chim. Acta*, 164 (1984) 279.
- 19 Y. Inoue, K. Wada, M. Ouchi, A. Tai and T. Hakushi, *Chem. Lett.*, (1988) 1005.
- 20 O. Ryba and J. Petranek, *Talanta*, 23 (1976) 158.
- 21 M. Yamaguchi, A. Jyo and N. Ishibashi, *Anal. Chim. Acta*, 136 (1982) 399.
- 22 A.O. Okorodudu, R.W. Burnett, R.B. McComb and G.N. Bowers, *Clin. Chem.*, 36 (1990) 104.
- 23 V.P.Y. Gadzekpo, J.M. Hungerford, A.M. Kadry, Y.A. Ibrahim, R.Y. Xie and G.D. Christian, *Anal. Chem.*, 58 (1986) 1948.
- 24 K. Kimura, H. Oishi, T. Miura and T. Shono, *Anal. Chem.*, 59 (1987) 2331.

Liquid–liquid extraction of lanthanides with a highly acidic extractant, 3-phenyl-4-benzoyl-5-isoxazolone, in the presence and absence of tri-*n*-octylphosphine oxide

Quyen Thi Hanh Le, Shigeo Umetani, Hideki Takahara and Masakazu Matsui

Institute for Chemical Research, Kyoto University, Uji, Kyoto 611 (Japan)

(Received 23rd July 1992)

Abstract

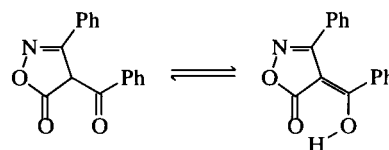
A highly acidic β -diketone, 3-phenyl-4-benzoyl-5-isoxazolone (HPBI), was synthesized and the acid dissociation constant and the partition constant between an organic solvent and 0.1 M sodium perchlorate solution were determined by a liquid–liquid distribution method. The extraction of lanthanides with HPBI was investigated in the presence and absence of tri-*n*-octylphosphine oxide. HPBI was found to be a very powerful extractant for lanthanides owing to its strong acidity. The acidity and extractability are discussed on the basis of the molecular structure optimized by a semi-empirical MNDO/H calculation.

Keywords: Extraction; Lanthanides

In the liquid–liquid extraction of metal ions, fluorinated substituents have often been introduced in extractant molecules. The acidity of the extractant is enhanced by the strong electron-withdrawing nature of the fluorinated substituent, and therefore metal ions are extractable from an acidic region. The acid dissociation constant (pK_a) of 2-thenoyltrifluoroacetone (HTTA), one of the most representative β -diketones, is reported to be 6.23, whereas that of acetylacetone is 8.82 [1]. Many metal ions are extractable from a more acidic region with HTTA. 4-Acyl-5-pyrazolones are also promising extractants. Their acid dissociation constants are 2.5–4.0, i.e., they are much stronger than HTTA [2,3]. Apparently the presence of a five-membered heterocyclic group leads to strong acidity. In addition, the combination of acylpyrazolones and neutral ligands such as tri-*n*-octylphosphine oxide (TOPO) and polydentate phosphine oxides has made it possible to extract quantitatively alkaline earth

metals [4,5] and lithium [6,7], which are known to be hardly extractable elements.

Recently, novel extractants derived from 5-isoxazolone have been developed [8–11]. Their acid dissociation constants are reported to be about 1.3 [12], so they are much more acidic than acylpyrazolones. In this present work, 3-phenyl-4-benzoyl-5-isoxazolone (HPBI) was synthesized and its acid dissociation constant and its partition constant between an organic phase and 0.1 M sodium perchlorate aqueous phase was determined precisely by a liquid–liquid distribution method. The liquid–liquid extraction of lanthanides in the presence and absence of TOPO was also examined.



3-Phenyl-4-benzoyl-5-isoxazolone (HPBI)

Correspondence to: S. Umetani, Institute for Chemical Research, Kyoto University, Uji, Kyoto 611 (Japan).

EXPERIMENTAL

Chemicals and apparatus

HPBI was synthesized by a method analogous to that for 3-phenyl-4-acetyl-5-isoxazolone [13]. 3-Phenyl-5-isoxazolone (3.2 g) and benzoic anhydride (4.5 g) were dissolved in dioxane (100 ml). After adding sodium benzoate (5.8 g), the mixture was refluxed for 2 h, the colour turning red–brown. After the mixture had cooled, sodium benzoate was removed by filtration. Addition of water (200 ml) and acidification with hydrochloric acid gave a yellow precipitate of HPBI. This precipitate was collected, washed with water and dried in vacuo; yield 3.3 g (62%), m.p. 146°C. Elemental analysis: calculated for $C_{16}H_{11}NO_3$, C 72.45, H 4.18, N 5.28; found, C 72.43, H 4.10, N 5.23%. 1H NMR ($CDCl_3$); δ 7.06–7.46 ppm (m, Ph).

TOPO was purchased from Dojindo and used as received. Other chemicals were of analytical-reagent grade. Water was demineralized and distilled.

Metal ion concentrations were measured with a Japan Jarrell-Ash Model ICAP-500 inductively coupled argon plasma atomic emission spectrometer. A Shimadzu UV-2200 spectrophotometer with 1-cm quartz cells was employed for spectrophotometric measurements. pH measurements were made with a Hitachi–Horiba F-8L pH meter equipped with a glass electrode. 1H NMR spectra were measured with a Varian VXR-200 spectrometer (200 MHz) at 25°C in $CDCl_3$.

A semi-empirical MNDO/H calculation was performed on a Cray Y-MP2E/264 computer using UniChem MNDO90 (Cray Research).

Distribution of HPBI

A 10-ml aliquot of an aqueous phase containing 0.1 M sodium perchlorate was adjusted to the desired pH with hydrochloric acid or sodium hydroxide solution. The aqueous phase was shaken with an equal volume of the organic phase containing a suitable amount of HPBI in a 30-ml centrifuge tube for 1 h at 25°C. After centrifugation, the pH of the aqueous phase was measured and taken as the equilibrium value. The HPBI concentration in the organic phase was deter-

mined spectrophotometrically. The HPBI concentration in the aqueous phase was measured after dilution with sodium hydroxide solution to complete the dissociation of the ligand.

Extraction of lanthanides

A 10-ml aliquot of an aqueous phase containing 1×10^{-4} M Ln^{3+} and 0.1 M sodium perchlorate was adjusted to the desired pH with hydrochloric acid or sodium hydroxide solution. The aqueous phase was shaken with an equal volume of chloroform containing the required amount of HPBI and TOPO in a 30-ml centrifuge tube for 1 h at 25°C. A shaking time of 1 h was found to be long enough for equilibration. After centrifugation, the pH of the aqueous phase was measured and taken as the equilibrium value. The metal concentration in the aqueous phase was determined by inductively coupled plasma atomic emission spectrometry and that in the chloroform phase was determined after stripping with 1 M hydrochloric acid. The sum of the metal concentrations in the two phases agreed well with the initial concentrations.

RESULTS AND DISCUSSION

Distribution of HPBI

In general, β -diketone-type chelating agents show keto–enol tautomerism. However, the absence of a methyne proton (CH) peak for the 4-position of the isoxazolone ring characteristic of a keto form in the 1H NMR spectrum indicates that HPBI exists quantitatively in the enol form in $CDCl_3$.

The acid dissociation constant (K_a) and the partition constant (P_{HA}) were determined by a liquid–liquid distribution method. The distribution ratio of HPBI (HA) between the organic and the aqueous phase, D_{HA} , can be written as

$$D_{HA} = \frac{[HA]_o}{([HA] + [A^-])}$$

$$= P_{HA} / (1 + K_a [H^+]^{-1}) \quad (1)$$

where P_{HA} and K_a are defined as $[HA]_o/[HA]$ and $[H^+][A^-]/[HA]$, respectively. The subscript o denotes the species in the organic phase. When

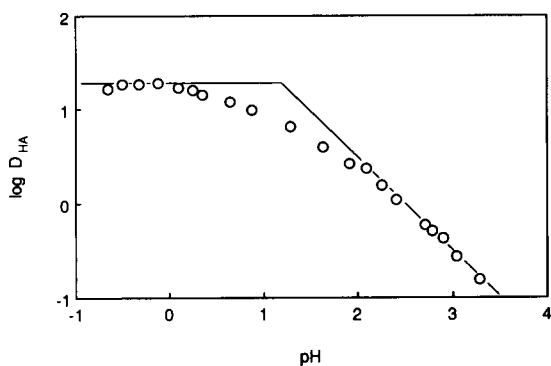


Fig. 1. Distribution of HPBI between cyclohexane and water.

the hydrogen ion concentration is high enough, D_{HA} is equal to P_{HA} , while $\log D_{HA}$ corresponds to $\log P_{HA} + pK_a - \text{pH}$ for low hydrogen ion concentrations. In Fig. 1 the relationship between $\log D_{HA}$ and pH for the cyclohexane–water system is shown. Analysing the plots on the basis of Eqn. 1 gives the values of $\log P_{HA}$ and pK_a as 1.24 and 1.23, respectively. The pK_a value is close to the reported value [12]. Although the molecular weight is similar, $\log P_{HA}$ value is much smaller than that of HPMBP (2.33) [3]. The oxygen atom at the 1-position of the isoxazolone ring, which is exposed to the solvent unlike the nitrogen atom at the 1-position of the pyrazolone ring, would decrease the hydrophobicity.

The distributions of HPBI between chloroform–water and benzene–water were also examined and are shown in Fig. 2. The plots were straight lines with a slope of -1 . The $\log P_{HA}$ values, obtained employing a pK_a value of 1.23 were 2.88 and 2.33 for the chloroform–water and benzene–water systems, respectively.

A ball-and-stick representation based on the MNDO/H optimized structure is shown in Fig. 3. All geometric parameters were fully optimized. Two phenyl groups are fixed face to face and this structure is supported by the ^1H NMR spectral data. The phenyl signals of HPBI appear as a multiplet at 7.06–7.46 ppm, whereas those of benzoic anhydride and 3-phenyl-5-isoxazolone appear at 7.5–8.2 ppm. This clearly indicates that the stacking of two phenyl groups leads to upfield shifts of the ring protons due to the ring current effect.

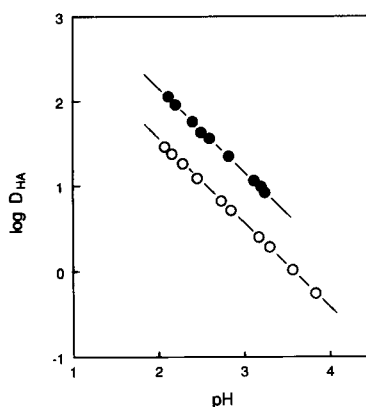


Fig. 2. Distribution of HPBI in chloroform–water and benzene–water systems. ● = Chloroform; ○ = benzene.

The strong acidity of acylpyrazolones and acylisoxazolones could be partly attributed to the heterocyclic π -electron conjugation system, which contains electronegative nitrogens and oxygens. It is interesting to compare the distance between the two donating oxygen atoms. The O–O distances for HTTA, HPMBP, and HPBI obtained from MNDO/H optimized structures are 2.5, 2.7 and 2.9 Å, respectively. The O–O distance should be significant with respect to the stability of the

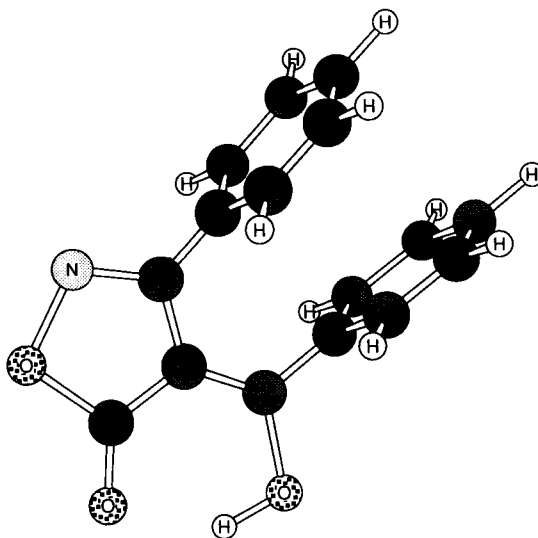


Fig. 3. Ball-and-stick representation based on the MNDO/H optimized structure of HPBI.

TABLE 1

Extraction constants for lanthanides with HPBI, HPMTFP, HPMBP and HTTA

Lanthanide	HPBI ($pK_a = 1.23^a$)		HPMTFP ($pK_a = 2.56^b$): Log K_{ex}^c	HPMBP ($pK_a = 3.92^b$): Log K_{ex}^f	HTTA ($pK_a = 6.23^c$): Log K_{ex}^g
	$pH_{1/2}^d$	Log K_{ex}			
La ³⁺	2.59	-1.77	-6.18	-7.18	-10.51
Pr ³⁺	2.40	-1.20	-4.98	-6.17	-8.85
Eu ³⁺	2.13	-0.39	-3.78	-5.33	-7.66 (-8.68) ^h
Ho ³⁺	2.12	-0.36	-3.36	-4.71	-7.25
Yb ³⁺	2.10	-0.30	-3.15	-4.24	-6.72

^a This work. ^b Taken from [3]. ^c Taken from [1]. ^d [HPBI]_o = 0.01 M in chloroform. ^e Taken from [14]. ^f Taken from [15]. ^g Taken from [16]. ^h Taken from [17]. Extraction into chloroform.

intramolecular hydrogen bonding and the formation of metal complexes.

The electronegativity of oxygen is larger than that of nitrogen, but such a great enhancement in acidity on changing from acylpyrazolone to acylisoxazolone could not be attributed merely to replacement of nitrogen with oxygen. The larger O–O distance in HPBI would decrease the stability of the intramolecular hydrogen bonding, resulting in a great enhancement of acidity. The effect of the O–O distance on acidity and complex formation is now under examination in further detail.

Extraction of lanthanides with HPBI

In the extraction of lanthanides (Ln³⁺), the overall extraction equilibrium and the extraction constant can be written as



$$K_{ex} = [Ln(PBI)_3_o][H^+]^3 / [Ln^{3+}][HPBI_o]^3 \quad (3)$$

$$\log K_{ex} = \log D - 3 \log [HPBI]_o - 3pH \quad (4)$$

TABLE 2

Stability constants of the adducts with TOPO

Extractant	Parameter	La	Pr	Eu	Ho	Yb
HPBI	Log $K_{ex,2}$	6.38	7.25	7.50	7.20	6.46
	Log β_1	5.05	5.14	5.11	5.13	5.53
	Log β_2	8.15	8.45	7.89	7.56	6.76
HPMTFP ^a	Log $K_{ex,2}$	4.20	5.19	6.06	6.08	5.68
	Log β_1	–	–	5.88	5.90	6.31
	Log β_2	10.38	10.17	9.84	9.44	8.70
HPMOP ^b	Log $K_{ex,1}$	–	-4.15	-2.82	–	-0.08
	Log β_1	–	4.34	4.15	–	4.40

^a Taken from [14]. ^b 1-Phenyl-3-methyl-4-octanoyl-5-pyrazolone. Taken from [18].

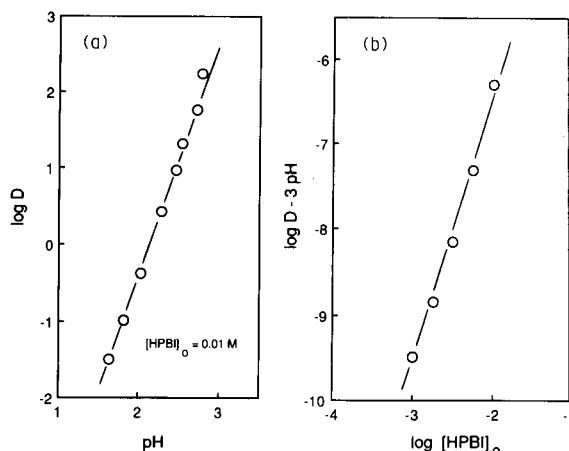


Fig. 4. Plots of (a) log D vs. pH and (b) log $D - 3pH$ vs. log [HPBI]_o in the extraction of europium.

where $D = [Ln(PBI)_3]_o / [Ln^{3+}]$ is the distribution ratio of Ln³⁺.

Figure 4 shows plots of log D vs. pH and log $D - 3pH$ vs. log [HPBI]_o in the extraction of europium into chloroform. The plots are straight

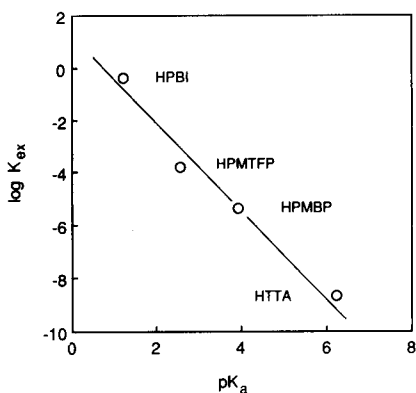


Fig. 5. Plots of $\log K_{\text{ex}}$ vs. $\text{p}K_{\text{a}}$ for the extraction of europium.

lines with a slope very close to 3, indicating that three molecules of HPBI react with one molecule of Ln, releasing three molecules of hydrogen, and that no neutral HPBI as a self-adduct is involved in the extracted species. After having confirmed the validity of Eqns. 3 and 4, the $\text{pH}_{1/2}$ values, at which half the metal ions are extracted, read from the plots of $\log D$ vs. pH for each lanthanide, were employed to obtain K_{ex} on the basis of Eqn. 4.

Table 1 gives the $\text{pH}_{1/2}$ and the $\log K_{\text{ex}}$ values for HPBI together with those for HTTA, 1-phenyl-3-methyl-4-benzoyl-5-pyrazolone (HPMBP) and 1-phenyl-3-methyl-4-trifluoroacetyl-5-pyrazolone (HPMTFP) for comparison. The extraction constants were obtained employing chloroform as the organic solvent, except for HTTA, where the organic phase was benzene. It is found to be possible to extract lanthanides quantitatively below pH 3 with 0.01 M HPBI. The extraction constants obviously increase as the acidity increases.

Figure 5 shows typical plots of $\log K_{\text{ex}}$ vs. $\text{p}K_{\text{a}}$ for each extractant in the extraction of europium, where the $\log K_{\text{ex}}$ value for HTTA is also that into chloroform (see Table 1). As can be seen in Fig. 5, $\log K_{\text{ex}}$ increases linearly as $\text{p}K_{\text{a}}$ decreases. The separation factor defined by $\log [K_{\text{ex}}(\text{Yb})/K_{\text{ex}}(\text{La})]$ is 1.47, 3.03, 2.94 and 3.79 for HPBI, HPMTFP, HPMBP and HTTA, respectively. The separation of lanthanides becomes poorer as the extractability increases. These re-

sults would strongly suggest the relationship between the separability and the acidity, that is, the O–O distance.

Extraction of lanthanides with HPBI and TOPO

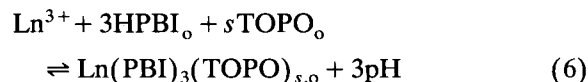
In the extraction of lanthanides in the presence of TOPO, the distribution ratio, D^* , can be expressed as

$$D^* = \{[\text{Ln}(\text{PBI})_3]_o + [\text{Ln}(\text{PBI})_3(\text{TOPO})]_o + \dots + [\text{Ln}(\text{PBI})_3(\text{TOPO})_s]_o\} / [\text{Ln}^{3+}]$$

Dividing D^* by D , the distribution ratio in the absence of TOPO, gives

$$D^*/D = 1 + \sum \beta_s [\text{TOPO}]_o^s \quad (5)$$

where β_s is an adduct formation constant, defined as $[\text{Ln}(\text{PBI})_3(\text{TOPO})_s]_o / [\text{Ln}(\text{PBI})_3]_o [\text{TOPO}]_o^s$. In the higher $[\text{TOPO}]_o$ region where $\text{Ln}(\text{PBI})_3(\text{TOPO})_s$ could be considered to be the predominant extracted species, the extraction equilibrium and the synergistic extraction constant, $K_{\text{ex},s}$, are expressed simply as follows:



$$K_{\text{ex},s} = [\text{Ln}(\text{PBI})_3(\text{TOPO})_s]_o [\text{H}^+]^3 / [\text{Ln}^{3+}] [\text{HPBI}]_o^3 [\text{TOPO}]_o^s \quad (7)$$

$$\log K_{\text{ex},s} = \log D^* - 3 \log [\text{HPBI}]_o - s \log [\text{TOPO}]_o - 3\text{pH} \quad (8)$$

The synergistic extraction of europium with a combination of 0.01 M HPBI and 0.01 M TOPO was examined. The plot of $\log D^*/D$ vs. pH was a straight line with a slope of 3, as predicted from Eqn. 8. Figure 6 shows a plot of $\log D^*/D$ vs. $\log [\text{TOPO}]_o$ in the synergistic extraction of europium as a typical example. The slope of the straight portion in the higher TOPO concentration region is 2 and decreases at lower TOPO concentrations. This change in slope indicates that the extracted species with HPBI and TOPO depends on $[\text{TOPO}]_o$ and that the extracted species, $\text{Eu}(\text{PBI})_3(\text{TOPO})$, in the lower TOPO concentration region changes to $\text{Eu}(\text{PBI})_3(\text{TOPO})_2$ at higher concentrations. The adduct formation constants were calculated by non-lin-

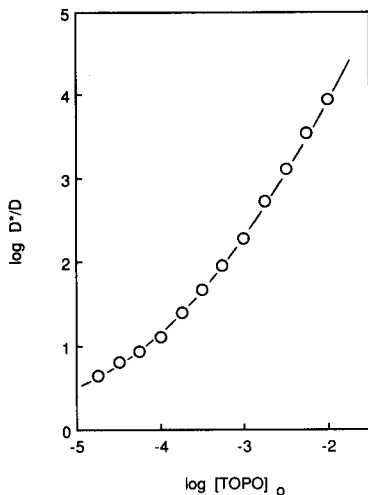


Fig. 6. Effect of $[\text{TOPO}]_0$ in the synergistic extraction of europium with HPBI into chloroform.

ear least-squares methods on the basis of Eqn. 5 and are summarized in Table 2 together with those for some acylpyrazolones for comparison.

In the synergistic extraction of lanthanides with acylpyrazolone and TOPO, the number of TOPO moieties in the extracted species is 1 when the substituent at the 4-position of the pyrazolone ring is aliphatic [18–20] and 2 when it is aromatic or perfluorinated [14,19,21]. The number of TOPO moieties in the extracted species with HPBI is 2, in analogy with aroyl- or perfluoroacylpyrazolones. The adduct formation constants for HPBI are larger than those for 1-phenyl-3-methyl-4-octanoyl-5-pyrazolone (HPMOP) and smaller than those for HPMTFP. The stability for the HTTA–TOPO–Eu system ($\log \beta_1 = 4.95$, $\log \beta_2 = 7.68$ [22]) is similar to that for the HPBI–TOPO–Eu system. It is known that stable adduct formation reactions are usually brought about by strongly acidic extractants. However, the order of the adduct formation reactions does not obey the order of the acidity of extractants to the extent discussed here. The stability of the adduct formation reaction probably depends on the acidity of extractants, but the strong acidity is caused in different ways, namely the electron-withdrawing substituent such as a perfluoroalkyl group, the heterocyclic structure and the O–O distance, which has a significant effect on hydrogen bond-

ing. These modes seem not to be equivalent for the stability of the adduct formation reaction.

The difference in the extraction constants between HPMTFP and HPBI decreases on adding TOPO owing to the very stable adduct formation in the HPMTFP–TOPO system; nevertheless, those for HPBI are still larger than those for HPMTFP. The order of the adduct formation constants is $\text{La} < \text{Pr} > \text{Eu} > \text{Ho} > \text{Yb}$. Consequently, the values of $\log K_{\text{ex},2}$ do not decrease as the atomic number increases, unlike $\log K_{\text{ex}}$, but have a maximum at Eu. A similar tendency has been reported for the HPMTFP–TOPO and HPMTFP–bidentate phosphine oxide systems [14].

This research was partly supported by a Grant-in-Aid for Scientific Research (03453042) from the Ministry of Education, Science and Culture of Japan. Computation time was provided by the Supercomputer Laboratory, Institute for Chemical Research, Kyoto University.

REFERENCES

- 1 C. Keller and H. Schreck, *J. Inorg. Nucl. Chem.*, 31 (1969) 1121.
- 2 S. Umetani, M. Matsui, J. Tôei and T. Shigematsu, *Anal. Chim. Acta*, 113 (1980) 315.
- 3 S. Umetani and M. Matsui, *Bull. Chem. Soc. Jpn.*, 56 (1983) 3426.
- 4 S. Umetani, K. Sasayama and M. Matsui, *Anal. Chim. Acta*, 134 (1982) 327.
- 5 S. Umetani, S. Kihara and M. Matsui, *Chem. Lett.*, (1986) 1545.
- 6 S. Umetani, K. Maeda, S. Kihara and M. Matsui, *Talanta*, 34 (1987) 779.
- 7 H. Mukai, S. Miyazaki, S. Umetani, S. Kihara and M. Matsui, *Anal. Chim. Acta*, 220 (1989) 111.
- 8 A. Jyothi and G.N. Rao, *Chem. Scr.*, 27 (1987) 367.
- 9 A. Jyothi and G.N. Rao, *Bull. Chem. Soc. Jpn.*, 61 (1988) 4497.
- 10 A. Jyothi and G.N. Rao, *Polyhedron*, 8 (1989) 1111.
- 11 A. Jyothi and G.N. Rao, *Talanta*, 37 (1990) 431.
- 12 R.H. Wiley, A. Quilico, G. Speroni, L.C. Behr and R.C. McKee, *The Chemistry of Heterocyclic Compounds*, Interscience, New York, 1962, p. 143.
- 13 F. Korte and K. Störko, *Chem. Ber.*, 94 (1961) 1956.
- 14 S. Umetani and H. Freiser, *Inorg. Chem.*, 26 (1987) 3179.
- 15 A. Roy and K. Nag, *J. Inorg. Nucl. Chem.*, 40 (1978) 331.
- 16 J. Stary, *The Solvent Extraction of Metal Chelates*, Pergamon, Oxford, 1964.

- 17 T. Sekine and D. Dyrssen, *Talanta*, 11 (1964) 867.
- 18 O. Tochiyama and H. Freiser, *Anal. Chim. Acta*, 131 (1981) 233.
- 19 K. Sasayama, S. Umetani and M. Matsui, *Anal. Chim. Acta*, 149 (1983) 253.
- 20 Y. Sasaki and H. Freiser, *Inorg. Chem.*, 22 (1983) 2289.
- 21 H. Mukai, S. Miyazaki, S. Umetani, S. Kihara and M. Matsui, *Anal Chim Acta*, 239 (1990) 277.
- 22 K. Akiba, M. Wada and T. Kanno, *J. Inorg. Nucl. Chem.*, 43 (1981) 1031.

Optimized prediction of ^{13}C NMR spectra using increments

Lingran Chen ¹ and Wolfgang Robien

University of Vienna, Währingerstrasse 38, A-1090 Vienna (Austria)

(Received 30th March 1992; revised manuscript received 31st August 1992)

Abstract

A novel approach for the prediction of the ^{13}C NMR spectrum of a given structure using a new algorithm of increment calculation [optimized prediction of spectra using increments (OPSI)] is presented. The algorithm is based on substructure search strategies starting from the parent ring system and taking into account all possible combinations of partial structures to generate the given target structure. This scheme allows the prediction of the ^{13}C NMR spectrum of any polysubstituted ring system without predefined parameter tables or already prepared substructure/subspectrum files using always the complete information content of a large database. Stereochemical influences are automatically detected and used for the calculation; furthermore, expectation ranges and standard deviations for each shift value can be obtained.

Keywords: Nuclear magnetic resonance spectrometry; Increments; Spectral prediction

Spectrum estimation is a key step during manual and computer-assisted structure elucidation processes. Practical solutions for this type of problem are the well established methods of increment calculations [1,2] and the application of the HOSE code [3]. Since the first additivity relationship published by Grant and Paul [4] for the prediction of ^{13}C NMR spectral data for simple hydrocarbons, many publications have dealt with this problem for different classes of compounds [5–9]. This approach usually allows a good prediction of the chemical shift values for a restricted class of very similar compounds. A more general parameter set for chemical shift prediction has been published recently [10,11]. Stereo-

chemical influences on chemical shifts are taken into account using additional terms derived from typical examples due to a certain arrangement of atoms within the molecular framework [12].

The common feature of all these additivity models is that they must use a set of parameters that have been derived from a set of carefully selected reference compounds. Therefore, each model must hold large tables of specifically derived parameters for a comparably narrow class of compounds. As the variety of organic molecules is extremely large, it is a difficult task to derive models even only for the most prominent classes of molecules. In order to describe the simple class of monosubstituted benzenes with respect to 100 different functional groups, it is necessary to keep a table with one parent value, 400 increment values and 5050 values for *ortho* interaction. When applying such a model to a certain target structure the result will simply consist of expected chemical shift values without any infor-

Correspondence to: W. Robien, Department of Organic Chemistry, University of Vienna, Währingerstrasse 38, A-1090 Vienna (Austria).

¹ On leave from University of Science and Technology of China, Hefei, Anhui 23006 (China).

mation about expectation range and standard deviation.

The approach presented here [optimized prediction of spectra using increments (OPSI)] uses directly the information content of a large ^{13}C NMR database instead of already prepared tables taking into account all possible combinations of substructural fragments, therefore including automatically stereochemical interactions between the individual substituents.

METHOD

The algorithm is based on the analysis of the user-defined target structure with respect to its substitution pattern. The best understanding of the basic problem can be achieved by consideration of a simple example taken from the above-mentioned field of polysubstituted benzene

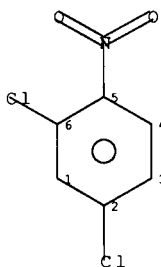
derivatives. 2,4-Dichloronitrobenzene is taken as an example (Fig. 1). The traditional way of solving this problem is a simple look-up algorithm using a table containing the increments for mono-substituted benzenes and adding these increments of the two functional groups Cl and NO_2 to the chemical shift value of benzene, leading to six shift values of the target structure with no information about their reliability.

The approach starts with an analysis of the substitution pattern of the target structure and then systematically removes all substituents from the benzene ring leading to a total of six partial structures shown in Fig. 2.

The next step is simply a search for all those six partial structures in the CSEARCH-NMR database system [13]. Suppose all six partial structures have been found, then four different ways of estimating the chemical shift values of the target structure can be generated as shown in Fig.

C-13 NMR DATENBANK: B #-4208 SADT-4261 C0-4261 25/03/1992 14:43:03
BENZENE, 2,4-DICHLORO-1-NITRO-,

SADTLER RESEARCH, COPYRIGHT 1991
 $\text{C}_6\text{H}_3\text{Cl}_2\text{NO}_2$ MWT= 192.0
 CDCl_3



C - 1: 131.60D
C - 2: 139.30S
C - 3: 128.10D
C - 4: 126.80D
C - 5: 146.30S
C - 6: 128.10S

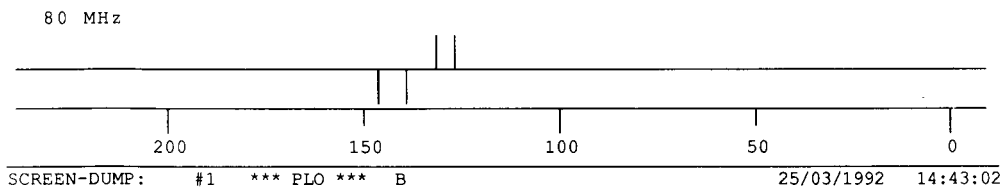
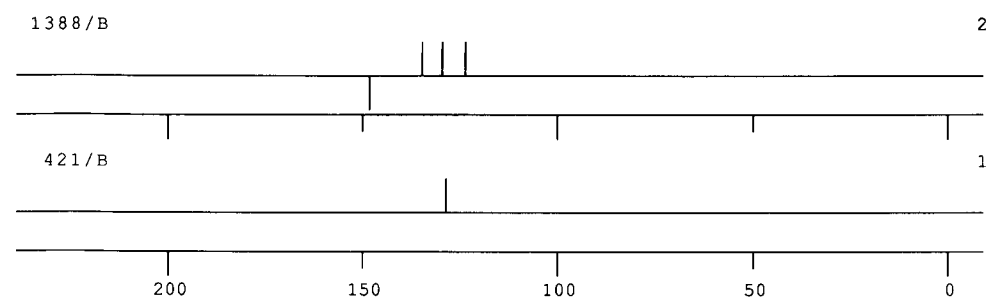
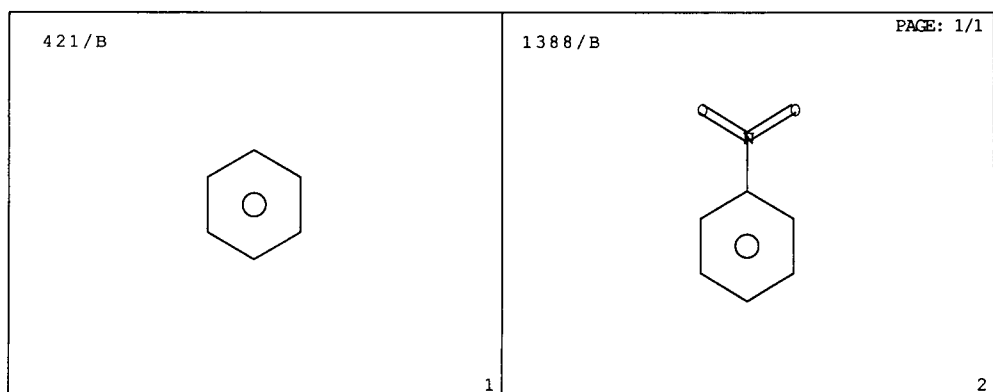
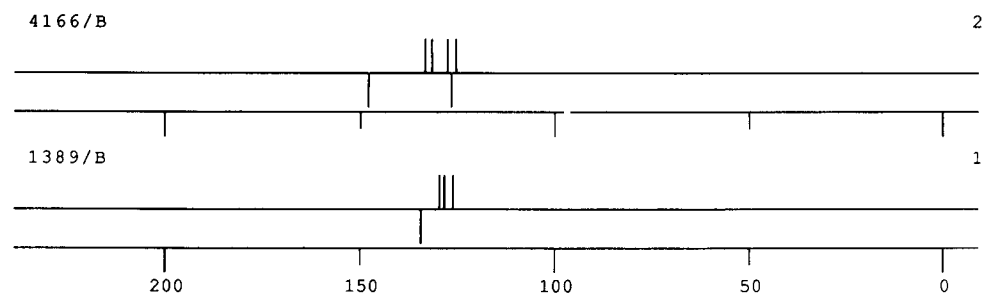
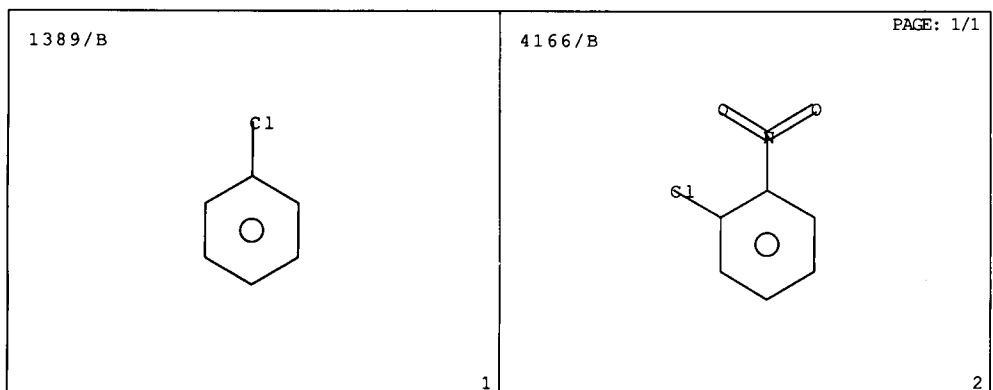


Fig. 1. Datasheet as generated by the CSEARCH software showing the target compound for the example selected.



SCREEN-DUMP: #6 *** MUL *** B 25/03/1992 14:47:28



SCREEN-DUMP: #7 *** MUL *** B 25/03/1992 14:50:42

Fig. 2. Spectral data for the six partial structures involved in the calculation.

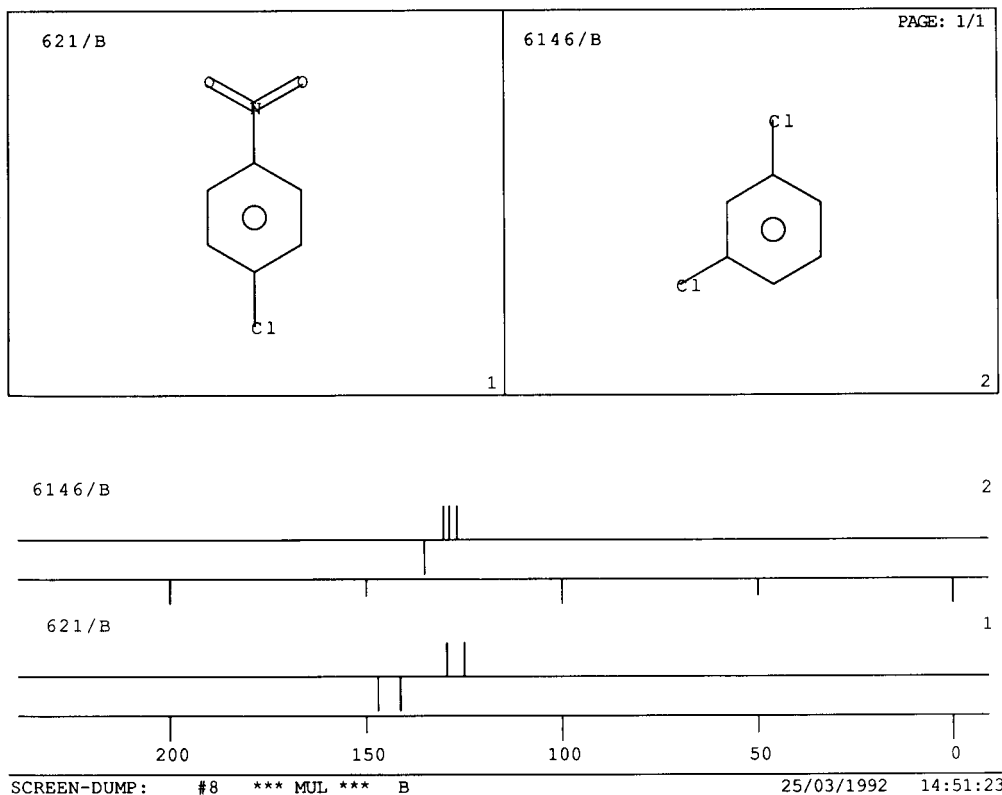


Fig. 2 (continued).

3 and Table 1. The best result obtained is derived from estimating way 1 starting from *o*-chloronitrobenzene and adding the shift increments calculated from chlorobenzene automatically taking into account the steric interaction between the two substituents in the *ortho* position.

TABLE 1

Measured chemical shift values and four sets of calculated chemical shift values (ppm) for 2,4-dichloronitrobenzene ^a

	Measured	Way 1	Way 2	Way 3	Way 4
C-1	131.6	131.9	129.8	129.7	129.7
C-2	139.3	139.3	141.4	142.6	141.9
C-3	128.1	127.9	127.8	127.5	127.5
C-4	126.8	126.7	125.3	126.2	125.9
C-5	146.3	146.0	146.6	147.1	146.3
C-6	128.1	127.9	130.1	130.9	130.6
Deviation		0.2	1.6	2.0	1.7

^a Data taken from the Sadtler collection of ¹³C NMR spectra. For convenience the same numbering scheme as in Fig. 1 is used.

From this example it can be seen that the approach presented here is entirely general and does not contain any compound-specific restriction, except that at least one ring must be present in the target structure. This method is totally equivalent to any increment table which can be deduced from the database itself; it should explicitly pointed out that this is valid for any parent compound (= ring system) contained in the database and for any substituent represented by the reference data itself. This approach has the advantages that no disk space necessary for storing any table and there is perfect utilization of the actual database contents.

DESCRIPTION OF THE ALGORITHM

The algorithm consists of five main parts as follows.

(1) Perception of substituted positions: first the MCSS algorithm [14] is used to detect ring systems in the target structure. For a structure containing no isolated ring systems, the substituted positions at the ring can be easily detected by simply removing all the acyclic substituents from the target structure. For those structures which have isolated ring systems, the procedures are more complicated [15].

(2) Generation of all possible cutways: according to the number of substituted positions perceived in the target structure, all the possible different ways of systematically cutting off the substituents from the target structure are calculated. For a structure with four substituents, for example, a total of fifteen cutways must be considered.

(3) Generation of partial structures and searching for identities occurring in the database:

according to each cutway and corresponding substituted positions perceived, each time a specific number of substituents is cut off from the target structure to generate one partial structure, then the identical structure search for this partial structure is performed over all databases accessed. As the identical structure search is the slowest step in the whole procedure, because of massive input/output operations, the duplicate cutways are deleted through the analysis of the target structure by means of the MCSS algorithm to avoid producing the duplicate partial structures.

(4) Generation of all possible estimating ways: after all the cutways have been processed and the identical structure of the parent structure and at least one identical structure of the other partial structures have been found in the database, all the possible combinations of the parent structure

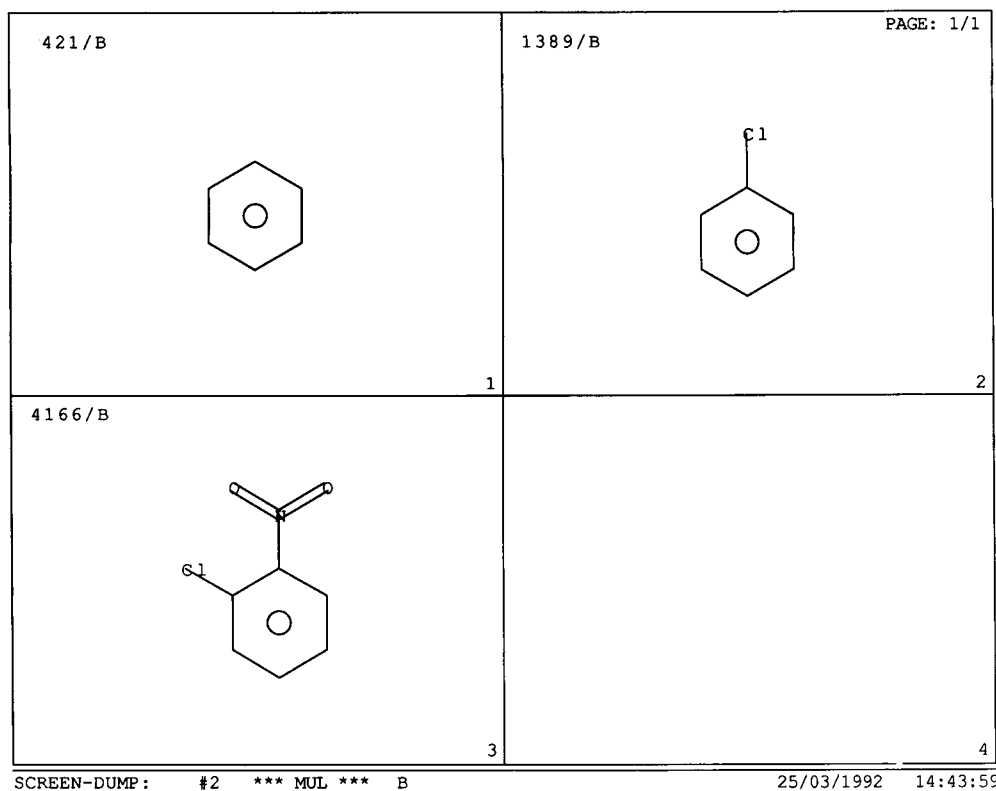
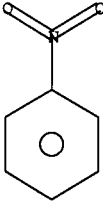
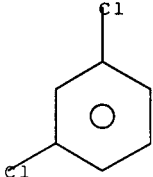


Fig. 3. Structures used to generate the four different estimating ways leading to the expected chemical shift values of 2,4-dichloronitrobenzene as given in Table 1.

421/B 	1388/B PAGE: 1/1 
6146/B 	
SCREEN-DUMP: #3 *** MUL *** B	25/03/1992 14:44:41

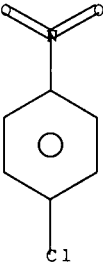
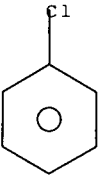
421/B 	621/B PAGE: 1/1 
1389/B 	
SCREEN-DUMP: #4 *** MUL *** B	25/03/1992 14:45:28

Fig. 3 (continued).

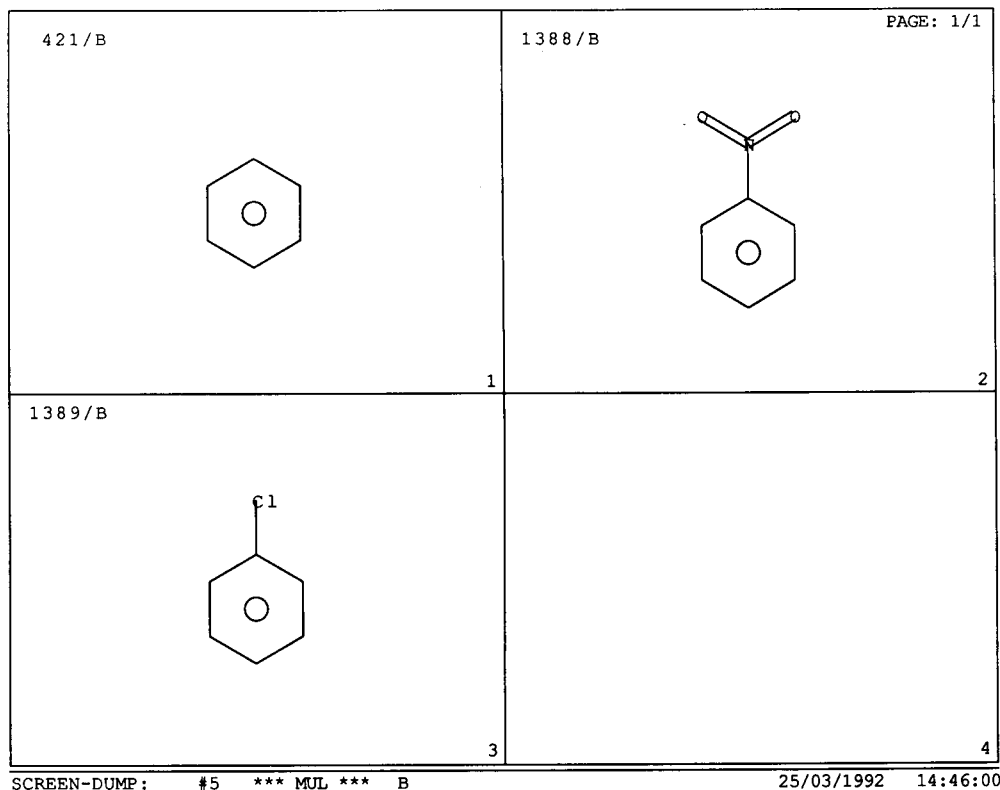


Fig. 3 (continued).

and other partial structures (called estimating ways) are calculated. The fact that the number of estimating ways increases dramatically with increase in the number of substituents considered implies that a good strategy would be that each estimating way generated is immediately used to calculate the chemical shift values. However, when a target structure contains identical substituents, duplicate estimating ways may be generated. In order to avoid this overhead of unnecessary estimating ways, all already generated combinations must be stored. By using an efficient strategy based on a general combination model [15], only a small part of the complete set of estimating ways needs to be stored. Besides, although the theoretical number of estimating ways is very large for polysubstituted target structures, only a small number of these combinations will be generated because usually not all partial structural fragments necessary are represented within the reference data collection.

(5) Calculation of chemical shift values: in accordance with each estimating way, one set of chemical shift values can be calculated. First, the parent structure is compared with the target structure by means of the MCSS algorithm to generate the atom-by-atom correspondences between the two structures. This information is used to assign the chemical shift values of the parent structure to the corresponding carbon atoms in the target structure as their base value. Then, each partial structure included in the estimating way is compared with the target structure. The chemical shift increments are calculated from the atom-by-atom correspondences and added to the corresponding intermediate result, leading to one set of predicted chemical shift values.

The great advantage of this method over other published increment approaches is that usually more than one set of shift values can be obtained because of the different estimating ways. The deviation allows the calculation of expectation

ranges instead of simple expectation values, giving some insight into steric influences between the substituents. A detailed comparison of the OPSI approach with other well established methods for spectrum estimation has been presented elsewhere [16].

EXPERIMENTAL

The algorithm was implemented in FORTRAN-77 under a UNIX operating system on a Silicon Graphics Workstation and on an IBM-R/6000 workstation. The program consists of ca. 7000 lines of source code. The databases used hold about 80 000 ^{13}C NMR spectra including the collections from University of Vienna, Sadtler Research Laboratories and the German Cancer Research Centre.

Lingran Chen is grateful to the Austrian Academic Exchange Service for financial support. The authors express their gratitude to the staff of the University Computing Centre for helpful discussions during program development. This work was supported within the European Academic Supercomputing Initiative (EASI).

REFERENCES

- 1 M.O. Kalinowski, S. Berger and S. Braun, *Carbon-13 NMR Spectroscopy*, Wiley, New York, 1988.
- 2 E. Pretsch, J.T. Clerc, J. Seibl and W. Simon, *Tables of Spectral Data for Structure Elucidation of Organic Compounds*, Springer, Berlin, 2nd edn., 1989.
- 3 W. Bremser, *Anal. Chim. Acta*, 103 (1978) 355.
- 4 D.M. Grant and E.G. Paul, *J. Am. Chem. Soc.*, 86 (1964) 2984.
- 5 L.P. Lindemann and J.Q. Adams, *Anal. Chem.*, 43 (1971) 1245.
- 6 A. Ejchart, *Org. Magn. Reson.*, 13 (1980) 368.
- 7 A. Ejchart, *Org. Magn. Reson.*, 15 (1981) 22.
- 8 Y.A. Shahab and H.A. Al-Wahab, *J. Chem. Soc., Perkin Trans. 2*, (1988) 255.
- 9 V.I. Dostovalova, L.A. Fedorov and J. Paasivirta, *Magn. Reson. Chem.*, 29 (1991) 830.
- 10 A. Fürst, E. Pretsch and W. Robien, *Anal. Chim. Acta*, 233 (1990) 213.
- 11 E. Pretsch, A. Fürst and W. Robien, *Anal. Chim. Acta*, 248 (1991) 415.
- 12 D. Ströhl, S. Thomas, E. Kleinpeter, R. Radeaglia, J. Brunn, GDCh-Tagung, Fortschritte und Anwendungen in der Magnetischen Resonanzspektroskopie, Todtmoos, Germany, 29 September–2 October 1991.
- 13 H. Kalchauer and W. Robien, *J. Chem. Inf. Comput. Sci.*, 25 (1985) 103.
- 14 L. Chen and W. Robien, *J. Chem. Inf. Comput. Sci.*, 32 (1992) 501.
- 15 L. Chen, Thesis, University of Vienna, in preparation.
- 16 L. Chen and W. Robien, *Fresenius' J. Anal. Chem.*, 344 (1992) 214.

Characteristics and application of an electrochemical concentration modulator in correlation chromatography

Part 2. Computational aspects, modelling and application

M. Engelsma, H.F.M. Boelens, D.J. Louwerse, W.Th. Kok and H.C. Smit

University of Amsterdam, Laboratory for Analytical Chemistry, Amsterdam (Netherlands)

(Received 20th February 1992; revised manuscript received 28th September 1992)

Abstract

An electrochemical cell was used as an injection device in correlation chromatography. The use of a conventional injection control signal combined with a conventional deconvolution method leads to the appearance of ghost peaks in the correlogram. Several methods to suppress or correct for the presence of ghost peaks in the correlogram were studied, taking into account the electrochemical cell characteristics determined in the first part of this paper. An overview is given of existing time-domain deconvolution methods with emphasis on the shape of the virtual injection. Fourier-domain deconvolution methods are discussed and compared with time-domain methods. An improved model for the modulation process taking place in the electrochemical cell is used to calculate the real injection pattern. Three alternative methods to diminish the ghost peak phenomenon have been compared. First, deconvolution of the detector signal with a calculated or experimentally determined input pattern was examined. Secondly, intrinsic correction properties of correlation chromatography were used to remove the ghost peaks. Finally, the effect of adjusting the signal used to control the potentiostat was tested. The latter method proved to be the best solution. Calibration curves were measured to test the linearity of the method.

Keywords: Chromatography; Voltammetry; Concentration modulation; Deconvolution; Electrochemical concentration modulator; Ghost peaks

In the first part of this paper [1] the potential advantages of an electrochemical concentration modulator over a mechanical modulator in correlation chromatography (CC) were explained as the absence of mechanical parts (wear and tear) and the gain in selectivity. Recent work by Mars and Smit [2] shows that wear and tear is much less a problem because very strong materials are used in valve fittings and rotors. Selectivity is gained because only compounds that are electrochemically active in the applied potential window are affected. This results in simpler correlograms

and in a reduction of correlation noise. Correlation noise [3–5] is caused by non-linearity and non-stationarity in the system and is proportional to the total peak intensity.

The first work done on electrochemical concentration modulation (ECM) by Carney and Phillips [6] showed that resulting correlograms were strongly dependent on the pH of the eluent, on the potential window used as modulation interval, on the pulse duration and on the composition of the sample matrix.

In the first part of this paper we have characterized the properties of ECM by systematic measurements with a standard compound. The electrochemistry of the quinone–hydroquinone couple is reversible and it has a moderate half-

Correspondence to: H.C. Smit, University of Amsterdam, Laboratory for Analytical Chemistry, Nieuwe Achtergracht 166, 1018 WV Amsterdam (Netherlands).

wave potential. Despite this carefully selected model, problems occurred with partly an electrochemical and partly a CC origin. It was shown that the step response of the electrode potential and the relative position of the half-wave potential in the potential modulation interval are responsible for the generation of ghost peaks [7]. The large surface area of the porous graphite working electrode and the position of the reference electrode in the cell are responsible for this slow response. It was also shown that the intensities of both complementary and non-complementary ghost peaks depend on whether the injection error is symmetrical or asymmetrical and on the time scale of the electrode potential delay.

The position of the lowest order non-complementary ghost peak in the correlogram can be calculated beforehand since it depends only on the pseudo random binary sequence (PRBS) used as the base pattern for the injection sequence. Not every aspect of the modulator's behaviour could be accounted for. For instance the effect of the analyte concentration on the ghost peak intensity remained unexplained, although the decreasing effect on the time constants used to describe the cell response function may be involved.

In the present paper deconvolution methods are proposed which may be used to correct for injection errors, thereby eliminating ghost peaks. Since the deconvolution method seems to play a crucial role, the history of deconvolution methods is discussed in short and the relation between different methods is discussed. Resolution-enhancing properties of some methods are observed. A model of the injection process is presented which provides a more accurate description of the form of the actual injection pattern. Furthermore correction methods intrinsic to CC are explained and applied. A calibration curve was constructed to check the linearity.

THEORY

All signals described are discrete sets of g points (a sequence). Injection signals are based on an n -bit pseudo random binary sequence. Each

PRBS bit corresponds to a so-called clock period (cp) in the injection sequence. Each cp has a duration t_{cp} and contains w equidistant points, so $g = n \cdot w$. A "1" in the PRBS means that an injection will take place in the corresponding cp which will be referred to as an "injection clock period" (i-cp). A "0" indicates that no injection will take place in the corresponding "non-injection clock period" (ni-cp). Discrete circular convolution between arbitrary signals x and y

$$z_k = \sum_{i=0}^{g-1} x_i \cdot y_{k-i}$$

is abbreviated to $z = x \star y$. Discrete circular cross-correlation between signals x and y

$$z_k = \sum_{i=0}^{g-1} x_i \cdot y_{k+i}$$

is abbreviated to $z = x \otimes y$.

Noise is considered to be absent. A thorough description of the effect of the deconvolution operation on the noise in the signal for normal CC is discussed elsewhere [8].

The general principle of CC

In normal chromatography a chromatogram y_{nc} can be described by

$$y_{nc} = b_w \star h_{chrom} \quad (1)$$

where b_w is the injection profile consisting of the actual injection represented by a block of w points of value "1" which is completed with zero's to g points (Fig. 1).

The exact (discrete) impulse response h_{chrom} of the chromatographic system cannot be measured because of the injection width. It can be measured approximately when the peaks are wide relative to the width of the injection (and to the volume of the detection device). Then the injection can be represented by one point of value "1".

The detector signal y_{cc} in CC can be described as a convolution of the actual (ideal or non-ideal) injection pattern x_{real} and the impulse response of the chromatographic system h_{chrom}

$$y_{cc} = x_{real} \star h_{chrom} \quad (2)$$

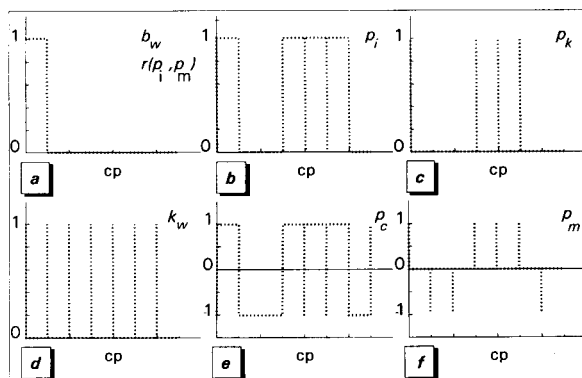


Fig. 1. Example signals based on a 7-bit PRBS. (a) Block function b_w ; (b) injection signal p_i ; (c) Kronecker sequence p_k ; (d) Kronecker comb k_w ; (e) conventional time-domain deconvolution signal p_c ; (f) resolution maintaining time-domain deconvolution signal p_m . The x -axis units are clock periods (cp); one cp contains w sample points and spans t_{cp} s.

The resulting superimposed collection of chromatograms can be deconvoluted to a comprehensible correlogram h_{cc} by performing a cross-correlation with a suitable signal z_d . The correlogram will resemble a normal chromatogram with an improved signal-to-noise ratio [9].

$$h_{cc} = y_{cc} \otimes z_d = (x_{real} \star h_{chrom}) \otimes z_d \quad (3)$$

Since the convolution operation is commutative we can write

$$h_{cc} = h_{chrom} \star (x_{real} \otimes z_d) = h_{chrom} \star r(x_{real}, z_d) \quad (4)$$

where $r(x_{real}, z_d)$ is the cross-correlation function between the actual injection pattern x_{real} and the signal z_d used for deconvolution. The use of the letter h in h_{cc} is not entirely correct since it is an impulse response only when $r(x_{real}, z_d)$ is a Kronecker delta function. However, its use is more or less a convention in CC literature. Compared to Eqn. 1 the single-injection function b_w is replaced by the so-called virtual injection $r(x_{real}, z_d)$ of the system. The virtual injection in CC is used for diagnostic purposes. It can be calculated approximately from the detector signal y_{cc} when the real impulse response h_{chrom} is known. It can also be calculated when the injection pattern x_{real} is measured. Ideally the virtual injection is a flat baseline with a spike at zero

time. When injection errors occur the baseline can be disturbed by ghost peaks and correlation noise.

The convolution of the virtual injection with the impulse response of the chromatographic system h_{chrom} will result in a correlogram in which each normal peak has its own set of individual satellite ghost peaks with equal positions and intensities relative to the real parent peak [7]. The quality of the virtual injection determines the quality of the CC part of the system, while the impulse response h_{chrom} determines the chromatographic quality. Therefore the impulse response h_{chrom} is ignored in the further treatment.

When an injection error is compound-specific the ghost peak patterns can be different for each sample component and each component may have a (slightly) different virtual injection. The shape of the virtual injection depends on the real injection pattern and on the deconvolution signal z_d . Therefore it is necessary to pay some attention to conventions regarding the deconvolution signal and its effect on the virtual injection.

The deconvolution signal in CC

p_i is the normal CC PRBS-based input signal, based on an n -bit PRBS, with n cp's, consisting of w points each (see for example Fig. 1b, where $n = 7$). All values within one cp are equal. p_k , a Kronecker input pattern is identical to p_i except that only the first point in a cp can be non-zero (Fig. 1c). It is constructed by multiplying p_i point by point, denoted by the “ \cdot ” sign, with a Kronecker comb k_w (Fig. 1d) under the condition that the distance between the “points” of the comb is equal to w points:

$$p_k = p_i \cdot k_w \quad (5)$$

p_c (Fig. 1e) is the conventionally used deconvolution signal. It has the same values as p_i except that each zero is replaced by (-1) . p_m (Fig. 1f) is the deconvolution signal used more recently in our group because of its favourable resolution characteristics, which will be discussed later. It was introduced recently by Mulder et al. [10].

The normal input signal p_i can be written as a convolution of the Kronecker pattern p_k and b_w :

$$p_i = p_k \star b_w \quad (6)$$

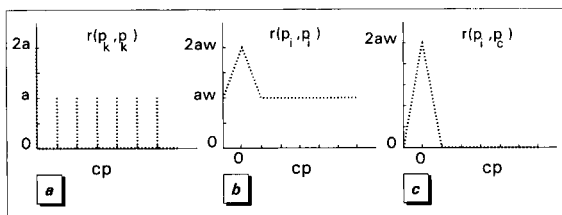


Fig. 2. Example signals based on a 7-bit PRBS with w points per clock period. (a) Autocorrelation function of a Kronecker sequence; (b) autocorrelation function of an injection signal; (c) cross-correlation function of an injection signal and the conventional deconvolution signal of Fig. 1e.

Now the virtual injection can be described for different deconvolution signals z_d in terms of the defined signals; p_i itself can be used as the deconvolution signal. Then a cross-correlation amounts to calculating the autocorrelation function $r(p_i, p_i)$ of the normal PRBS p_i :

$$\begin{aligned} r(p_i, p_i) &= p_i \otimes p_i = (p_k \star b_w) \otimes (p_k \star b_w) \\ &= (p_k \otimes p_k) \star b_w \star b_w \\ &= r(p_k, p_k) \star b_w \star b_w \end{aligned} \quad (7)$$

in $r(p_k, p_k)$ only the first point in each cp has a non-zero value. The first point (at zero shift) will have the value $(n+1)/2$, since only there all non-zero points are in eclipse and a PRBS of length n contains $(n+1)/2$ points of value 1. All other first points in subsequent cp's are of value $(n+1)/4$. As an example Fig. 2a shows $r(p_k, p_k)$ for a 7-bit PRBS-based signal with w points per cp. This signal can be expressed as $r(p_k, p_k) = a(\Delta + k_w)$, where $a = (n+1)/4$, Δ is a Kronecker delta function and k_w is a Kronecker comb. Then

$$\begin{aligned} r(p_i, p_i) &= a \cdot (\Delta + k_w) \star b_w \star b_w \\ &= a \cdot [(\Delta \star b_w) + (k_w \star b_w)] \star b_w \end{aligned} \quad (8)$$

Since $(\Delta \star b_w) = b_w$ and $(k_w \star b_w) = \mathbf{1}$ is a constant background

$$\begin{aligned} r(p_i, p_i) &= a \cdot (b_w + \mathbf{1}) \star b_w \\ &= a \cdot (b_w \star b_w) + a \cdot (\mathbf{1} \star b_w) \\ &= a \cdot d_{2w} + a \cdot w \end{aligned} \quad (9)$$

This is illustrated in Fig. 2b. The use of p_i as a deconvolution signal results in a virtual injection

$r(p_i, p_i)$ which broadens all peaks in the impulse response h_{chrom} with the triangular signal d_{2w} with a baseline width of two cp's. Also it gives an offset baseline in the correlogram. Compared to the chromatogram y_{nc} resulting from a single injection, the correlogram will be additionally broadened by a moving average filter of width w , which is equivalent to a low-pass filtering operation.

To avoid the offset the correlogram was usually calculated using p_c which can be written in terms of a signal p_m and b_w as $p_c = p_m \star b_w$. Then

$$\begin{aligned} r(p_i, p_c) &= p_i \otimes p_c = (p_k \star b_w) \otimes (p_m \star b_w) \\ &= (p_k \otimes p_m) \star b_w \star b_w \end{aligned} \quad (10)$$

It has been shown [10] that $r(p_k, p_m) = 2a \cdot \Delta$, so

$$\begin{aligned} r(p_i, p_c) &= 2a \cdot \Delta \star b_w \star b_w = 2a \cdot b_w \star b_w \\ &= 2a \cdot d_{2w} \end{aligned} \quad (11)$$

As a result the virtual injection has a triangular shape (Fig. 2c), and still gives an extra broadening compared to a single injection. Obviously one of the convolutions with the block function can be omitted by cross-correlating with p_m instead of with p_c :

$$\begin{aligned} r(p_i, p_m) &= p_i \otimes p_m = (b_w \star p_k) \otimes p_m \\ &= b_w \star 2a \cdot \Delta = 2a \cdot b_w \end{aligned} \quad (12)$$

which was already shown in Fig. 1a. Thus using p_m as deconvolution signal results in a virtual injection b_w . This deconvolution method will not result in an additional broadening of the virtual injection. Compared to the single-injection chromatogram y_{nc} the peak broadening is similar. The advantage compared to the single-injection method is the higher signal-to-noise ratio.

The difference between the last two methods vanishes when a cp contains only one point. Then the virtual injection would become a Kronecker delta function. In order to achieve this latter property when more than one detection point is sampled per cp a signal z_d has to be found with the characteristic that regardless of the number of points per cp:

$$p_i \otimes z_d = \Delta \quad (13)$$

Such a deconvolution would result in resolution enhancement. Alas, when a PRBS-based injection pattern is used with more than one point per cp the desired z_d does not exist. This can be illustrated by stating the problem in a matrix formalism. The cyclic convolution of the PRBS-based input pattern x and the impulse response h can be written as a multiplication of a square ($g \times g$) circulant matrix \mathbf{X} consisting of columns with cyclicly permuted input-sequence elements p_i [11] and a ($1 \times g$) column matrix \mathbf{H} , which contains the chromatographic impulse response h_{chrom} .

$$\mathbf{Y} = \mathbf{X} \cdot \mathbf{H} \quad (14)$$

where \mathbf{Y} is a ($1 \times g$) column matrix containing the detector signal y_{cc} . Calculating \mathbf{H} from the known \mathbf{Y} and \mathbf{X} amounts to calculating the inverse matrix \mathbf{X}^{-1} since

$$\mathbf{X}^{-1} \cdot \mathbf{Y} = \mathbf{X}^{-1} \cdot \mathbf{X} \cdot \mathbf{H} = \mathbf{1} \cdot \mathbf{H} \quad (15)$$

Where $\mathbf{1}$ is the square ($g \times g$) identity matrix. \mathbf{X}^{-1} only exists when the matrix \mathbf{X} is non-singular, i.e. its determinant should be non-zero. Remembering that the input signal p_i can be written as the convolution of p_k and b_w , or in matrix formalism

$$\mathbf{P}^i = \mathbf{P}^k \cdot \mathbf{B}^w \quad (16)$$

where \mathbf{P}^i is a ($1 \times g$) column matrix containing the elements of p_i ; \mathbf{P}^k is a square ($g \times g$) circulant matrix consisting of columns of cyclicly permuted input sequence elements p_k and \mathbf{B}^w is a ($1 \times g$) vector matrix containing the signal b_w . Since the square matrix \mathbf{X} consists of cyclicly permuted columns of p_i it can be written as the matrix product of square matrices \mathbf{P}^k and \mathbf{S}^w , where \mathbf{S}^w consists of cyclicly permuted columns containing the elements of b_w :

$$\mathbf{X} = \mathbf{P}^k \cdot \mathbf{S}^w \quad (17)$$

So

$$\mathbf{X}^{-1} = (\mathbf{P}^k \cdot \mathbf{S}^w)^{-1} = (\mathbf{S}^w)^{-1} \cdot (\mathbf{P}^k)^{-1} \quad (18)$$

\mathbf{P}^k can readily be inverted, resulting in a circulant matrix consisting of cyclicly permuted rows of the signal p_m . The matrix \mathbf{S}^w is however singular. This is caused by “matching” dimensions be-

tween the number w of serried points with value “1” in the columns (rows) of \mathbf{S}^w and g , the total number of points.

Whenever g is a whole multiple of the number of w , two or more equal columns (rows) can be constructed by application of a standard theorem for determinants [12]. This theorem states that the determinant of a matrix is not changed by adding to the elements of its i -row (column) the corresponding elements of another row (column). Elements 1 to w of the first column are “1”, the rest is zero. Elements $(w + 1)$ to $(2 \cdot w)$ in the w -th column are also “1”. Adding the contents of every w -th column (g/w columns) to the first column means that every element in the column has value “1”. The same operation can be carried out with other columns. As a result \mathbf{S}^w is singular and cannot be inverted. So for every PRBS-based injection signal p_i with more than one point per cp the inverse cannot be calculated.

In CC sometimes a so-called duty-cycle injection pattern is used. This means that only a part of an i-cp is used to inject. As a consequence only w_1 of the w points in an i-cp are “1”. When $w_1 > 1$ the corresponding matrix is not always singular. If g is not a whole multiple of w_1 , \mathbf{S}^w is not singular and \mathbf{X}^{-1} exists. This means that for a 7-bit PRBS-based injection signal with 5 points per cp no inverse exists when all 5 points in an i-cp have the value “1”. For a 7-bit PRBS based injection signal with 6 points per cp no inverse exists when 2, 3 or all 6 points in an i-cp have the value “1”. Only when duty-cycle injection patterns with 1, 4 or 5 points are used the inverse can be calculated.

Next to the matter of singularity the accuracy of the inverted result is important. Prior to application of the inverted matrix it should be checked whether the matrix \mathbf{X} is ill-conditioned [13] (the determinant is near zero), otherwise unwanted effects, i.e. excessive noise, may appear in the correlogram.

General frequency-domain deconvolution theory applied to CC

The time-domain deconvolution method used in CC is a special case of the general principle, which is most easily stated in the Fourier domain.

For some forms of CC it is more natural to perform calculations in the Fourier domain. For example: multiplex chromatography used by Phillips [14], where non-PRBS-based pseudo random injection sequences are used, and single-sequence correlation chromatography, introduced by Louwerse et al. [15], which is partly PRBS-based.

The convolution of impulse response h_{chrom} and some arbitrary injection pattern x can, according to the convolution theorem, be described in the Fourier domain as the product of the two signals: (capitals represent the complex frequency-domain signal)

$$Y_{\text{cc}} = H_{\text{chrom}} \cdot X \quad (19)$$

where Y_{cc} , H_{chrom} and X have real and imaginary parts. At this point it is important to realize that, in the absence of noise, by performing this multiplication, frequencies with zero amplitude in either H_{chrom} or X also have zero intensity in the detector signal Y_{cc} . The convoluted time-domain signal (the detector signal) can be found using an inverse Fourier transformation

$$y_{\text{cc}} = \text{IFT}[Y_{\text{cc}}] = \text{IFT}[H_{\text{chrom}} \cdot X] \quad (20)$$

Deconvolution of h_{chrom} from y_{cc} is performed in the Fourier domain as a complex division by X :

$$h_{\text{chrom}} = \text{IFT}[Y_{\text{cc}}/X] \quad (21)$$

A complex division is carried out by multiplication of both sides of the quotient by the complex conjugate of the denominator, causing the denominator to become a real number.

$$h_{\text{chrom}} = \text{IFT}[Y_{\text{cc}} \cdot X^*/X \cdot X^*] \quad (22)$$

Since multiplication with a complex conjugate in the frequency domain is equal to a correlation operation in the time domain

$$h_{\text{chrom}} = \text{IFT}[R_{y_{\text{cc}},x}/G_{x,x}] \quad (23)$$

where $R_{y_{\text{cc}},x}$ is the Fourier transform of $r(y_{\text{cc}}, x)$, the cross-correlation function of y_{cc} and x . The Fourier transform of $r(x, x)$, the autocorrelation function of x , is equal to the power spectrum $G_{x,x}$ of the signal x . For the special case that x is a PRBS-based injection signal with one point per cp $r(x, x)$ is equal to $\{(n+1)/4\}[2\Delta+1]$ in ac-

cordance with Eqn. 7 and the discussion following it. Then

$$h_{\text{chrom}} = a + \text{IFT}[b^{-1} \cdot Y_{\text{cc}} \cdot X^*] \quad (24)$$

where a is a constant representing the offset in the deconvolugram and b is the Fourier transform of the delta function, a horizontal line at offset b in the Fourier domain. Equation 24 is the Fourier-domain analogue of Eqns. 3 and 4 for this special case. When this deconvolution method is used the real impulse response h_{chrom} is calculated instead of the broadened correlogram h_{cc} . Compared to the normal chromatogram resulting from a single injection, the broadening by the injection width is eliminated. The virtual injection is a Kronecker delta function, even when more points per cp are used.

There are potential problems involved with this method. A first problem occurs when the detector signal contains noise, which is very likely. In that case, high-frequency noise may be amplified. This effect is beyond the scope of the present investigation. A general consideration is that the gain in signal-to-noise ratio achieved with CC may be sacrificed for a gain in resolution. The balance between these effects is a subject for future research. A second problem is that the power spectrum $G_{x,x}$ may contain near-zero or even zero values. When this happens in the frequency range where noise contributions are predominating, a filtering operation can be readily carried out. However, when it occurs in the frequency range which contains analytical information a major problem is at hand [15]. This problem could be dealt with by multiplying both the numerator and the denominator of the quotient with a function which has zero values at the same frequencies as $G_{x,x}$ and defining the quotient of two zero's to be zero. Another method is to replace extreme quotient values caused by very small power spectrum values by the average of two neighbouring points. It is beyond doubt that such manipulations will limit the analytical value of the results unless one knows exactly what the effects on the analytical signals will be. If possible it is better to use an injection pattern with a power spectrum without zero values (white noise characteristics). It is interesting to pay some at-

tention to the PRBS-based injection pattern with more points per cp. Following Eqn. 21 the frequency-domain deconvolution can essentially be written as

$$h_{\text{chrom}} = \text{IFT}[Y_{\text{cc}}/P_i] = \text{IFT}[Y_{\text{cc}}/(P_k \cdot B_w)] \quad (25)$$

B_w is the source of division problems. The discrete Fourier transform of b_w can be written [16] as

$$B_{w,u} = \sum_{k=0}^{w_1-1} \exp[-i \cdot 2 \cdot \pi \cdot u \cdot k/g],$$

$$u = 0 \dots g - 1 \quad (26)$$

where $B_{w,u}$ is the value of the u -th point in the frequency domain, $i^2 = -1$ and w_1 is the number of points equal to "1" in b_w . Equation 26 can be expanded in sine and cosine terms:

$$B_{w,u} = \sum_{k=0}^{w_1-1} \cos[2 \cdot \pi \cdot u \cdot k/g]$$

$$- i \sum_{k=0}^{w_1-1} \sin[2 \cdot \pi \cdot u \cdot k/g] \quad (27)$$

For all points u of B_w for which the condition holds that

$$u \cdot w_1 = g \cdot n \quad (28)$$

where n is a whole number. The cosine and sine terms in Eqn. 27 represent the sum of equidistantly sampled values of respectively the cosine and sine function over one period ($2 \cdot \pi$). As a consequence the sum of these sampled points is zero for both the real and the imaginary part, so $B_{w,u} = 0$ and the division of Eqn. 26 cannot be carried out. Unfortunately this is always so when a PRBS-based injection pattern p_i is used with more points per cp, then $w_1 = w$. Zero values may also occur in the frequency-domain representation of a duty-cycle injection signal when the number of points representing the actual injection time w_1 answers to the condition in Eqn. 28. This difficulty may be considered as the Fourier method analogue of the time-domain matrix inversion problem. Of course Y_{cc} should have zero values at the same places as B_w since $Y_{\text{cc}} = H_{\text{chrom}} \cdot P_i$ and P_i equals $P_k \cdot B_w$. However, when the actual injection profile differs from the ideal

one or the measurement is disturbed by noise, the zero-crossings may differ and the problem cannot be resolved straightforwardly. In practice the number of digits used in the calculation will also contribute to the problem. It should be emphasized that these problems may be circumvented by the methods mentioned before.

It is interesting to compare this method with the deconvolution method in the time domain proposed recently by Mulder et al. [10] (Eqn. 12). When this equation is combined with Eqn. 4 and translated to the frequency domain it becomes

$$h_{\text{cc}} = \text{IFT}[Y_{\text{cc}} \cdot P_m^*] = \text{IFT}[H_{\text{chrom}} \cdot P_i \cdot P_m^*] \quad (29)$$

where P_m^* is the complex conjugate of P_m , the Fourier transformed deconvolution signal used in Eqn. 13. According to Eqn. 7 we may write

$$h_{\text{cc}} = \text{IFT}[H_{\text{chrom}} \cdot P_k \cdot B_w \cdot P_m^*] \quad (30)$$

We know already from the time domain that $p_k \otimes p_m = \Delta$, and $\text{FT}[\Delta] = 1$, so

$$h_{\text{cc}} = \text{IFT}[H_{\text{chrom}} \cdot B_w \cdot 1] = \text{IFT}[H_{\text{chrom}} \cdot B_w]$$

$$= h_{\text{chrom}} \star b_w \quad (31)$$

So using p_m as a deconvolution signal implies CC is used in the signal-enhancing mode while maintaining the resolution achieved with a single injection of a width equal to one cp. On the other hand the problems involving division by zero will not occur.

Consequences of using non-PRBS injection signals

So far we have more or less assumed the injection pattern to be PRBS-based, that means it can be described by a simple relation in which the values of successive PRBS bits are multiplied by some factor, yielding a concentration y-axis. Even an injection pattern resulting from a convolution of the PRBS with some clearly defined finite function is not problematic, it just results in a virtual injection which is the convolution of the basic form and this additional function. Of course this would be visible in the correlogram but apart from a change in peak shape no serious errors would result from the correlation process. When a real injection pattern is used which cannot be linearly related to a PRBS the correlation method

in the time domain utilizing the reported deconvolution signals will result in ghost peaks and/or correlation noise. Seen from the CC point of view any deviation from the ideal PRBS-based shape is an injection error. Injection errors may be decomposed into time-shifted and/or mirror-imaged versions of the basic PRBS shape. When these error parts of the injection profile are correlated with a conventional deconvolution signal the result is a ghost peak at some position along the time axis in the virtual injection. To solve the problem either the injection should be improved and the normal correlation method can be used or the exact profile of the injection must be known to the user and the calculation has to be performed in the Fourier domain. In the latter case the following deconvolution method must be used. When the detector signal is $Y = X_{\text{real}} \cdot H_{\text{chrom}}$, the impulse response h_{chrom} should be calculated by dividing the Fourier transformed detector signal by the Fourier transform of the actual input signal:

$$h_{\text{chrom}} = \text{IFT}[Y/X_{\text{real}}] \quad (32)$$

Depending on the actual shape of the input pattern it may be necessary to apply some windowing method in the Fourier domain to suppress high-frequency noise. When this method is used it is always necessary to pay special attention to the Fourier transform of the input pattern or its power spectrum in view of division-by-zero problems.

MODELS AND CORRECTION METHODS

The main problem in the application of ECM-CC are the ghost peaks. They result from a non-ideal injection pattern combined with a deconvolution procedure based on an ideal pattern. Several methods will be discussed that either do not assume an ideal injection pattern or force the system to apply an ideal injection pattern. All methods make use of the formalism established above.

Modelling of the injection pattern in EMC-CC

The previous discussion indicates the necessity to know the shape of the actual injection profile.

This may be acquired by making a sufficiently accurate model of the modulation process and calculating it. In our first paper on ECM injection in CC [1] we found the time-dependent behaviour during the charge build-up on the working electrode in combination with the half-wave potential of the sample component to be the factors responsible in the generation process of ghost peaks. To be able to calculate the injection profile the model found in our previous paper has to be more accurate.

When we assume the working electrode to be infinitely small, the system to be describable by Nernst law and chemical reaction equilibria to be reached instantaneously after a potential change then

$$E_t = E_{1/2} + (R \cdot T/n \cdot F) \cdot \ln\{c_t^{\text{ox}}/c_t^{\text{red}}\} \quad (33)$$

where $E_{1/2}$ is the half-wave potential of a sample compound, E_t is the working electrode potential at time t and c_t^{ox} and c_t^{red} are respectively the concentrations of the oxidized and reduced form of the compound at time t . This equation can be written as

$$c_t^{\text{ox}} = c_t^{\text{red}} \cdot \exp[n_f \cdot (E_t - E_{1/2})] \quad (34)$$

where $n_f = n \cdot F/R \cdot T$. The total concentration is $c_0 = c_t^{\text{red}} + c_t^{\text{ox}}$. Assuming a constant sample concentration results in

$$c_t^{\text{ox}} = c_0 / \{1 + \exp[n_f \cdot (E_t - E_{1/2})]\} \quad (35)$$

E_t can be described as the convolution of the potential control signal $p_{e,t}$ supplied by the computer and the instrument response function $h_{\text{cell},t}$ of the potentiostat–electrochemical cell combination.

$$E_t = p_{e,t} \star h_{\text{cell},t} \quad (36)$$

The expression for the injection profile becomes $x_{\text{real},t} = c_0$

$$/ \left\{ 1 + \exp \left[n_f \cdot \left\{ (p_{e,t} \star h_{\text{cell},t}) - E_{1/2} \right\} \right] \right\} \quad (37)$$

As was found in our previous paper the instrument function can be described best by the sum of two exponential terms:

$$h_{\text{cell},t} = A_1 \cdot \exp[-t/\tau_1] + A_2 \cdot \exp[-t/\tau_2] \quad (38)$$

The control signal supplied by the computer $p_{e,t}$ is a PRBS-based signal with specific values for the upper and lower potential levels (E_{upper} and E_{lower}) and is related to $p_{n,t}$, the normal PRBS-based injection pattern:

$$p_{e,t} = p_{n,t} \cdot E_{\text{upper}} - (p_{n,t} - 1) \cdot E_{\text{lower}} \quad (39)$$

Now all terms in Eqn. 37 are known or can be measured and $x_{\text{real},t}$ can be calculated. However, one should note that $E_{1/2}$, A_1 , τ_1 , A_2 and τ_2 depend upon the specific experimental conditions. This implies that for each change in these conditions all parameters have to be determined. Furthermore the model might not be entirely correct which means the theoretical description should be expanded and more parameters may be involved.

Virtually speeding up the modulator

The answer to all correlation-related problems involved in using an electrochemical concentration modulator in CC is to use a cell with a fast response to changes in the control signal. When the time constant is zero the ghost peak problem would be solved. Therefore the selection of the fastest modulator available and “fast” experimental conditions should have priority over the use of error correction or prevention techniques. A working electrode that combines a relatively small electrode surface with a coulometric characteristic, optimally placed reference and counter electrodes and highly viscous eluents with high salt concentrations should be used. When this approach is not sufficient the modulator can be speeded up virtually. The speed of the charge build-up on the electrode surface is governed by the time constants of the cell. The time to reach a certain potential is, however, also determined by the value of the control potential, applied by the computer to the potentiostat adder circuit. By not simply applying a PRBS-based control signal but by anticipating on the cell response function h_{cell} it is possible to force the actual working electrode potential to follow the desired sharp-edged PRBS-based shape. A potentiostat can be equipped with a build-in feedback loop circuitry, which compensates automatically. It is however known that these circuits can easily oscillate [17].

Therefore it seems wiser to calculate or experimentally determine the optimal control signal. Using this control signal does not alter the time constants of the cell but virtually speeds up the electrode potential changes. Since Eqn. 36 shows the relationship between the working electrode potential, the cell response function and the applied control signal, it is easy to derive a relation for the theoretical shape of the control signal necessary to obtain a perfect PRBS-shaped electrode potential:

$$x_{\text{control}} = \text{IFT}[P_e/H_{\text{cell}}] \quad (40)$$

where P_e is the Fourier transform of the desired PRBS-shaped signal and H_{cell} is the Fourier transform of the cell response function.

Deconvolution with the measured injection profile

Laborious determinations of time constants and calculation of the injection profile can be avoided by performing a calibration measurement. There are three possible ways to do this. First, a monitoring detector can be positioned between the modulator and the column and the in- and output can be measured simultaneously in one run (Fig. 3a). The measured input signal $x_{\text{meas,pre-column}}$ will be the injection profile convoluted with the broadening function of the connective tubing $h_{\text{tubing},1}$ and the instrument function of the detector $h_{\text{det},1}$:

$$x_{\text{meas,pre-column}} = x_{\text{real}} \star h_{\text{tubing},1} \star h_{\text{det},1} \quad (41)$$

This signal can be used in Eqn. 28 after a transformation to the frequency domain. It should be realized that the same bandspreading function is contained by the impulse response h_{chrom} , since

$$h_{\text{chrom}} = h_{\text{tubing},1} \star h_{\text{det},1} \star h'_{\text{chrom}} \star h_{\text{tubing},2} \star h_{\text{tubing},3} \star h_{\text{det},2} \quad (42)$$

where h'_{chrom} is the impulse response of the chromatographic system without any extra-column broadening contributions, $h_{\text{tubing},2}$ is the broadening caused by the tubing between the first detector and the column, $h_{\text{tubing},3}$ the broadening caused by the tubing between the column and the second detector, and $h_{\text{det},2}$ is the instrument

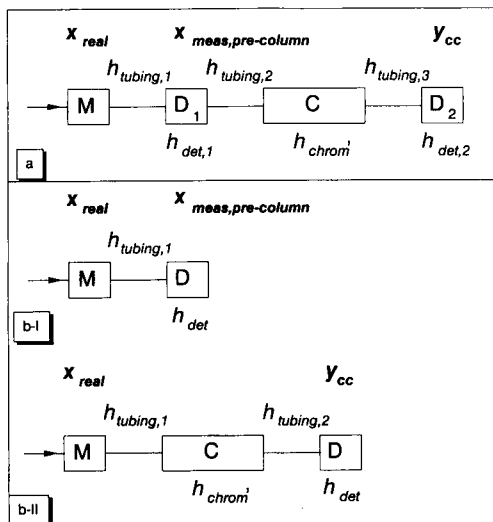


Fig. 3. Deconvolution with a measured input profile. Experimental set-up, signals and broadening effects. (a) One-run measurement with two detectors; (b-I,II) two-run measurement with one detector; M = modulator cell; C = column; D = detector. See text for further explanations.

function of the detector at the column outlet. The equation for the detector signal becomes

$$y_{cc} = x_{real} \star h_{tubing,1} \star h_{det,1} \star h_{tubing,2} \star h'_{chrom} \star h_{tubing,3} \star h_{det,2} \quad (43)$$

The word “deconvolugram” will be used for results obtained by a deconvolution procedure which results in something else than the normal impulse response h_{chrom} of the chromatographic system. Now the deconvolugram r_d can be calculated, using

$$\begin{aligned} r_d &= \text{IFT} [Y_{cc} / X_{meas,pre-column}] \\ &= \text{IFT} [X_{real} \cdot H_{tubing,1} \cdot H_{det,1} \cdot H_{tubing,2} \cdot H'_{chrom} \\ &\quad \cdot H_{tubing,3} \cdot H_{det,2} / (X_{real} \cdot H_{tubing,1} \cdot H_{det,1})] \\ &= \text{IFT} [H'_{chrom} \cdot H_{tubing,2} \cdot H_{tubing,3} \cdot H_{det,2}] \quad (44) \end{aligned}$$

So the deconvoluted signal will contain a broadening contribution caused by the tubing and the second detector. The injection broadening is nevertheless eliminated. A second method is to perform two runs. In the first run the detector (only

one is used) is connected directly to the modulator cell (see Fig. 3bI). The signal measured is $x_{meas,pre-column}$ which is composed of

$$X_{meas,pre-column} = X_{real} \cdot H_{tubing,1} \cdot H_{det} \quad (45)$$

$H_{tubing,1}$ is caused by the connective tubing between the modulator and the detector. In the next run the column is connected between the modulator and the detector. There is some additional broadening due to the connection between the column and the detector (see Fig. 3bII), causing $H_{tubing,2}$. The measured detector signal can be described in the Fourier domain as

$$Y_{cc} = X_{real} \cdot H_{tubing,1} \cdot H'_{chrom} \cdot H_{tubing,2} \cdot H_{det} \quad (46)$$

So the deconvolugram r_d will look like

$$\begin{aligned} r_d &= \text{IFT} [X_{real} \cdot H_{tubing,1} \cdot H'_{chrom} \cdot H_{tubing,2} \cdot H_{det} \\ &\quad / (X_{real} \cdot H_{tubing,1} \cdot H_{det})] \\ &= \text{IFT} [H'_{chrom} \cdot H_{tubing,2}] \quad (47) \end{aligned}$$

As a result the deconvolution operation will also remove broadening effects due to the detector instrument function, while the only broadening left to consider is the one caused by the tubing connecting the modulator with the column. A third possibility is to measure the detector signal in the usual system, behind the column (Fig. 3bII), and use a special calibration compound which elutes very fast under the experimental conditions used for the chromatographic determination. The measured calibration signal $x_{meas,post-column}$ can be described by

$$x_{meas,post-column} = x_{real} \star h_{chrom,cal} \quad (48)$$

where $h_{chrom,cal}$ is the impulse response of the chromatographic system to a spike-shaped “injection” of the calibration compound. The broadening contributions can be summed in

$$h_{extra-column} = h_{tubing,1} \star h_{tubing,2} \star h_{det}$$

Since

$$h_{chrom,cal} = h'_{chrom,cal,t=0} \star h_{extra-column} \star \Delta_{t,cal} \quad (49)$$

where $h'_{chrom,cal,t=0}$ is the impulse response of the chromatographic system for the calibration compound, corrected for broadening $h_{extra-column}$ in

the parts of the system other than the column and shifted in time to $t = 0$.

$\Delta_{t,\text{cal}}$ is a Kronecker delta function shifted to the retention time of the calibration compound.

$$x_{\text{meas,post-column}} = x_{\text{real}} \star h'_{\text{chrom,cal},t=0} \star h_{\text{extra-column}} \star \Delta_{t,\text{cal}} \quad (50)$$

The detector signal for the sample solution can be described as

$$y_{\text{cc}} = x_{\text{real}} \star h'_{\text{chrom}} \star h_{\text{extra-column}} \quad (51)$$

Using $x_{\text{meas,post-column}}$ as a deconvolution signal in the Fourier domain results in a deconvolugram r_{d} :

$$\begin{aligned} r_{\text{d}} &= \text{IFT} \left[Y_{\text{cc}} / X_{\text{meas,post-column}} \right] \\ &= \text{IFT} \left\{ X_{\text{real}} \cdot H'_{\text{chrom}} \cdot H_{\text{extra-column}} / \left[X_{\text{real}} \cdot H_{\text{extra-column}} \cdot H'_{\text{chrom,cal},t=0} \cdot \text{FT}(\Delta_{t,\text{cal}}) \right] \right\} \\ &= \text{IFT} \left\{ H'_{\text{chrom}} / \left[H'_{\text{chrom,cal},t=0} \cdot \text{FT}(\Delta_{t,\text{cal}}) \right] \right\} \\ &= \text{IFT} \left\{ H'_{\text{chrom}} \cdot \text{FT}(\Delta_{-t,\text{cal}}) / \left[H_{\text{chrom,cal},t=0} \cdot \text{FT}(\Delta_{t,\text{cal}}) \cdot \text{FT}(\Delta_{-t,\text{cal}}) \right] \right\} \\ &= \text{IFT} \left[H'_{\text{chrom}} \cdot \text{FT}(\Delta_{-t,\text{cal}}) / (H_{\text{chrom,cal},t=0}) \right] \quad (52) \end{aligned}$$

Where Δ_{-t} is a Kronecker delta function shifted to minus the retention time of the calibration compound. As a result the deconvolugram is a time-shifted version of the normal correlogram, in which all extra-column broadening effects are eliminated. The effect on the peak shapes will depend on the precise shape of $h_{\text{chrom,cal},t=0}$.

CC's intrinsic ghost peak correction method

Mulder et al. [7] have developed a theoretical base for a method to correct for non-complementary ghost peaks which are the most intolerable for short-term effects. As was illustrated in part one of this paper [1], an asymmetrically disturbed injection pattern can be decomposed into an ideal part with a lower amplitude, a so-called complementary part and a non-complementary part. Cross-correlating the erroneous pattern with p_m results in a virtual injection with ghost peaks. The individual ghost peaks can be traced directly to the complementary and non-complementary parts

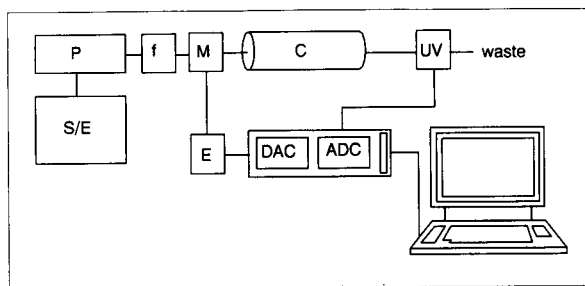


Fig. 4. Experimental set-up for time-domain correlation and Fourier-domain deconvolution experiments; the column was left out during input profile measurements. S/E = sample/eluent solution; P = pump; f = solvent filter; M = modulation cell; C = column; UV = detector; E = potentiostat; DAC = digital-to-analog interface; ADC = analog-to-digital interface.

of the injection pattern. Mulder et al. [7] showed that the sign of non-complementary ghost peaks relative to the real peak sign changed when a bit-inverted PRBS-based injection control signal is used. This means we can correct for the presence of non-complementary ghost peaks by performing two CC runs, one with a normal control signal and one with an “inverted” control signal and by then subtracting the “inverted” from the normal correlogram. It does not matter whether the signals are first subtracted and then correlated or are first correlated and then subtracted. The former method is faster, since only one cross correlation has to be performed. The latter method gives the separate correlograms and hence gives more insight in the quality of the injection.

EXPERIMENTAL

The basic experimental set-up was already described in detail in part one of this paper. Figure 4 shows the set-up used in the present investigations. For the injection pattern measurements the UV detector (Waters Model 441, 254 nm) was directly connected to the modulator cell (ESA, Model 5020 guard cell). A Kratos Model SF-400 pump, equipped with a liquid pulse damper, supplied a constant flow of 0.60 ml min^{-1} . A $20 \text{ cm} \times 3 \text{ mm}$ i.d. column was used, packed with $5\text{-}\mu\text{m}$ Zorbax ODS particles. Mixtures of 20:80

and 65:35 (v/v) of methanol (Merck, p.a.) and aqueous (Baker, LC-reagent) phosphate (Merck, p.a.) buffer pH 3.5 were used as an eluent. Hydroquinone (Gold Label, 99 + %; Aldrich) was used as a test compound.

Two computer programs were developed in our laboratory to handle the data acquisition and control tasks on an Acorn micro computer, Model BBC Master, equipped with an intelligent ADC/DAC interface (Cambridge Electronic Design, Model 1401). The DAC interface was connected to the external input of a PAR Model 174A potentiostat. The potentiostat applied the control signals to the modulator cell. In the potential control signal generation program pulse shapes can be defined in three modes. In the first mode the "injection" or "non-injection" potential levels are stored without modification. For the other modes the pulse shape for ni-cp's and i-cp's can be defined with the requested resolution (points per cp). We used 20 points per cp. In the second mode the contents of all cp's are substituted by the defined pulse shapes for i-cp's or ni-cp's. In the third mode only the first of a train of successive i-cp's or ni-cp's is substituted by the appropriate defined pulse shape. The fol-

lowing cp's in the train preserve their original shape. Apart from this, the program generates the PRBS using a default or user-defined generation mask and generates the bit-inverted version of the injection pattern. The data acquisition and control program uses data generated by the previous program, to control the electrode potential and sample the data from the detector. The measured signal is then transferred from the BBC-Econet by means of a serial port to a HP 1000 mini-computer where it can be converted to the appropriate data format and used for further processing. Simulation studies were performed on a Laser 386SX personal computer with a 80387SX co-processor. The programs running on the PC were developed in Turbo-C 2.0 (Borland).

RESULTS AND DISCUSSION

An overview of solutions to the ghost peak problem

Table 1 lists possible correction methods and requirements. The methods can be classed as potential resolution-enhancing methods (i–iii) where the calculations have to be performed in

TABLE 1
Overview of solutions

No.	Basic method	Resolution enhancement ^a	Calculation type ^b	Measurements required	Extra step
i	Measured input pre-column	y	f	Actual input pattern in the same run or in pre-run	–
ii	Measured input post-column	y	f	Calibration run with fast eluting test compound	Correction for time shift
iii	Calculated input profile	y	f	Cell response function, exact $E_{1/2}$	Optimization
iv	CC's intrinsic correction methods	n	t	Run with bit-inverted injection pattern	Subtraction of correlograms
v	Adjustment of potential control signal	n	t	Cell response function	Optimization

^a Resolution enhancement caused by the deconvolution method; y = yes, n = no. ^b f = frequency domain calculation; t = time domain calculation.

the frequency domain or as the more conventional methods that are applicable in the time domain but could also be used in the frequency domain (iv–v). Methods (i) and (ii) require measuring of the actual input signal (i) or a calibration signal (ii). Method (iv) requires measurement of an extra detection sequence while using a bit-inverted injection sequence. Methods (iii) and (v) require knowledge of the response function of the modulator cell for the experimental conditions used.

Deconvolution with the actual input signal

In the first publication concerning CC, Izawa [18] already mentioned the monitoring of the input signal as a security measurement. In the same paper a picture is shown of a gas chromatographic CC system with a measurement system for the actual input. However, in the subsequent time-domain correlation the input control signal is used instead. In their next paper Izawa et al. [19] show the same picture, but the actual input signal is not mentioned at all. In our experiments the measurement of the actual input signal in an LC-CC experiment in the same run as the detec-

tor signal, followed by a deconvolution according to Eqn. 44, was not feasible since a non-destructive detector capable of withstanding the high pressures before the column was not available. To measure the input signal (Fig. 5a) used for the deconvolution, the UV detector was directly connected to the modulator cell. Figure 5b shows the detector signal when the column was connected. A 10^{-5} mol l^{-1} hydroquinone solution in methanol–phosphate buffer pH 3.5 (65:35, v/v) was used as sample/eluent. The modulation interval applied was 0.7/–0.3 V and a 63-cp injection sequence was used. Cp duration was 10 s and 5 data points were sampled in one cp. All time-domain deconvolutions (cross-correlations) are performed with the p_m type of signal, as was shown in Fig. 1f, so Eqn. 12 is relevant for the virtual injection.

A cross-correlation operation on the signal measured directly after the modulation cell results in the correlogram in Fig. 5c. Prominent are the f_3 ghost peak at point 293 (58 cp from the real peak) and f_5 at point 269 (53 cp from the real peak). The same operation on the signal measured with a column in the system yields the

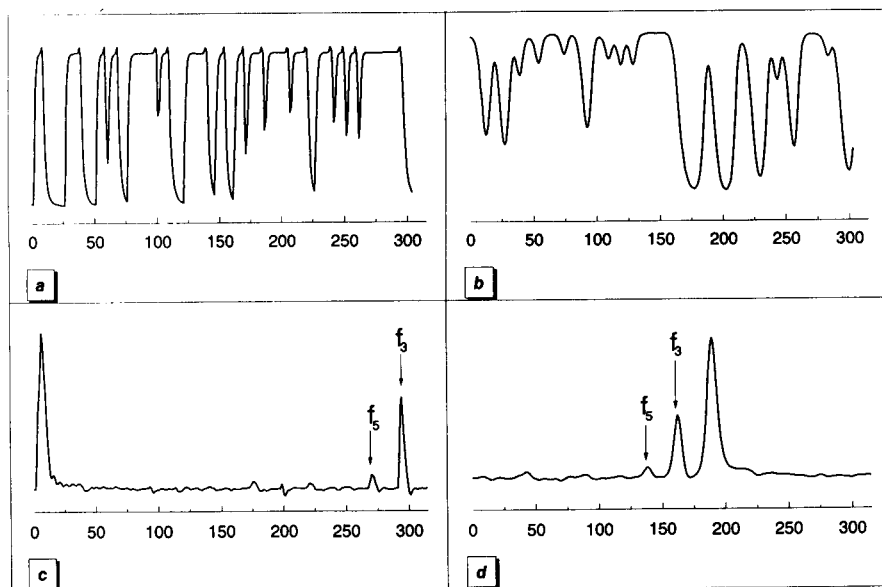


Fig. 5. (a) Measured injection profile (with experimental set-up of Fig. 3b-I); (b) measured detector signal (with experimental set-up of Fig. 3b-II) for the same sample as was used in (a); (c) correlogram of (a); (d) correlogram of (b); x-axis: data points; y-axis: UV absorbance. See text for further explanations.

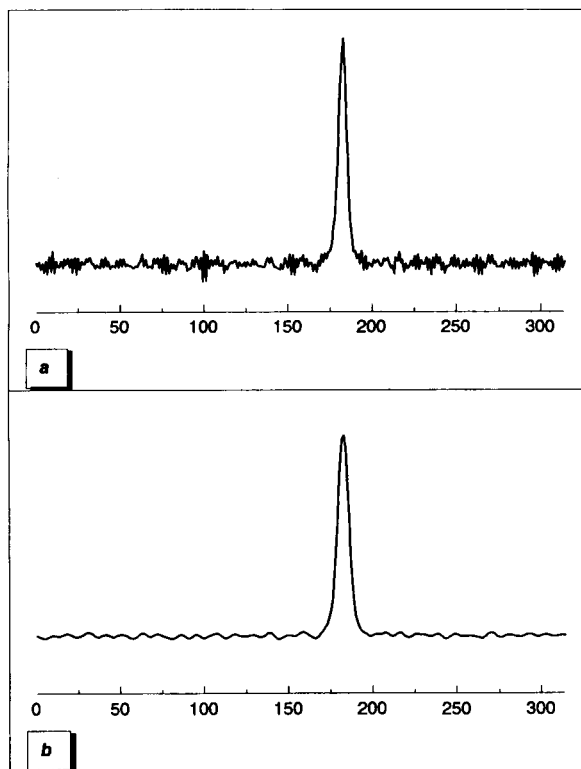


Fig. 6. Deconvolugrams obtained by using the signal in Fig. 5a to deconvolute the signal in Fig. 5b. (a) Unfiltered; (b) filtered with a hamming window.

correlogram in Fig. 5d. Here too, the f_3 ghost peak at point 162 in the correlogram (58 or -5 cp from the real peak) and f_5 at point 138 (53 or -10 cp from the real peak) are the most pronounced. Both ghost peaks are of the non-complementary type. Furthermore, the baseline is very uneven which may indicate the presence of some other non-stationarity in the system. When the measured input signal $x_{\text{meas,pre-column}}$ is used to deconvolute the detector signal according to eqn. 47 and no additional filtering is used a noisy deconvolugram emerges (Fig. 6a). Application of a low-pass filtering hamming window (to reduce sidelobes) with a cut-off frequency of 0.09 Hz (sample frequency is 0.5 Hz) gives a more reasonable picture (Fig. 6b). It should be emphasized that this type of filtering also results in deformation and broadening of the peak. The cut-off frequency is chosen from the power spectrum of the detector signal. These correlograms can be

compared with the correlogram in Fig. 5d which was calculated using a time-domain cross-correlation with a p_m type of deconvolution signal. The baseline of the deconvolugram is still rather uneven but the main ghost peaks are gone and the real peak is sharpened. To give a global indication of the influence of the different methods on the peak width the full width at half height (fwhh) was measured. The fwhh is 10 s in the unfiltered signal and 16 s in the filtered signal while the fwhh in the conventional correlogram is 19 s. Probably, the diaphragm pulse dampener in the pump was responsible for the baseline perturbation. The pressure may have been too low in the columnless experiment to obtain a good pulse damping performance.

This method is only applicable when the ghost peak generating injection error is not compound-specific or, in other words, when compounds are analyzed with the same modulation characteristics.

Deconvolution with a calibration signal

Sharpening of a broadened peak by a division in the Fourier domain by a somewhat less broadened peak under the condition that both peaks can be described with the same basic equation is known in the literature [20]. This deconvolution method can only be applied without distortion of the analytical signal when the broadening effect can be described by a convolution with a broadening function [21]. The broadening can then be eliminated by a deconvolution with this broadening function. Therefore deconvolution of the detector signal for a real sample by the separately recorded signal from a fast-eluting calibration compound is expected to result in a sharpened but undistorted peak shape. The retention times of the deconvoluted peaks in the deconvolugram are relative to the retention time of the calibration compound. Simulations were carried out to demonstrate the effect of this approach. The impulse response of a chromatographic system was simulated for three "compounds", one calibration compound and two sample components. Gaussian peak shapes were assumed. Table 2 lists the parameters used and Fig. 7a1–c1 shows the simulated impulse responses for the calibration

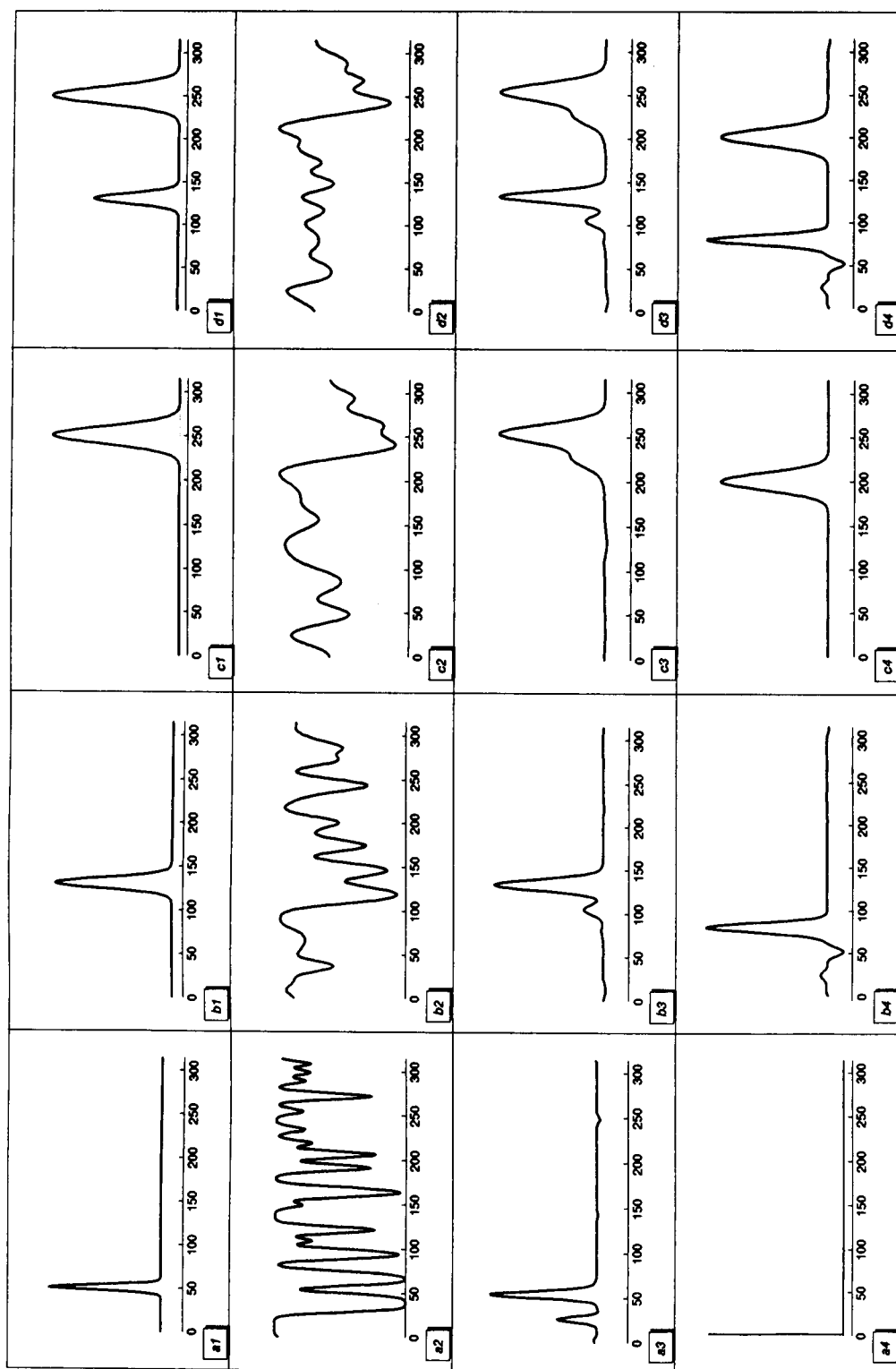


Fig. 7. Simulation results of calibration run deconvolution method. (a1) Calibration compound peak; (b1) component 1; (c1) component 2; (d1) mixture of component 1 and 2; (a2–d2) corresponding detector signals in a CC experiment; (a3–d3) time-domain correlograms; (a4–d4) deconvoluted signals when the signal in (a2) is used as the deconvolution signal. For further details see text.

TABLE 2

Component and peak parameters

Component	t_{ret} (points)	σ (points)	$E_{1/2}$ (V)
Calibration	50	3	0.1
1	130	6	0.0
2	250	10	0.1

compound and sample component 1 and 2. The chromatogram for the mixture is shown in Fig. 7d1. Next, using the potential response function parameters listed in Table 3 in Eqn. 38, the real potential profile for the working electrode was generated for a 63-bit PRBS-based injection signal with 5 points per cp. The corresponding injection profiles were generated from Eqn. 37. The injection profiles for the calibration compound and for component 2 are identical since the $E_{1/2}$ values are identical. Next, the corresponding detector signals were calculated by convoluting the injection profiles with the chromatograms. The results are shown in Fig. 7a2–c2. The detector signals for sample component 1 (Fig. 7b2) and component 2 (Fig. 7c2) were added, resulting in the detector signal for a two-component sample (Fig. 7d2). Conventional time-domain cross-correlation of the signals in Fig. 7a2–d2, using a p_m -type of signal, results in the correlograms in Fig. 7a3–d3.

Fig. 7a4–d4 shows the deconvolugrams when the injection profile for the calibration compound (Fig. 7a2) is used as $x_{\text{meas,post-column}}$ in Eqn. 52. The deconvolugram for the second mixture component (Fig. 7c4) is ghost peak free, while the conventional correlogram (Fig. 7c3) shows a large ghost peak, partly overlapping the real peak. The peak widths of components 1 and 2 in Fig. 7b4 and c4 are only slightly less than the original

widths but the broadening caused by the injection profile is completely compensated by the deconvolution with the equally broadened calibration signal.

Both the deconvolugram (Fig. 7b4) and the normal correlogram (Fig. 7b3) for compound 1 are disturbed. Fig. 7d4 shows the deconvolugram of the mixture. The retention time of all components is shifted as was predicted. This method is applicable in ECM-CC when the $E_{1/2}$'s of all components match and in conventional CC or other forms of modulation CC where the injection error is independent of the characteristics of the injected compound. It should be noted that the presence of noise in the signals will limit the applicability of this method even more.

Deconvolution with a calculated input profile

When the cell response function and the half-wave potential of the injected compounds are known it is possible to calculate the expected injection profile and to use this signal to deconvolute the detector signal. In our previous paper we determined the cell potential response and found it can be described as a sum of two exponential functions. Using the time constants and scale factors found in our previous investigation, which are listed in Table 4, (set 1) and Eqn. 37, we calculated the injection profile for quinone using the half-wave potential of -0.10 V. This profile and the corresponding virtual injection are shown in Fig. 8a1 and a2. For comparison Fig. 5c shows the experimental virtual injection obtained in the experiment in which the detector was directly connected to the modulator. The latter signal is somewhat broadened by the connecting tubing. It is clear that the calculated signal shows some features of the measured signal but it is not optimal. By varying the parameters for the poten-

TABLE 3

Impulse response and PRBS parameters

Modulation interval	E_{upper} (V)	0.7	E_{lower} (V)	-0.3
Potential impulse response parameters	A_1	1.0	τ_1 (s)	0.48
	A_2	0.7	τ_2 (s)	6.2
Injection sequence	Base PRBS length	63	Points per cp	5

TABLE 4

Impulse response parameters and half-wave potential values used for a deconvolution with a calculated input pattern

Set	A_1	τ_1 (s)	A_2	τ_2 (s)	$E_{1/2}$ (V)
1 (measured in part 1)	1.2	0.29	0.68	4.3	-0.1
2 (optimized)	0.98	0.73	0.61	8.6	-0.05

tial impulse response function and the value for the half-wave potential a somewhat better matching signal was obtained (Fig. 8b1 and b2). Figure 8a3–b3 shows the results from a deconvolution of

the detector signal, obtained in the system with a column, with the calculated signals. These results should in the first place be compared with the conventional correlogram in Fig. 5d. It is striking that the time constants in the response function parameters have to be doubled to reach some result. Compared to the results with the measured injection signal in Fig. 5a the quality is poor. This may be improved by the use of a better electrochemical model, incorporating the potential drop inside the electrode [22] or reaction kinetics inside the porous electrode flow channels [23]. Nevertheless, the method will always suffer from several drawbacks. As was shown in our previous paper the ghost peak pattern, and therefore the modulator response function, is different

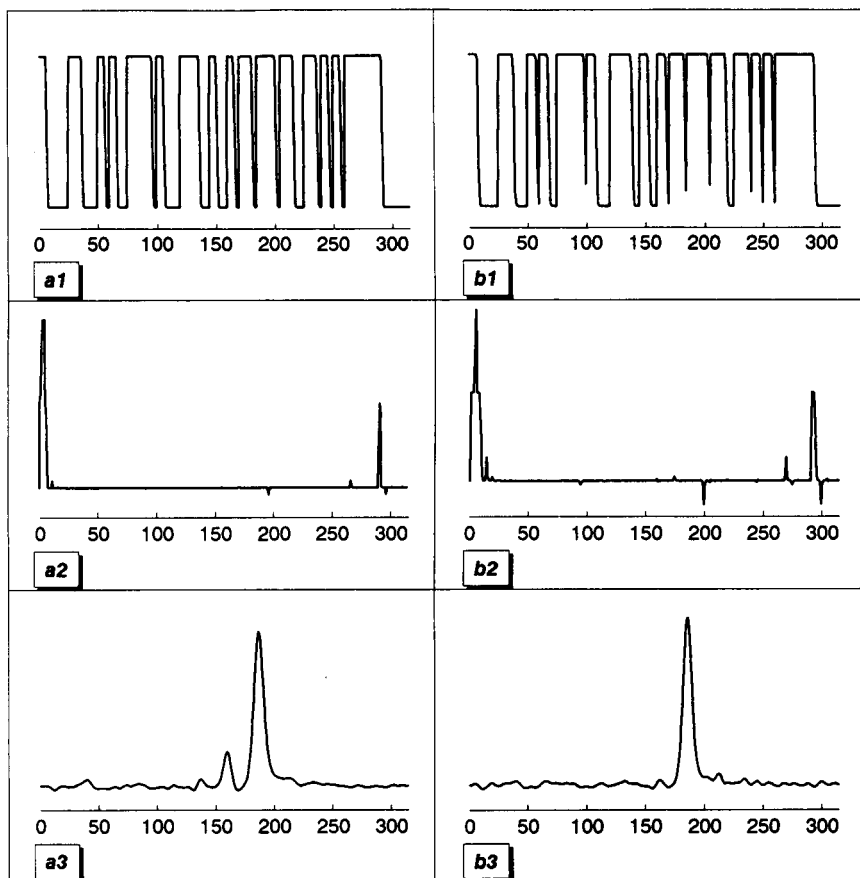


Fig. 8. Calculated injection profiles for hydroquinone using the parameters of Table 4, the first set (a1) and the second set (b1); (a2–b2) time-domain correlograms of the signals in (a1–b1); (a3–b3) deconvoluted signals of the measured detector signal in Fig. 5b when the calculated injection profiles of (a1–b1) are used as deconvolution signal.

when the concentration of the analyzed compounds changes. Secondly, when the compounds to be analyzed have differing half-wave potentials the method cannot be used. Finally, each change in composition of the mobile phase will result in a change of the cell response. Therefore frequent measurement of the cell response and recalculation of the input pattern is necessary.

Using CC's intrinsic ghost peak compensation methods

To check the feasibility of this method experiments were performed using normal and bit-inverted PRBS-based injection sequences. The experiments were carried out using a 10^{-5} mol l^{-1} hydroquinone solution and a 31-bit PRBS-based injection pattern. A 0.2/0.3 V potential modulation interval was used. The correlogram resulting from the normal injection sequence is shown as the upper trace in Fig. 9a. The lower trace represents the correlogram resulting from a bit-inverted PRBS-based injection pattern. The upper trace in Fig. 9b shows the difference between these two, while the lower trace depicts the sum signal. It is clear that the f_3 and f_5 ghost peaks have disappeared from the difference signal. However, the second-order complementary ghost peak f_7 is enlarged. This correction method, which was recognized by Mulder et al. [7], does not suffer from the limitations of the methods discussed thus far. It is independent of the number of components and their half-wave potentials.

It only requires a second experiment and thereby improves the signal-to-noise ratio since the correction procedure is in fact a signal-averaging operation. An additional advantage is that non-complementary components of the correlation noise in the baseline will also vanish. The only drawback is the magnification of complementary ghost peaks. The occurrence of this type of ghost peak on other places than next to the real peak ("broadening") indicates that the effect of an injection error stretches out over several cp's. In that case the best solution is to revise the injection system.

Adjustment of the potential control signal

Using eqn. 40 a control signal can be calculated that compensates for the response function of the charge build-up on the working electrode if there is no feed-back or non-linearity in the system. It is assumed that time behaviour does not alter in time or under differing experimental circumstances. Figure 10 shows the calculated control signal. We can, however, only approximate this signal using a digital control system. The computer controls the potential step-wise in time steps. The resolution of the potential is defined by the number of bits in the D/A converter and the potential range to cover, while the time-step size after which the potential can be changed is limited in principle only by the speed of the interface but in practice it seemed reasonable to limit the number of points in one cp to 20 points.

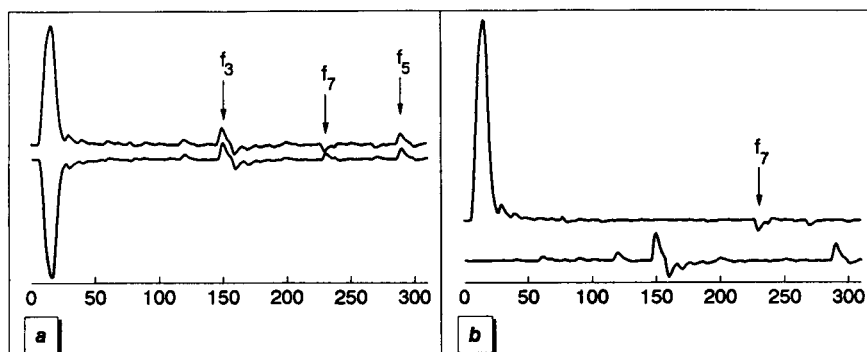


Fig. 9. (a) Upper trace: correlogram of a normal PRBS-based detector signal; lower trace: correlogram of a bit-inverted PRBS-based detector signal; (b) upper trace: difference between the correlograms in (a); lower trace: sum of the detector signals in (a). See text for further details.

First we applied a conventional 63-bit PRBS-based block shaped control signal to the potentiostat. The control signal, the resulting injection pattern and correlogram are shown in Fig. 11a, b and c. Since the purpose of these experiments was to force the ECM to supply an ideal injection pattern the normal time-domain correlation procedure with p_m as deconvolution signal was used. Next we started experimenting with a signal resembling the one we calculated in Fig. 10 with charging and discharging pulses.

Figure 12a shows the signal we used after some optimization in an ECM-CC experiment. Figure 12b and c shows the detector signal and the correlogram.

Since there was still a f_3 ghost peak visible we went one step further and applied a duty-cycle PRBS-based control signal. With this signal we intended to eliminate the influence of one cp on the other. The electrode charging and discharging process was to take place in one cp, so the begin situation in each next cp was the same as in the one before, whether or not an injection had taken place. After some experiments it was clear that the control shape shown in Fig. 13a yielded the best results. Nearly all traces of ghost peaks had vanished as can be seen in Fig. 13c. This method is independent of the half-wave potentials of the compounds to analyze. It will depend upon the experimental conditions, however, and frequent re-optimization will remain necessary. Furthermore, since a duty-cycle is used, the sample throughput is less than when the whole cp is used

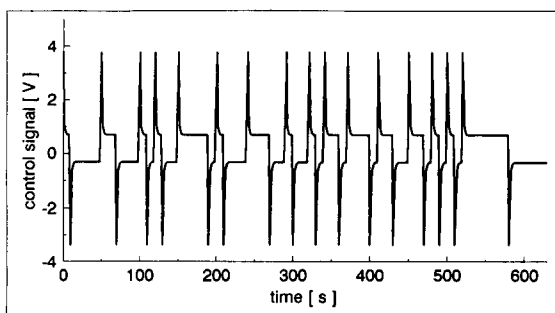


Fig. 10. Calculated potential control signal necessary to compensate for the response function of the ECM.

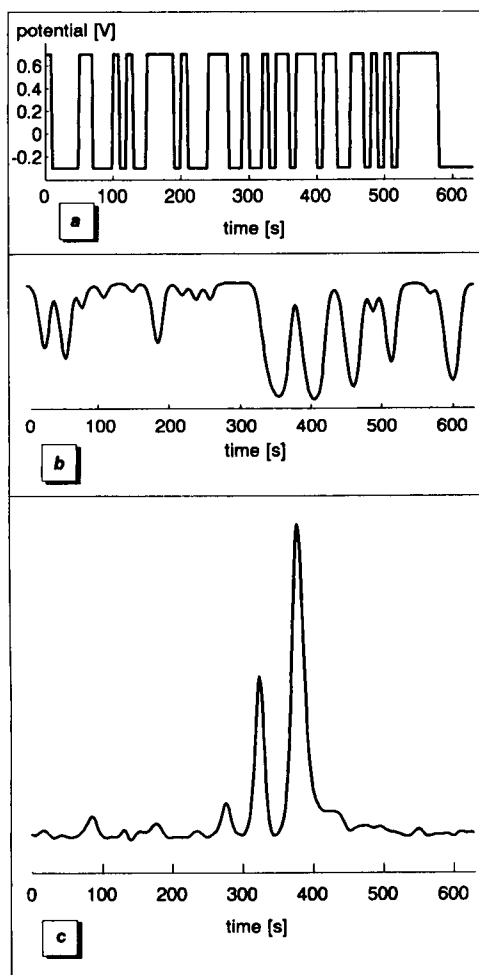


Fig. 11. (a) Block-shaped potential control signal; (b) detector signal; (c) correlogram for a 63-bit PRBS-signal-based correlation experiment using a 10^{-5} mol l^{-1} solution of hydroquinone in eluent as sample.

for the injection. As a consequence the gain in signal-to-noise ratio will be correspondingly lower.

Linearity

Only the duty-cycle control signal is relevant for analytical purposes according to Fig. 13a. For comparison the potential control signals shown in Fig. 11a and 12a were also used in a calibration experiment to check the linearity. Another purpose of the calibration experiments was to check whether the correlograms for different concentrations remain without ghost peak, since we found

in our previous work the ghost peak pattern to be dependent on the concentration. The tested concentration range of hydroquinone in the eluent was 10^{-4} to 10^{-8} mol l^{-1} . The correlograms for the duty-cycle control signal show no ghost peaks for the whole concentration range. Figure 14a shows the calibration plots on a log-log scale. Table 5 displays the least-squares data. More linearity information is gained from a linearity plot [24]. Figure 14b shows a variation on the linearity plot for the three methods. The quotient of the absorbance difference and the concentration difference for two successive concentrations in the measured range were plotted against the logarithm of the concentration difference. A per-

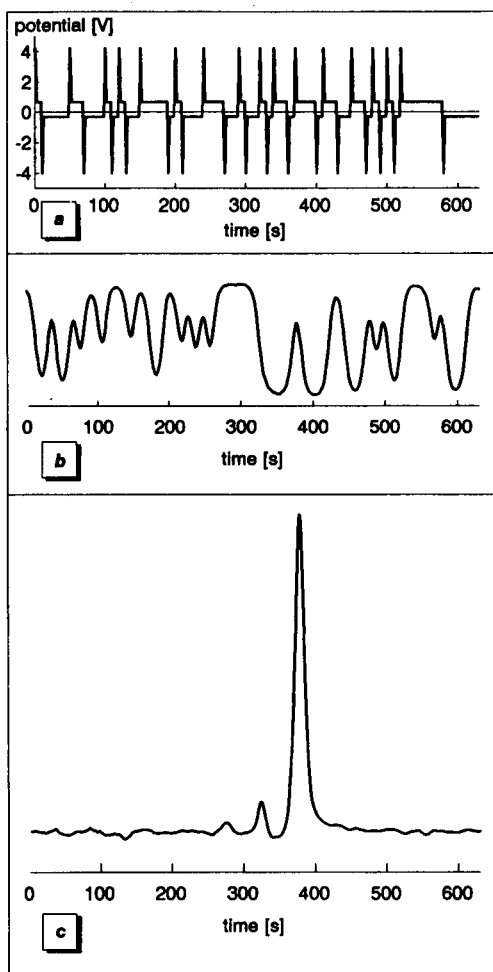


Fig. 12. (a) Adjusted potential control signal; (b) detector; (c) correlogram. Other experimental conditions as in Fig. 11.

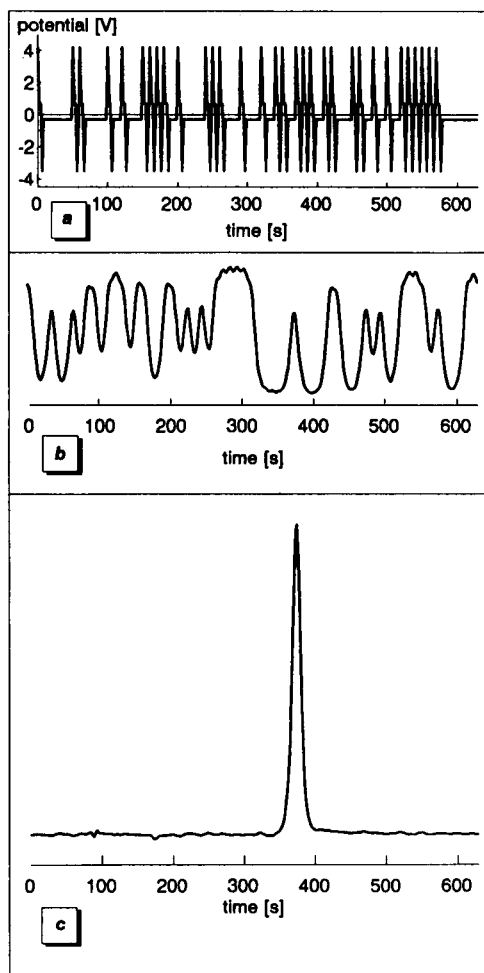


Fig. 13. (a) Duty-cycle potential control signal; (b) detector signal; (c) correlogram. Other experimental conditions as in Fig. 11.

fectly linear method would yield a horizontal line. As can be seen from Table 5 and Fig. 14b the duty-cycle method delivers agreeable results.

Conclusion

A chemical concentration modulator may be used as a selective injection device in CC. This can, however, not be done on a routine base with the modulator tested in this investigation unless some laborious precautionary measures are taken. Of all methods discussed in this paper only two are useful in standard analysis. The adjustment of the control signal can be used as a first step. The

TABLE 5

Least-squares fit data (5 observations)

Method	Constant	Slope	r^2
Normal control signal	4.21	1.1270	0.99955
Adjusted control signal	3.69	1.0010	0.99985
Duty-cycle control signal	3.52	0.9999	0.99991

intrinsic ghost peak correction method can be used when it is not possible to optimize the control signal frequently, or when persistent lower-order ghost peaks occur in the correlograms. The best solution, however, seems to select a faster modulator cell. Presently there are other cells commercially available with a better internal geometry and a smaller internal volume. The only problem is the capability to withstand the pressure regime between pump and the column. One cell in particular has been proven to yield excellent results [25]. It should be noted that a major drawback of all tested commercially available coulometric flow-through cells is the absence of a possibility to clean or renew the porous graphite working electrode. It can be recommended for future investigations to develop a

cell based on the one reported by Schieffer [26]. This cell, which is capable of withstanding the high pressures at the modulation site, can be taken apart for cleaning purposes.

Frequency-domain deconvolution can yield a higher resolution correlogram than can be obtained with the reported time-domain cross-correlations. The price to pay is a more unpredictable result and a gain of the baseline noise, requiring additional filter procedures. An optimum between resolution and noise can probably be found using modern digital filters.

The discussion about the origin of ghost peaks in using an electrochemical concentration modulator can be generalized to chemical and physical concentration modulators. The action of all chemical or physical modulators is based on the change in some physical or chemical parameter of a cell or cell constituent (i.e. temperature or potential). The change in this parameter is never instantaneous. Also, the compound will react to the modulated parameter in a compound-specific way. The combination of these two factors inevitably produces ghost peaks when the change in the parameter responsible for the modulation process is not fast enough.

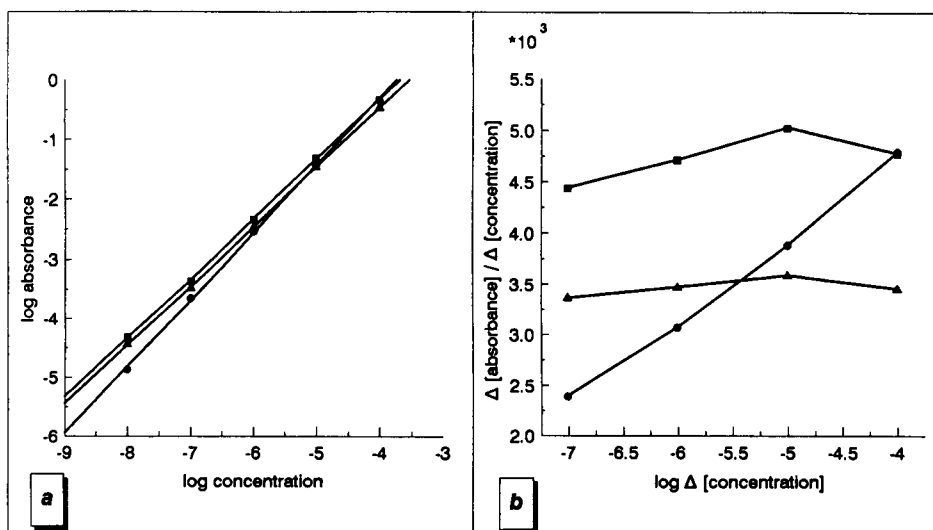


Fig. 14. (a) Log-log calibration curves for hydroquinone; a normal control signal (solid circle), an adjusted control signal (solid square) and a duty-cycle control signal (solid triangle) as in Figs. 11a, 12a and 13a were used; (b) linearity plot for the same experiments.

LIST OF SYMBOLS

a, A_1, A_2	Scaling factors		
b_w	Block function; $b_{w,i} = 1$ for $i = 0, w$; $b_{w,i} = 0$ for $i = w, (n \cdot w) - 1$	p_c	Potential control signal from computer to potentiostat
c_t^{ox}	Concentration of oxidized form at time t	p_i	Ideal injection pattern, based on an n -bit PRBS; all points in an i-cp are "1", all points in an ni-cp are "0"
c_t^{red}	Concentration of reduced form at time t	p_k	Kronecker PRBS-based sequence; each first point in an i-cp is "1", all other points are "0"
c_0	Total concentration, oxidized and reduced form	p_m	PRBS-based deconvolution signal; each first point in an i-cp is "1", each first point in an ni-cp is "-1", all other points are "0"
d_{2w}	Triangular function; baseline width $2 \cdot w$; maximum w		
$E_{1/2}$	Half-wave potential	R	Gas constant
E_t	Working electrode potential at time t	r_d	Deconvolugram, result from frequency-domain deconvolution procedure, comparable to correlogram
F	Faraday's constant		
g	Total number of points in a signal, equals $(n \cdot w)$ always	$r(x, y)$	Cross-correlation function of x and y
$G_{x,x}$	Power spectrum of signal x	$r(x_{\text{real}}, z_d)$	Virtual injection, cross-correlation between the real input pattern and a suitable deconvolution signal
h_{cc}	Correlogram, resulting from a time-domain correlation procedure	S^w	Circulant matrix with columns of cyclicly permuted b_w
$h_{\text{cell}}, h_{\text{cell},t}$	Potential impulse response to electrochemical cell	T	Absolute temperature
h_{chrom}	Impulse response of the total chromatographic system	t_{cp}	Clock period length in time units
h'_{chrom}	Idem, without the broadening contributions of tubing and detector cell volume	w	Clock period length in number of data points
$h_{\text{chrom,cal}}$	Impulse response of total chromatographic system for a calibration compound	w_1	Number of serried points in b_w of values "1"
$h'_{\text{chrom,cal},t=0}$	Idem, without broadening contributions of tubing and detector cell volume, peak maximum shifted from $t = t_{\text{ret}}$ to 0	x	Arbitrary injection signal
$h_{\text{extra-column}}$	All extra-column peak-broadening contributions	$x_{\text{meas,post-column}}$	Detector signal for a calibration compound measured behind the column; used as deconvolution signal
$h_{\text{tubing},1,2,3}$	Peak-broadening functions for connecting tubing	$x_{\text{meas,pre-column}}$	Detector signal for a calibration compound measured directly behind the modulator; used as deconvolution signal
k_w	Kronecker comb point-to-point distance w points	x_{real}	Real injection pattern
n	Number of bits in PRBS		
p_c	Conventional PRBS-based time-domain deconvolution		

y_{cc}	Detector signal in cc
z_d	Deconvolution signal used in the time domain
Δ	Kronecker delta function
Δ_{t_r}	Idem, maximum shifted to retention time t_r
$\tau_{1,2}$	Time constants

REFERENCES

- M. Engelsma, D.J. Louwerson, H.F.M. Boelens, W.Th. Kok and H.C. Smit, *Anal. Chim. Acta*, 228 (1990) 209.
- C. Mars and H.C. Smit, *Anal. Chim. Acta*, 228 (1990) 193.
- T.T. Lub and H.C. Smit, *Anal. Chim. Acta*, 112 (1979) 341.
- M. Kaljurand and E. Küllik, *Computerized Multiple Input Chromatography*, Ellis Horwood, Chichester, 1989, p. 53.
- S. Frazer and M.F. Burke, *Anal. Chim. Acta*, 177 (1985) 15.
- D.P. Carney and J.B. Phillips, *Anal. Chem.*, 58 (1986) 1251.
- R. Mulder, P.J. Hoogerbrugge and H.C. Smit, *Chemom. Intell. Lab. Syst.*, 1 (1987) 243.
- M. Kaljurand and E. Küllik, *Computerized Multiple Input Chromatography*, Ellis Horwood, Chichester, 1989, p. 42.
- H.C. Smit, *Chromatographia*, 3 (1970) 515.
- R. Mulder, C. Mars and H.C. Smit, *Chemom. Intell. Lab. Syst.*, 12 (1991) 155.
- M. Kaljurand and E. Küllik, *Computerized Multiple Input Chromatography*, Ellis Horwood, Chichester, 1989, p. 38.
- F. Ayres, Jr., *Theory and Problems of Matrices*, McGraw-Hill, New York, 1962, p. 22.
- L. Fox, *Introduction to Numerical Linear Algebra*, Clarendon, Oxford, 1964.
- J.B. Phillips, *Anal. Chem.*, 52 (1980) 468A.
- D.J. Louwerson, H.F.M. Boelens and H.C. Smit, *Anal. Chim. Acta*, 256 (1992) 349.
- E. Oran Brigham, *The Fast Fourier Transform*, Prentice-Hall, Englewood Cliffs, NJ, 1974.
- D. Britz, *J. Electroanal. Chem.*, 88 (1978) 309.
- K. Izawa, in A.B. Littlewood (Ed.), *Gas Chromatography*, Institute of Petroleum, London, 1966, p. 147.
- K. Izawa, F. Furuta, T. Fujiwara and N. Suyama, *Ind. Ch. Belge*, 32 (1967) 223.
- D.W. Krimse and A.W. Westerberg, *Anal. Chem.*, 43 (1971) 1035.
- T. Vladimiroff, *J. Chromatogr.*, 55 (1971) 175.
- R.E. Sioda, *J. Electroanal. Chem. Interfacial Electrochem.*, 56 (1974) 149.
- R. Alkire and R. Gould, *J. Electrochem. Soc.*, 123 (1976) 1842.
- C.A. Dorschel, J.L. Ekmanis, J.E. Oberholtzer, F. Vincent Warren, Jr. and B. Bidlingmeyer, *Anal. Chem.*, 61 (1989) 951A.
- M. Engelsma, W.Th. Kok and H.C. Smit, *J. Chromatogr.*, 506 (1990) 201.
- G.W. Schieffer, *Anal. Chem.*, 53 (1981) 126.

Ambient error weighted partial least-squares regression: a new receptor model

Shizoom Wang

Department of Environmental Engineering, National Chung Hsing University, Taichung (Taiwan)

Timothy Larson

Department of Civil Engineering, University of Washington, Seattle, WA 98195 (USA)

(Received 26th June 1992; revised manuscript received 4th September 1992)

Abstract

In the proposed model, both the ambient data and the source profiles were weighted by the ambient mass scaled ambient error. The comparison between this model and the effective variance weighted chemical mass balance-type model was done using NBS test data sets. The compared results show that the ambient error weighted partial least-squares regression model was better in predicting the emissions from each source. However, the effective variance weighted chemical mass balance model did better in predicting the ambient concentration of each species, which can easily be understood from the formulation of these different approaches.

Keywords: Partial least-squares regression; Receptor models

Ever since Friedlander [1] proposed the idea of a chemical mass balance receptor model, a number of different types of receptor models have been proposed. Currently, the most widely used receptor models are the chemical mass balance type proposed by Watson et al. [2] and the factor analysis type proposed by Hopke [3]. Neither approach solves all the problems associated with receptor models, most important the multicollinearity problem and the factor-source recognition problem. Vong et al. [4] proposed partial least-squares regression (PLS) as a new approach to solve these two problems. In this new approach, the independent latent structures of the source profiles were established. The mass collected was then apportioned among the latent

structures instead of the original source profiles. However, Vong et al.'s model did not consider the measurement errors inherent in either the source profiles or the ambient measurements. This paper extends the work done by Vong et al. by attempting to utilize the information supplied by the measurement errors.

ALGORITHM

For the PLS model, the source profiles were decomposed as follows [4]:

$$X = TP' + \epsilon_x \quad (1)$$

$$Y = UQ' + \epsilon_y \quad (2)$$

where X is the matrix for source profiles and Y is an identity matrix of the same rank as X . The reason for choosing Y an identity matrix is that it is hoped to establish the independence of the

Correspondence to: S. Wang, Department of Environmental Engineering, National Chung Hsing University, Taichung (Taiwan).

sources through the latent structures of the source profiles. Matrices P and Q are the latent structures of X and Y , respectively. The relationship between X and Y is established through regressing each column of U against the corresponding column of T :

$$\hat{b}_j = U_{.j}^t \times T_j \quad (3)$$

where T_j represents the j th column of matrix T and $U_{.j}$ the corresponding column of U . The total number of b s depends on the number of variables chosen. Once the relationship has been established, the matrix Y can be predicted as follows:

$$\hat{Y} = \begin{bmatrix} b_1 & & \\ & b_j & \\ & & b_m \end{bmatrix} TQ^t + \epsilon \quad (4)$$

Once the predicted \hat{Y} is the same as an identity matrix, we say that the source profiles are independent. The Y in Eqn. 2 is exact, but the \hat{Y} is not.

As for the weighting, there are two ways to use the information supplied by errors. The first is the effective error weighting. The ambient errors are first scaled to the same units as the source errors for each species by dividing each ambient error by its respective measured filter mass. In this way the measurement errors for a given ambient sample are in units of mass percentage instead of mass per air volume. The source profile X is first scaled by this new ambient error and the ambient data is scaled by its own error. After the source contribution prediction has been made, both the errors of source profile X and ambient data are combined as an "effective" error. The mass scaled ambient error, $\epsilon_{amb,i}$, and the "effective" error, ϵ_i , are calculated as follows:

$$\epsilon_{amb,i} = \frac{\sigma_{amb,i}}{\text{mass}_{amb}} \quad (5)$$

$$\epsilon_i = \epsilon_{amb,i} + \sigma_{X_{ij}} \hat{Y}_j \quad (6)$$

where $\sigma_{amb,i}$ is the error for the i th species of the ambient sample ($\mu\text{g m}^{-3}$), mass_{amb} is the mass of this sample ($\mu\text{g m}^{-3}$), $\sigma_{X_{ij}}$ is the error for the i th species of source j ($\mu\text{g } \mu\text{g}^{-1}$) and Y_j is the

fractional apportionment predicted for source j and also the j th element of the main diagonal of \hat{Y} .

Once the new \hat{y} has been found, Eqn. 6 is used to update the effective error. The source profile X is then scaled by this new effective error. New \hat{y} can be found by Eqns. 1–4. The predicted \hat{y} is the fractional contribution of total mass from each source. The whole procedure is repeated until the predicted \hat{y} converges. The converging criterion is defined as

$$\frac{\hat{y}_{j,\text{new}} - \hat{y}_{j,\text{old}}}{\hat{y}_{j,\text{old}}} < 0.01$$

Unlike the effective variance weighted chemical mass balance-type receptor models, this new error weighted PLS converges asymptotically.

The second weighting scheme is the ambient error weighting scheme. Both the source profiles and ambient data are scaled by the ambient errors. The adjusted ambient error is mass scaled ambient error calculated in Eqn. 5. This second scheme does not need iteration.

All calculations are done using MacII-Matlab [5] on a Macintosh personal computer, and the graphs are constructed using Macspin [6], version 3.01, on the same computer.

RESULTS

In order to compare the effects of different weighting schemes, some artificial samples were generated using a generating equation similar to that used by Currie et al. [7] to generate the samples in the Quail Roost data sets. A set of 50 artificial samples were generated using the same source profiles as used by Currie et al. [7]. The results are given in Table 1 and show that the ambient error weighting scheme is better than the effective error weighting scheme. The "No weighting" scheme is the same algorithm as reported by Vong et al. [4] with the exception that similar sources are not combined.

The integrity of the model was tested using artificial samples composed of random numbers. This test was conducted with both the PLS model and the effective variance weighted chemical mass

TABLE 1

Comparison of apportionments predicted by different weighting schemes

True	No weighting	Ambient error weighting	Effective error weighting ^a
0.243	2.525	0.233	-1.870
0.027	-1.486	0.098	1.490
1.903	2.123	2.500	2.180
4.667	4.661	6.030	4.620
0.112	-0.071	0.086	-1.100
1.651	2.325	2.860	9.470
0.084	-1.000	-0.242	-3.170
0.723	0.778	0.870	1.300
4.469	3.558	5.980	6.820
2.236	2.942	2.750	1.150
0.275	0.204	0.387	0.688
0.935	0.868	1.370	1.630
1.535	1.528	2.020	1.750

^a See text for details.

balance model (EV-CMB). The source profiles used for this testing were those used by Wang et al. [8]. Both models predicted the expected strange results: unreasonably high and also negative contributions were observed. The residual sum of squares based on observed versus predicted ambient concentrations showed that both models performed poorly as expected. The explanation for this can be seen by plotting these random samples in source space using the technique reported by Vong et al. [4] and Larson and Vong [9]. Figure 1 shows the results for two extreme samples (that with the largest residual sum of squares and that with the smallest). Both sample points lie outside the source polygon. This implies that these samples cannot be produced by the hypothesized sources. With the EV-CMB model, we only know there is something wrong with the predicted results, but we do not know why. With ambient error weighted PLS, it is easy to conclude that the implausible results are due to a mismatch between the source profiles and the sample profile and not to problems with source profile collinearity.

The other comparison between ambient error weighted PLS and EV-CMB was done by tests using Quail Roost data sets I–III. Figures 2–4 show the results for both models. As set I is a

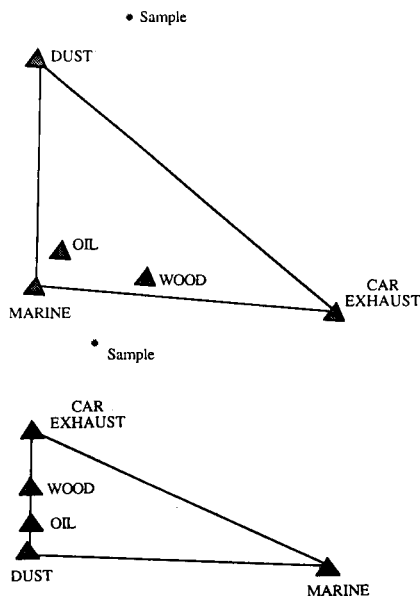


Fig. 1. Projection of randomly generated samples and five sources on to PLS components 1 and 2. As the axes have been rotated, they are not shown.

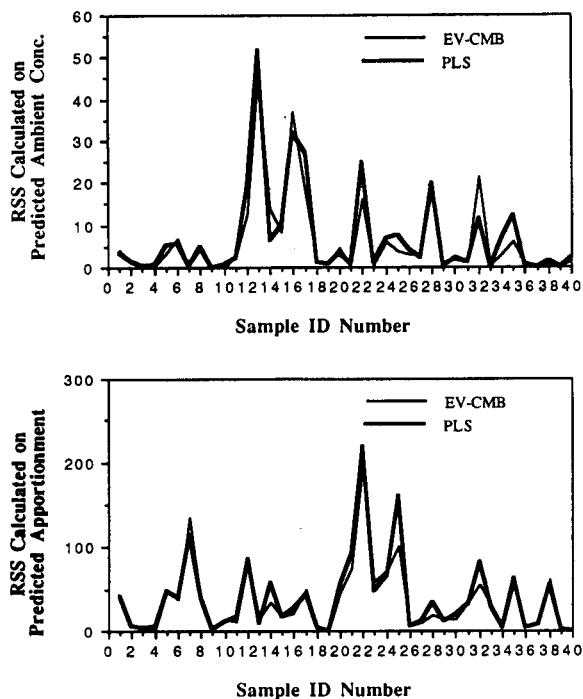


Fig. 2. Residual sum of squares for Quail Roost set I.

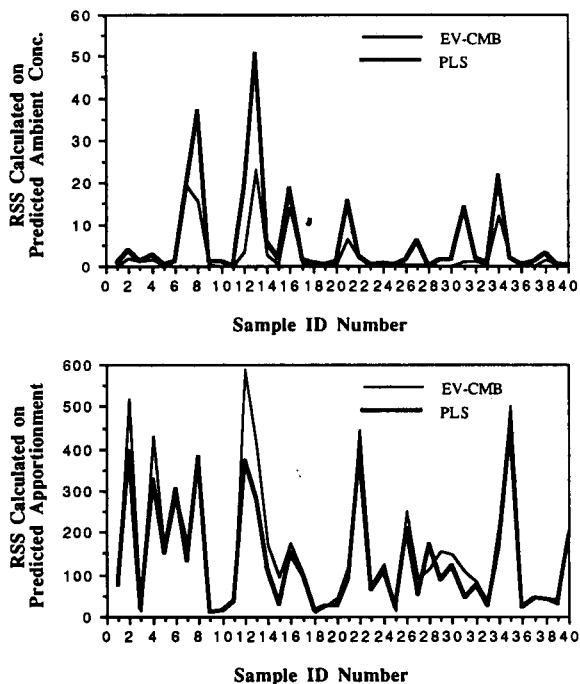


Fig. 3. Residual sum of squares for Quail Roost set II.

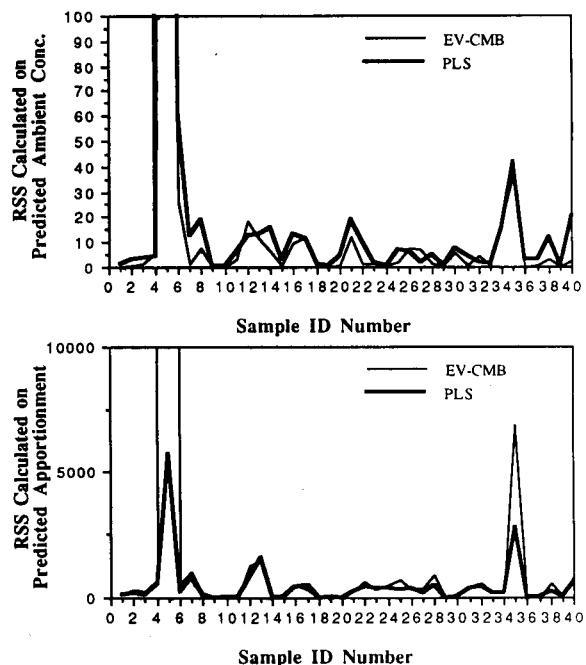


Fig. 4. Residual sum of squares for Quail Roost set III.

simple set, both models performed about the same. In contrast, for sets II and III ambient error weighted PLS did better than EV-CMB in predicting the apportionment. However, for predicting the ambient concentration for each species, EV-CMB was better than ambient error weighted PLS. This is understandable because EV-CMB uses the absolute ambient concentration of each species for calculation, whereas ambient error weighted PLS used the ambient mass fraction of each species to apportion the source contributions. As set III is perturbed with more randomness, the residual sum of squares value for set III was much larger than both sets I and II. The residual sum of squares values increased from set I to set II to set III. This is consistent with the increased complexity of the three sets.

DISCUSSION

Like Hopke's factor analysis model, the ambient error weighted PLS uses the latent structure to represent the source profiles. The problem associated with this type of model is to determine the number of factors used to represent the original source profiles. Most workers choose an eigenvalue of 1 as the cut-off, a somewhat subjective criterion. Vong et al. [4] proposed the partial least-squares regression as an alternative approach. However, in testing their model against the Quail Roost sets, they combined similar sources into one compound source. In this way, the collinearity problem was not adequately addressed. Unlike the model proposed by Vong et al., the ambient error weighted PLS model presented here does not combine source profiles. The latent structure is based on the ambient error weighted source profiles. Table 2 shows the variance apportioned among latent variables for sample 12 of set II. Even though the first four latent variables can explain 99.7% of the total variance of the source profiles, all five latent variables are still needed to predict the independence of the source profiles, i.e., in order for the predicted Y to be an identity matrix.

The reason why the "effective" error weighting scheme did not work as well in predicting the

TABLE 2

Variance apportionment among latent variables for sample No. 12 of Quail Roost test set II

LV No.	Percentage variance captured by PLS model			
	X-block		Y-block	
	This LV	Total	This LV	Total
1	94.0422	94.0422	7.6923	7.6923
2	4.3487	98.3909	7.6923	15.3846
3	0.9454	99.3363	7.6923	23.0769
4	0.3881	99.7244	7.6923	30.7692
5	0.1663	99.8907	7.6923	38.4615
6	0.0763	99.9670	7.6923	46.1538
7	0.0135	99.9806	7.6923	53.8462
8	0.0122	99.9928	7.6923	61.5385
9	0.0042	99.9970	7.6923	69.2308
10	0.0016	99.9986	7.6923	76.9231
11	0.0008	99.9995	7.6923	84.6154
12	0.0004	99.9999	7.6923	92.3077
13	0.0001	100.0000	7.6923	100.0000

apportionment is because the scheme is iterative. With each iteration, the source profiles were changed by the “effective” error. The latent structure is sensitive to the change of the source profiles. Therefore, the “effective” error weighting scheme is unstable unless an additional constraint (such as making the sum of the fractional apportionments equal to 1) is imposed. This constraint might be too restrictive and unreasonable because the observed mass collected on the ambient sample might not in fact be the sum of the mass emitted by all sources used in the source profiles.

Conclusion

The “effective” error weighted PLS is iterative and changes with each iteration. Therefore, the “effective” error weighting process is unstable unless an additional constraint (such as forcing the sum of the fractional apportionments to 1) is imposed. The ambient error weighted PLS is a plausible way to do weighting for the PLS algorithm.

Neither EV-CMB nor ambient error weighted PLS can predict the “true” apportionment of all the samples in the Quail Roost data sets. For most samples in the Quail Roost data sets, the results predicted by PLS are close to those predicted by EV-CMB. However, for some samples (those samples of set II), ambient error weighted PLS outperformed EV-CMB (the residual sum of squares was less). Neither model can perform well once the samples are perturbed with too much randomness (as with set III).

The PLS regression model is mathematically identical with the principal component regression (PCR) model when the *Y* matrix is exactly the identity matrix. This is not always the case. There may be tradeoffs that the user will accept with respect to the collinearity of the source profiles (i.e., the magnitude of the diagonal elements of *Y*). This additional feature distinguishes PLS from PCR.

REFERENCES

- 1 S.K. Friedlander, *Environ. Sci. Technol.*, 7 (1973) 235.
- 2 J.G. Watson, N.F. Robinson, J.C. Chow, R.C. Henry, B.M. Kim, T.G. Pace, E.L. Meyer and Q. Nguyen, *Environ. Software*, 5 (1990) 38.
- 3 P.K. Hopke, in E.S. Macias and P.K. Hopke (Eds.), *Atmospheric Aerosol: Source/Air Quality Relationships* (ACS Symposium Series, No. 167), American Chemical Society, Washington, DC, 1981, p. 21.
- 4 R.J. Vong, P. Geladi, S. Wold and K. Esbensen, *J. Chemometr.*, 2 (1988) 281.
- 5 *MacII-Matlab User's Manual* (Version 1.2), Math Works, Natick, MA, 1989.
- 6 *Macspin User's Manual* (Version 3.01), Abacus Concepts, Berkeley, CA, 1991.
- 7 L.A. Currie, R.W. Gerlach, C.W. Lewis, W.D. Balfour, J.A. Cooper, S.L. Dattner, R.T. De Cesar, G.E. Gordon, S.L. Heisler, P.K. Hopke, J.J. Shah, G.D. Thurston and H.J. Williamson, *Atmos. Environ.*, 18 (1984) 1517.
- 8 S. Wang, D. Kalman and T.V. Larson presented at the 84th Annual Meeting of Air and Waste Management Association (AWMA), 1991, paper 91-136.4.
- 9 T.V. Larson and R.J. Vong, in J.G. Watson (Ed.), *AWMA Transactions TR-14*, Air and Waste Management Association (AWMA), Pittsburgh, PA, 1989, p. 391.

Computer method for the simultaneous kinetic determination of compounds in mixtures based on the use of diode-array spectrophotometry

Andreu Cladera, Enrique Gómez, José Manuel Estela and Víctor Cerdà

Departamento de Química, Universitat de les Illes Balears, E-07071 Palma de Mallorca (Spain)

Juan Luis Cerdà

Departamento de Matemática Aplicada y Análisis, Universitat de Barcelona, Plaça Universitat, E-08071 Barcelona (Spain)

(Received 15th June 1992; revised manuscript received 25th September 1992)

Abstract

A computer method for the treatment of kinetic data provided by a diode-array spectrophotometer was developed. The method relies on a non-linear regression procedure for estimating the rate constants and concentrations of mixture components. The underlying principle of this method is fitting the absorption matrix obtained as a function of time and wavelength to a theoretical kinetic equation. This allows the resolution of mixtures of compounds with similar rate constants in a simultaneous fashion provided that they or their reaction products feature appreciable spectral differences from one another. The proposed method was applied to the resolution of Co(II) ($0.1\text{--}1.0\ \mu\text{g ml}^{-1}$)–Ni(II) ($0.5\text{--}5.0\ \mu\text{g ml}^{-1}$) mixtures based on displacement from their the EGTA complexes by 4-(2'-pyridylazo)resorcinol.

Keywords: Kinetic methods; UV–Visible spectrophotometry; Cobalt; Computer fitting; Nickel

Kinetic methods have been widely used in the last few decades in catalytic and non-catalytic determinations of various chemical species, particularly metal ions, on account of their advantages over equilibrium methods. The different techniques and procedures associated with this type of method have been reviewed [1–4].

Among kinetic methods, differential reaction rate methods have chiefly been used for resolving two or more chemical species with similar features present in the same sample. Because of their basis, their success depends critically on the

difference between the rate constants of the species concerned. This has curtailed their application and, in some instances, they require a number of sample aliquots to be used in order to achieve different working conditions so as to be able to determine the different analytes.

Recently, several groups have developed new procedures for the simultaneous resolution of kinetic processes. Using non-linear regression methods, Rutan and Brown [5] applied the extended Kalman filter to multi-wavelength kinetic data. Pardue and co-workers [6,7] mathematically modelled the kinetic response on the simultaneous determination of catalysts based on the differences in rates of inhibition by a common inhibitor. However, the former method has only

Correspondence to: V. Cerdà, Departamento de Química, Universitat de les Illes Balears, E-07071 Palma de Mallorca (Spain).

been applied to determinations with one reaction and a constant rate, and in the latter, because of its differential basis, the errors increase dramatically when the ratios of rate constants are near to unity. More recently, Schechter and Schröder [8] studied kinetic determinations in simulated systems of mixed first- and second-order reactions using the Levenberg–Marquardt method for non-linear least-squares fitting. In practice, the algorithm does not perform better when more information is given, which is a disadvantage regarding the available multi-channel detectors.

In continuation of studies into the resolution of multi-component systems [9–13], in this work a kinetic method for the simultaneous determination of several components in mixtures was developed on the basis both of the kinetic equation of the reaction involved and of spectral data obtained at regular intervals from a diode-array spectrophotometer. The rate constants and concentrations of the analytes are determined by using the Newton–Gauss non-linear regression optimization model in the form of a computerized algorithm. Unlike alternatives, the proposed method does not require appreciable differences between the reaction rates of the components of the mixture as resolution is essentially based on spectral data.

The applicability of the proposed method was checked on the model reported by Tanaka et al. [14], who used the displacement of Co(II) and Ni(II) from their complexes with ethylene glycol bis(2-aminoethyl ether)-*N,N,N',N'*-tetraacetic acid (EGTA) by 4-(2'-pyridylazo)resorcinol (PAR) to determine both ions simultaneously by differential kinetic analysis. The present method allows the rate constants and concentrations of Co(II) and Ni(II) to be determined over the ranges 0.1–1.0 and 0.5–5.0 $\mu\text{g ml}^{-1}$, respectively.

MATHEMATICAL BASIS

As a rule, for a kinetic reaction involving a single component that is monitored spectrophotometrically through the disappearance of the reactant or the formation of a product, the ab-

sorbance changes with time according to the following equation:

$$A = f(C, t, \lambda) \quad (1)$$

where A is the absorbance measured at wavelength λ , f is a function describing the kinetics of the process and usually dependent on one or more rate constants, C is the initial concentration of the monitored compound and t is time. For a mixture of n components in the absence of interactions:

$$A_{j,t} = \sum_{i=1}^n f_i(C_i, t, j) \quad \forall i = 1 \dots m \text{ and} \\ t = 0 \dots t_f \quad (2)$$

where $A_{j,t}$ is the absorbance measured at wavelength j at time t , f_i is the kinetic function of component i and C_i its initial concentration. This equation defines a system of $m \times (t_f + 1)$ non-linear equations that can be solved by one of the many procedures available for this purpose. One such procedure is the Newton–Gauss algorithm, which optimizes the values of the parameters to be determined in order to minimize the sum of the squares of the residuals ($A_{\text{exp}} - A_{\text{cal}}$) and accomplishes rapid convergence by employing the partial derivatives of the f_i functions with respect to each variable to be determined.

Solving the aforementioned equation system requires the determination of the molar absorptivity, rate constant and concentration of each component present in the mixture, which can be achieved in various ways. One involves calculating every parameter simultaneously by performing a series of experiments with different concentrations obtained by addition of known amounts of the analytes. This entails solving a system of $k \times m \times (t_f + 1)$ equations, k being the number of additions.

A second alternative entails determining the molar absorptivity of each component to be assayed over the working wavelength range by using solutions of the individual components in equilibrium, after which additions of known amounts of the components are used to determine the rate constant and concentration of each by using the previously calculated molar absorptivities.

A third procedure involves calculating the absorptivity and reaction constant of each component from standard solutions and solving the equation system for the concentration of each mixture component only.

Each of these three methods has its own assets and weaknesses from the computational and experimental points of view. Thus, the first involves laborious computations owing to the large number of parameters to be optimized. Inasmuch as absorptivities can be calculated individually with greater accuracy and convenience, the second alternative appears to be more interesting than the first. The third option is even more advantageous than the second, provided that reliable rate constant values can be obtained, as the computational and experimental aspects are much more straightforward (only a single measurement per sample need be done, irrespective of the number of components it contains). However, the second option is not overcomplicated in the calculations and allows for the multiple standard addition method to be used. Moreover, it is insensitive to fluctuations in the rate constants arising from environmental factors.

The proposed method relies on differences not only in the rate constants, but also in the spectral features of the species to be determined. Hence, unlike the differential kinetic methods used so far for this purpose, it does not require differences between the rate constants of the components.

EXPERIMENTAL

Apparatus and software^a

Experimental data were acquired by using a Hewlett-Packard HP8452A diode-array spectrophotometer furnished with quartz cuvettes of 1-cm path length and interfaced with a PC compatible computer. Absorption spectra were recorded as a function of time with the aid of DARRAY [15], a computer program developed

in this laboratory. The acquired data were subsequently processed by another program, NGOPT, which was developed for this purpose, NGOPT is written in QuickBasic and allows mathematical expressions of the type described under Mathematical Basis to be solved by using the Newton–Gauss algorithm. It uses the function to be optimized and its partial derivatives with respect to each parameter to be determined as input data and the spectrum of a pure standard of each component (from which it calculates the molar absorptivity) and those corresponding to the kinetics of the samples as data files.

Reagents

The solutions used included 3×10^{-3} M EGTA, 4×10^{-3} M PAR, 0.06 M borate–boric acid buffer (pH 8.5) containing 0.3 M NaClO₄ and Co(II) and Ni(II) working standard solutions prepared by dilution of stock standard solutions containing 1000 $\mu\text{g ml}^{-1}$ of either ion. All solutions were prepared in water purified using a Millipore Milli-Q system.

Procedure

In a 4-ml spectrophotometric cuvette are placed 1 ml of sample containing 0.3–3 $\mu\text{g ml}^{-1}$ cobalt and 1.5–15 $\mu\text{g ml}^{-1}$ nickel, 1 ml of 3×10^{-3} M EGTA, 1 ml of buffer (pH 8.5) and 150 μl of 4×10^{-3} M PAR. The mixture is homogenized and, after a preset time (12 s), kinetic data are acquired at a rate of 2 min^{-1} for 15 min over the wavelength range 490–570 nm in 2-nm steps against a blank prepared similarly but containing no sample. All these operations are performed at room temperature (20–23°C). The acquired data are stored in a file that is subsequently processed by the program NGOPT.

The molar absorptivities of Co(II) and Ni(II) are determined by a similar procedure using pure standards of the metal ions at concentrations between 0.2 and 0.6 $\mu\text{g ml}^{-1}$ and adding EGTA last so that equilibrium can be attained in a few minutes. The absorption spectra recorded under these conditions are standardized to unit concentration and averaged, and finally transferred for processing by the program NGOPT.

^a The software used in this work can be obtained from SCIWARE, Banco de Programas, Departamento de Química, Universitat de les Illes Balears, E-07071 Palma de Mallorca, Spain.

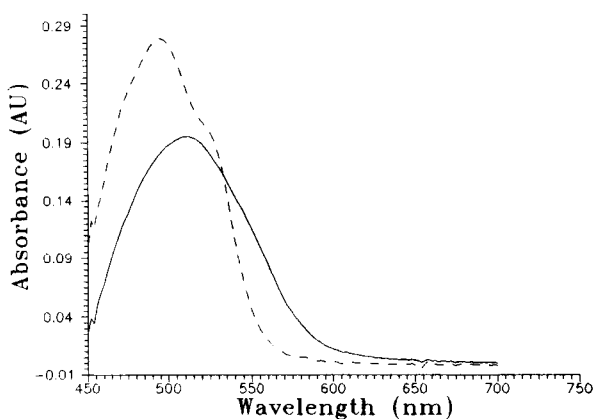
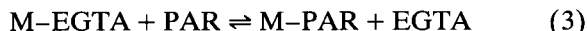


Fig. 1. Absorption spectra of the (—) Co(II)-PAR and (---) Ni(II)-PAR complexes at a concentration of $0.2 \mu\text{g ml}^{-1}$.

RESULTS AND DISCUSSION

The applicability of the proposed method was checked on the chemical model proposed by Tanaka et al. [14] namely the displacement of EGTA from its complexes with metal ions by the ligand PAR:



The model was applied to mixtures of Co(II) and Ni(II). Figure 1 shows the absorption spectra of the PAR complexes of the two ions after subtraction of the contribution of the ligand^a. In the presence of excess of EGTA and PAR and at pH 8–10, the process is of pseudo-first order and the corresponding integrated kinetic equations are

$$[\text{Co-PAR}] = C_{\text{Co}}[1 - \exp(k_{\text{Co}}t)] \quad (4)$$

$$[\text{Ni-PAR}] = C_{\text{Ni}}[1 - \exp(k_{\text{Ni}}t)] \quad (5)$$

where C_{Co} and C_{Ni} are the concentrations of cobalt and nickel, in the cuvette, and k_{Co} and k_{Ni} are their respective rate constants.

By substituting Eqns. 4 and 5 in Eqn. 2 and assuming the absorbance due to the disappearance of PAR to be negligible, one has

$$A_{j,t} = \epsilon_{\text{Co},j} b C_{\text{Co}} [1 - \exp(k_{\text{Co}}t)] + \epsilon_{\text{Ni},j} b C_{\text{Ni}} \times [1 - \exp(k_{\text{Ni}}t)] \quad (6)$$

^a The species being monitored are presumably Co(PAR)_n and Ni(PAR)_n where $n = 2-3$ which implies rapid addition of the extra PAR molecules.

where $\epsilon_{\text{Co},j}$ and $\epsilon_{\text{Ni},j}$ are the molar absorptivities of the Co-PAR and Ni-PAR complexes, respectively, at wavelength j , and b is the cuvette path length.

By making known additions of each metal ion on the starting sample, Eqn. 6 can be converted into

$$A_{j,t} = \epsilon_{\text{Co},j} b (C_{\text{Co}} + C_{\text{Co}}^{\text{ad}}) [1 - \exp(k_{\text{Co}}t)] + \epsilon_{\text{Ni},j} b (C_{\text{Ni}} + C_{\text{Ni}}^{\text{ad}}) + [1 - \exp(k_{\text{Ni}}t)] \quad (7)$$

where $C_{\text{Co}}^{\text{ad}}$ and $C_{\text{Ni}}^{\text{ad}}$ are the added Co and Ni concentrations, respectively.

Table 1 lists the results obtained by applying Eqn. 6 to the resolution of Co and Ni in a series of synthetic samples. The molar absorptivities were calculated by using the standardized spectra obtained from Co and Ni standards containing 0.2, 0.4 and 0.6 $\mu\text{g ml}^{-1}$ of either ion. The rate constants were calculated from the kinetic data obtained for three mixtures containing known concentrations of the two metal ions. As can be seen in Table 1, the concentrations obtained for cobalt were consistent, whereas those of nickel were underestimated in those instances where

TABLE 1

Results obtained in the resolution of synthetic mixtures of Co and Ni by optimizing their concentrations with the known values of their rate constants [$k_{\text{Co}} = (9.6 \pm 0.2) \times 10^{-4} \text{ s}^{-1}$, $k_{\text{Ni}} = (4.3 \pm 0.4) \times 10^{-5} \text{ s}^{-1}$]

Sample No.	Added ($\mu\text{g ml}^{-1}$)		Found ($\mu\text{g ml}^{-1}$)		RMS ^a $\times 10^3$
	Co	Ni	Co	Ni	
1	0.00	5.00	0.04	4.98	3.06
2	2.00	0.00	2.06	0.00	9.99
3	0.10	0.50	0.10	0.50	0.80
4	0.10	4.00	0.10	4.18	1.16
5	0.30	2.50	0.30	2.79	2.30
6	0.50	1.00	0.49	1.10	2.27
7	0.70	0.50	0.68	0.47	2.29
8	0.80	4.00	0.76	4.09	2.63
9	2.00	2.00	2.02	1.24	9.72
10	2.50	1.00	2.53	0.00	14.74
11	1.50	3.00	1.54	1.94	5.82
12	3.00	5.00	3.03	3.43	24.77
13	2.00	7.00	2.03	5.92	14.34

^a RMS = mean of the sum of residuals calculated by the program NGOPT from the equation $\text{RMS} = [1/n \sum_{i=1}^n (A_{\text{exp}} - A_{\text{calc}})^2]^{1/2}$, where n is the number of experimental data.

the cobalt concentration present in the mixture was higher than $1 \mu\text{g ml}^{-1}$. This can be attributed to the greater displacement rate of the cobalt ion, which does not conform to the proposed model at times where the nickel substitution has not developed to an appreciable extent. Accordingly, unlike in differential kinetic methods, the applicability of the proposed method will be inversely proportional to the difference between the rate constants of the analytes.

Table 2 lists the results obtained in the simultaneous determination of the concentrations and rate constants of Co and Ni in a series of synthetic samples to which two successive additions were made (the first of $0.2 \mu\text{g ml}^{-1}$ Co and the second of $1 \mu\text{g ml}^{-1}$ Ni) and later Eqn. 7 was applied. The constant rate deviations among the different samples must be attributed to the fact that they were obtained in different working sessions without a thermostat. Thus, the results found matched the expectations except for samples 7 and 9, in which the amount of Ni added was insufficient for the program NGOPT to determine its influence on account of the high absorbance signal corresponding to the relatively large excess of Co present when the proposed additions were made. This problem was overcome in samples 8 and 10 by increasing the concentration of Ni in the second addition ($2 \mu\text{g ml}^{-1}$ Ni), which provided significantly better results. All the same, sample 10 was subject to negative errors

probably arising from lack of fulfillment of the proposed theoretical equation at such high Co and Ni concentrations. This must be true particularly in the case of standard additions as the ion concentrations in such solutions are even higher.

Conclusions

The results show that the proposed method can take advantage of the possibilities of diode-array detectors to be applied satisfactorily to the simultaneous determination of several compounds involved in a kinetic process.

Unlike differential kinetic methods, it does not require large differences between the rate constants of the species involved as the spectral data used allow for ready discrimination of the analytes. In fact, according to the experimental results obtained, the closer the rates in question are, the better the mixture resolution and the broader the determination range will be. Unlike the use of the Kalman filter algorithm [5], for the determination of the analytes the proposed method uses two different reactions with their corresponding rate constants which allow great versatility in the working chemical system. The chief limitation of the method is the need for each kinetic process involved to result in a measurable spectral change and the availability of resolvable spectra, whether overlapped or not, of the reactants or their reaction products.

Of the two experimental alternatives tried, the

TABLE 2

Results and standard deviations ($n = 3$) obtained in the resolution of synthetic samples by simultaneously optimizing concentrations and rate constants

Sample	Added ^a ($\mu\text{g ml}^{-1}$)		Found ($\mu\text{g ml}^{-1}$)		$k_{\text{Co}} \times 10^4$	$k_{\text{Ni}} \times 10^5$	RMS ^b $\times 10^3$
	Co	Ni	Co	Ni			
1	0.33	0.00	0.31 ± 0.06	0.00 ± 0.10	8.8 ± 0.4	3.4 ± 0.6	4.69
2	0.00	5.00	0.05 ± 0.02	5.46 ± 0.04	9.3 ± 0.1	3.7 ± 0.3	4.66
3	0.10	0.50	0.11 ± 0.01	0.40 ± 0.10	8.7 ± 0.3	4.3 ± 0.9	0.96
4	0.10	4.00	0.10 ± 0.01	4.20 ± 0.05	9.6 ± 0.1	4.2 ± 0.1	1.58
5	0.30	2.50	0.28 ± 0.02	2.02 ± 0.20	10.2 ± 0.5	6.2 ± 0.3	3.28
6	0.50	1.00	0.45 ± 0.01	0.94 ± 0.04	10.7 ± 0.2	5.0 ± 0.05	2.52
7	0.70	0.50	0.71 ± 0.03	2.41 ± 1.41	8.9 ± 0.4	1.1 ± 0.7	3.31
8	0.70	0.50	0.65 ± 0.01	0.49 ± 0.05	11.0 ± 0.2	4.3 ± 0.9	3.58
9	0.80	4.00	0.79 ± 0.04	14.8 ± 1.6	9.9 ± 0.6	1.2 ± 0.1	6.82
10	0.80	4.00	0.54 ± 0.02	3.29 ± 0.33	13.8 ± 0.4	5.2 ± 0.1	3.27

^a Additions: the first was of $0.2 \mu\text{g ml}^{-1}$ Co and the second $1 \mu\text{g ml}^{-1}$ Ni, except for samples 8 and 10, to which $0.2 \mu\text{g ml}^{-1}$ Co and $2 \mu\text{g ml}^{-1}$ Ni were added. ^b See footnote to Table 1.

first is simpler to apply but requires stricter control of the working conditions because the kinetic parameters are not re-calculated. On the other hand, the second alternative (standard additions) overcomes potential multiplicative interferences due to the sample matrix. This latter method, however, is more laborious, particularly as regards designing the addition series, which must be done very carefully in order to avoid spurious results. This is particularly true of kinetic processes taking place at different rates, in which the faster one may mask the changes due to the slower one. On the other hand, both options allow additive interferences arising from background absorption to be overcome by extrapolation to time zero. This can be readily implemented in the equations to be optimized.

The experimental results obtained in the chemical model selected using both alternatives are satisfactory except in some limiting cases. The concentration working range and deviations are similar to those obtained by Tanaka et al. [14], despite the few experimental data that they reported.

Finally, it should be noted that, despite the fact that the proposed method was applied to a mixture of only two components in this work, it can be used equally well for mixtures of several components of diverse nature provided that a suitable chemical model is available.

The authors express their gratitude to the Dirección General de Investigación en Ciencia y Tecnología (DGICYT) for financial support of this work as part of Project PB 90-0359.

REFERENCES

- 1 K.B. Yatsimirskii, *Kinetic Methods of Analysis*, Pergamon, Oxford, 1966.
- 2 H.A. Mottola and H.B. Mark, Jr., *Anal. Chem.*, 58 (1986) 264.
- 3 D. Pérez-Bendito and M. Silva, *Kinetic Methods in Analytical Chemistry*, Horwood, Chichester, 1988.
- 4 H.L. Pardue, *Anal. Chim. Acta*, 216 (1989) 69.
- 5 S.C. Rutan and S.D. Brown, *Anal. Chim. Acta*, 167 (1985) 23.
- 6 W.E. Weiser and H.L. Pardue, *Anal. Chem.*, 58 (1986) 2523.
- 7 C.P. Fitzpatrick and H.L. Pardue, *Anal. Chem.*, 61 (1989) 2551.
- 8 I. Schechter and H. Schröder, *Anal. Chem.*, 64 (1992) 325.
- 9 E. Gómez, J.M. Estela and V. Cerdà, *Anal. Chim. Acta*, 249 (1991) 513.
- 10 E. Gómez, J.M. Estela, V. Cerdà and M. Blanco, *Fresenius' J. Anal. Chem.*, 342 (1992) 318.
- 11 A. Cladera, A. Caro, E. Gómez, J.M. Estela and V. Cerdà, *Fresenius' J. Anal. Chem.*, 342 (1992) 322.
- 12 A. Cladera, A. Caro, E. Gómez, J.M. Estela and V. Cerdà, *Talanta*, 39 (1992) 887.
- 13 G. Turnes, A. Cladera, E. Gómez, J.M. Estela and V. Cerdà, *J. Electroanal. Chem.*, 338 (1992) 49.
- 14 M. Tanaka, S. Funahashi and K. Shirai, *Anal. Chim. Acta*, 39 (1967) 437.
- 15 A. Cladera, E. Gómez, J.M. Estela and V. Cerdà, *Analyst*, 116 (1991) 913.

BOOK REVIEWS

E. Heftmann (Ed.), *Chromatography, 5th Edition. Part A: Fundamentals and Techniques. Part B: Applications (Journal of Chromatography Library, Vol. 51A and B)*, Elsevier, Amsterdam, 1992 (ISBN 0-444-88237-5). Part A, xxxvi + 552 pp., Part B, xxxii + 630 pp. Price US \$333.50/Dfl. 650.00.

This comprehensive description of chromatographic methods and their applications is an updating and revision of the 4th edition published in 1983. So much has changed over the last 9 years that a new overview of the subject is both desirable and timely.

The editor has brought together 37 authors to cover the full width of separation methods. The first volume concentrates on the different techniques and gives similar prominence to each. This has the effect of apparently playing down the role of liquid chromatography and gas-liquid chromatography, but these techniques have been comprehensively covered in other works. Instead we are reminded of counter-current chromatography, affinity chromatography, and field flow fractionation as methods with potential but which are probably underused. Supercritical fluid chromatography (SFC) has a chapter but the more recently developed method of capillary zone electrophoresis (CZE) appears only as a small section within electrophoresis.

The second volume concentrates on applications of chromatographic methods, an initial chapter on inorganic samples and then chapters on the major biochemical areas; proteins, lipids, carbohydrates, nucleic acids, porphyrins and phenolics. There is only one chapter on drug compounds, although it starts by noting that this is the largest application area for chromatography with 16% of papers. As this represents some 10 000 papers since the 4th edition of *Chromatography*, it is clear why a detailed coverage would be impossible. Instead the chapter surveys the area with examples from the individual drug groups. It includes a brief section of chiral separations,

which even a few years later have now gained much greater importance.

The last few chapters are devoted to more specific areas, fossil fuels, synthetic polymers, pesticides, and environmental samples. These last chapters in particular demonstrate the way in which new methods such as SFC have become accepted. By the next edition CZE is likely to show a similar impact on biochemical methods.

As always, the problem with a work of this size is that it is difficult for the editor to ensure that the individual contributions are up-to-date. Overall the coverage is good with most chapters including references to the late 1980s or 1990, which is as recent as might be permitted by the publishing schedule. However, new and expanding areas are inevitably under-represented partly because they are research rather than application areas and the methods are often not yet fully accepted or developed. CZE and chiral separations are two notable problem areas. Overall, these volumes present an up-to-date comprehensive coverage of an enormous area of analytical chemistry but which would need to be supplemented for many users by more specific texts in particular areas of interest.

Roger M. Smith

D. Cagniant (Ed.), *Complexation Chromatography*, Marcel Dekker, New York, 1992 (ISBN 0-8247-8577-0). vii + 294 pp. Price US \$114.50.

A glance at the cover of this book showing the separation of hydrocarbons will quickly dispel any thoughts that the subject matter involves the separation of inorganic complexes. Here, complexation encompasses the wider Lewis acid-base concept of electron donor-acceptor (EDA) interactions exploited for the separation of organic compounds. For chromatographic purposes the formation of EDA complexes must be labile and relatively weak, and as expected ligand interac-

tion with metal ions is the most commonly used process. However, EDA interactions involving charge transfer complexes (CTC) between organic compounds is also being increasingly exploited for difficult separations. This book covers these areas in some detail, with a good balance between background theory and principles and a large number of practical examples. A survey of the types of packings used in EDA complex separations is followed by chapters on developments in CTC chromatography, argentation chromatography, ligand-exchange chromatography of chiral molecules and a special topics chapter on the analysis of coal and petroleum products. I found this a fascinating book and thoroughly recommend it to all interested in the separation of organic compounds. Like me, many will be genuinely surprised at the diversity of compounds amenable to separation by this approach.

P. Jones

Frieder Scheller and Florian Schubert, *Biosensors (Techniques and Instrumentation in Analytical Chemistry, Vol. 11)*, Elsevier, Amsterdam, 1992 (ISBN 0-444-98783-5). x + 359 pp. Price US \$161.50/Dfl. 315.00.

The authors define biosensors as "devices incorporating a biologically active element in contact with a physico-chemical signal transducer and an electronic signal processor". The development of biosensors is an area of great current activity; the appearance of this book provides a good basis for understanding the fundamental concepts of the subject, and obtaining a comprehensive account of developments up to ca. 1989.

There are four major chapters. The first deals with the fundamentals of biosensors, largely in respect of enzyme-based systems. In the next two chapters there are detailed descriptions of sensors based either on metabolic effects, i.e., chemical conversion, generally brought about by enzymes, or on affinity effects (protein binding, enzyme binding (including inhibitors and activators), and immuno-interactions). A wide range of

signal transducers is used to monitor the sensing effects, and problems of interfacing are discussed in detail. The fourth chapter discusses applications of biosensors, for clinical and food analysis, bioprocess control and environmental monitoring.

The book is well written and illustrated. It provides a clear and comprehensive account of biosensors, and will serve as an excellent source book for some years. So rapid is the rate of progress, however, that a second edition will undoubtedly be needed in the not too distant future.

Alan Townshend

Anthony P.F. Turner (Ed.), *Advances in Biosensors, Vol. 2*, JAI Press, London, 1992 (ISBN 1-55938-270-8). xii + 343 pp. Price £54.00.

This is the second volume of a "research annual" describing advances in biosensor technology emanating from the laboratories of prominent scientists involved in this area of research. As such the chapters reflect work being carried out at the "cutting edge", and allow the reader critically to assess the current state-of-the-art in this multi-disciplinary subject. Although the chapters are not critical reviews, they provide an important source of information, especially for newcomers to the field. The nine chapters in this present volume reflect advances in amperometric, optical, acoustic wave and surface plasmon resonance detection, as well as describing new developments in bioelectrochemistry and microfabrication of devices, particularly for in vivo applications. The volume is to be welcomed as an additional source of information not present in the primary literature. By its very nature, however, there is a certain degree of overlap in the coverage of the respective authors, but the book can be recommended for purchase by all those interested in chemical and biological sensor development.

Malcolm R. Smyth

P.T. Moseley, J.O.W. Norris and D.E. Williams, *Techniques and Mechanisms in Gas Sensing*, Adam Hilger, Bristol, 1991 (ISBN 0-7503-0074-4). xv + 390 pp. Price £59.00.

Gas sensors are developing very rapidly, both in the techniques available, and in their fabrication and range of application. This book, in the same series as *Solid State Gas Sensors* edited by P.T. Moseley and B.C. Tofield (1987), gives an up-to-date account of the principles and operation of all well-known gas sensors. There are fourteen chapters, written by acknowledged experts in their field. Five chapters are devoted to metal oxide semiconductor sensors, and there are descriptions of sensors based on metal phthalocyanines, colorimetry, optical fibres, infrared spectroscopy and surface acoustic waves. Further chapters are devoted to liquid electrolyte fuel cells, humidity sensing and the measurement of oxygen by its paramagnetism. The book concludes with a timely article on pattern recognition in gas sensing.

The appearance of this book, providing a detailed yet readable and comprehensive account of a subject of such great current interest, is most welcome.

Alan Townshend

Malcolm R. Smyth and Johannes G. Vos (Eds.), *Analytical Voltammetry* (Vol. XXVII of *Wilson and Wilson's Comprehensive Analytical Chemistry*, series editor: G. Svehla), Elsevier, Amsterdam, 1992 (ISBN 0-444-88938-8). xxvi + 578 pp. Price US \$283.00/Dfl. 495.00.

This volume on analytical voltammetry is one of a long series on analytical chemistry. The chapters in this volume are individually written by different authors, some including the editors. The quality of the chapters is variable. The chapters are on Theory, Instrumentation, Biological Molecules, Pharmacy, Environmental Science (Inorganic and Organic Species), Modified Elec-

trodes, and Amperometric Sensors. The last two are on currently very popular research topics (modified electrodes and biosensors).

The chapters are thoroughly written and generally well-referenced. Each chapter has its own reference list of between 200 and 500 references. As such the book contains an enormous amount of information and is quite comprehensive, which was the aim of the editors.

The theory is aimed at beginners in voltammetry but it is presented in such a manner that it is quite unreadable (theory is not my strong point anyway). No derivations are given, just the final equations underlying voltammetry and polarography. This is useful if you know what you are looking for but references are given so you can go back to the original literature.

The chapter on Instrumentation is well-written, describing many kinds of electrodes and basic instruments. Problems (and their causes) associated with some of the electrodes are also set out. Circuit diagrams are given and explained for simple and improved potentiostats. The use of computers to control the potentiostat is indicated.

The application chapters include many biological applications (in vivo) and are well-researched: many examples are given. The chapter on pharmaceutical applications (by the Bersier brothers) is similarly well done, giving many examples of successful drug analyses; it is quite interesting reading because of the clear explanations.

The chapter on inorganic species in the environment unfortunately suffers from some erroneous statements regarding sample storage: freezing is recommended for water samples, for instance, which is known to cause losses of several elements. This chapter is weak on actual natural water applications (including chemical speciation) but many examples and references are available nevertheless.

The chapter on organic and organometallic species in the environment is very knowledgeably written and many examples of applications are given including descriptions of the sources of the contaminants. This chapter also includes some information on how to determine the chemical speciation of inorganic elements by complexation

reactions. It is a broad and interesting chapter, a useful source of information.

Modified electrodes are a popular topic with many (in my opinion sometimes rather optimistic) promises. This chapter is big on theory and thin on successful applications. There appears to be a misunderstanding in the use of the concentration terms pM and picomole (which indicates a quantity rather than a concentration) which makes a big difference when discussing detection limits; furthermore different concentration scales (ng and μM) are occasionally mixed within one sentence. This field is still developing and there is undoubted potential for environmental applications including in vivo (intra-cellular) measurements.

The last chapter (Biosensors) is somewhat weaker, giving statements sometimes unsupported by references. Even so, many useful examples are given in this area which is still developing.

On the whole this book provides a large amount of information, and the major part is well-written and interesting to read.

I recommend this book as a reference source for the title topic for researchers and analytical chemists at postgraduate level.

C.M.G. van den Berg

William B. Guenther, *Unified Equilibrium Calculations*, Wiley, New York, 1991 (ISBN 0-471-53854-X). xv + 313 pp. Price £56.00.

Imagine a solution containing citric acid (tri-basic acid), oxalic acid (dibasic) and sodium hydroxide. Now calculate the pH of the mixture, and the concentrations of each of the seven organic species present. Most chemists blanch at the thought of this type of calculation. This book explains how to do such complicated calculations of pH and speciation.

Firstly, a straightforward method of writing down the sums to be done is presented. Secondly, the author shows how to do the calculations using

a computer spreadsheet (such as Lotus 1-2-3, or Excel). Sample calculations are presented for many types of system. Calculations involving the formation of complexes by metal ions and ligands are included. When copper(II) ions are mixed with hydroxide and ammonia, up to nine separate copper complexes may be involved, and the author shows how his systematic method deals with pH and speciation calculations for such systems. Calculations where one or more species precipitate out of solution are also discussed. The methods presented are the result of many years of thought and quickly give answers for complicated mixtures. This book is no easy read, but by persistence you can quickly master these tricky calculations.

J.R. Chipperfield

Alan F. Williams, C. Floriani and A.E. Merbach (Eds.), *Perspectives in Coordination Chemistry*, VCH, Weinheim and Helvetia Chimica Acta, Basel, 1992 (ISBN 3-527-28487-7). 486 pp. Price DM 148.00.

This collection of 23 monographs in contemporary coordination chemistry is intended as a tribute to the hundredth anniversary of Alfred Werner's seminal papers in the field. As might be expected the topics presented cover a wide range of chemistry including studies of bonding, synthesis and reactivity in biomimic, organometallic and catalytic chemistry. Although this book is not directly targeted at analytical chemists three sections relating to molecular recognition and ion selective ligation by macrocyclic species (F. Vögtle, R.D. Hancock, M.W. Hosseini) would perhaps be of greatest use. These rational approaches present insights in to how highly selective inclusion phenomena may be brought about by ligand design. However, in total this volume has a strong inorganic flavour and will most appeal to analytical chemists with inorganic biases.

S. Woodward

Louise Voress, *Instrumentation in Analytical Chemistry, 1988–1991*, American Chemical Society, Washington, DC, 1992 [ISBN 0-8412-2209-9 (paperback)]. xv + 478 pp. US \$28.95.

This is a useful collection of relevant articles that appeared in the “A” pages of *Analytical Chemistry* during 1988–1991, reprinted in their original format, but without the use of colour. The topics are divided into Robotics, Computers and Laboratory Data Management (5 articles), Atomic and Molecular Spectroscopy (16), Electroanalytical Chemistry and Chemical Sensors (9), Separations (7), Mass Spectrometry (8) and Surface Analysis (5), each section having its own introduction. There is a good subject index. Seeing all these articles together gives a tremendous impression of how broad analytical science has become, and how rapidly its advance is continuing.

Benjamin Chu, *Laser Light Scattering*, 2nd edn., Academic Press, San Diego, 1991 (ISBN 0-12-174551-1). ix + 343 pp.

This edition is a complete update of the original 1974 text. In it the author has made considerable efforts to make the text more “user-friendly” to those without formal training in electrodynamics. A lot of the more complex mathematics is

now assigned to appendices. Nevertheless, much mathematical detail necessarily remains. After a chapter on light scattering theory, there is a comprehensive account of optical mixing spectroscopy, photocorrelation spectroscopy and interferometry as applied to laser light scattering, and details of experimental methods and data analysis. Analytical scientists who use light scattering extensively for particle sizing and in nephelometry and turbidimetry, will find the text generally informative, but without particular attention to these applications. The only application included is polymer particle sizing.

E. Buncl and G.W. Kabalka (Eds.), *Synthesis and Applications of Isotopically Labelled Compounds 1991*, Elsevier, Amsterdam, 1992 (ISBN 0-444-89280-X). xxvii + 784 pp. Price US \$320.00/Dfl. 560.00.

These are the *Proceedings of the 4th International Symposium* held at Toronto, 3–7 September, 1992, produced from camera-ready copy on high quality paper. It includes 3 plenary lectures, numerous oral presentations on the synthesis and applications of isotopically-labelled compounds (6 pages each) and poster presentations (4 pages each). One section deals with the analysis of such labelled compounds. Otherwise the volume will only be of general interest to analytical chemists.

ANALYTICA CHIMICA ACTA, VOL. 272 (1993)

AUTHOR INDEX

- Appriou, P., see Blain, S. 91
- Baker, M., see Christie, I. 145
- Baldo, M.A.
—, Daniele, S. and Mazzocchin, G.A.
Voltammetry with microelectrodes in wine: determination of the total acidity 151
- Barakat, S.A.
—, Burns, D.T. and Harriott, M.
Flow-injection extraction spectrophotometric determination of chromium(VI) with the benzyltributylammonium cation 135
- Bartsch, R.A.
—, Goo, M.-J., Christian, G.D., Wen, X., Czech, B.P., Chapoteau, E. and Kumar, A.
Influence of ring substituents and matrix on lithium/sodium selectivity of 14-crown-4 and benzo-13-crown-4 compounds 285
- Battagliarin, M., see Milella, E. 99
- Beinrohr, E., see Lee, M.L. 193
- Blain, S.
—, Appriou, P. and Handel, H.
Preconcentration of trace metals from sea water with the chelating resin Chelamine 91
- Boelens, H.F.M., see Engelsma, M. 309
- Bourdillon, C., see Huet, D. 205
- Burns, D.T., see Barakat, S.A. 135
- Buydens, L.
—, Schoenmakers, P., Maris, F. and Hindriks, H.
Expert systems in chromatography. Results of the ESCA project 41
- Calokerinos, A.C., see Psarellis, I.M. 265
- Cerdà, J.L., see Cladera, A. 339
- Cerdà, V., see Cladera, A. 339
- Chapoteau, E., see Bartsch, R.A. 285
- Chen, L.
— and Robien, W.
Optimized prediction of ^{13}C NMR spectra using increments 301
- Chen, S.-Z., see Zhang, Z.-Q. 227
- Christian, G.D., see Bartsch, R.A. 285
- Christie, I.
—, Leeds, S., Baker, M., Keedy, F. and Vadgama, P.
Direct electrochemical determination of paracetamol in plasma 145
- Cladera, A.
—, Gómez, E., Estela, J.M., Cerdà, V. and Cerdà, J.L.
Computer method for the simultaneous kinetic determination of compounds in mixtures based on the use of diode-array spectrophotometry 339
- Crowley, J.J., see Shanahan, P. 271
- Czech, B.P., see Bartsch, R.A. 285
- Daniele, S., see Baldo, M.A. 151
- Dembiński, B., see Mikulski, R. 233
- Donnelly, D.F., see Shanahan, P. 271
- Emaus, W.J.M.
— and Henning, H.J.
Determination of bromide in sodium chloride matrices by flow-injection analysis using blank peak elimination and kinetic discrimination 245
- Engelsma, M.
—, Boelens, H.F.M., Louwerse, D.J., Kok, W.Th. and Smit, H.C.
Characteristics and application of an electrochemical concentration modulator in correlation chromatography. Part 2. Computational aspects, modelling and application 309
- Estela, J.M., see Cladera, A. 339
- Fang, Y.
—, Tong, W., He, P., Wang, R. and Jin, L.
Four-potential-step differential amperometry in a dual-potential sequence mode 139
- Feinberg, M.H.
—, Ireland-Ripert, J. and Mourel, R.M.
Optimization procedure of open vessel microwave digestion for Kjeldahl nitrogen determination in foods 83
- Fu, X.-T.
—, Wang, C.-M. and Zhang, Y.-X.
Polarographic study of the Eu(III)-triethylenetetra-aminehexaacetic acid complex and determination of europium by oscillopolarography 221
- Fukaya, T.
—, Imura, H. and Suzuki, N.
Stoichiometric ion-pair extraction and determination of barium(II) with macrocyclic crown ether and cryptand 279
- Glennon, J.D., see Shanahan, P. 271
- Gómez, E., see Cladera, A. 339
- Goo, M.-J., see Bartsch, R.A. 285
- Guo, Q.-L., see Yan, X.-P. 105

- Hadjiioannou, T.P., see Halvatzis, S.A. 251
- Halvatzis, S.A.
—, Timotheou-Potamia, M.M. and Hadjiioannou, T.P.
Continuous-flow chemiluminometric determination of dihyalazine, rifampicin and rifamycin SV by oxidation with *N*-bromosuccinimide 251
- Handel, H., see Blain, S. 91
- Harriott, M., see Barakat, S.A. 135
- He, P., see Fang, Y. 139
- Henning, H.J., see Emaus, W.J.M. 245
- Hindriks, H., see Buydens, L. 41
- Hoke, S.H., see Jordan, J.M. 115
- Horiguchi, K., see Kaku, S. 213
- Huet, D.
— and Bourdillon, C.
Automatic apparatus for heterogeneous enzyme immunoassays based on electrocatalytic detection of the enzyme and electrochemical regeneration of the solid phase 205
- Imura, H., see Fukaya, T. 279
- Ireland-Ripert, J., see Feinberg, M.H. 83
- Ishizuki, T.
—, Tsuzuki, M., Yuchi, A., Ozawa, T., Wada, H. and Nakagawa, G.
Synthesis of 2-[2-(4-methylquinoly)azo]-5-diethylamino-phenol and its use for the spectrophotometric determination of nickel 161
- Jarvis, T.D.
— and Kalivas, J.H.
Condition index evolving profile library searches: gas chromatography-Fourier transform infrared spectrometry application 53
- Jin, L., see Fang, Y. 139
- Jordan, J.M.
—, Hoke, S.H. and Pardue, H.L.
Evaluation of different data-processing options for a flow system with a well-stirred mixing chamber 115
—, Love, M.D. and Pardue, H.L.
Evaluation of a predictive curve-fitting method for processing data from flow systems. Part 1. Flow system with a mixing chamber 125
- Kaku, S.
—, Nakanishi, S., Horiguchi, K. and Sato, M.
Amperometric enzyme immunoassay for urinary human serum albumin using plasma-treated membrane 213
- Kalivas, J.H., see Jarvis, T.D. 53
- Karakelle, M., see Lakowicz, J.R. 179
- Keedy, F., see Christie, I. 145
- Kok, W.Th., see Engelsma, M. 309
- Korenaga, T.
—, Zhou, X., Okada, K., Moriwake, T. and Shinoda, S.
Determination of chemical oxygen demand by a flow-injection method using cerium(IV) sulphate as oxidizing agent 237
- Kumar, A., see Bartsch, R.A. 285
- Lakowicz, J.R.
—, Szmazinski, H. and Karakelle, M.
Optical sensing of pH and pCO₂ using phase-modulation fluorimetry and resonance energy transfer 179
- Larson, T., see Wang, S. 333
- Le, Q.T.H.
—, Umetani, S., Takahara, H. and Matsui, M.
Liquid-liquid extraction of lanthanides with a highly acidic extractant, 3-phenyl-4-benzoyl-5-isoxazolone, in the presence and absence of tri-*n*-octylphosphine oxide 293
- Lee, M.L.
—, Tölg, G., Beinrohr, E. and Tschöpel, P.
Preconcentration of palladium, platinum and rhodium by on-line sorbent extraction for graphite furnace atomic absorption spectrometry and inductively coupled plasma atomic emission spectrometry 193
- Leeds, S., see Christie, I. 145
- Liang, Y.-Z., see Xie, Y.-L. 61
- Lin, C.-C., see Lo, J.-M. 169
- Lin, H.-M., see Zhang, Z.-Q. 227
- Lo, J.-M.
—, Lin, C.-C. and Yeh, S.-J.
Extraction constants of Te⁴⁺, Sb³⁺, Se⁴⁺, MoO₂⁺ and Ga³⁺ with dithiocarbamates 169
- Louwerse, D.J., see Engelsma, M. 309
- Love, M.D., see Jordan, J.M. 125
- Maris, F., see Buydens, L. 41
- Matsui, M., see Le, Q.T.H. 293
- Mazzetto, G., see Milella, E. 99
- Mazzocchin, G.A., see Baldo, M.A. 151
- Meregalli, L., see Milella, E. 99
- Mikulski, R.
— and Dembiński, B.
Determination of colloidal electrolytes: conductimetric titration of hydroxyzine hydrochloride with ammonium molybdate 233
- Milella, E.
—, Sentimenti, E., Mazzetto, G., Meragalli, L. and Battagliarin, M.
Direct determination of trace elements in indium phosphide by atomic absorption spectrometry 99
- Moriwake, T., see Korenaga, T. 237
- Mourel, R.M., see Feinberg, M.H. 83
- Nakagawa, G., see Ishizuki, T. 161
- Nakanishi, S., see Kaku, S. 213
- Ni, Z.-M., see Yan, X.-P. 105
- Nomura, T.
—, Ohno, Y. and Takaji, Y.
Single drop method for determination of ions using an electrodeless piezoelectric quartz crystal 187
- O'Gara, F., see Shanahan, P. 271
- Ohno, Y., see Nomura, T. 187
- Okada, K., see Korenaga, T. 237
- Ozawa, T., see Ishizuki, T. 161

- Pardue, H.L., see Jordan, J.M. 115, 125
- Psarellis, I.M.
—, Sarantonis, E.G. and Calokerinos, A.C.
Flow-injection chemiluminometric determination of sodium cyclamate 265
- Robien, W., see Chen, L. 301
- Sarantonis, E.G., see Psarellis, I.M. 265
- Sato, M., see Kaku, S. 213
- Schoenmakers, P., see Buydens, L. 41
- Schwedt, G., see Stein, K. 73
- Sentimenti, E., see Milella, E. 99
- Shanahan, P.
—, Glennon, J.D., Crowley, J.J., Donnelly, D.F. and O'Gara, F.
Liquid chromatographic assay of microbially derived phloroglucinol antibiotics for establishing the biosynthetic route to production, and the factors affecting their regulation 271
- Shinoda, S., see Korenaga, T. 237
- Smit, H.C., see Engelsma, M. 309
- Stein, K.
— and Schwedt, G.
Comparison of immobilization methods for the development of an acetylcholinesterase biosensor 73
- Suzuki, N., see Fukaya, T. 279
- Szmacinski, H., see Lakowicz, J.R. 179
- Takahara, H., see Le, Q.T.H. 293
- Takaji, Y., see Nomura, T. 187
- Timotheou-Potamia, M.M., see Halvatzis, S.A. 251
- Tölg, G., see Lee, M.L. 193
- Tong, W., see Fang, Y. 139
- Tschöpel, P., see Lee, M.L. 193
- Tsuzuki, M., see Ishizuki, T. 161
- Umetani, S., see Le, Q.T.H. 293
- Vadgama, P., see Christie, I. 145
- Wada, H., see Ishizuki, T. 161
- Wang, C.-M., see Fu, X.-T. 221
- Wang, R., see Fang, Y. 139
- Wang, S.
— and Larson, T.
Ambient error weighted partial least-squares regression: a new receptor model 333
- Wen, X., see Bartsch, R.A. 285
- Wyatt, P.J.
Light scattering and the absolute characterization of macromolecules. Review 1
- Xie, Y.-L.
—, Liang, Y.-Z. and Yu, R.-Q.
Quantitative calibration of multi-component systems with a known range of possibly co-existing species 61
- Yan, X.-P.
—, Ni, Z.-M. and Guo, Q.-L.
In situ concentration of mercury vapour in a palladium-coated graphite tube: determination of mercury by atomic absorption spectrometry 105
- Yeh, S.-J., see Lo, J.-M. 169
- Yu, R.-Q., see Xie, Y.-L. 61
- Yuchi, A., see Ishizuki, T. 161
- Zhang, H., see Zhang, Z.-Q. 227
- Zhang, Y.-X., see Fu, X.-T. 221
- Zhang, Z.-Q.
—, Chen, S.-Z., Lin, H.-M. and Zhang, H.
Simultaneous determination of copper, nickel, lead, cobalt and cadmium by adsorptive voltammetry 227
- Zhou, X., see Korenaga, T. 237

NEWS BRIEF

EUCMOS XXI

FROM August 23 to 26, 1992, the 21st European Congress on Molecular Spectroscopy, EUCMOS XXI, was held at the Technical university of Vienna with more than 400 participants from 40 countries. At the opening ceremony, in the presence of the organizing committee, the importance of this conference in the long series of EUCMOS conferences was emphasized. During the opening ceremony, two meritorious scientists were awarded by Prof. J.F.K. Huber: Prof. Jeanette G. Grasselli (Athens, Ohio, USA) was elected honorary member of the Austrian Society for Analytical Chemistry; Prof. B. Schrader (Essen, Germany) was awarded the Friedrich-Emich medal for his achievements in the field of Raman microscopy.

The opening lecture from H. Fuchs (Ludwigshafen, Germany) marked the first scientific highlight, during which the possibilities and new developments in the field of

atomic force and scanning tunneling microscopy. An absolute highlight was the Nobel lecture, held by the Nobel laureate for Chemistry 1991, Prof. Richard R. Ernst (ETH Zürich, Switzerland). The programme during the following days was intense with plenary, keynote and contributed lectures and poster presentations on several topics. For the first time, the "Vienna Opt(r)ode Workshop" — taking place this year for the third time — was held during the course of this conference with international experts in this field as contributors, thus forming a link between classical spectroscopy and optical sensor development.

The numerous excellent contributions resulted in the conference being of a very high scientific level according to the opinion of the participants. The organization was tight to enable a smooth-run-

ning conference, yet there were many possibilities for scientific and personal exchange.

We hope that all participants will remember EUCMOS XXI as an outstanding scientific and social event.

R. KELLNER
and E. ROSENBERG
Vienna, Austria

CAC-92

THE Fifth International Conference on Chemometrics in Analytical Chemistry (CAC-92), was held in Montreal, Canada on July 14–17, 1992. This marked the first time that the conference had been held in North America and provided an excellent opportunity

Views and opinions expressed in this section do not necessarily reflect those of the Publisher or Editors. No responsibility is assumed by the Publisher for any injury and/or damage to persons or property as a matter of products liability, negligence or otherwise, or from any use or operation of any methods, products, instructions or ideas contained in the material herein.

for North Americans who do not regularly attend the meeting to interact with their European counterparts. Over 100 participants attended this year's conference.

Seventy-three papers and posters were submitted from about a dozen countries, with the largest representations from the USA and The Netherlands.

The format for the four day meeting, held at the Hotel Meridien in Montreal, consisted of two parallel sessions of 25-minute talks interspersed with one-hour plenary lectures in the morning, afternoon and evening. The talks encompassed a broad spectrum of topics in chemometrics and provoked considerable discussion. Interest in the applications of neural networks has not waned, and problems and perspectives in multivariate calibration continued to generate strong interest. There were eight plenary lectures. Professor Stan Deming of the University of Houston opened the proceedings with his lecture "Chemometrics in Analytical Chemistry: A Brief History and a Long Future". Professor Clifford Spiegelman of Texas A&M University discussed approaches to receptor modelling with air pollution data from the region of El Paso, Texas. A lecture entitled "Chemometrics in Mass Spectrometry: An Old Cap with a New Feather", was held by Prof. Kurt Varmuza of the Technical University of Vienna. Professor Robert Meglen of the University of Colorado speculated on the role of fractal methods for exploratory data analysis. Advances in the analysis of ordered data sets via evolutionary factor analysis methods were discussed by Prof. D.L. Massart of Belgium.

The area of neural networks as a means of getting "coloured information from a black box" was reviewed by Prof. G. Kateman of the Catholic University of Nijmegen. Professor H.C. Smit of the University of Amsterdam discussed the power of signal processing methods, particularly matched filters, in extracting analytical information. The problem of nonlinear calibration with neural networks, and its relationship to the world of baseball, was addressed by Prof. Steven Brown of the University of Delaware. The final plenary lecture was delivered by Svante Wold of Umeå University who discussed some unique multivariate approaches to the rather formidable task of modelling the properties of large biomolecules and how this relates to chemical processes.

At the conference dinner the 1992 Elsevier Chemometrics Award was presented to Lutgarde Buydens of the Catholic University of Nijmegen. The hard work of the organizing committee resulted in a smooth and productive meeting, and in particular the efforts of the local organizers (Prof. Philip Hopke, Prof. Barry Lavine, and Jan Lavine) were gratefully acknowledged.

PETER WENTZELL
Dalhousie University
Halifax, Canada

ESEAC'92

DURING ESEAC '92 (Noordwijkerhout, May 31st to June 3rd, 1992) it was suggested that a Newsletter be started

in order to intensify the exchange of information among European electroanalysts. It is proposed that the Newsletter should appear twice a year with issues in late autumn and early summer. All the activities of the various European national electroanalytical working groups will be reported (authors of correspondence from the respective groups will be given with full postal addresses, phone and fax numbers). Conference and meetings relevant to electroanalysts will be announced and short reviews given. Personalalia (call for chairs and acceptance, honours, jubilees, obituaries) will also have a place. Book reviews will be welcome. It is also planned to have limited space for companies to present new products and advertisements. These, however, will be charged for in order to cover printing and mailing costs. Scientific papers will not be published.

For more information, please contact Dr. Wolfgang Frenzel, Technische Universität Berlin, Institute für Technischen Umweltschutz, Fachgebiet Luftreinhaltung, Sekr. KF2, Str. d. 17 Juni 135, W-1000 Berlin 12, Germany. Tel. +49 30-314-25218; Fax +49 30-314-23850.

Readers are invited to send any news item that they would like to have considered for publication in this section to:
ACA Newsbrief
Elsevier Science Publishers
P.O. Box 330,
1000 AH Amsterdam,
The Netherlands
Fax: [+31] 20 5862 845

Announcements of meetings

15th INTERNATIONAL SYMPOSIUM ON CAPILLARY CHROMATOGRAPHY, RIVA DEL GARDA, ITALY, MAY 24-28, 1993

The scientific program of this symposium will feature:

- The latest developments in: micro separation techniques, capillary gas chromatography (CGC), capillary GC-MS, GC-FTIR and GC-AES, micro-HPLC, supercritical fluid chromatography (SFC), capillary zone electrophoresis (MEKC).
- New methods and applications in: environmental analysis, pharmaceutical analysis, petroleum and petrochemicals, foods and beverages, biochemical separations, organic chemicals, drug testing, flavors and fragrances, proteins and peptides, trace analysis, sample preparation techniques; and new columns and instrumentation.

The program will include review papers, invited papers, poster sessions, discussion sessions and workshop seminars.

A limited number of scholarships will be awarded to students and young scientists. Application

forms may be requested by writing to Prof. Dr. P. Sandra,

Advanced registration fees accepted prior to April 25, 1993 are 300 ECU, on-site registration is 330 ECU and student registration fees are 150 ECU.

For further details contact: Prof. Dr. P. Sandra, I.O.P.M.S., Kennedy-park 20, B-8500 Kortrijk, Belgium. Tel.: +32 56-204-960; Fax: +32 56-204-859.

CHEMOMETRICS III, BRNO, CZECHOSLOVAKIA, JULY 11-15, 1993

Chemometrics III, the Third Czechoslovak Chemometric Conference with international participation, is organized by Masaryk University, Brno, and the Chemometric Group of the Czech Chemical Society. The Scientific Program will deal with:

Chemometrics in Analytical Chemistry

- analytical and statistical methods of quality control
- multivariable calibration
- non-linear regression and optimisation
- analysis of variance and residuals
- principal component analysis and pattern recognition

- education in analytical chemometrics

Physico-organic Chemometrics

- correlation analysis in chemistry (CAIC)
- quantitative structure-activity relationship (QSAR)
- experimental design and syntheses optimisation
- calculations in kinetics and thermodynamics
- confluent analysis
- education in physico-organic chemometrics

Contributions will be presented as plenary and main lectures, and selected oral communications and posters. The conference language will be English.

An exhibition of personal computers and demonstration and purchase of commercial software will be organized. The Conference fee will be about US\$ 200.

For further details, contact: RNDr. Josef Havel, Dept. of Analytical Chemistry, Masaryk University, Kotlarska 2, CS-61137 Brno. Tel.: +42 5-7129284; Telex: +42 5-740108; or RNDr. Miroslav Holik, Research Institute of Fine Chemicals, Lachema, Karasek 28, CS-62133 Brno. Tel.: +42 5-773077/270; Telex: +42 5-771121.

1994 WINTER CONFERENCE ON PLASMA SPECTRO-CHEMISTRY, SAN DIEGO, CA, USA, JANUARY 10-15, 1994

The 1994 Winter Conference on Plasma Spectrochemistry will be held Monday January 10 to Saturday January 15, 1994 in San Diego,

California. Short courses highlighting special topics will be offered Friday through Sunday, January 7-9. A three-day exhibition of spectroscopic instrumentation and accessories will be included. The Sixth Winter Conference on Flow Injection Analysis will be held consecutively on January 5-7.

Program features and Symposia will include:

- Automation, Expert Systems, and Robotics with Plasma Spectroscopy
- Chemometric Applications in Plasma Spectrochemistry
- Chromatography with Plasma Source Detection
- Elemental Speciation-Plasma Techniques
- Flow Injection Plasma Spectrometry
- Glow Discharge and Low Pressure Plasma Atomic and Mass Spectrometry
- Laser-Assisted Plasma Spectrochemistry
- Mechanisms and Process in Plasma Sources
- Modern Sample Preparation and Calibration Techniques
- New Instrumentation for Plasma Spectrochemistry
- Plasma Source Mass Spectrometry
- Process Control, Remote, and On-line Plasma Analysis
- Sample Introduction Techniques and phenomena
- Spectrochemical Applications of Plasma Sources
- Transform Interferometry for Plasma Sources

Titles and a 50-word abstracts for submitted lecture or poster papers are solicited by July 2, 1993. Extended conference abstracts are requested by October 8, 1993.

For further information, contact Dr. R. Barnes, ICP Information Newsletter, Department of Chemistry, GRC Towers, University of Massachusetts, Amherst, MA 01003-0035, USA. Tel.: +1 413-545-2294; Fax: +1 413-545-4490.

**EUCMOS XXII. XXIInd
EUROPEAN CONGRESS ON
MOLECULAR
SPECTROSCOPY, ESSEN,
GERMANY, SEPTEMBER
11-16, 1994**

The scope of the congress will cover all methods and applications of molecular spectroscopy, from theory to problem solving. The purpose is to catalyse international co-operation and exchange of ideas. Plenary lectures will deal with new developments and topics of general interest. Poster sessions and workshops with contributed papers will provide the opportunity to present and discuss new results.

EUCMOS XXII is especially intended to help colleagues from Western Europe to establish new contacts. Limited funds are available for those who contribute a poster or paper. The key topics will be:

- Industrial, Medical, and Environmental Problems
- Sensors, Remote Spectroscopy, Astrophysics
- Molecular Electronics, Semi- and Superconductors
- Solid State, Effects of Phase, Order, Temperature, Pressure
- Space Resolution, Surfaces, Nanostructures, Microscopy, Mapping, Tomography
- Time Resolution, Transients, Relaxation
- Resonance and Non-linear Phenomena
- Biomolecules, Chirality
- Structure, Interaction, Modelling
- New Techniques

For further details contact: Congress Secretariat, Gesellschaft Deutscher Chemiker, Abt. Tagungen, P.O. Box 900440, W-6000 Frankfurt 90, Germany. Tel.: +49 69 7917-366; Fax +49 69 7917-475; Telex 4 170 497 gdch d.

**Announcements are
included free of charge.
Information on
planned events should
be sent well in
advance [preferably 6
months or more] to:
ACA Newsbrief,
Elsevier Science
Publishers
P.O. Box 330, 1000 AH
Amsterdam,
The Netherlands
Fax: (+31) 20 5862 845**

Calendar of forthcoming meetings

★ indicates new or amended entry

February 9-10, 1993

Tokyo, Japan

CHEMSPEC ASIA 93. Exhibition. *Contact:* Jane Malcolm-Coe, PR & Publicity Manager, FMJ International Publications Ltd., Queensway House, 2 Queensway, Redhill, Surrey RH1 1QS, UK. Tel.: +44 737-768611. Fax: +44 737-761685.

★ February 17, 1993

Hull, UK

Recent Developments in X-Ray Fluorescence Spectrometry. *Contact:* Analytical Division, Royal Society of Chemistry, Burlington House, Piccadilly, London W1V 0BN, UK. Tel.: +44 71 437-8656.

★ February 23-26, 1993

Montreux, Switzerland

2nd International Symposium on Automation, Robotics and Artificial Intelligence Applied to Analytical Chemistry and 2nd International Conference on Robotics in Laboratory Medicine. *Contact:* J. van der Greef, TNO and University of Leiden, P.O. Box 360, 3700 AJ Zeist, The Netherlands. Tel.: +31 3404 44144; Fax: +31 3404 5722.

★ March 1-3, 1993

Amsterdam, The Netherlands

Good Laboratory Practices. A Three Day Intensive Course with Workshop. *Contact:* The Center for Professional Advancement, Oudezijds Voorburgwal 316A, 1012 GM Amsterdam, The Netherlands. Tel.: +31 20 6382806; Fax: +31 20 6202136; Telex: 10662 (cfpa nl).

March 8-12, 1993

Atlanta, GA, USA

PITTCON '93. 44th Pittsburgh Conference and Exposition on Analytical Chemistry and Applied Spectroscopy.

Contact: Linda S. Briggs, Pittsburgh Conference, 300 Penn Center Blvd., #332, Pittsburgh, PA 15235, USA. Tel. 412 825-3220; Fax: 412 825-3224. (Further details published in Vol. 268, No. 2).

★ March 11, 1993

Glasgow, UK

Chemometrics for Analytical Chemists — An Introduction. *Contact:* Analytical Division, Royal Society of Chemistry, Burlington House, Piccadilly, London W1V 0BN, UK. Tel.: +44 71 437-8656.

March 19, 1993

Antwerp, Belgium

Symposium on Possibilities and Limitations of Chiral Separation Techniques. *Contact:* Royal Flemish Chemical Society (KVCV), Working Part on Chromatography, c/o Dr. R. Smits, BASF Antwerpen N.V., Central Laboratory, Scheldelaan, B-2040 Antwerp, Belgium. Tel.: +32 3 568 2831; Fax: +32 3 568 3250; Telex: 31047 basant b.

★ March 14-18, 1993

Banff, Alta., Canada

VIIth International Symposium on Bioluminescence and Chemiluminescence. *Contact:* Dr. A.A. Szalay, 6-30 Med. Sci. Bldg., University of Alberta, Edmonton, Alta., T6G 2H7, Canada. Tel: 403 492-1774; Fax: 403 492-1782.

★ March 22-24, 1993

York, UK

Quality Compliance and Validation in Spectrophotometry. *Contact:* Dr. Terry Threlfall, Industrial Liaison Executive, Department of Chemistry, University of York, Heslington, York YO1 5DD, UK. Tel.: +44 904 432576 or 432511.

April 4-7, 1993

Clwydd, Wales, UK

Ion Exchange Processes. *Contact:* Haydn Hughes, Faculty of Science, The North East Wales Institute, Connah's Quay, Clwydd CH5 4BR, Wales, UK.

★ April 18-21, 1993

Baltimore, MD, USA

Fourth International Symposium on Pharmaceutical and Biomedical Analysis. *Contact:* Shirley E. Schlessinger, Symposium Manager, Suite 1015, 400 East Randolph Drive, Chicago, IL 60601, USA. Tel.: +1 312 527-2011.

April 20-21, 1993

Pontypridd, Wales, UK

The Interpretation of Vibrational Spectra. The Infrared and Raman Discussion Group and the University of Glamorgan Residential School. *Contact:* Mrs. Stephanie Williams, Faculty of Science and Engineering, University of Glamorgan, Pontypridd, Mid Glamorgan CF37 1DL, Wales, UK.

April 20-23, 1993

Brussels, Belgium

5th European Congress on Biopharmaceutics and Pharmacokinetics. *Contact:* Mrs. F. Rey, 3/17 Avenue de l'Observatoire B-1180 Brussels, Belgium. Tel.: +32 2 375 1648; Fax: +32 2 375 3299.

★ May 3-5, 1993

Veldhoven, The Netherlands

EuroResidue II. International Conference on Residues of Veterinary Drugs in Food. *Contact:* Dr. N. Haagsma, Section of Food Chemistry, Department of the Science of Food of Animal Origin, Faculty of Veterinary Medicine, University of Utrecht, P.O. Box 80.175, NL-3508 TD Utrecht, The Netherlands. Tel.: +31 30 535365 or 535367; Fax: +31 30 532365.

May 3-5, 1993

Szombathely, Hungary

5th Symposium on the Analysis of Steroids. *Contact:* Prof. S. Görög, c/o Chemical Works of Gedeon Richter Ltd., P.O. Box 27, H-1475 Budapest, Hungary. Tel.: +36 1-1574 566; Fax: +36 1-1571 578; Telex: 22-5067 richt h. (Further details published in Vol. 268, No. 2).

May 9-14, 1993
Hamburg, Germany

HPLC '93. 17th International Symposium on Column Liquid Chromatography. *Contact:* Gesellschaft Deutscher Chemiker, Abteilung Tagungen, Varrentrappstr. 40-42, D-6000 Frankfurt am Main 90, Germany. Tel.: +49 69-7917-360; Fax: +49 69-7917-475.

May 12-14, 1993
Paris, France

Spectral Analysis of Complex Structures. *Contact:* Uppsala University, School of Engineering, P.O. Box 534, S-75121 Uppsala, Sweden.

★ May 24-28, 1993
Riva del Garda, Italy

15th International Symposium on Capillary Chromatography. *Contact:* Prof. Dr. P. Sandra, I.O.P.M.S., Kennedypark 20, B-8500 Kortrijk, Belgium. Tel.: +32 56-204-960; Fax: +32 56-204-859. (See "Announcements" for further details).

May 25-27, 1993
Ghent, Belgium

Vth International Symposium on Quantitative Luminescence Spectrometry in Biomedical Sciences. *Contact:* Dr. Willy R.G. Baeyens, Symposium Chairman, University of Ghent, Pharmaceutical Institute, Harelbekestraat 72, 9000 Ghent, Belgium.

June 2-4, 1993
Stockholm, Sweden

Symposium on Analysis of Peptides. *Contact:* Swedish Academy of Pharmaceutical Sciences, P.O.Box 1136, S-111 81 Stockholm, Sweden. Tel.: +46 8 245085; Fax: +46 8 205511.

June 3-4, 1993
Brno, Czechoslovakia

European Conference on Analytical Chemistry and Pharmaceuticals, Chromatography and Spectroscopy, and Thermal Analysis. *Contact:* Dr. V.M. Bhatnagar, Alena Chemicals of Canada, P.O. Box 1779, Cornwall, Ont., Canada K6H 5V7. Tel.: 613 932-7702.

★ June 6-8, 1993
Malvern, PA, USA

Fifth Symposium on Chemically Modified Surfaces. *Contact:* Dr. Ivan E. Leigh, CertainTeed Corp., 1400 Union

Meeting Road, P.O. Box 1100, Blue Bell, PA 19422-0761, USA. Tel.: (215) 341-6622; Fax: (215) 341-6291.

June 7-9, 1993
Lyon, France

European Seminar on InfraRed Spectroscopy. *Contact:* G. Lachenal, Université Lyon I, Laboratoire des Matériaux Plastiques et des Biomatériaux, 69622 Villeurbanne Cédex, France. Fax: +33 78 89 25 83. (Further details published in Vol. 268, No. 2).

June 8-11, 1993
Egham, UK

Seventh International LIMS Conference. *Contact:* John Boothe, Programme Chairman, JB Scientific, P.O. Box 5, Riseley, Reading RG7 1YL, UK. Tel.: +44 734 883125; Fax: +44 734 885604.

June 9-12, 1993
Dortmund, Germany

22nd International Roland W. Frei Memorial Symposium on Environmental Analytical Chemistry. *Contact:* Mrs. M. Frei-Hausler, P.O. Box 46, CH-4123 Allschwil 2, Switzerland. Fax: +41 61-4820805.

June 13-17, 1993
Århus, Denmark

3rd Scandinavian Symposium on Chemometrics. *Contact:* SSC3 Secretariat, Department of Chemical Technology, Danish Technological Institute, Teknologiparken, DK-8000 Århus C, Denmark. Tel.: +45 86-142400; Fax: +45 86-147445.

★ June 13-17, 1993
Florence, Italy

6th European Congress on Biotechnology. *Contact:* Congress Secretariat, c/o Professor Laura Frontali, Department of Cell and Developmental Biology, University of Rome "La Sapienza", P. Aldo Moro 5, 00185 Rome, Italy. Tel.: +39 6 445-3950; Fax: +39 6 449-12351.

June 14-16, 1993
Arlington, VA, USA

PREP-93, 10th International Symposium on Preparative Chromatography. *Contact:* Barr Enterprises, P.O. Box 279, Walkersville, MD 21793, USA. Tel.: 301 898-3772; Fax: 301 898-5596. (Further details published in Vol. 268, No. 2).

June 23-24, 1993
Basle, Switzerland

CHEMSPEC EUROPE 93. *Contact:* Jane Malcolm-Coe, PR & Publicity Manager, FMJ International Publications Ltd., Queensway House, 2 Queensway, Redhill, Surrey RH1 1QS, UK. Tel.: +44 737-768611. Fax: +44 737-761685.

June 27-30, 1993
Santa Barbara, CA, USA

Fullerenes '93. The First International Interdisciplinary Colloquium on the Science and Technology of the Fullerenes. *Contact:* In North America: Kim Cavallero, Pergamon Seminars, 660 White Plains Road, Tarrytown, NY 10591-5153, USA. Tel.: 914 333-2550; Fax: 914 333-2468. All other countries: Gill Spear, Pergamon Seminars, c/o Elsevier Advanced Technology, Mayfield House, 256 Banbury Road, Oxford OX2 7DH, UK. Tel.: +44 865 512242; Fax: +44 865 310981.

June 29-July 4, 1993
York, UK.

XXVIII Colloquium Spectroscopicum Internationale. *Contact:* Department of Chemistry (CSI Secretariat), Loughborough University of Technology, Loughborough, Leics. LE11 3TU, UK.

July 7-9, 1993
York, UK.

Modern Ultraviolet Spectrometry. *Contact:* Dr. Tom Frost, Wellcome Foundations Ltd., Dartford Hill, Dartford DA1 5AH, UK. Tel: +44 322 223-488; Fax: +44 322 289-285.

★ July 11-14, 1993
Crete, Greece

Sixth International Symposium on Polymer Analysis and Characterization. *Contact:* Judith A. Sjöberg, Professional Association Management, 815 Don Gaspar, Santa Fe, NM 87501, USA. Tel.: (505) 989-4735; Fax: (505) 989-1073.

★ July 11-15, 1993
Brno, Czechoslovakia

Chenometrics III. Third Czechoslovak Chemometric Conference with international participation. *Contact:* RNDr. Josef Havel, Dept. of Analytical Chemistry, Masaryk University, Kotlarska 2, CS-61137 Brno. Tel.: +42 5-7129284; Telex: +42 5-740108; or RNDr. Miroslav

Holik, Research Institute of Fine Chemicals, Lachema, Karasek 28, CS-62133 Brno. Tel.: +42 5-773077/270; Telex: +42 5-771121. (See "Announcements" for further details).

July 19-21, 1993
Guildford, UK

6th Symposium on Handling of Environmental and Biological Samples in Chromatography. Contact: Mrs. M. Frei-Häusler, IAEAC Secretariat, Postfach 46, CH-4123 Allschwil 2, Switzerland.

August 9-11, 1993
Winnipeg, Canada

3rd Soil and Sediment Residue Analysis Workshop. International Association of Environmental Analytical Chemistry. Contact: Dr. G.R. Barrie Webster, Pesticide Research Laboratory, Department of Soil Science, University of Manitoba, Winnipeg, MB, Canada R3T 2N2. Tel.: (204) 474-6039; Fax: (204) 272-6019. Prof. Dr. J. Tarradella, IGE-Ecole Polytechnique, Federale de Lausanne, 1015 Lausanne, Switzerland. Tel.: +41 21 6932712; Fax: +41 21 6932727.

★ August 9-13, 1993
Beijing, China

ASIANALYSIS II. Second Asian Conference on Analytical Chemistry. Contact: Prof. Erkang Wang, 109 Sitalin Street, Changchun Institute of Applied Chemistry, Chinese Academy of Sciences, Changchun, Jilin 130022, China.

August 15-20, 1993
Beijing, China

34th IUPAC Congress: Chemistry for the 21st Century. Contact: Prof. Xinqi Song, Secretary-General of 34th IUPAC Congress, c/o Chinese Chemical Society, P.O. Box 2709, Beijing 100080, China.

★ August 21-24, 1993
Bologna, Italy

CHESM-93. Chemometrics and Environmetrics Meeting. Contact: Prof. Daniela Cocchi, Dipartimento di Scienze Statistiche "Paolo Fortunati", Università di Bologna, Via Belle Arti 41, I-40126 Bologna, Italy. Tel.: +39 51-258234; Fax: +39 51-232153; Email: cocchi%statbo.cineca.it@icnucev.m.cnuce.cnr.it.

August 23-27, 1993
Budapest, Hungary

9th Danube Symposium on Chromatography. Contact: Prof. L. Szepezy, Symposium Secretariat, Department of Chemical Technology, Technical University of Budapest, Budafoki ut 8, H-1521 Budapest, Hungary. Tel. +36 1 186-9000; Fax +36 1 181-2755; Telex 225931 muegy h. (Further details published in Vol. 264, No. 2).

★ August 23-27, 1993
Calgary, Canada

9th International Conference on Fourier Transform Spectroscopy. Contact: Conference Office, The University of Calgary, 2500 University Drive NW, Calgary, Alta. T2N 1N4, Canada. Tel.: +1 403 220-5051; Fax: +1 403 289-7287.

September 5-10, 1993
Loutraki, Greece

5th European Conference on the Spectroscopy of Biological Molecules. Contact: Professor Theo Theophanides, Chairman of ECSBM '93, Department of Chemical Engineering, National Technical University of Athens, Zografou Campus, Zografou 15780, Athens, Greece. Tel.: +30 1-7792438; Fax+ +30 1-7700989. (Further details published in Vol. 268, No. 2).

September 5-11, 1993
Edinburgh, UK.

Euroanalysis VIII. Contact: Miss P.E. Hutchinson, Analytical Division, The Royal Society of Chemistry, Burlington House, Piccadilly, London W1V 0BN, UK. Tel.: +44 71 437 8656; Fax: + 44 71 734 1227; Telex: 268001. (Further details published in Vol. 252, No. 1-2).

September 7-10, 1993
Verona and Soave, Italy

Applications of HPLC and CE in the BioSciences (12th International Symposium on Biomedical Applications of Chromatography and Electrophoresis and 2nd International Symposium on the Applications of HPLC in Enzyme Chemistry). Contact: Dr. F. Tagliaro, Scientific Secretariat, c/o Istituto di Medicina Legale, Policlinico Borgo Roma, I-37134 Verona, Italy. Tel.: +39 45 807-4618; Fax: +39 45 505-259. (Further details published in Vol. 268, No. 2).

September 8-10, 1993
Prague, Czechoslovakia

International Association of Environmental Analytical Chemistry 4th Workshop on Chemistry and Fate of Modern Pesticides and Related Pollutants. Contact: Dr. J. Hajslova, Institute of Chemical Technology, Department of Food Chemistry and Analysis, Suchbatarova 5, 16628 Prague 6-Dejvice, Czechoslovakia. Fax: +42 23-114769.

★ September 19-22, 1993
Research Triangle Park, NC, USA

2nd National Symposium on Planar Chromatography: Modern Thin-Layer Chromatography. Contact: Janet E. Cunningham, Barr Enterprises, P.O. Box 279, Walkersville, MD 21793, USA. Tel.: (301) 898-3772; Fax: (301) 898-5596.

★ October 5-8, 1993
Beijing, China

4th ISEC. Fourth International Seminar on Electroanalytical Chemistry. Contact: Prof. Erkang Wang, 109 Sitalin Street, Changchun Institute of Applied Chemistry, Chinese Academy of Sciences, Changchun, Jilin 130022, China.

★ October 8-13, 1993
Beijing, China

5th BCEIA. Fifth International Beijing Conference and Exhibition on Instrumental Analysis. Contact: General Service Office, 5th BCEIA, Room 5412, Building No. 4, Xi Yuan Hotel, Er Li Gou, Beijing 100046, China.

November 1-4, 1993
Oslo, Norway

LAB '93, Laboratory Exhibition. Contact: Norges Varemesse, P.O. Box 130, Skoyen, 0212 Oslo 2, Norway. Tel.: +47 2-43 90100; Fax: +47 2-43 1914.

★ January 10-15, 1994
San Diego, CA, USA

1994 Winter Conference on Plasma Spectrochemistry. Contact: Dr. R. Barnes, ICP Information Newsletter, Department of Chemistry, GRC Towers, University of Massachusetts, Amherst, MA 01003-0035, USA. Tel.: +1 413-545-2294; Fax: +1 413-545-4490. (See "Announcements" for further details).

February 22-25, 1994**Antwerp, Belgium**

HTC 3. Third International Symposium on Hyphenated Techniques in Chromatography. *Contact:* Royal Flemish Chemical Society (KVCV), Working Part on Chromatography, c/o Dr. R. Smits, BASF Anstwerpen N.V., Central Laboratory, Scheldelaan, B-2040 Antwerp, Belgium. Tel.: +32 3 568 2831; Fax: +32 3 568 3250; Telex: 31047 basant b. (Further detailed published in Vol. 268, No. 2).

February 28-March 4, 1994**Chicago, IL, USA**

PITTCO '94. Pittsburgh Conference on Analytical Chemistry and Applied Spectroscopy. *Contact:* Pittsburgh Conference, Suite 332, 300 Penn Center Blvd., Pittsburgh, PA 15235-9962, USA.

April 19-22, 1994**Munich, Germany**

ANALYTICA 94. 14th International Trade Fair for Biochemical and Instrumental Analysis with International Conference. *Contact:* Bernhard Schauder, ANALYTICA Press Office, Münchener Messe- und Ausstellungs-Gesellschaft mbh, Messgelände, Postfach 12 10 09, D-8000 Munich 12, Germany. Tel.: +49 89-51070; Fax: +49 89-5107506; Telex: 5212086 ameg d.

May 8-13, 1994**Minneapolis, MN, USA**

HPLC '94. 18th International Symposium on High Performance Liquid Chromatography. *Contact:* Janet E. Cunningham, Barr Enterprises, P.O. Box 279, Walkersville, MD 21793, USA. Tel.: (301) 898-3772; Fax: (301) 898-5596.

June 19-24, 1994**Bournemouth, UK**

20th International Symposium on Chromatography. *Contact:* The Executive Secretary, Chromatographic Society, Suite 4, Clarendon Chambers, 32 Clarendon Street, Nottingham NG1 5JD, UK. Tel.: +44 603-500596; Fax: +44 602-500614.

★ July 1994**Maastricht, The Netherlands**

International Chemometrics Research Meeting. *Contact:* Laboratory for Analytical Chemistry, Faculty of Science, Catholic University of Nijmegen, Toernooiveld 1, 6525 ED Nijmegen, The Netherlands.

★ September 11-16, 1994**Essen, Germany**

EUCMOS XXII. XXII European Congress on Molecular Spectroscopy. *Contact:* Congress Secretariat, Gesellschaft Deutscher Chemiker, Abt. Tagungen, P.O. Box 900440, W-6000 Frankfurt 90,

Germany. Tel.: +49 69 7917-366; Fax +49 69 7917-475; Telex 4 170 497 gdch d. (See "Announcements" for further details).

September 21-23, 1994**Stockholm, Sweden**

5th International Symposium on Pharmaceutical and Biomedical Analysis: *Contact:* Swedish Academy of Pharmaceutical Sciences, P.O. Box 1136, S-111 81 Stockholm, Sweden. Tel.: +46 8 245085; Fax: +46 8 205511.

★ September 22-24, 1994**Constanta, Romania**

12th Conference on Analytical Chemistry. *Contact:* Dr. Gabirel-Lucian Radu, Romanian Society of Analytical Chemistry, 13 Blvd. Carol I, Sector 3, 70346 Bucharest, Romania.

March 6-10, 1995

PITTCO '95. Pittsburgh Conference on Analytical Chemistry and Applied Spectroscopy. *Contact:* Pittsburgh Conference, Suite 332, 300 Penn Center Blvd., Pittsburgh, PA 15235-9962, USA.

★ July 9-15, 1995**Hull, UK**

SAC 95. *Contact:* Analytical Division, The Royal Society of Chemistry, Burlington House, Piccadilly, London W1V 0BN, UK. Tel.: +44 71 437-8656; Fax: +44 71 734-1227.

10th INTERNATIONAL SYMPOSIUM ON PREPARATIVE CHROMATOGRAPHY

CALL FOR PAPERS

JUNE 14 - 16, 1993

Send Abstracts to:
Prep-93 Symposium Manager
Barr Enterprises
P.O. Box 279
Walkersville, MD 21793 USA

Abstracts received after December 1, 1992
will be considered for poster presentation.



ARLINGTON, VIRGINIA
USA

CHAIRMAN:

Professor Georges Guiochon
Oak Ridge National Laboratory
and University of Tennessee

SYMPOSIUM MANAGER:

Mrs. Janet Cunningham
Barr Enterprises
P.O. Box 279
Walkersville, MD 21793 USA
Phone: (301) 898-3772
Fax: (301) 898-5596

PUBLICATION SCHEDULE FOR 1993

	S'92	O'92	N'92	D'92	J	F	M	A	M
Analytica Chimica Acta	267/1 267/2	268/1 268/2	269/1 269/2	270/1 270/2	271/1 271/2	272/1 272/2 273/1-2	274/1 274/2	275/1 275/2	276/1 276/2
Vibrational Spectroscopy		4/1			4/2		4/3		

INFORMATION FOR AUTHORS

Manuscripts. The language of the journal is English. English linguistic improvement is provided as part of the normal editorial processing. Authors should submit three copies of the manuscript in clear double-spaced typing on one side of the paper only. *Vibrational Spectroscopy* also accepts papers in English only.

Abstract. All papers and reviews begin with an Abstract (50–250 words) which should comprise a factual account of the contents of the paper, with emphasis on new information.

Figures. Figures should be prepared in black waterproof drawing ink on drawing or tracing paper of the same size as that on which the manuscript is typed. One original (or sharp glossy print) and two photostat (or other) copies are required. Attention should be given to line thickness, lettering (which should be kept to a minimum) and spacing on axes of graphs, to ensure suitability for reduction in size on printing. Axes of a graph should be clearly labelled, along the axes, outside the graph itself. All figures should be numbered with Arabic numerals, and require descriptive legends which should be typed on a separate sheet of paper. Simple straight-line graphs are not acceptable, because they can readily be described in the text by means of an equation or a sentence. Claims of linearity should be supported by regression data that include slope, intercept, standard deviations of the slope and intercept, standard error and the number of data points; correlation coefficients are optional. Photographs should be glossy prints and be as rich in contrast as possible; colour photographs cannot be accepted. Line diagrams are generally preferred to photographs of equipment.

Computer outputs for reproduction as figures must be good quality on blank paper, and should preferably be submitted as glossy prints.

Nomenclature, abbreviations and symbols. In general, the recommendations of the International Union of Pure and Applied Chemistry (IUPAC) should be followed, and attention should be given to the recommendations of the Analytical Chemistry Division in the journal *Pure and Applied Chemistry* (see also *IUPAC Compendium of Analytical Nomenclature, Definitive Rules, 1987*).

References. The references should be collected at the end of the paper, numbered in the order of their appearance in the text (*not* alphabetically) and typed on a separate sheet.

Reprints. Fifty reprints will be supplied free of charge. Additional reprints (minimum 100) can be ordered. An order form containing price quotations will be sent to the authors together with the proofs of their article.

Papers dealing with vibrational spectroscopy should be sent to: Dr J.G. Grasselli, 150 Greentree Road, Chagrin Falls, OH 44022, U.S.A. Telefax: (+ 1-216) 2473360 (Americas, Canada, Australia and New Zealand) or Dr J.H. van der Maas, Department of Analytical Molecule Spectrometry, Faculty of Chemistry, University of Utrecht, P.O. Box 80083, 3508 TB Utrecht, The Netherlands. Telefax: (+ 31-30) 518219 (all other countries).

© 1993, ELSEVIER SCIENCE PUBLISHERS B.V. All rights reserved.

0003-2670/93/\$06.00

No part of this publication may be reproduced, stored in a retrieval system or transmitted in any form or by any means, electronic, mechanical, photocopying, recording or otherwise, without the prior written permission of the publisher, Elsevier Science Publishers B.V., Copyright and Permissions Dept., P.O. Box 521, 1000 AM Amsterdam, The Netherlands.

Upon acceptance of an article by the journal, the author(s) will be asked to transfer copyright of the article to the publisher. The transfer will ensure the widest possible dissemination of information.

Special regulations for readers in the U.S.A.—This journal has been registered with the Copyright Clearance Center, Inc. Consent is given for copying of articles for personal or internal use, or for the personal use of specific clients. This consent is given on the condition that the copier pays through the Center the per-copy fee for copying beyond that permitted by Sections 107 or 108 of the U.S. Copyright Law. The per-copy fee is stated in the code-line at the bottom of the first page of each article. The appropriate fee, together with a copy of the first page of the article, should be forwarded to the Copyright Clearance Center, Inc., 27 Congress Street, Salem, MA 01970, U.S.A. If no code-line appears, broad consent to copy has not been given and permission to copy must be obtained directly from the author(s). All articles published prior to 1980 may be copied for a per-copy fee of US \$2.25, also payable through the Center. This consent does not extend to other kinds of copying, such as for general distribution, resale, advertising and promotion purposes, or for creating new collective works. Special written permission must be obtained from the publisher for such copying.

No responsibility is assumed by the publisher for any injury and/or damage to persons or property as a matter of products liability, negligence or otherwise, or from any use or operation of any methods, products, instructions or ideas contained in the material herein.

Although all advertising material is expected to conform to ethical (medical) standards, inclusion in this publication does not constitute a guarantee or endorsement of the quality or value of such product or of the claims made of it by its manufacturer.

This issue is printed on acid-free paper.

PRINTED IN THE NETHERLANDS

Atomic Absorption Spectrometry

Theory, Design and Applications

edited by S.J. Haswell, School of Chemistry, University of Hull, Hull, UK

Analytical Spectroscopy Library Volume 5

Atomic absorption spectroscopy is now a well-established technique for the determination of trace elements covering a wide range of analyte types. The early theory and instrumentation chapters incorporate recent trends in instrumental design and methodology, in particular those associated with electrothermal techniques and background correction. The major thrust of the book is represented by 14 application chapters which give an extensive well referenced review of the practical use of the technique written by experts drawn from their own speciality areas. These include the determination of trace elements in areas as diverse as environmental, chemical and industrial analysis.

Whilst the book is primarily concerned with atomic absorption spectroscopy, any analyst involved in sample handling prior to trace elemental analysis will find this book a valuable compendium of methodology drawn from a very wide range of applications. For the current user of the technique the well referenced sections critically evaluate the state-of-the-art, while for the newer user the text will form the basis of a good laboratory handbook which offers a comprehensive instruction on the theory and instrumental design in atomic absorption spectroscopy.

Contents:

1. Basic principles (*J.F. Tyson*). 2. Instrumental requirements and optimisation

(*S.J. Haswell*). 3. Practical techniques (*S.J. Haswell*). 4a. Waters, sewage and effluents (*M. Blankley, A. Henson and K.C. Thompson*). 4b. Application of atomic absorption spectrometry to marine analysis (*H. Haraguchi and T. Akagi*). 4c. Analysis of airborne particles in workplace atmospheres (*J.C. Septon*). 4d. Application of atomic absorption spectrometry to the analysis of foods (*T.C. Rains*). 4e. Applications of atomic absorption spectrometry in ferrous metallurgy (*K. Ohls and D. Sommer*). 4f. The analysis of non-ferrous metals by atomic absorption spectrometry (*M.R. North*). 4g. Atomic absorption methods in applied geochemistry (*M. Thompson and E.K. Banerjee*). 4h. Applications of atomic absorption spectrometry in the petroleum industry (*J. Marshall*). 4i. Methods for the analysis of glasses and ceramics by atomic absorption spectrometry (*W.M. Wise, R. A. Burdo and D.E. Goforth*). 4j. Clinical applications of flame techniques (*A. Taylor*). 4k. Elemental analysis of body fluids and tissues by electrothermal atomization and atomic absorption spectrometry (*H.T. Delves and I.L. Shuttler*). 4l. Forensic science (*I.M. Dale*). 4m. Fine, industrial and other chemicals (*L. Ebdon and A.S. Fisher*). 4n. Analysis of polluted soils (*M. Cresser*). Subject Index.

1992 xx + 530 pages

Price: US \$ 177.00 / Dfl. 345.00

ISBN 0-444-88217-0



Elsevier Science Publishers

P.O. Box 211, 1000 AE Amsterdam, The Netherlands

P.O. Box 882, Madison Square Station, New York, NY 10159, USA



0003-2670(19930212)272:2;1-K

2000.36

- 2 8. 2536